

PERSISTENT ANOMALIES OF THE
EXTRATROPICAL NORTHERN HEMISPHERE WINTER TIME CIRCULATION

by

RANDALL M. DOLE

B.S., Cornell University
(1975)

SUBMITTED TO THE DEPARTMENT OF
METEOROLOGY AND PHYSICAL OCEANOGRAPHY
IN PARTIAL FULFILLMENT OF THE
REQUIREMENTS FOR THE DEGREE OF

DOCTOR OF PHILOSOPHY

at the

MASSACHUSETTS INSTITUTE OF TECHNOLOGY

January 1982

© Massachusetts Institute of Technology 1982

Signature of Author.

Department of Meteorology and Physical Oceanography
A 1 1 January, 1982

Certified by

Frederick Sanders
Thesis Supervisor

Accepted by.

Chairman, Departmental Committee on Graduate Students
Ronald G. Prinn

WITHDRAWN
RECEIVED
MASSACHUSETTS INSTITUTE
OF TECHNOLOGY
MIT LIBRARIES



Room 14-0551
77 Massachusetts Avenue
Cambridge, MA 02139
Ph: 617.253.5668 Fax: 617.253.1690
Email: docs@mit.edu
<http://libraries.mit.edu/docs>

DISCLAIMER OF QUALITY

Due to the condition of the original material, there are unavoidable flaws in this reproduction. We have made every effort possible to provide you with the best copy available. If you are dissatisfied with this product and find it unusable, please contact Document Services as soon as possible.

Thank you.

Author apparently miss numbered some pages.
Page 19 does not exist.

PERSISTENT ANOMALIES OF THE
EXTRATROPICAL NORTHERN HEMISPHERE WINTERTIME CIRCULATION

by

RANDALL M. DOLE

Submitted to the Department of Meteorology and Physical Oceanography
in January 1982 in partial fulfillment of the requirements for the
degree of Doctor of Philosophy.

ABSTRACT

We have studied the geographical, structural and temporal characteristics of anomalies that persist beyond the periods associated with synoptic-scale variability and have examined the relationship that these persistent anomalies have to changes in storm activity. There are three major regions for the occurrence of persistent anomalies: the north-central North Pacific, the eastern North Atlantic, and the northern Soviet Union. For each region, the maximum in the frequency of occurrence of positive anomalies is approximately co-located with, and has a comparable value to, the corresponding maxima of negative anomalies. For sufficiently long durations, the number of events decays nearly exponentially with increasing durations, resembling the behavior obtained from a first-order autoregressive process.

Analyses of horizontal structure provide evidence for the recurrence of certain preferred anomaly patterns. To a first approximation, persistent positive and negative anomaly patterns for a region can be described as opposite phases of the same basic pattern. Most of the cases appear as unusually strong enhancements of the primary regional pattern of low-frequency variability. One phase of this pattern usually resembles blocking; the other, a regional high-index flow. Systematic changes in the storm paths and in the locations and intensities of the major surface centers of action accompany the persistent anomalies. The corresponding vertical structures display maximum height anomalies in the upper troposphere and little tilt with height.

Composite time analyses indicate that development rates are often rapid (full establishment in less than a week). There is little evidence of an atmospheric precursor until just prior to onset. Following onset, anomaly centers develop and intensify downstream from the main center, leading to the establishment of the persistent anomaly pattern. Intensification occurs with little evidence of phase propagation. The anomalies often display greater westward vertical tilts during than following development. Break-downs occur rapidly. Until just prior to breakdown, the patterns closely resemble the patterns following development.

Contributions of transient eddies toward maintaining local, time-mean balances of heat, vorticity and potential vorticity are then examined to study how changes in storm activity are related to changes in the mean flow. Comparisons between corresponding positive and negative cases show well-defined differences in most heat budget terms, but few significant differences in most vorticity and potential vorticity terms. Many of the systematic differences in the eddy terms appear qualitatively consistent with changes expected for developing baroclinic waves on a spatially varying mean flow. Differences in the time-mean diabatic heating appear mainly related to changes in the storm paths. The results are generally consistent with similar calculations for climatological-mean flows; thus, the qualitative relations already established between long-term mean flows and storm activity also appear in anomalous flows having durations of a few weeks.

Thesis Supervisor: Professor Frederick Sanders
Title: Professor of Meteorology

ACKNOWLEDGEMENTS

My experiences have been made much richer and more enjoyable by my relationships with a number of the faculty and staff in the Department. I was privileged to have Prof. Jule Charney as advisor for most of this research. His insights and infectious enthusiasm for understanding meteorological phenomena were always inspirational. As advisor during the final portion of the thesis, Prof. Frederick Sanders was supportive of my efforts, but also provided useful criticisms and alternative viewpoints. Throughout my studies, Prof. Mark Cane was a ready source for advice and consultation; he, in addition to Profs. Glenn Flierl and Peter Stone, gave several helpful comments on early versions of the thesis. Insightful and constructive criticisms and suggestions were also provided by Drs. Claude Frankignoul and Neil Gordon. Ms. Isabelle Kole exhibited extraordinary patience and skill in drafting the several hundred figures that are in this thesis, and Ms. Virginia Mills displayed considerable good humor while typing (and re-typing) the final draft. The research was supported by National Science Foundation grant NSF-g 76-20070 ATM. Calculations were carried out on both the GSFC and NCAR computer systems.

I have also benefitted from several stimulating discussions with Profs. K. K. Tung and Ed Harrison of MIT, Prof. Dick Lindzen and Dr. Ed Sarachik of Harvard, Prof. Lance Bosart and Steve Colucci of SUNYA, Drs. Maurice Blackmon and Chuck Leith of NCAR, and Drs. Gabriel Lau and Isaac Held of GFDL. The latter two have graciously provided me with early drafts of some of their research, while Dr. Blackmon generously allowed me access to his NCAR data sets.

I have greatly enjoyed my friendships with former and present students in the Department, particularly Drs. Lee Branscome, Brian Reinhold and George Huffman. Lee was an excellent sounding board for various (often wild) ideas. Brian's marathon running served as excellent preparation for our often lengthy, but always stimulating, discussions of persistent phenomena. George's ready advice, patience and good humor, if not legendary, should be: he helped considerably to ease the difficulties and to add to the enjoyment of my graduate studies.

My friends, particularly Al Lush and Bob Posner, were sources of unflagging support throughout the years. Finally, my family and especially my wife, Ellen, to whom this thesis is dedicated, were always with me, selflessly providing their encouragement, help and love.

Table of Contents

	<u>Page</u>
I. Introduction	7
A. Background and statement of objectives	7
B. Outline of thesis	9
II. Review	11
A. Definitions of blocking	11
B. Observational studies	15
1. Geographical and seasonal variability	15
2. Structure	20
3. Characteristics of time evolution	21
4. Budget studies	24
5. Summary of observational results	25
C. Proposed mechanisms	25
D. Discussion	35
III. Geographic distribution	39
A. Introduction	39
B. Data set	39
C. Procedure	39
1. Anomaly: definition and measures	39
a. Zonal height anomalies	40
b. Temporal height anomalies	41
c. Standardized height anomalies	42
2. Method for defining cases	43
D. Geographic distributions	45
1. Zonal height anomalies	46
2. Temporal height anomalies	50
3. Standardized height anomalies	61
E. Discussion	65
F. Conclusion	68
IV. Structure	70
A. Introduction	70
B. Horizontal structure	70
C. Vertical structure	102
D. Discussion	112
E. Conclusions	121
V. Time evolution	123
A. Introduction	123
B. Data set	123
C. Development	124
D. Breakdown	153
E. Discussion	162

	<u>Page</u>
VI. Interactions with transient eddies and the maintenance of persistent anomalies.	166
A. Introduction	166
B. Procedure.	167
C. Differences in mean flows and storm paths.	168
D. Budgets.	174
1. Heat budgets.	174
2. Vorticity budgets	183
E. Discussion	193
F. Conclusions.	196
VII. Conclusion.	198
Appendix 1. NMC Data Set	205
Appendix 2. Case dates	208
Appendix 3. Empirical orthogonal function analysis	212
Appendix 4. Vertical motion calculations	215
References	218
Acknowledgements	226

I. INTRODUCTION

A. Background and Statement of Objectives

Weather forecasters commonly use their familiarity with "analogue" cases in preparing short-range predictions. Observational meteorologists frequently suggest that there may also be some recurrent flow patterns that typically persist beyond the periods associated with synoptic-scale variability. The prototypical example cited is the phenomenon of blocking, often described as having considerable persistence and a tendency toward the recurrence of qualitatively similar flow patterns (Namias, 1947; Elliott and Smith, 1949; Rex 1950 a,b; Sumner, 1954). The descriptions presented in these studies suggest coherent forms of low-frequency behavior. Nevertheless, our current understanding of the nature and characteristics of recurrent persistent flow anomalies remains quite limited. A challenging problem facing meteorologists is to determine if these earlier observations can be placed within a more general and systematic framework.

The close association of persistent flow anomalies with prolonged abnormal weather conditions suggests that their accurate prediction is fundamental to skillful extended-range weather forecasting. Recent estimates (see e.g., Leith, 1978), however, suggest that our current limit of predictive skill is within the range of durations attributed to synoptic-scale fluctuations. This present practical limit is appreciably less than the limits estimated by predictability theory (Leith, 1978).

Although the reasons for our lack of skill at extended range forecasting have not been fully elucidated, a multiplicity of con-

tributing factors can readily be imagined. Indeed, a discussion by von Neumann (1957) on a strategy for weather prediction anticipates the intrinsic difficulty of the problem. Von Neumann states that

It seems quite plausible from general experience that in any mathematical problem it is easiest to determine the solution for shorter periods, over which the extrapolation parameter is comparatively small. The next most difficult problem to solve is that of determining the asymptotic conditions - that is, the conditions that exist over periods for which the extrapolation parameter is very large, say near infinity. Finally, the most difficult is the intermediate range problem, for which the extrapolation parameter is neither very small nor very large... On the basis of these considerations, it follows that there is a perfectly logical approach...to the problem of weather prediction. The approach is to try first short-range forecasts, then long-range forecasts of those properties of the circulation that can perpetuate themselves over arbitrarily long periods of time (other things being equal), and only finally to attempt to forecast for medium-long time periods...

In many respects, research on large scale atmospheric phenomena has paralleled von Neumann's prescription. One focus for study has been the short period fluctuations; another, the long-term mean flow. To a first approximation, the behavior of the former conforms with that expected of disturbances developing as a result of baroclinic instability (Charney, 1947; Eady, 1949) and decaying by barotropic and frictional processes; the latter appears to be a response mainly to forcing by topography and geographically-fixed heat sources and sinks.

In comparison, our current understanding of the causes and characteristics of intermediate scale phenomena, or persistent anomalies, is far more primitive. We do not yet have a generally accepted theory of persistent anomalies, although there has been much recent

effort devoted to this problem. A major obstacle hindering our progress has been the lack of an adequate empirical description of the typical characteristics of these features. Moreover, we do not yet know how changes in storm behaviors are related to changes in the mean flow accompanying the persistent anomalies. This hinders our understanding of phenomena such as blocking, where major deformations of the mean flow are accompanied by significant changes in the location of, and activity along, storm paths.

The two general objectives of this thesis are, first, to ascertain systematic behaviors of anomalies that persist beyond the periods associated with synoptic-scale variability and, second, to examine the relationship that these persistent anomalies have to changes in storm activity. The specific objectives are:

- 1) to determine whether persistent anomalies preferentially occur in specific geographic regions;
- 2) to determine whether persistent anomalies are associated with recurrent flow patterns;
- 3) to describe typical life cycles of persistent anomalies; and
- 4) to examine how changes in storm activity are related to mean flow changes associated with persistent anomalies.

B. Outline of Thesis

Chapter 2 reviews research in this area with emphasis on blocking studies. The main theme of Chapter 3 is to identify the geographical distribution of persistent anomalies and to relate this distribution to other features of the Northern Hemisphere wintertime circulation. Chapter 4 provides detailed analyses of the structure of persistent

anomalies and examines evidence for the existence of recurrent, large-scale anomaly patterns. Chapter 5 furnishes descriptions of time evolution. Chapter 6 compares the relative roles of mean and eddy terms in local, time-mean budgets of heat, vorticity and potential vorticity during persistent anomalous periods. This forms a basis for examining how changes in storm activity are related to changes in the mean flow. Chapter 7 consists of concluding remarks and suggestions for further research.

II. REVIEW

There is a vast but diffuse body of literature relating to persistent anomalies, including studies on blocking, teleconnections* and weather regimes. We will not attempt a comprehensive review of this research. Rather, our main objectives are to evaluate prior phenomenological and theoretical studies in order to define the principal problems requiring further investigation. The majority of studies in this area have focused on blocking and, accordingly, we emphasize that subject. Since no review of blocking presently exists, our discussion is rather thorough; for the more casual reader, brief summaries of the salient observational and theoretical results are provided at the ends of the corresponding sections. The last section more extensively discusses and outlines the primary outstanding problems.

A. Definitions of blocking

In common with many other terms in synoptic meteorology, "blocking" has been defined by a number of different criteria. Perhaps the most frequent use of the term has been to indicate the existence of a quasi-stationary, persistent and usually strong anticyclone or ridge located at mid- to high-latitudes (Glossary of Meteorology, 1959). Some investigators (Rex, 1950a, b; 1951) additionally require the existence of a "split" in the upper-level westerlies (the occurrence of multiple maxima in the zonal wind at fixed longitude and pressure). An idea implicit in much of the research is that the major deformation of the westerlies associated with blocking appears to obstruct or divert ("block") migratory disturbances from their predominantly

*We will not review teleconnection research in detail, since Wallace and Gutzler (1981) provide a good recent summary of the main results.

eastward movement along the climatological mean storm paths. This "steering flow" definition of blocking has never been applied directly, nor adequately evaluated observationally, although Petterssen (1956) provides a time sequence of frontal analyses to illustrate this concept (Fig. 2.1).

The most important differences among the various selection criteria center about three factors:

- 1) the relative importance attached to various structural characteristics of the flow;
- 2) the variations in emphasis placed on persistence;
- 3) the types of data used for primary identification (i.e., surface synoptic, 500 mb synoptic, 700 mb mean).

The principal criteria that have been used to define blocking can be sufficiently illustrated by examining those used by Namias (1947), Elliott and Smith (1949), Rex (1950a,b) and White and Clark (1975).

Namias (1947) associates two characteristics with blocking:

- 1) A "retardation" of the zonal circulation in a limited sector of the hemisphere throughout the depth of the troposphere, which moves westward with time; and
- 2) a synoptic manifestation of a warm anticyclone in high latitudes and a cold cyclone in lower latitudes. Namias employs 5-day mean charts at sea level and 10,000 ft. He identifies blocking situations by large positive pressure anomalies at high latitudes, but applies no specific objective criterion.

Elliott and Smith (1949) also place most emphasis on the structural characteristics of blocking; in particular, they define blocking as

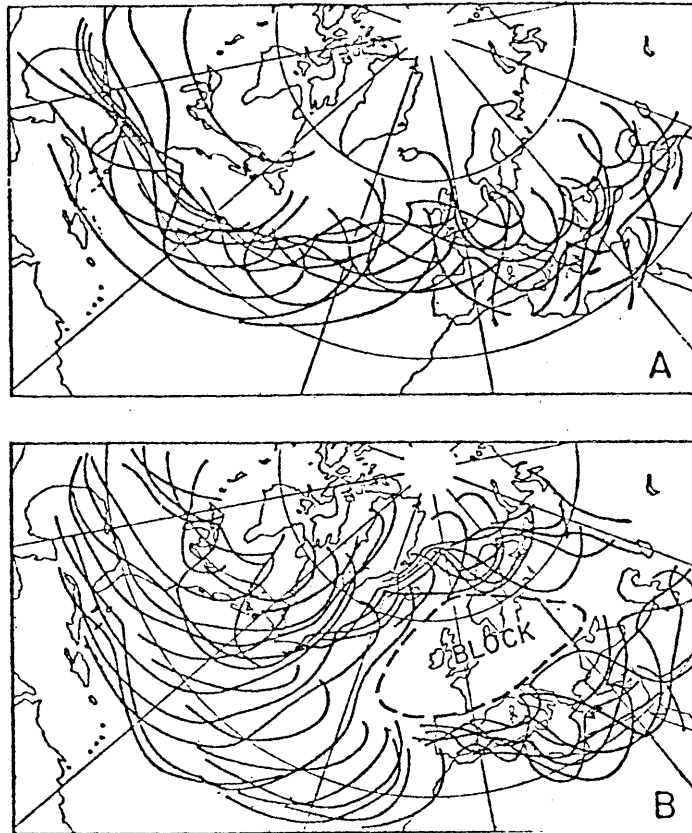


Fig. 2.1

Positions of fronts during two successive
10-day periods:

- A) preceding the formation,
- B) following the establishment of, a
blocking high (from Petterssen, 1956)

A state of circulation in which the normal flow is interrupted in a sector . . . by strong persistent, meridional-type flow. Synoptically . . . a persistent high at high latitudes (is present) . . . obstructing the normal eastward progress of migratory cyclones and anticyclones. The high is linked, as a rule, to simultaneous abnormally deep depressions either upstream or downstream or both, which are often trapped in low latitudes.

For objective criteria they use excessive positive surface pressure departures (+20 mb) in a band at least 15 degrees longitude wide over a period of at least three consecutive days.

Rex (1950a) develops considerably more detailed criteria for identifying blocking patterns. Rex states that

a blocking case must exhibit the following characteristics:

- 1) The basic westerly current must split into two branches.
- 2) Each branch current must transport an appreciable mass.
- 3) The double-jet system must extend over at least 45° of longitude.
- 4) The pattern must persist with recognizable continuity for at least ten days.

Blocking is said to be initiated when 1) occurs, and to have dissipated whenever any of conditions 1) - 4) are no longer met.

White and Clark (1975) investigated blocking situations over the central North Pacific using monthly mean 700 mb height data.

Consequently, their definition of blocking is somewhat less restrictive than that of Rex (1950a). They state that

A blocking ridge exists when a sharp transition in the mid-latitude westerlies from a zonal type upstream to a meridional type downstream occurs with an amplitude exceeding five degrees of latitude.

For ease of comparison, the different criteria used in investigations of blocking are summarized in Table 2.1, which also lists the data sources and primary objectives of each of the studies.

B. Observational studies

The majority of observational studies on blocking were performed from the late 1940's through the mid-1950's. The primary objectives of these investigations were to provide synoptic analyses of blocking cases (Berggren, Bolin and Rossby, 1949; Rex, 1950a) and to establish a climatology of blocking (Rex, 1950b; Brezowsky, Flohn and Hess, 1951; Sanders, 1953; Sumner, 1954). Aside from statistical summaries presented in the climatology studies, quantitative results are quite limited. The lack of uniformity in the criteria used by different researchers, as previously discussed, must also be considered in interpreting and comparing the results cited in this section.

1. Geographical and seasonal variability

The most comprehensive study of the seasonal and geographic distribution of blocking is that of Rex (1950b). In common with most blocking studies, Rex concentrated on blocking situations located over the Northern Hemisphere oceans with most emphasis on North Atlantic blocking. The less thorough analysis of North Pacific blocking is primarily a manifestation of the inadequate data coverage that existed in that region during the period considered (1933-1940, 1945-1949). Several results obtained by Rex are pertinent; he states that:

Table 2.1

<u>Study</u>	<u>Criteria</u>	<u>Type of Study</u>	<u>Data</u>
Namias (1947)	large pressure anomalies at high latitudes, no time criterion	synoptic- climatological	5-day mean charts at sea level and 10,000 feet
Elliot and Smith (1949)	excessive positive pressure departures in a band 15° longitude wide over 3 days	climatological	daily surface pressure values for Jan.-Feb. 1900-1939
Berggren, <u>et al.</u> , (1949)	subjectively identified	synoptic	mult. level data for Feb., 1948 case
Rex (1950a) (1950b) (1951)	split westerly flow over at least 45° of longitude, sharp transition from zonal to meridional flow, recognizable continuity for at least 10 days.	synoptic- climatological	500 mb z and surface synoptic charts: 1933-1940; 1945-1949
Sumner (1954)	well formed cellular structure north of 50° N subjectively identified, no minimum time criteria	climatological	500 mb and 500 mb - 1000 mb thickness, 1949-1952
White and Clark (1975)	sharp transition in mid- latitude westerlies to a meridional-type flow with amplitude exceeding 5° of latitude	climatological	monthly mean 700 mb data, 1950-1970
Hartman and Ghan (1980)	continuous high heights in confined region for at least 6 days	climatological budget	NMC analyses of z, T for 10 winters 1965-66 through 1974-75

- 1) Blocking activity is most frequently initiated in two relatively narrow longitudinal zones in the northern hemisphere, one (Atlantic) centered aloft at 10°W longitude and the other (Pacific) at 150°W longitude.*
- 2) Both Atlantic and Pacific blocks . . . normally persist for a period of 12 to 16 days and are relatively stable in position.
- 3) Regular seasonal and irregular yearly variations in both Atlantic and Pacific blocking activity occur. These variations are strong, in excess of 50%, and in the case of the seasonal trends are essentially in phase in both Atlantic and Pacific.
- 4) Atlantic blocks exceed Pacific blocks in frequency of occurrence, apparently by a factor of two to one.

The differences in frequency of occurrence between Atlantic and Pacific blocks may be due in part to the deficient data coverage over the latter region during the period considered, as observed by Rex. Note that although Rex states that the seasonal variations of the frequency of Atlantic and Pacific blocking are approximately in phase, he observes in an earlier paper that "it is more usual to find only one block in the hemispheric flow pattern . . . double blocks are normally short-lived. One or the other dissipates, leaving a single block which may persist for several weeks." (Rex, 1950a). Also, any estimate of duration depends on the particular selection criteria. In this study, Rex (1950b) insists that

*The longitudes given by Rex refer to the upstream location of the split in the westerly flow and not to the position of the anti-cyclone center, which is the usual convention.

"the pattern must persist with recognizable continuity for at least ten days " although the particular minimum duration appears somewhat arbitrary.

Sumner (1954) examines the climatology of blocking for North Atlantic and western European regions over 1949-1952. Although Sumner uses substantially different selection criteria than Rex (the principal differences are that Sumner does not apply a minimum duration criterion and does not require a split flow, cf. Table 2.1) his results on the whole confirm Rex's conclusions on Atlantic blocking. The most serious discrepancy concerns the seasonal variations of blocking: Rex finds a seasonal maximum in late winter to early spring and a late summer minimum, while Sumner includes these but also shows a second maximum in November and a second minimum in January. Brezowsky, Flohn and Hess (1951), using surface pressure data for the period 1881-1950, indicate a primary maximum of blocking in late spring, a minimum in summer, and also a weak secondary maximum in autumn. It is not clear to what extent differences among the selection criteria and data sources account for these discrepancies.

The above studies focused on blocking over the North Atlantic and western Europe. White and Clark (1975) investigate blocking activity over the central North Pacific. Recall that White and Clark use monthly mean charts so that they have no values for the duration of individual features. Their analysis of blocking frequency shows a pronounced winter maximum and a late spring minimum. This is in conflict with some of the conclusions given by Rex (1950b) on Pacific blocking, especially his assertion that the seasonal variations in

Atlantic and Pacific blocking frequencies are approximately in phase. The longitudinal distribution of Pacific blocking found by White and Clark shows a maximum in frequency of occurrence near 170°W or about 20°W of the maximum indicated by Rex, despite Rex's use of the upstream position of the split flow, rather than the ridge axis, to locate cases. Additionally, White and Clark indicate that the inter-annual variability in blocking activity appears to fluctuate in concert with the Southern Oscillation. They associate frequent blocking activity with below-normal sea surface temperatures over the central and eastern equatorial Pacific.

2. Structure

Previous studies have concentrated on the horizontal structure of blocking "patterns" and, indeed, this has been used as the sole basis for defining cases (e.g., Sumner, 1954; 1959). This emphasis was no doubt partially motivated by data availability, but it was also influenced by the primacy of barotropic models in early theories of blocking (e.g., Yeh, 1949; Rossby, 1950). Apparently these studies also sometimes affected the choice of horizontal structural models used for defining cases observationally; an important objective of Rex's (1950a) study, for example, was to test a theory by Rossby (1950) accounting for a rapid downstream decrease in the zonal flow, suggesting a current "split." Although Rex focuses on split flows, he also observes (Rex, 1950a) that "no sharp distinction may exist" between these flows and amplified wave patterns not accompanied by a split flow, which his criteria exclude at the outset.

Nevertheless, there are several suggestions in the literature

of particular recurrent, persistent flow patterns. Rex (1951) provides composites of the surface pressure and 500 mb heights for three winter cases of European blocking. He notes "a remarkable agreement in the location and relative orientation of the various features" for the cases analyzed. A typical aspect of the flow patterns identified by Rex is an intense warm anticyclone located to the north of a cold-core cyclone. This is similar to the description of blocking cases provided by Namias (1947). Sumner (1954) presents flow patterns typical of Atlantic and European blocking (Fig. 2.2). White and Clark (1975) compare a mid-Pacific blocking pattern with a more "normal" winter flow pattern (Fig. 2.3). An important limitation of these earlier studies is that, owing to data availability, comparisons are generally carried out over limited regions.

3. Characteristics of time evolution

Case analyses are described by Berggren, et al., (1949) and Rex (1950a). In these studies, blocking develops in about a week. Typical durations for cases are from one to three weeks, with a mean duration of close to two weeks (Rex, 1950b; Sumner, 1954). In some years, blocks may persist or recur frequently in the same region for most of a season (e.g., Namias, 1964). The primary focus in these studies is on describing zonal propagation characteristics; little attention has been given to time evolution in the meridional direction, or to the evolution of the vertical structure. Early studies suggest that blocking is characterized by a slow westward development (Namias, 1947), which Palmen and Newton (1969) associate with the successive development of new warm

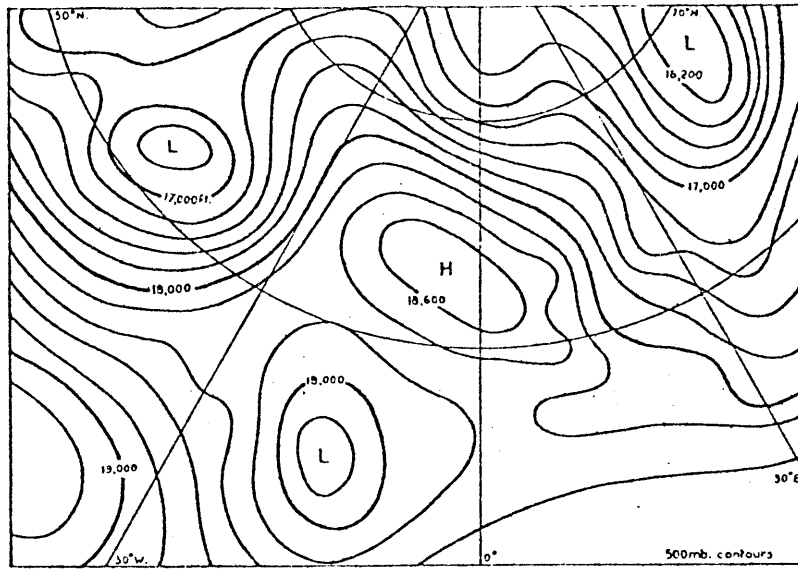


Fig. 2.2a

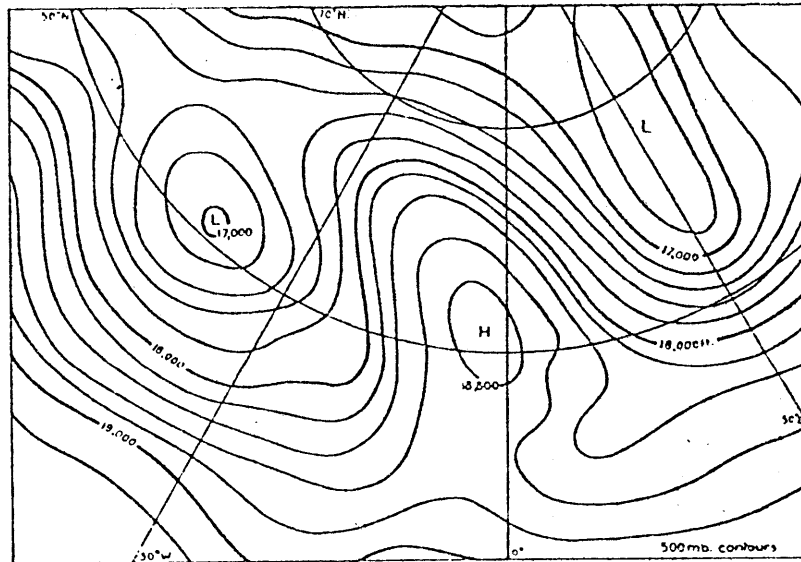


Fig. 2.2b

500 mb height analyses (units: ft.) presenting examples of typical Atlantic blocking patterns.

a) diffluent pattern

b) meridional pattern (from Sumner, 1954).

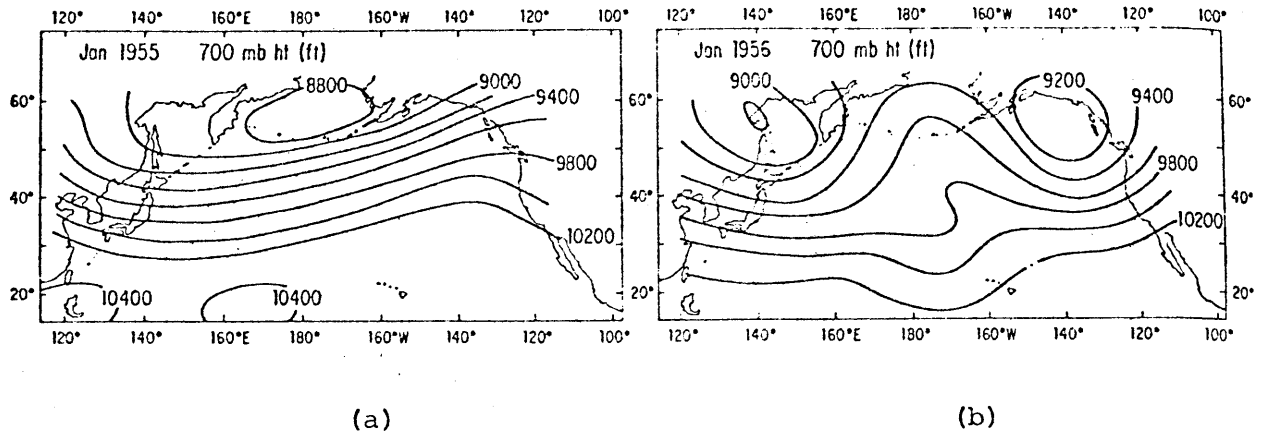


Fig. 2.3

Monthly mean maps of the 700 mb heights (units: ft.) for
a) "normal" wintertime flow pattern (Jan. 1955);
b) a Pacific blocking pattern (Jan. 1966).
(from White and Clark, 1975).

anticyclones to the west of the main ridge. Elliott and Smith (1949) also describe a situation in which a series of mobile anticyclones appears to merge with and to reinforce the quasi-stationary blocking ridge. Rex (1950a), however, finds a trend toward retrogression during the developing stages and progression in the decaying stages of blocking.

4. Budget studies

There have been few diagnostic analyses of blocking conducted up until now. Green (1977) summarizes transient-eddy momentum flux calculations over western Europe for July 1976. From these results, he suggests that transient-eddy vorticity flux divergence occurred in the region of the blocking anticyclone during this period and speculates that this mechanism may have played an important role in maintaining this system. Savijarvi (1977b), however, calculates the time-mean vorticity budget for a case of strong Atlantic blocking and finds no clear evidence that transient eddies act to maintain the block during the period considered.

Hartmann and Ghan (1980) compare vorticity and heat budgets for blocking and transient ridges for both the Atlantic and Pacific oceanic regions. In most respects the local balances for the blocking and transient ridges were similar. In the Pacific the main differences are associated with reduced eastward advection of relative vorticity during blocking due to a decreased zonal flow. In the Atlantic baroclinic mechanisms appear relatively more important for blocking than transient ridges.

5. Summary of observational results

Despite the inconsistencies between studies, several general observations can be made about the nature of blocking activity:

1) There are strongly favored geographical locations for the occurrence of blocking. The studies indicate that eastern portions of oceans in the Northern Hemisphere are particularly favored, and that blocking of extended duration over continents is rare. Atlantic blocking appears to be more prevalent than Pacific blocking.

2) The persistence of blocking varies considerably and may extend for over a month, but the typical duration is about two weeks.

3) There are marked seasonal and annual variations in the incidence of blocking. Since considerable discrepancies exist between studies it is difficult to make firm generalizations. The data suggest, however, that Atlantic-European blocking occurs most frequently in the spring and that Pacific blocking occurs most commonly in winter.

4) Qualitative evidence suggests that there are favored flow patterns associated with blocking.

5) Strongly systematic zonal propagation characteristics are not apparent.

C. Proposed mechanisms

In addition to examining past observational research, it is also useful to examine theories of blocking in order to determine the current outstanding questions. As for the observational studies, different investigators have emphasized various aspects of the phenomenon. Perhaps the earliest theoretical study of blocking is that of Yeh (1949). Yeh considers the energy dispersion characteristics of a

barotropic atmosphere. He suggests that the westward movement of the breakdown in the zonal flow as described by Berggren, et al., (1949) and Namias (1947) can be accounted for by upstream energy dispersion. Yeh finds that an initial solitary disturbance disperses more slowly at high than at low latitudes and speculates that this provides an explanation for the greater persistence of blocking highs in these regions.

The first non-linear model of blocking is that of Rossby (1950). Rossby's model is also of interest as the earliest example of a geophysical flow system in which multiple equilibrium states may exist for a fixed external driving. From observations (Berggren et al., 1949) indicating that blocking is associated with a rapid breakdown in the zonal flow, Rossby (1950) suggests that blocking is a geophysical analogue of a hydraulic jump. He derives a critical zonal speed above which two possible types of flow may occur, one of which bears some similarity to "split" westerly flows.

Thompson (1957) derives a prognostic equation for the zonally-averaged zonal flow in a non-divergent barotropic model. He is able to reproduce the splitting of a westerly flow into two jets in a manner similar to that described by Rex (1950a).

Namias (1964) examines blocking activity over Northern Europe for the period 1958-1960 using 700 mb monthly mean data. He finds that anomalous North Atlantic sea surface temperatures and a deficient snow cover over the Scandanavian peninsula are present during the period of

frequent and persistent blocking. He postulates that blocking results from a positive feedback between the anomalous atmospheric and surface conditions in this region. Namias suggests that anomalous sea-surface temperature gradients lead to altered patterns of cyclogenesis which then encourage the formation of blocking in certain regions, primarily by barotropic processes. According to Namias, the long wave patterns associated with blocking then favor the maintenance of the anomalous sea-surface temperature gradients. Green (1977), and more recently Austin (1980) also propose that transient eddies may be important in maintaining the vorticity anomalies associated with blocking patterns.

White and Clark (1975) investigate blocking over the central North Pacific using monthly mean 700 mb data for the period 1950-1970. They determine that the occurrence of blocking is correlated with anomalies in the sensible heat transfer from the ocean surface and suggest that baroclinic instability induced by sensible heat exchange is the mechanism responsible for blocking development. For theoretical support they apply the results of Haltiner's (1967) analysis of the effects of diabatic heating on baroclinic instability. Haltiner uses a two-layer quasi-geostrophic model on a β -plane and includes sensible heat exchange with a lower boundary having a fixed, prescribed temperature. In this model, for typical values of the vertical wind shear and for the wavelengths of interest (~7000 km) perturbations are stable, but can be destabilized by diabatic heat exchange (parameterized as a Newtonian cooling) with the lower boundary.

Geisler (1977) criticizes the use by White and Clark of Haltiner's model, since Geisler and Garcia (1977) find that in a continuously-

stratified model Newtonian cooling acts to reduce the growth rates at all wavelengths with the greatest reductions occurring at long wavelengths. At wavelengths of around 7000 km and a value of the Newtonian cooling coefficient close to that used by Haltiner (1967), perturbations do not amplify at all. Geisler and Garcia also find that the unstable modes in their model propagate eastward with a phase speed of about 1 ms^{-1} greater than the basic state surface wind, and thus would not remain geographically stationary for a westerly surface flow.

Egger (1978) proposes that blocking develops through the non-linear interactions between forced standing waves and a slowly moving free wave. To test this hypothesis he constructs three simple low order spectral models (truncated at zonal wavenumber 3 and allowing only two meridional modes) on a β -plane:

- 1) the first model is barotropic, includes non-zonal forcing but neglects wave-mean flow interactions;

- 2) the second model is similar to the first but allows wave-mean flow interactions to occur;

- 3) the third model is a two-level quasi-geostrophic model which allows for the effects of baroclinicity. Dissipative effects are neglected in all three models. Steady, stationary forcing is applied in the form of vorticity sources at (zonal wavenumber, meridional wavenumber) (1,1) and (3,1). The initial zonal wind is chosen such that free Rossby wave mode (2,2) will be stationary. In the first model, this free wave is found to amplify non-linearly and persists for about a month. More complicated, but qualitatively similar, behaviors exist in the second and third models. Egger finds that

blocking does not occur when the vorticity sources are suppressed.

More recently, Egger (1979) includes a weak vorticity damping (dissipation time scale ~20 days) and replaces the fixed vorticity sources by orographic forcing for a barotropic atmosphere. He then finds that unless the initial state is very near a blocking configuration, blocking does not subsequently develop.

Egger's studies do not consider the problem of direct external forcing at the wavelength of interest. This problem has recently received increased attention, most extensively by Tung and Lindzen (1979a,b).

The basic question Tung and Lindzen consider is why stationary waves of certain scales are selectively amplified during blocking situations. They propose that this amplification is due to a resonant response of the long waves to forcing by topography and land-sea differential heating.

Tung and Lindzen (1979a) first consider the problem of resonance of a barotropic, non-sheared, time-varying flow on a β -plane. A resonant response is obtained when the zonal flow is varied such that the frequency of a normal mode (Rossby wave in this problem) becomes equal to the frequency of the forcing (which is zero for stationary forcing). In the linear theory, amplification continues until equilibration is achieved between the forcing and damping. Certain scales are favored for resonance since:

a) the resonance wind speed $U = \frac{\beta}{k^2 + \ell^2}$, can only be achieved for certain waves;

b) for the atmosphere, the forcing varies with wavenumber.

For the linear theory, the final amplitude achieved by the damped

"resonant" response is directly proportional to the amplitude of the forcing at that wavenumber.

c) damping mechanisms are also scale dependent; in particular, smaller scales are more severely damped. For reasonable values of the forcing and with damping by Ekman pumping (damping time scale ~ 5 days) wave amplitudes typical of those associated with blocking are achieved within several days. An examination of the off-resonant response shows that the wave amplification is not particularly sensitive to being at exact resonance as long as the period of the free Rossby wave is greater than roughly twice the damping time scale.

Tung and Lindzen (1979b) extend the previous results to the case of an atmosphere in which vertical shear of the mean flow is included. The time behavior is qualitatively similar to that found in the barotropic case. The equilibrium resonant amplitude at the lower boundary is unchanged, although the resonant wave may now possess a non-trivial vertical structure. Wave responses to a number of physically realizable profiles are studied in order to determine the most favorable conditions for resonance. Smaller scale waves (zonal wavenumber $k \geq 3$) can be made resonant rather easily by introducing small changes in the tropospheric wind profile. The behavior of the ultra-long waves ($k = 1-2$) strongly depends on the wind structure of the stratosphere; in particular, a polar night jet maximum at latitudes lower than is typically observed appears favorable for resonance of these waves.

Tung and Lindzen addressed the problem of the initial development of large amplitude flow anomalies. Charney and DeVore (1979) attempt to account for the persistence of these features. They propose that,

owing to non-linearity, a multiplicity of equilibrium states may exist for an atmosphere having zonally asymmetric forcing and fixed external driving, of which more than one of the states may be stable or only weakly unstable. They suggest that blocking is an example of one of the atmosphere's meta-stable equilibrium states.

In order to study this problem, Charney and DeVore examine the properties of a highly-truncated spectral model of a homogeneous β -plane atmosphere. For the case of topographic forcing three equilibrium solutions exist for a certain range of external forcing. Two of the equilibria are stable and correspond to a strong zonal flow having a small wave amplitude and to a weak zonal flow with a large wave amplitude, the latter case resembling some blocking flows. The stable equilibria were subsequently confirmed in grid point model calculations. Multiple stable equilibria were also found in the spectral model when the wave field was instead forced directly (simulating zonally-asymmetric thermal forcing), but were not confirmed in the grid point model calculations.

Charney and Strauss (1980) extend the analysis of Charney and DeVore (1979) to a two-layer quasi-geostrophic baroclinic model forced by topography. Multiple stationary equilibrium states also occur in this model. As in Charney and DeVore (1979), the equilibrium states arise from an orographic instability, but the energy for the growth is now derived from the potential energy, rather than the kinetic energy, of the mean flow.

In addition to the multiple equilibria studies, recent analyses of quasi-stationary waves in simple time dependent models have disclosed

similar pairs of flow states. Reinhold (1981) examines the time-dependent behavior of a model similar to that used by Charney and Strauss (1980), but retains two waves in the zonal direction to simulate the interaction of a baroclinically unstable synoptic-scale wave with a forced planetary-scale wave. For some parameter ranges he identifies pairs of persistent states characterized by nearly opposite phases of the planetary-scale wave.

Kalnay-Rivas and Merkin (1981) conduct time-dependent numerical experiments with a barotropic channel model to study the interactions between traveling disturbances and stationary waves generated by localized topographic forcing. They find that when vorticity perturbations are repeatedly introduced at certain distances upstream of the mountain (simulating, for example, recurrent, localized cyclogenesis), the steady part of the response can, in some cases, dominate the transient behavior, leading to quasi-steady flow configurations. Their results indicate that, depending on the character and location of the forcing relative to the topography, there are two favored quasi-steady flow patterns, corresponding to localized high- and low-index flows.

McWilliams (1980), in contrast, suggests that at least some blocking patterns resemble certain non-linear analytic solutions obtained to the homogeneous, equivalent barotropic model. These special free solutions, which McWilliams calls "equivalent modons", are of permanent form (non-dispersive) and are local (the perturbation is negligible at large distances from the modon center). In their simplest form, equivalent modons occur as vortex pairs, somewhat reminiscent of

the "high-over-low" structures frequently associated with blocking.

We might consider the resonance, equivalent modon, multiple equilibria and allied theories as presenting internal mechanisms for persistent anomalies: that is, the behaviors of interest occur even though external parameters and boundary conditions remain fixed. Changes in internal parameters (e.g., the mean zonal flow) presumably related to flow instabilities govern the character of the solutions. It is useful to consider a recent suggestion by Hoskins (1978) as an example of a theory in which persistent flow anomalies follow changes in external conditions.

Hoskins (1978), after Bjercknes (1966), suggests that over tropical regions anomalously warm sea surface temperature anomalies may lead to enhanced convection. He proposes that increased convective heating will be balanced by adiabatic cooling through upward motions, so that upper-level divergence and therefore forcing of anticyclonic vorticity can be expected over abnormally warm water. To simulate the effects of convective heating in the tropics on the large-scale flow, Hoskins forces the linearized barotropic vorticity equation on a sphere with a prescribed divergence over a region 60° longitude by 30° latitude centered at 15°N . The basic state in this experiment is the winter-mean zonally-averaged 300 mb zonal flow. The steady-state solution gives a stationary wave-train mainly north and east from the source region with largest responses in the height field at middle and high latitudes. The height perturbations in these regions somewhat resemble blocking patterns.

Discussion of proposed mechanisms

There are an almost bewildering variety of proposed mechanisms for blocking. Nevertheless, we may identify certain general characteristics that, at least in principle, help us to classify* the different theories:

- 1) whether or not zonal asymmetries in forcing are fundamental to the theory (i.e., a forced vs. a free response). Most of the theories discussed specify some form of zonally-asymmetric forcing; the most notable exception being the equivalent modon theory (McWilliams, 1980).
- 2) whether the flow anomalies result from changes in external (boundary) conditions or arise by internal processes. Hoskins (1978) presents an example of a theory of the former kind; the multiple-equilibria theories, of which Charney and DeVore (1978) is the prototype, are of the latter kind.
- 3) whether the feature and/or the forcing are local or non-local. Most theories including resonance (including most multiple equilibria theories) are non-local; Hoskins' (1978) theory has a local forcing but a non-local (wave) response; the equivalent modon theory of McWilliams (1980) is local.

*Our objective is to present some general distinctions as a guide to the subsequent investigation, rather than to develop a rigorous or exhaustive classification scheme.

4) whether or not transience (e.g., eddy forcings) plays an essential role in the dynamics (quasi-equilibrium vs. equilibrium models). In the theories of Green (1977) and Austin (1980), transient eddy forcings assume a fundamental role. Reinhold (1981) also finds that eddy forcings are important in determining regime-like behaviors in his model. In contrast, Charney and DeVore (1978) and Hoskins (1978) obtain equilibrium solutions by assuming that all transient terms vanish.

For our purposes, the above distinctions are the most useful, although others may certainly be made (e.g., linear vs. non-linear, barotropic vs. baroclinic, β -plane vs. spherical geometry). The following section discusses implications that the above concepts carry for our research.

D. Discussion

A fundamental objective of this thesis is to generalize blocking research to the analysis of persistent anomalies. In the past, blocking has been defined by a number of different methods. Common to all definitions is a requirement that the flow conform to specified spatial patterns; most frequently, the central feature is considered to be a strong, quasi-stationary ridge or anticyclone. This approach has proved highly useful for isolating certain flow patterns for study; nevertheless, it also has certain limitations:

1) Differences between the selection criteria in the various studies have frequently been motivated by subjective impressions concerning the importance of particular features. It is unclear to what extent these differences account for discrepancies among the results.

2) The long-term mean has not been removed from the data prior to defining cases. We therefore have an a priori basis for anticipating that most persistent, strong ridges or highs will show a geographic bias toward the climatological-mean ridge positions.

3) The past emphasis on ridges or highs has never been adequately justified and is perhaps misleading. Synoptic case studies often reveal a persistent large-scale flow pattern without providing an obvious indication on how to identify a single "key" feature.

We address these issues in Chapter III as follows:

1) by generalizing the method used to define cases and then testing the sensitivity of the results to changes in the selection criteria.

2) by determining the geographic distributions using data from which the long-term mean has been removed and then comparing the results with similar calculations that include the long-term mean.

3) by providing detailed comparisons between the characteristics of persistent positive anomalies and persistent negative anomalies.

Investigators have frequently remarked that qualitatively similar large scale flow patterns seem to recur in different blocking situations. Nevertheless, the evidence presented is not entirely

satisfying; since we expect some similarity to be forced by the restrictive definitions adopted in these studies. There have been few qualitative results, so interpretations are based primarily on subjective impressions concerning the relative importance of particular features. In Chapter IV we identify typical structures of persistent anomalies. An important question addressed is whether subjective impressions of blocking "patterns" can be associated with a particular feature (or features) which are objectively derived from observational data.

We have indicated that there is little concrete information on the temporal behavior of persistent anomalies. In chapter V we consider the question of how persistent anomalies evolve in time, placing particular attention on identifying typical time scales and isolating systematic propagation characteristics. Major extensions beyond previous research are analyses of the meridional propagation characteristics and the evolution of vertical structures during development.

Up until now, the relationship between mean flows and transient eddies during persistent anomaly periods has been the subject of considerable speculation but little quantitative analysis. We take up this problem in Chapter VI, first by examining the association between persistent anomalies and storm paths and second by evaluating relative contributions of transient-eddy and time-mean contributions to local balances of heat, vorticity and potential vorticity.

The results of the analyses in chapters III - VI provide some basis for addressing the theoretical issues previously raised. Indications of whether persistent anomalies are mainly forced or free

are provided by analyses of geographic variability (chapter III), spatial scales (chap IV) and propagation characteristics (chap V). Indications of the relative importance of external and internal processes are primarily provided by various temporal characteristics, some of which are examined in chapters III and IV and are more extensively studied in chapter V. Questions of localness are addressed through analyses of structure (chapter IV) and evolution (chapter V). The issue of the relative contributions by transient eddy and time-mean terms is the main focus of chapter VI. Chapter VII summarizes the results and discusses the theoretical implications of our study.

III. GEOGRAPHIC DISTRIBUTION

A. Introduction

We now consider the question of whether persistent anomalies preferentially occur in specific geographic regions. Following a brief description of the data set, we outline our method for defining persistent anomaly cases. We then present the results of the geographic distribution calculations.

B. Data Set

Data are derived from the National Meteorological Center (NMC)* final analyses of the Northern Hemisphere 500 mb heights. The data set consists of twice-daily analyses (00Z and 12Z) for the 14 consecutive 90-day winter seasons from December 1, 1963 - February 28, 1964 to December 1, 1976 - February 28, 1977. Data were spatially interpolated by a 16-point Bessel scheme (Jenne, 1970) from the NMC octagonal grid to a 5 degree latitude by 5 degree longitude grid over the region from 20N to 90N. Missing or obviously incorrect analyses were replaced with linearly-interpolated data. Less than one per cent of the 500 mb height analyses required replacement.

C. Procedure

We first propose a generalized definition and three alternative measures of "anomaly." We then describe our method for selecting cases.

1. Anomaly: definition and measures

Meteorologists conventionally define "anomaly" as the deviation of the value of an atmospheric variable x from its local long term mean:

* The NMC data set is discussed in Appendix 1.

$$x'(\lambda, \theta, p, t) = x(\lambda, \theta, p, t) - \bar{x}(\lambda, \theta, p, t) \quad (3.1)$$

where θ is the latitude, λ the longitude, p the pressure and t the time. The long term mean \bar{x} is in general a function of both position and time of year. We will find it helpful to instead consider a generalized definition of anomaly as

$$x' = s(x - \hat{x}) \quad (3.2)$$

where the scaling factor s and the reference value \hat{x} may be functions of both space and time. Applying this generalized definition, we now specify the three alternative measures of anomaly used in this study.

a. Zonal height anomalies (ZHA)

The zonal height anomaly z^* is defined as

$$z^* = \frac{\sin \theta_r}{\sin \theta} (z - [z]) \quad (3.3)$$

where the zonal-average height $[z]$ is defined by

$$[z] = \frac{1}{2\pi} \int_0^{2\pi} z \, d\lambda \quad (3.4)$$

The reference latitude $\theta_r = 45^\circ$ in all calculations.

The $(\sin \theta)^{-1}$ scaling factor is motivated by a recent study on atmospheric energy dispersion (Hoskins, Simmons and Andrews, 1977)

showing that height field analyses provide a poor indication of the meridional component of energy propagation. This shortcoming is due to the latitudinal variation of the Coriolis parameter, which biases height field responses toward high latitudes. Hoskins, et al. suggest that quantities like streamfunction or vorticity provide better indicators of horizontal energy propagation. Note that this normalization is similar to that used in obtaining a geostrophic streamfunction from height data.

Of the three anomaly measures, the ZHA correspond most closely to the magnitude criteria adopted in most observational studies of blocking. Recall that in these investigations, climatological deviations from zonality are retained in the data. Since these deviations are often considerable, a regional bias may be anticipated in the results.

b. Temporal height anomalies (THA)

The temporal height anomaly z' is defined as

$$z' = \frac{\sin \theta_r}{\sin \theta} (z - \bar{z}) \quad (3.5)$$

The climatological-mean value \bar{z} is determined as the local seasonal trend value. The seasonal trend time series at a point is obtained by a least-squares quadratic fit to the 14-winter mean time series for that point (e.g., the first value of the winter mean time series is the average of the 14 December 1, 00Z values, the second value is the average of the December 1, 12Z values, etc.).

Of the three measures, this measure, as a scaled version of eq. (3.1), is most closely identified with the traditional definition of an anomaly as the difference between observed and climatological-mean values. In contrast to ZHA's, there is no a priori reason for anticipating that high numbers of THA's will be associated with climatological-mean ridge or trough locations. There is, however, some basis for expecting that large THA's are more likely in regions characterized by high temporal variance.

c. Standardized height anomalies (SHA)

The standardized height anomaly z'_s is defined by

$$z'_s = \frac{(z - \bar{z})}{\sigma} \quad (3.6)$$

where \bar{z} is obtained as for the THA's and the local standard deviation σ is determined for the seasonally-detrended data.

SHA's can be considered as THA's scaled for regional variations in the height variance. Geographic variations in numbers of SHA's having certain values can occur if there are substantial regional differences in the shapes of the anomaly distributions (e.g., Gaussian vs. significantly non-Gaussian).

So far, we have refrained from stating our preference for one anomaly measure over the others. As suggested above, each of the measures provides some distinct information on the behavior of the height fields. In this and later chapters, however, we will focus primarily on persistent THA's. Our motivation for preferring THA's to ZHA's is, as we shall show, that the latter primarily

reflect the climatological-mean height structure. The long-term mean structure has been studied observationally (e.g., Blackmon, 1976) and theoretically (e.g., Charney and Eliassen, 1949; Smagorinsky, 1953) and, although related to our problem, is not our primary interest here. We prefer THA's over SHA's since, through the geostrophic relation, fields of the former provide a much better indication of associated wind and vorticity anomalies, and therefore are more amenable to direct physical interpretation.

2. Method for defining cases

Our definition of a persistent anomaly is simple and intuitive: a persistent anomaly is defined at a point if the anomaly at that point exceeds a threshold value for a sufficient duration. The method, illustrated in Fig. 3.1, is as follows:

- 1) Specify a "magnitude" criterion, M , and a duration criterion, T , where for positive anomaly cases $M \geq 0$ and for negative anomaly cases $M \leq 0$.
- 2) Define the occurrence of a persistent positive (negative) anomaly case at a particular grid point satisfying selection criteria (M, T) if the anomaly at that point remains equal to or greater (less) than M for at least T days.
- 3) Define the duration, D , for a positive (negative) case as the time from which the anomaly first becomes greater (less) than M to the time when the anomaly next becomes less (greater) than M at that point.

Note that these criteria act as lower bounds, so that all events which meet or exceed the threshold values are counted as persistent anomaly cases satisfying the specified criteria.

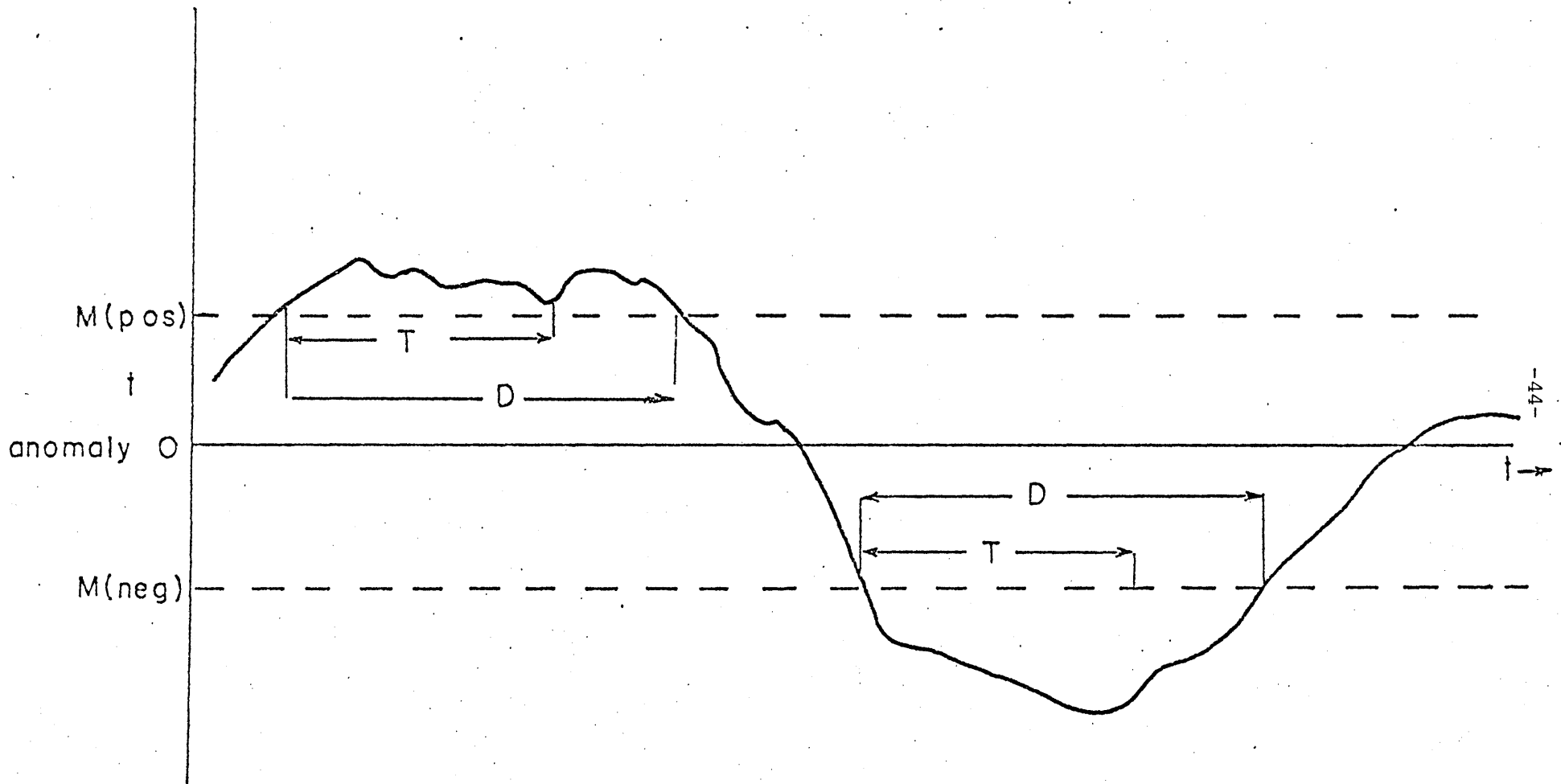


Fig. 3.1. Method for defining cases. See text for explanation.

The number of persistent anomaly cases occurring over the 14 winter seasons were determined for each point on the 5 degree latitude by 5 degree longitude grid for the following values of selection criteria:

1) ZHA:

$$M = \pm 0 \text{ m}, \pm 50 \text{ m}, \dots, \pm 250 \text{ m}$$

$$T = 5 \text{ days}, 10 \text{ days}, \dots, 25 \text{ days}$$

2) THA:

$$M = \pm 0 \text{ m}, \pm 50 \text{ m}, \dots, 250 \text{ m}$$

$$T = 5 \text{ days}, 10 \text{ days}, \dots, 25 \text{ days}$$

3) SHA:

$$M = \pm 0, \pm 0.2, \dots, \pm 1.0$$

$$T = 5 \text{ days}, 10 \text{ days}, \dots, 25 \text{ days}$$

D. Geographic Distributions

The definitions and criteria given previously provide the basis for performing the geographic distribution calculations. In describing the results, we place emphasis on features which are insensitive to changes in or show systematic variations over the values of the selection criteria. For display purposes, the results have been lightly post-smoothed by applying a nine-point spatial filter.

This filter effectively removes fluctuations having wavelengths of less than ~1500 km but does not otherwise affect the general character of the spatial variability.*

1. Zonal height anomalies

The zonal height anomalies have similar geographic distributions over a broad range of values of the selection criteria. Consequently, the basic results will be illustrated with one set of representative values.

Fig. 3.2a displays the number of positive anomaly cases satisfying (+100 m, 10 days). Major regions having maxima in the number of cases are centered over the eastern North Pacific (EPAC) and eastern North Atlantic (EATL), with slightly larger maxima occurring in the latter area. Fig. 3.2b shows the corresponding distribution for the negative anomaly cases satisfying (-100 m, 10 days) and Fig. 3.2c the sum of the numbers of positive and negative cases. Comparing these maps, we see that for ZHA's, regions having high numbers of positive anomaly cases and regions having high numbers of negative anomaly cases are almost mutually exclusive. Regions with the highest occurrence of negative anomalies are centered over the western North Pacific (WPAC) near Japan and to the north of Hudson Bay (HBAY). The maximum number of cases in WPAC exceeds that of HBAY by a ratio of over two to one and also exceeds the corresponding EPAC and EATL positive anomaly maxima. The relative dominance of the WPAC maximum over all other regional

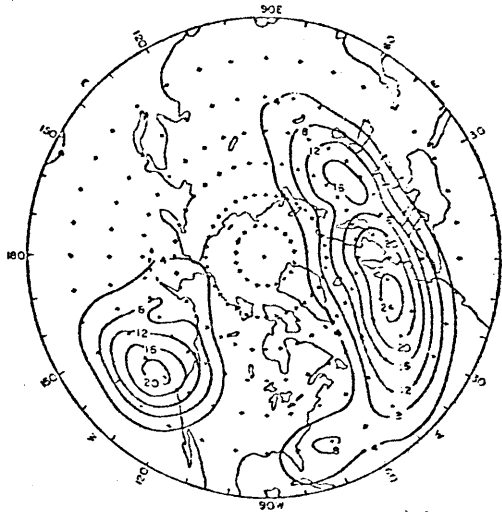
* Shapiro (1970) provides a detailed description of the response characteristics of the 9 point filter.

maxima is reproduced throughout the range of selection criteria and is especially evident at higher values of the magnitude and duration criteria. By this anomaly measure, then, the strongest and most persistent anomalies are the negative anomalies over the western North Pacific, rather than the positive anomalies which frequent the eastern North Atlantic and eastern North Pacific.

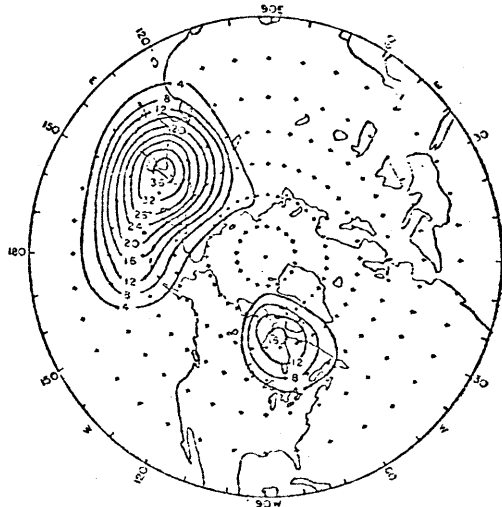
To a great extent, the regional patterns of the ZHA distributions reflect the structure of the climatological-mean 500 mb height field. Fig. 3.3a presents the 14-winter season average 500 mb heights and Fig. 3.3b displays the departure of the time-average heights from their zonal-average values. By comparing these figures to the corresponding maps for the ZHA distributions (Figs. 3.2a-c), we see that the majority of persistent positive ZHA's are associated with climatological-mean ridges, while most persistent negative ZHA's occur near the climatological-mean troughs.

The ZHA's have a considerably weaker relation to the distribution of the standard deviations of the 500 mb heights (Fig. 3.3c), indicating that regions of persistent large ZHA's are not necessarily regions of large (temporal) variance. The areas of maximum variance over the oceans lie roughly halfway between the major upstream troughs and downstream ridges, with the Atlantic variance maxima slightly nearer the mean ridge position. The third maxima over the northern Soviet Union appears near a weak mean trough downstream from the major Atlantic mean ridge. Note, however, that the regions between upstream ridges and downstream troughs over central North America and east-central Asia are characterized by relatively small variance.

(a)



(b)



(c)

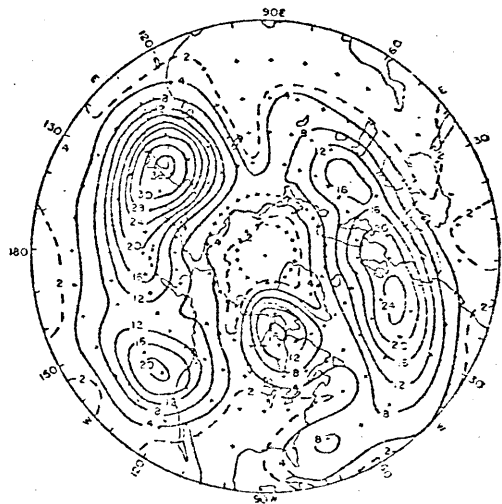
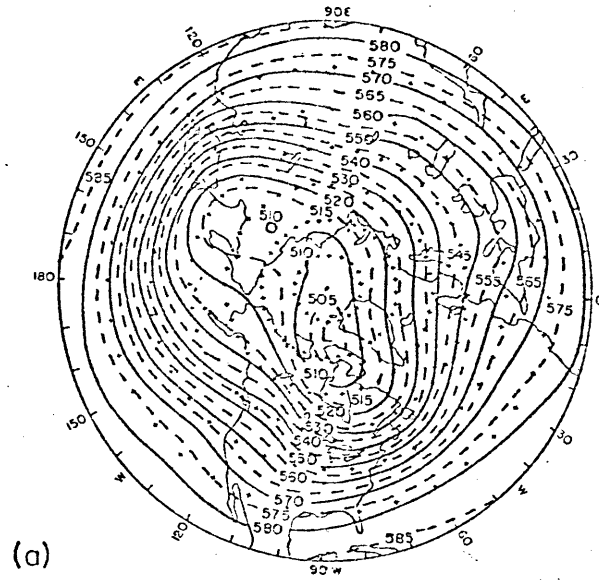
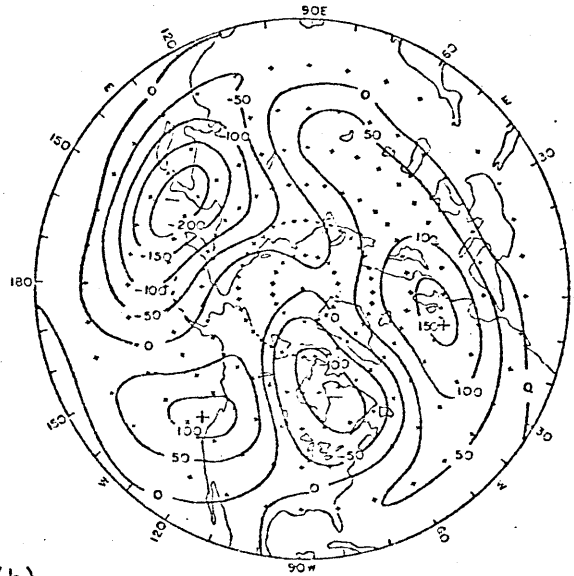


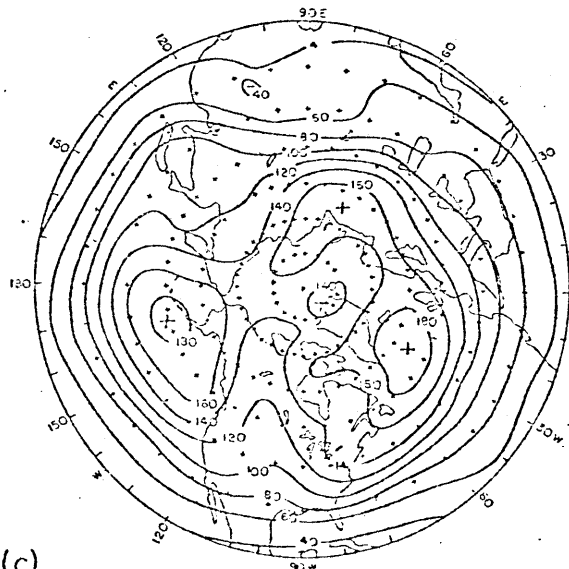
Fig. 3.2. Zonal height anomaly (ZHA) geographic distributions for (a) positive anomaly cases (100m, 10 days); (b) negative cases (-100m, 10 days); and (c) the sum of the cases in (a) and (b).



(a)



(b)



(c)

Fig. 3.3. Geographic distributions of (a) the climatological mean 500 mb heights (units: dam); (b) departure of climatological mean heights from their zonal average values (units:m); and (c) standard deviation of the 500 mb heights (units:m).

2. Temporal height anomalies

Fig. 3.4 presents the results of typical geographic distribution calculations for

- a) positive anomaly cases (100m, 10 days),
- b) negative anomaly cases (-100m, 10 days), and
- c) the corresponding "sum" distribution, obtained by adding the numbers of cases from the two previous distributions.

The three distributions shown are determined from data that have been lightly low-pass* filtered to remove brief (-1-2 day) interruptions by mobile transient disturbances. The total numbers of cases are increased by about 50 percent over the unfiltered values, but the regional characteristics are otherwise almost unchanged. We see that:

- 1) There are three primary regions for the occurrence of persistent THA: the North Pacific to the south of the Aleutians (PAC), the North Atlantic to the southeast of Greenland (ATL) and from the northern Soviet Union northeastward into the Arctic Ocean (NSU).

- 2) For each region the maximum in the frequency of occurrence of positive anomalies is approximately co-located with, and has a comparable magnitude to, the corresponding maxima of negative anomalies.

- 3) There is considerable latitudinal variability in the number of cases, despite the anomaly normalization, with maxima occurring near 50N for ATL and PAC regions and near 60N for NSU.

- 4) The range in the number of cases is substantial: the three major regions each have in excess of twenty cases over the 14 winter season, while parts of Asia, the subtropics and central North

*

The 17 point filter has a 10% response at periods of about 3 days, 50% at 5.5 days and 90% response at around 13 days.

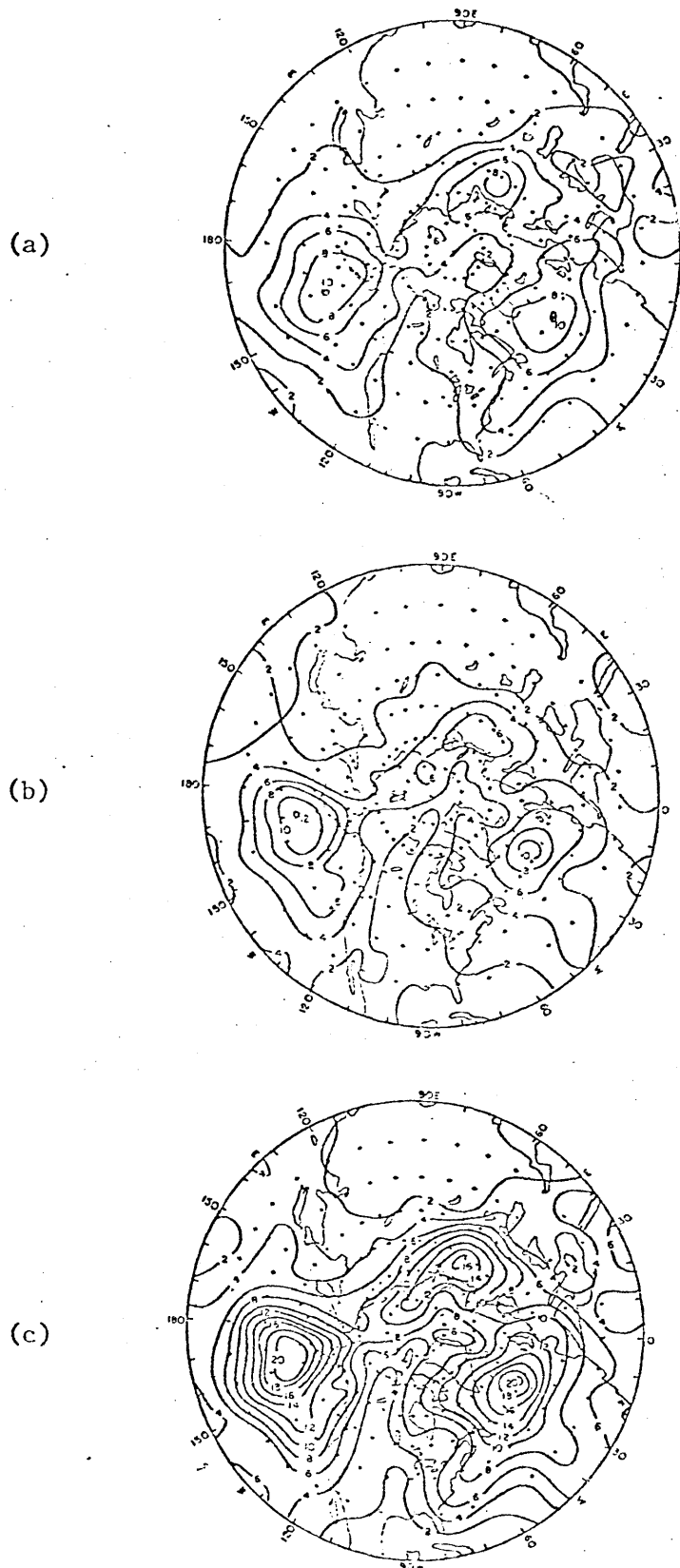


Fig. 3.4. Temporal height anomaly distributions for (a) positive anomaly cases (100m, 10 days); (b) negative anomaly cases (-100m, 10 days); and (c) the sum of the cases in (a) and (b).

America have less than two events satisfying these criteria over the period. Qualitatively similar distributions are obtained if the raw anomalies are defined as departures from the seasonal (rather than long-term) means, although the magnitudes of the maxima are slightly reduced (5%-25%). For relatively large magnitudes and short durations, ATL and PAC maxima exceed the maximum values over NSU, while for relatively small magnitudes and long durations the maxima are comparable.

Whereas the ZHA distributions primarily mirror the structure of the climatological-mean 500 mb height field, the THA distributions are closely related to the pattern of variance of the 500 mb heights (cf Fig. 3.3c). The PAC, ATL and NSU regions identified as having high numbers of major persistent anomaly cases correspond with the three major centers of large variance. This relationship is not surprising, since persistent anomalies can be expected to provide major contributions to the low-frequency variance (periods beyond 10 days) and, as Blackmon (1976) demonstrates, the height variance is dominated by low-frequency components.

Fig. 3.5 further illustrates regional variations in persistence. The numbers of events $y(n)$ exceeding the threshold criteria (M) for n or more consecutive days are shown on a semi-logarithmic diagram for:

- a) positive events (50m), for regions having high numbers of persistent anomalies, obtained by averaging the

distributions* of the three major persistent anomaly regions;

- b) negative events (-50m) for regions having high numbers of persistent anomalies, obtained similarly to a); and, for comparison:
- c) positive events (50m) for a region with relatively few persistent anomalies, centered over North America, and
- d) negative events (-50m) for the same region.

We notice that:

1) For durations beyond about 3 days, there are more cases in the persistent anomaly (PA) regions than in the non-persistent anomaly (NPA) regions. The ratio of the number of events in the two regions, $y(n)_{PA} / y(n)_{NPA}$, increases with increasing n .

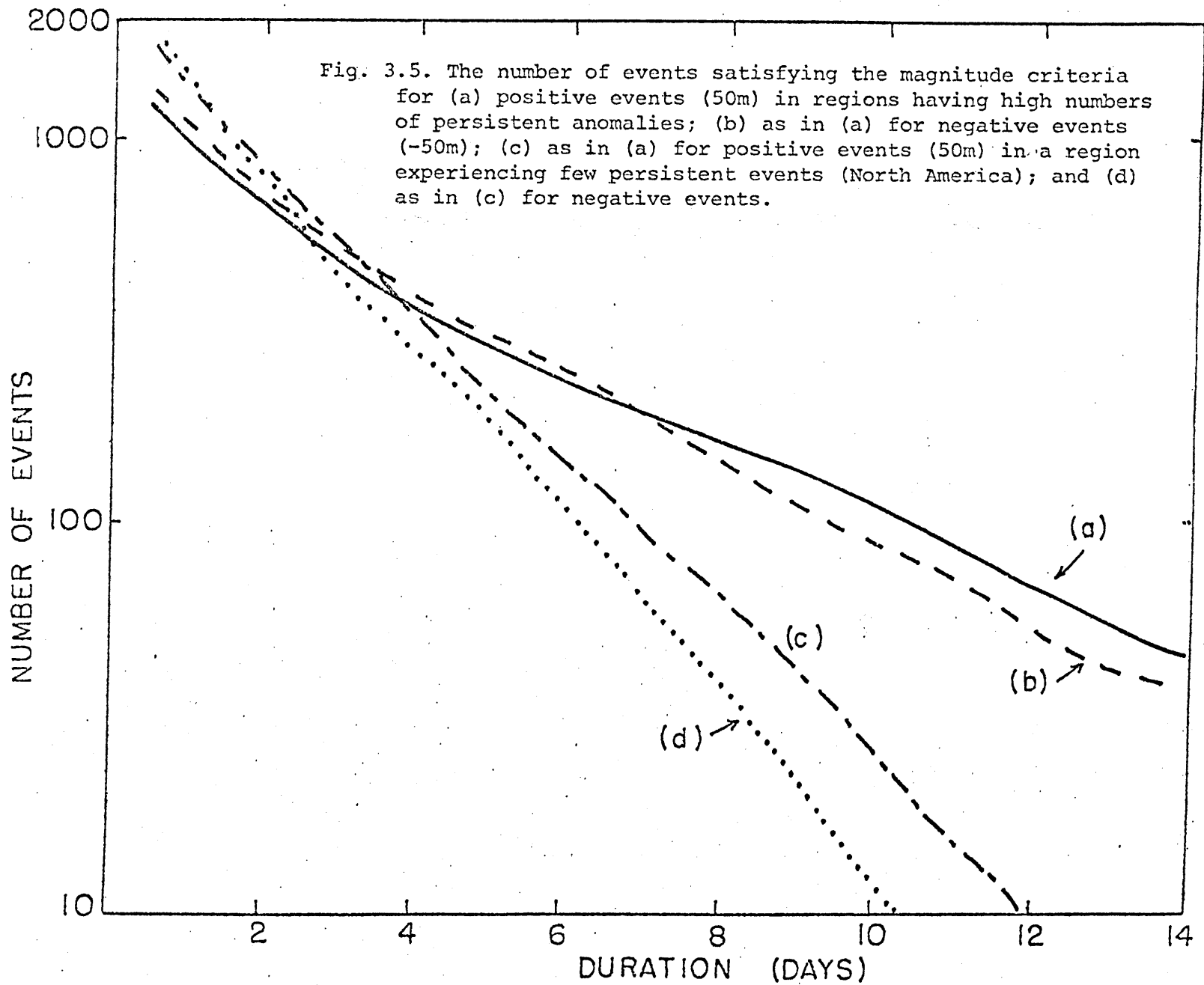
2) The distributions for the NPA region form nearly straight lines, whereas the slopes for the PA distributions vary as a function of duration.

Since the conditional probability that an event which has lasted n days will last at least $n+1$ days is given by

$$P(n+1 | n) = y(n+1)/y(n) , \quad (3.7)$$

a linear relationship in this display indicates that the persistence probability P is independent of the duration n ;

* The distribution for a region is determined by combining the distributions obtained at each of 9 points in a 10° latitude by 20° longitude box centered at a point within the region. The combined distributions are qualitatively similar to, and have smaller sampling errors than, the corresponding distributions at individual points.



conversely, if the relationship is non-linear, the persistence probability varies with the duration. Estimates of anomaly "half-lives" (the time required for half of the anomaly events to be terminated) can be obtained from this figure: for NPA, the half-life is about 1.5 days; for PA, the half-lives vary from about 1.5 days at very short durations to around 3.5 days after about $n=6$ days, with slightly more positive than negative cases at long durations. Although the shift in time scales appears small, the consequences are highly significant: for durations of about 10 days or longer, roughly an order of magnitude more events are observed than would be predicted by assuming a single distribution following the rapid decay rate.

The relatively constant slopes of the PA curves beyond about 5 days suggests that for longer durations $y(n)$ can be approximated by

$$y_s(n) = c_s e^{-n/\tau_s} \quad \text{for } 5 \leq n \leq 14 \text{ days} \quad (3.8)$$

where c_s and τ_s are constants associated with a slow decay process. These constants have been estimated by applying a non-linear least squares fit to the points between $n=6$ days and $n=14$ days. For durations of less than 6 days, residuals were calculated as the difference between the observed values and the estimated values for the slow decay process. The residuals

decayed rapidly and also nearly exponentially. This suggests an empirical model for $y(n)$ of the form

$$y(n) = c_s e^{-n/\tau_s} + c_f e^{-n/\tau_f}, 0.5 \text{ days} \leq n \leq 14 \text{ days} \quad (3.9)$$

where c_s, τ_s and c_f, τ_f are constants associated with the slow and fast decay processes, respectively. The values of the constants are $c_s = 2323, c_f = 2500, \tau_s = 5.1 \text{ days}, \tau_f = 1.1 \text{ days}$ for the positive cases, and $c_s = 3234, c_f = 2153, \tau_s = 4.0 \text{ days}, \tau_f = 0.3 \text{ days}$ for the negative cases. Corresponding values of explained variance are over 99 percent for both the positive and negative cases. The NA curves, in contrast, are dominated by a single decay process with a time constant of about 2 days.

The cumulative distributions in the PA regions can thus effectively be described as a sum of two simple decay processes whose time scales lie on either side of the comparable time scale for a region experiencing few persistent anomalies. Since the constants c_f and c_s have roughly the same values, at very short durations the numbers of events contributed by the "fast" and "slow" populations are about equal. In contrast, durations beyond about 5 days can be attributed almost entirely to the slow decay population. Comparison of the time constants also suggests that the positive events are typically slightly more persistent.

Many of the qualitative characteristics of these distributions are insensitive to variations in the magnitude criterion. This is illustrated in fig. 3.6, which presents results of similar calculations for the PA regions for values of M ranging between 0 and +200m for the positive cases and 0 and -200m for the negative cases. The tendency for relatively steeper slopes at short durations and shallower nearly constant slopes at longer durations is apparent throughout this range of criteria, although at large magnitudes the changes in slopes are relatively smaller. Values for the slow decay time constant range from about 2 days for $M = -200m$ to over 6 days for $M = +0m$. Negative anomalies typically display fewer events at long durations, particularly for large values of M .

For given magnitude and duration criteria, mean event durations can easily be obtained from fig. 3.6. For intermediate values of $M(50-100m)$ and durations of 10 days or longer, mean durations are around 14-15 days. Perhaps not coincidentally, this is close to the mean duration of blocking determined by Rex (1950b) using a similar 10-day minimum duration criterion.

Do distributions of anomaly values from the three regions display multiple modes, perhaps suggesting several preferred states? Fig. 3.7 displays histograms of anomaly values obtained from the 14 winter seasons of twice daily data for selected points from the three regions. Compared with normal distributions, these distributions are more rectangular, with fewer values near the mean and in the tails. This characteristic appears broadly typical of distributions throughout the key regions (cf. White, 1980). White (1980) calcu-

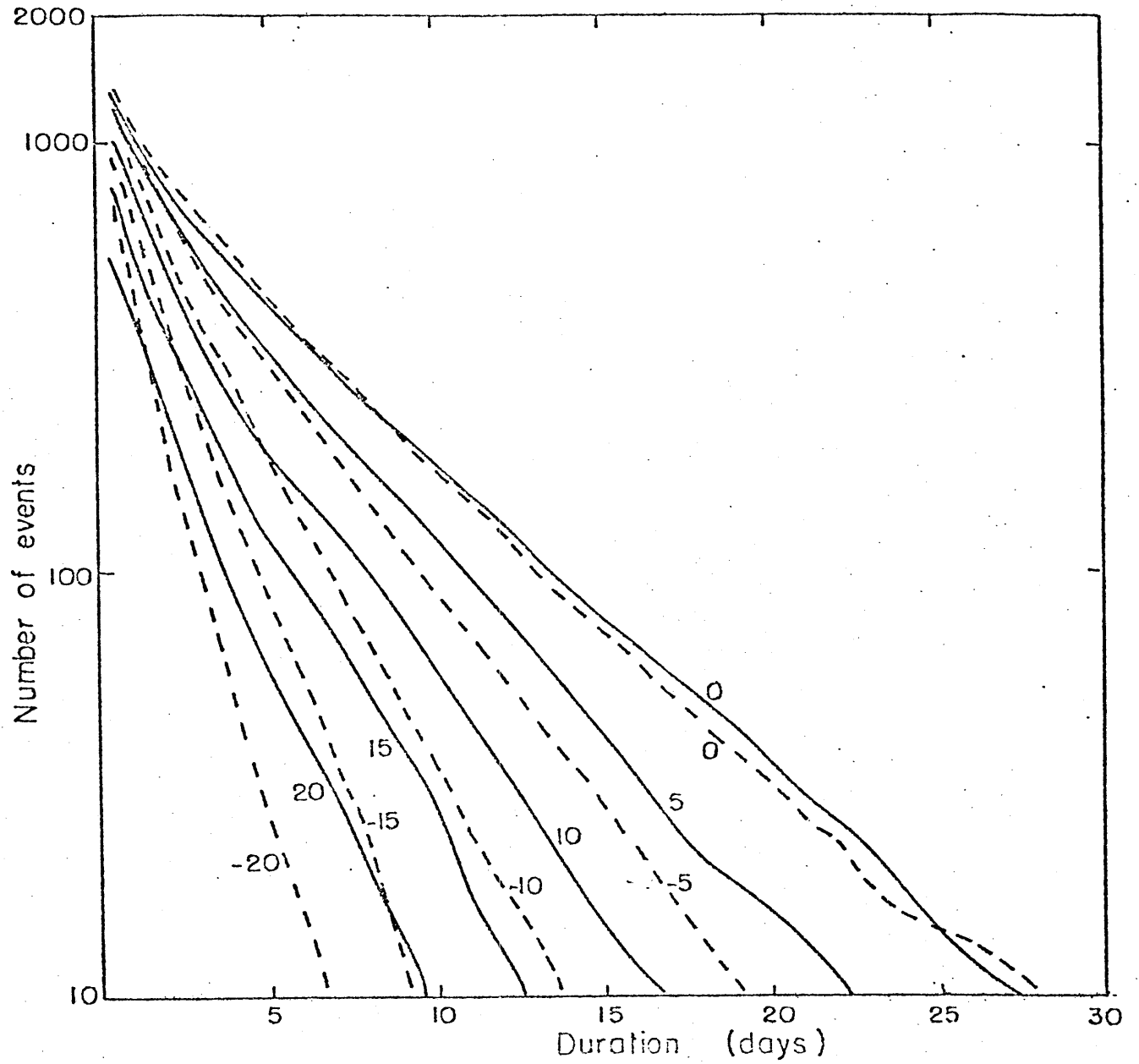


Fig. 3.6. As in Fig. 3.5. for the persistent anomaly regions for values of M ranging between 0m and 200m for the positive cases and 0m and -200m for the negative cases. Solid lines are for positive cases; dashed lines are for negative cases.

lates geographical distributions of the skewness and kurtosis (related to the third and fourth statistical moments, respectively) of the wintertime 500 mb heights. The skewness roughly measures the asymmetry and the kurtosis the "flatness" or peakedness of a distribution. Very crudely, strongly peaked distributions have high kurtosis and distributions with relatively few events near the mean have low kurtosis. For reasonable estimates of the number of degrees of freedom, White's analyses suggest that in all three regions the distributions are nearly symmetric but may have values of kurtosis significantly lower than the value for a normal distribution.

White has considered whether distributions with these characteristics might result from the superposition of two normal distributions with different means. He has argued that if one regime of a bimodal distribution consists of "blocking" and the other regime consists of a more "normal" state, then since blocking occurs much less than half of the time (according to Rex, 1950b), the resulting distributions should be much more asymmetric than are observed. Our results, however, suggest that the use of Rex's statistics together with the assumption of a "normal" state, may be misleading. We find that, for corresponding criteria, persistent positive anomalies and persistent negative anomalies occur about equally frequently. Thus, if we associate blocking with persistent positive anomalies (as White apparently does), then our results suggest there is another phenomenon corresponding with the persistent negative anomalies which is about as common. Accordingly, our analyses would lead us to expect that the distributions would be nearly symmetric, as the observations indicate.

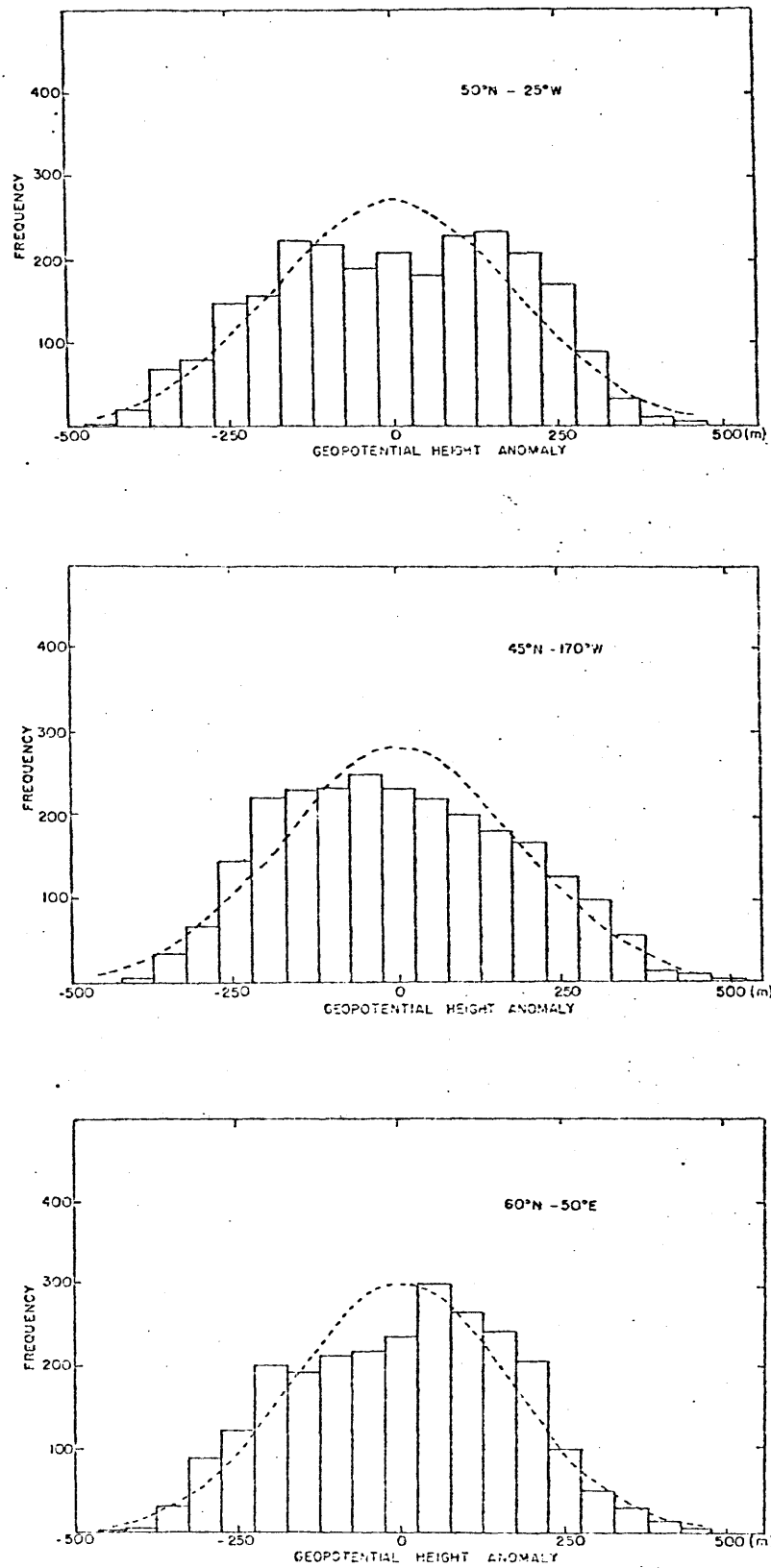


Fig. 3.7. Histograms of anomaly values for the 14 winter seasons of twice-daily data at (a) $50^{\circ}\text{N } 25^{\circ}\text{W}$; (b) $45^{\circ}\text{N } 170^{\circ}\text{W}$; and (c) $60^{\circ}\text{N } 50^{\circ}\text{E}$. Corresponding normal distributions having the same mean and variance are drawn in dashed lines.

3. Standardized height anomalies

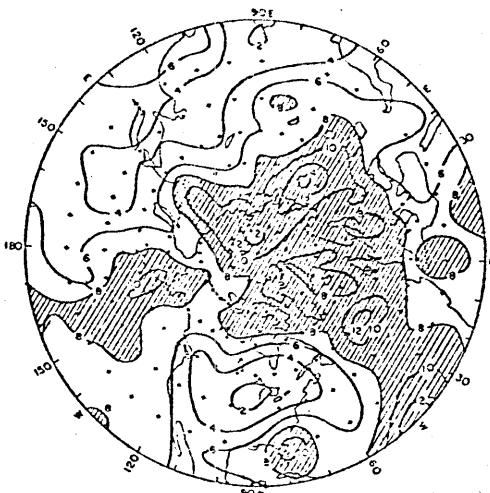
Fig. 3.8 presents geographical distributions for positive cases (0.4, 10 days), negative cases (-0.4, 10 days), and the corresponding sum of positive and negative cases, representative of intermediate values of magnitudes and durations. The most striking characteristics of these distributions are the large number of cases over polar latitudes, the relative minimum in cases at mid-latitudes and the secondary maxima over the subtropical central North Pacific and subtropical central North Atlantic. Compared with the ZHA and THA distributions, the SHA distributions display little zonal variability. Major mid-latitude maxima appear as southward extensions from the polar maximum to over the PAC, ATL and NSU regions previously described as having high numbers of THA's.

We can gain some understanding of the SHA distributions by examining the relative contributions of different frequency bands to the total height variance. Following a procedure similar to Blackmon (1976), we partition the 14 winter seasons of detrended anomaly data into frequency domains by application of two filters*:

- 1) a low-pass filter, retaining periods of greater than 10 days, and
- 2) a band-pass filter, retaining periods between about 2.5 and 6 days.

* Detailed characteristics of the filters are described by Blackmon (1976).

(a)



(b)



(c)

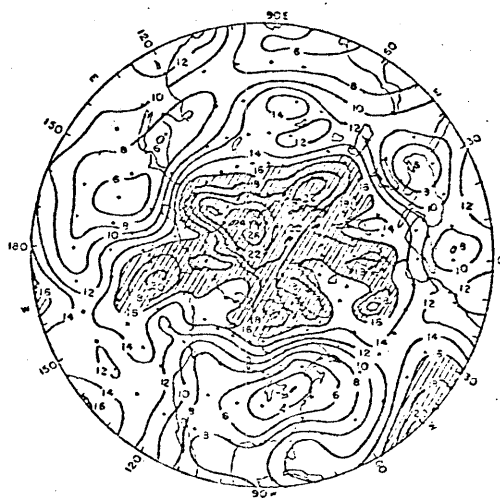


Fig. 3.8. Standardized height anomaly distributions for: (a) positive anomaly cases (0.4, 10 days); (b) negative anomaly cases (-0.4, 10 days); and (c) the sum of the cases in (a) and (b). Values above 8 are hatched in (a) and (b); values above 16 are hatched in (c).

Fig. 3.9a presents the root-mean-square (rms) heights for the low-pass filtered data. We see that the mid-latitude SHA maxima appear somewhat related to the regions of relatively large low-frequency variance. A more direct relation is indicated in the distribution of the rms heights for the band-pass data (Fig. 3.9b), which displays zonally elongated mid-latitude maxima extending from the eastern continents across the oceans in approximate conformance with the major storm paths (Sawyer, 1970; Blackmon, 1976; Blackmon, et. al., 1977). In contrast to the low-pass maxima, the regions of relatively large band-pass variance over the eastern continent -- western ocean regions correspond with relative minima in the SHA distributions; note however, that the SHA minima over the central and eastern oceans are displaced somewhat southward of the maxima in band-pass variance. We will see in the following chapter that these minima correspond more closely to nodal lines in the dominant spatial patterns of low-frequency variability. Similarly, the relative maxima over the central subtropical oceans appear to be related to secondary centers in these patterns while the PAC, ATL and NSU regions are associated with the primary centers.

The above relations suggest that regions with large numbers of SHA's are characterized by a relative predominance of low frequency fluctuations. Indeed, the SHA distributions somewhat resemble distributions for the characteristic time intervals between statistically-independent values of sea-level pressures (Madden, 1976) and 500 mb heights (Stefanick, 1981), with regions having high numbers of SHA's associated with relatively long characteristic time scales.

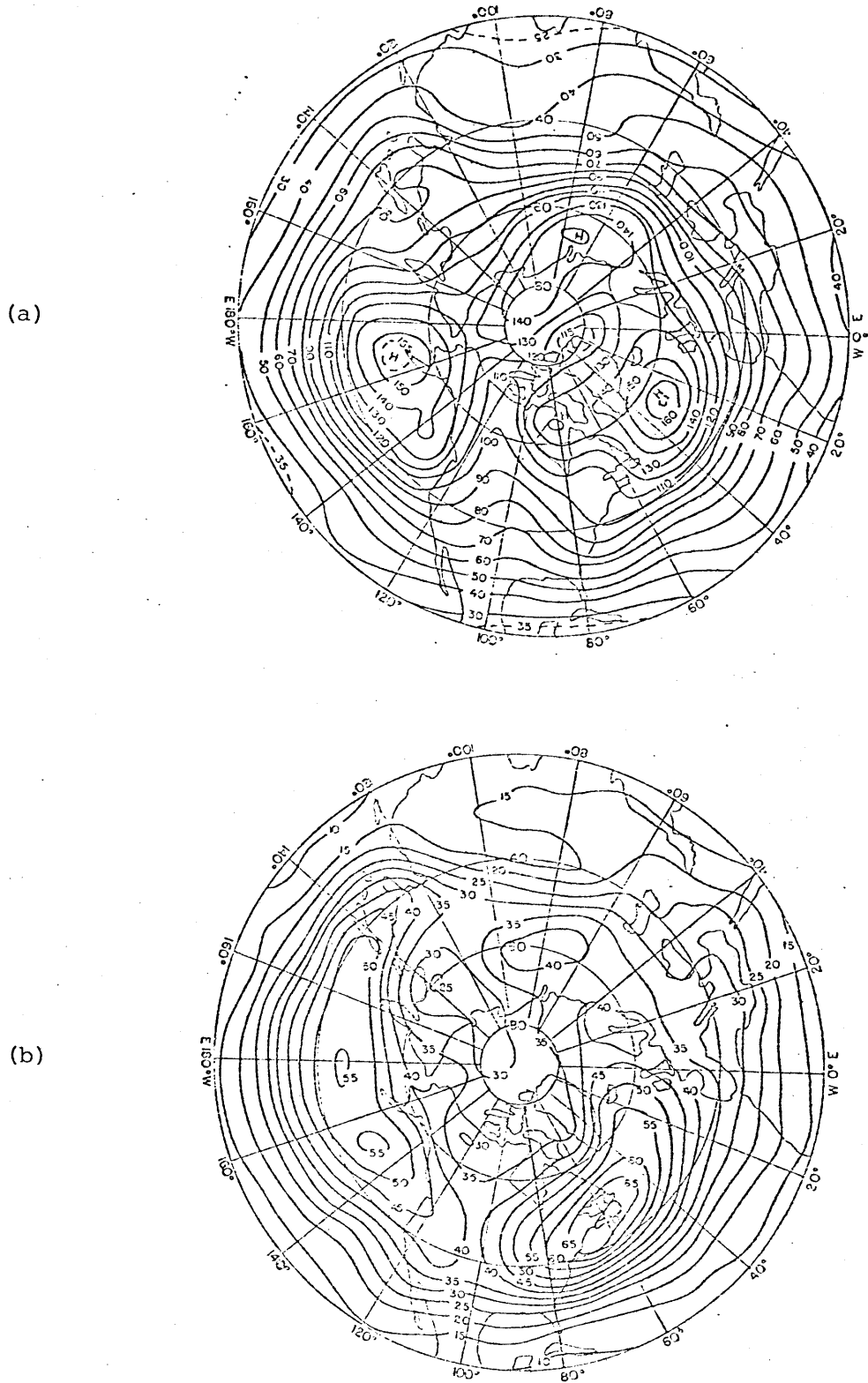


Fig. 3.9. Geographic distribution of (a) rms heights for the low-pass filtered data; and (b) rms heights for the band-pass filtered data.

E. Discussion

The main points to emerge from the previous analyses are:

For the zonal height anomalies (ZHA's),

- 1) Regions having high numbers of positive anomaly cases and regions having high numbers of negative anomaly cases are almost mutually exclusive.
- 2) The strongest and most persistent ZHA's are the negative anomalies over the western North Pacific, rather than the positive anomalies which frequent the eastern North Atlantic and eastern North Pacific.
- 3) The regional patterns of the ZHA distributions strongly reflect the structure of the climatological-mean height fields: the majority of persistent positive ZHA's are associated with climatological-mean ridges, while most persistent negative ZHA's occur near the climatological-mean troughs.

For the temporal height anomalies (THA's):

- 1) There are three primary areas of high occurrence: the North Pacific to the south of the Aleutians (PAC), the North Atlantic to the southeast of Greenland (ATL) and from the northern Soviet Union northeastward into the Arctic Ocean (NSU).
- 2) For each region, the maxima in the frequency of occurrence of positive anomalies is approximately co-located with the comparable maxima of negative anomalies.
- 3) For corresponding magnitude criteria, the numbers of positive and negative cases in each region are about the same, with slightly more positive cases at long durations.

- 4) The THA distributions are closely related to the pattern of variance of the 500 mb heights, with the PAC, ATL and NSU regions characterized by large temporal variance.
- 5) In persistent anomaly (PA) regions, the probability that an event which has lasted n days will last at least $n+1$ days increases up to about $n=5$ days and is thereafter nearly constant. For values of M around 50m - 100m and durations of 10 days or longer, roughly an order of magnitude more events are observed than would be predicted by assuming a single distribution following the initial rapid decay rate.
- 6) Distributions of anomaly values for points within these regions are nearly symmetric but have fewer values near the means and in the wings than corresponding normal distributions.

For the SHA distributions:

- 1) There are a large number of cases over polar latitudes, a relative minimum in cases at mid-latitudes and secondary maxima located over the subtropical central North Pacific and subtropical central North Atlantic.
- 2) The mean mid-latitude maxima appear as southward extensions from the polar maxima over the PAC, ATL and NSU regions.
- 3) The SHA distributions are somewhat similar to distributions for the characteristic time interval between statistically independent values of sea-level pressure (Madden, 1976) and 500 mb heights (Stefanick, 1981), with regions having high numbers of SHA's associated with relatively long characteristic time scales.

The results obtained here show several areas of broad agreement with the results described in blocking studies, but also some important differences. The locations of the PAC and ATL maxima in the frequency of occurrence of persistent positive THA are in approximate conformance with the locations of frequent blocking described by Rex (1950b), Sumner (1954) and White and Clark (1975). Not described in these studies are the roughly equal numbers of persistent negative anomalies that occur in these regions, nor the third area of frequent persistent anomalies centered over the northern Soviet Union. Also, Rex (1950b) finds that Atlantic blocking exceeds Pacific blocking by a factor of two to one, whereas our results suggest that persistent positive anomalies occur about equally frequently in the two regions.

Our results do not suggest a preferred duration for persistent anomalies, nor indicate any strong periodicities. Rather, for sufficiently long durations, the number of events decays exponentially with increasing durations. This is similar to distributions obtained for a first order autoregressive process (Parzen, 1962), suggesting that many of the persistent anomalies may arise from fluctuations, sometimes called "climate noise" (Leith, 1973), that are generally assumed to be unpredictable on long time scales. Nevertheless, there is some indication in our analyses, also supported by the results of others (Madden, 1976; Stefanick, 1981), that features in the PAC, ATL and NSU regions may decay somewhat more slowly than in other regions. Our results suggest that in the three persistent anomaly regions, anomalies persisting beyond about 5 days are almost entirely associated with this slow decay process.

Our results raise certain questions. We have observed that the geographical distribution of persistent THA is closely related to that of the variance. Recall, however, that the THA and variance maxima are not co-located with the storm paths but rather appear somewhat downstream of the main cyclogenesis regions. What determines the THA (and variance) distributions? Are they primarily a manifestation of slowly moving large amplitude baroclinic waves or are other, more subtle processes involved? In later chapters we will address this question observationally by identifying the typical characteristics of persistent anomalous features in these regions. We also noted an association between the SHA distributions and distributions of characteristic atmospheric time scales (Madden, 1976; Stefanick, 1981). In mid-latitudes there appears to be some relationship between these distributions and the locations of the storm tracks, suggesting the importance of flow instabilities in determining characteristic decorrelation times. Nevertheless, certain regions, such as the central North Pacific, appear to be characterized both by vigorous and highly transient storm activity and by relatively long characteristic time scales. What, then, determines the relatively great persistence of features occurring in these regions?

F. Conclusion

The results indicate that there are preferred regions for the occurrence of persistent anomalies. The regional characteristics of the distributions vary little for moderate changes in the values of the selection criteria, but vary substantially if different anomaly measures (e.g., ZHA, THA or SHA) are used. For the THA, there are

three major favored regions for persistence: the north-central North Pacific, the eastern North Atlantic and the northern Soviet Union. For each region, the maximum in the frequency of occurrence of positive anomalies is approximately co-located with, and has comparable values to, the corresponding maxima of negative anomalies. For durations beyond about a week, there are slightly more positive than negative anomaly cases. At long durations, the number of cases decreases exponentially for increasing durations, consistent with the distributions obtained from a first-order autoregressive process.

Our results help to sharpen the definition of persistent anomalies, but also raise further questions. In later chapters we address some of these questions by providing detailed analyses of persistent anomalies occurring within the three key regions.

IV. STRUCTURE

A. Introduction

We noted earlier that in previous investigations blocking was associated with the recurrence of certain flow patterns. Some qualitative similarity between patterns, however, appears to have been forced by the restrictive definitions adopted in those studies. The objective of this chapter is to identify typical structures of persistent anomalies. An important question to be addressed is whether subjective impressions of blocking "patterns" can be associated with a particular feature (or features) which are objectively derived from observational data.

We first provide a detailed analysis of the horizontal structure at one level (500 mb), and then examine characteristics of the full three-dimensional structure. Following this, we discuss our results in relation to several recent theories of long-lived phenomena.

B. Horizontal Structure

The data base for this portion of the study is the same as that used in Chapter III. As in Chapter III, the data were interpolated onto a 5 degree latitude-longitude grid prior to performing calculations. The following analyses focus on latitude-normalized time height-anomalies (THA's), which for brevity will be called "anomalies" in the remainder of this section. In the following discussion, we will emphasize results based on the selection criteria (+100m, 10 days). Our previous results indicate that this choice for the duration criterion ensures that the anomalies persisted beyond the periods typically associated with synoptic-scale variability. The choice of

magnitude thresholds of $\pm 100\text{m}$ ensures that the anomaly magnitudes are large relative to the noise level (e.g., observation and analysis errors). As a sensitivity check, several of the following calculations were also performed using other key points and different values for the selection criteria. The results of these calculations were substantially the same as the results to be described for the ($\pm 100\text{m}$, 10 days) criteria.

The results of the previous chapter indicate that there are three regions characterized by high numbers of persistent anomalies: the North Pacific to the south of the Aleutians (PAC), the North Atlantic to the west of the British Isles (ATL), and the northwest Soviet Union (NSU). Consequently, a large percentage of the Northern Hemisphere wintertime persistent anomaly cases can be studied by selecting cases from these regions. For each of these regions, the maximum in the frequency of occurrence of positive anomalies is approximately collocated with the comparable maximum of negative anomalies. As a first step toward selecting independent cases, we identify the point in each region having the greatest total (sum of positive and negative) number of cases (the "key" point). For this set of criteria the three key points are:

- 1). ATL, 50N 20W (ATL)
(9 positive cases, 6 negative cases);
- 2). PAC region, 50N, 165W (PAC)
(7 positive cases, 7 negative cases);
- 3). NSU region, 60N, 50E (NSU)
(8 positive cases, 6 negative cases).

The case dates and durations are listed in Appendix 2.

In the following discussion, cases defined at points within one of these regions are so identified by name (for example, a PAC positive anomaly case).

Composite or "grand mean" persistent anomaly maps were formed by first constructing time mean maps for each of the cases defined at the key points, then averaging the case means, taking each case as one realization. Grand means obtained by weighting the case means by the case durations and then averaging gave results nearly identical to those described below.

Figs. 4.1a and 4.1b show, respectively, composite anomaly maps for the PAC positive anomaly cases and PAC negative anomaly cases. Comparing these maps, we see that, in addition to the anomaly at the key point, there is a larger scale pattern evident which, to a first approximation, appears with opposite polarity in the two maps. The overall impression of this pattern is of a dominant center near the key point, a center of opposite sign located about 25 degrees of latitude to the south of the dominant center and a train of anomaly centers of alternating signs and decreasing magnitudes extending mostly downstream from the main center. The greatest discrepancies between the positive and negative patterns are the somewhat smaller zonal scales and more northward position of the positive pattern centers relative to the corresponding features of the negative pattern.

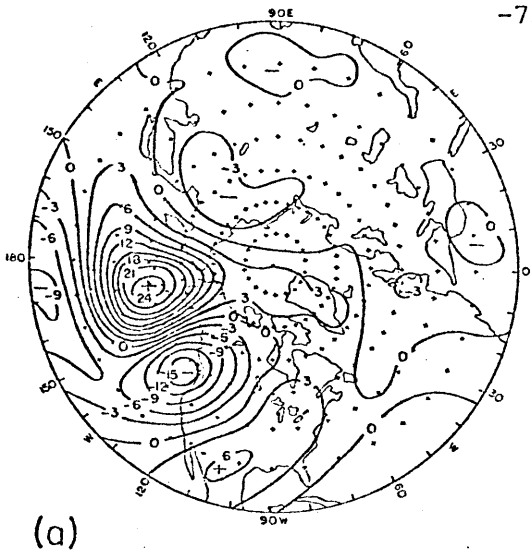
The statistical significances of the differences between means (null hypothesis of equal means), obtained by a two-sided t-test, are displayed in Fig. 4.1c. The principal centers of the pattern are associated with statistically significant differences at or above

the 99% confidence level.

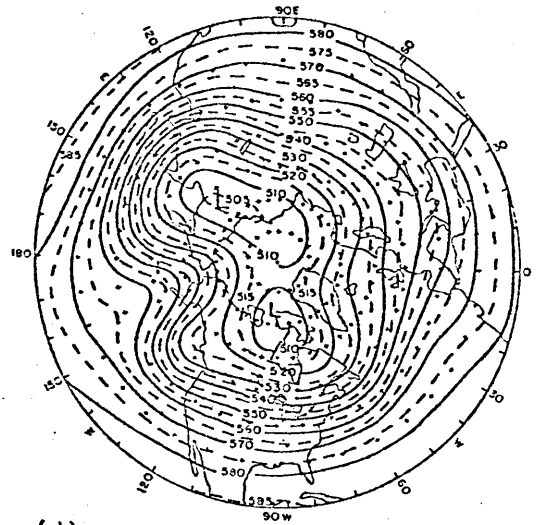
Figs. 4.1d and 4.1e present the corresponding composite of the heights for the positive and negative cases, respectively. The positive map displays a flow configuration typical of the central North Pacific blocking patterns described by White and Clark (1975). The principal features of the negative map are an intensified westerly flow across the central North Pacific, an amplified ridge along the west coast of North America and an enhanced trough in the East. It is interesting that the contrasting flows over the Pacific, which are often described as the two extreme stages of the index cycle (Namias, 1950), appear in the present analyses as opposite phases of a single basic anomaly pattern.

Similar analyses for the ATL cases and for the NSU cases are shown in Figs. 4.2 and 4.3, respectively. The pattern similarities between the ATL positive and negative anomaly maps are especially evident over the eastern North Atlantic, Europe and the Northern Soviet Union; the most striking discrepancies are in the relative intensity of the centers near the Aleutians. The ATL positive cases are typically associated with a strongly enhanced ridge over the eastern North Atlantic with a branch of westerlies far to the south. This flow configuration is reminiscent of the Atlantic blocking patterns described in the classical studies by Rex (1950a,b). The corresponding negative anomaly cases are associated with a single, intense westerly jet over the North Atlantic. The NSU pattern is somewhat less extensive, with the dominant center over the western Soviet Union straddled by weak centers of opposite sign located

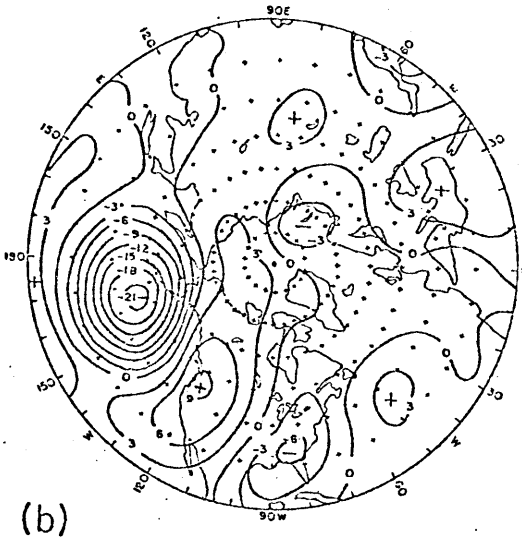
Fig. 4.1. (a) Composite anomaly maps (units:dam) for 7 PAC positive cases; (b) as in (a) for 7 PAC negative cases; (c) confidence levels for a two-sided t-test estimating the significance of the difference in means (a) - (b). Dashed at 95% confidence level, solid at 99% level; sign is the sign of the difference (a) - (b); (d) composite 500 mb heights (units:dam) for the positive cases; and (e) as in (d) for the negative cases.



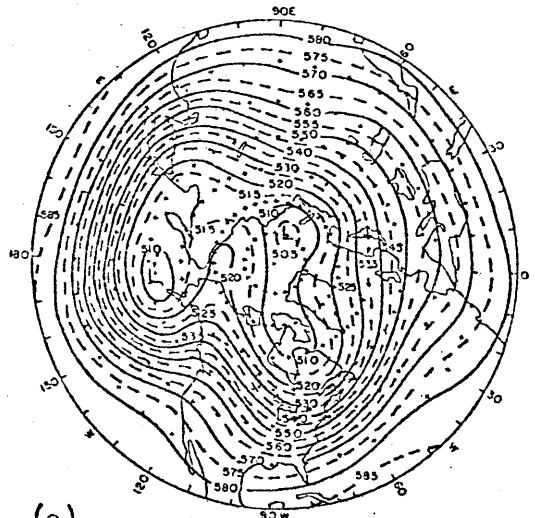
(a)



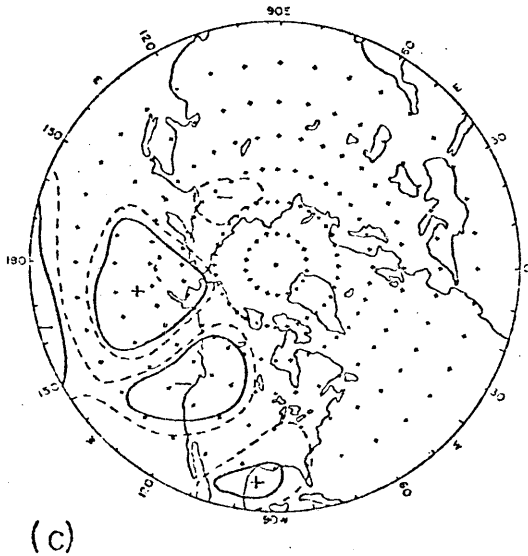
(d)



(b)



(e)



(c)

Fig. 4.1

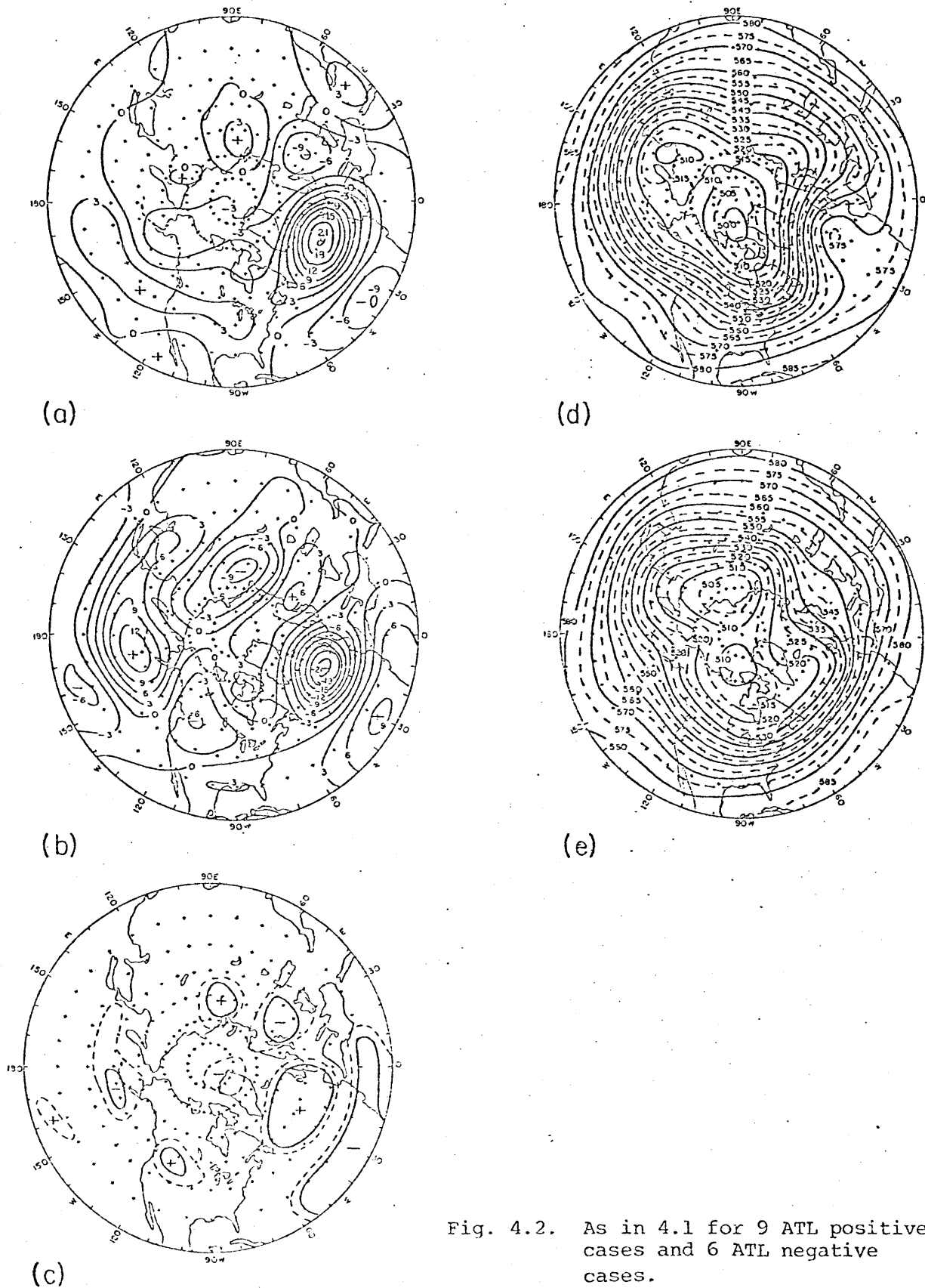
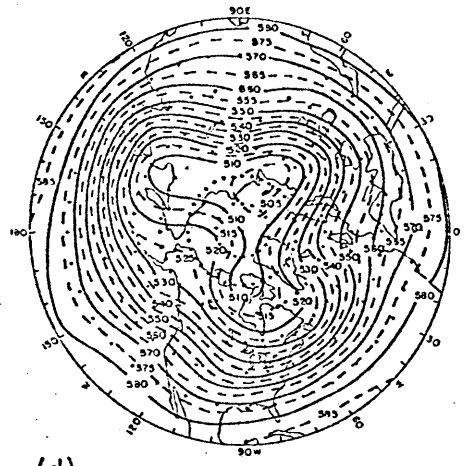


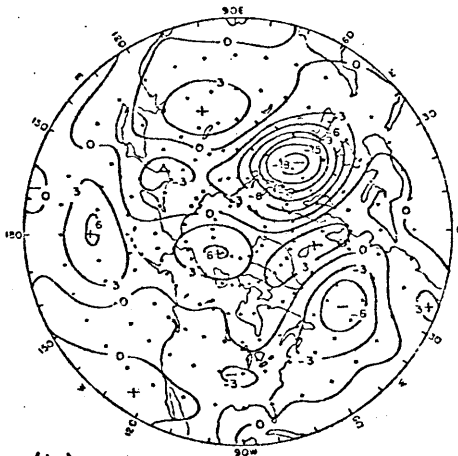
Fig. 4.2. As in 4.1 for 9 ATL positive cases and 6 ATL negative cases.



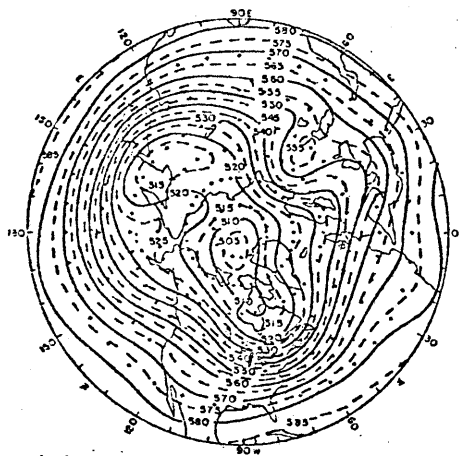
(a)



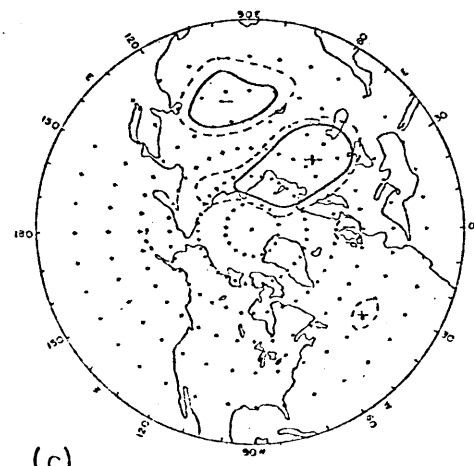
(d)



(b)



(e)



(c)

Fig. 4.3. As in 4.1 for 8 NSU positive cases and 6 NSU negative cases.

upstream near the British Isles and downstream over Northern China. The NSU positive cases display a blocking ridge and split westerly flow over the western Soviet Union. The corresponding negative cases show a deep trough over the key region.

For all three regions, then, persistent positive anomalies are associated with blocking ridges. Examination of individual case means for the PAC negative cases also frequently discloses a blocking ridge along the west coast. The PAC and ATL negative cases resemble regional high-index flows. For the PAC and ATL regions, high- and low-index zonal flows appear as opposite phases of the same basic anomaly pattern.

Concurrently with our study, Wallace and Gutzler (1981) have examined temporal correlation patterns between Northern Hemisphere gridpoints using 15 winters of monthly mean 500 mb NMC analyses. Two of the outstanding correlation patterns that they describe, the Pacific-North American (PNA) pattern and the Eastern Atlantic (EA) pattern, closely resemble our PAC and ATL patterns. As Wallace and Gutzler point out, these patterns qualitatively resemble solutions obtained in simple linear models for forced stationary waves on a sphere (Hoskins, et. al., 1977; Grose and Hoskins, 1979; Hoskins and Karoly, 1981). Wallace and Gutzler also note that the PAC pattern appears in other studies on teleconnections (e.g., Martin, 1953; O'Connor 1969; Dickson and Namias, 1976).

It is interesting that although Wallace and Gutzler use selection and data analysis procedures substantially different from ours, the

points that they choose for constructing the PNA and EA teleconnection maps (45N 165W and 50N 25W, respectively) are remarkably close to our key points. Empirical orthogonal function (EOF) analysis* reveals why both procedures lead to the same key regions.

An EOF analysis of the case mean patterns for a region enables us to extract the single spatial pattern that best describes the patterns of both the positive and negative anomaly cases. An EOF analysis of low-pass filtered data (periods beyond 10 days**) defines the dominant regional pattern of low-frequency variability. Fig. 4.4 displays for each of the three regions the principal EOF patterns calculated from the case data alone and the principal EOF patterns calculated from the 14 winter seasons of low-pass filtered data. Examination of the low-pass analyses reveals that the points selected by Wallace and Gutzler and ourselves correspond to the main centers of the dominant regional patterns of low-frequency variability. The principal EOF patterns calculated from the case data alone and the corresponding principal EOF patterns calculated from the 14 winter seasons of low-pass filtered data are virtually identical. This suggests that the cases we selected are predominantly enhancements of the primary regional pattern of low-frequency variability. Nevertheless, comparison of the explained variance and cumulative explained variance for the case and low-pass EOF's (Table 4.1) indicates that other patterns are also often important in describing the low frequency behavior of anomalies in this region.

* Lorenz (1956) and Davis (1976) thoroughly discuss the theory and methods of EOF analysis. A brief summary of this method is provided in Appendix 3.

** The low-pass filter described by Blackmon (1976).

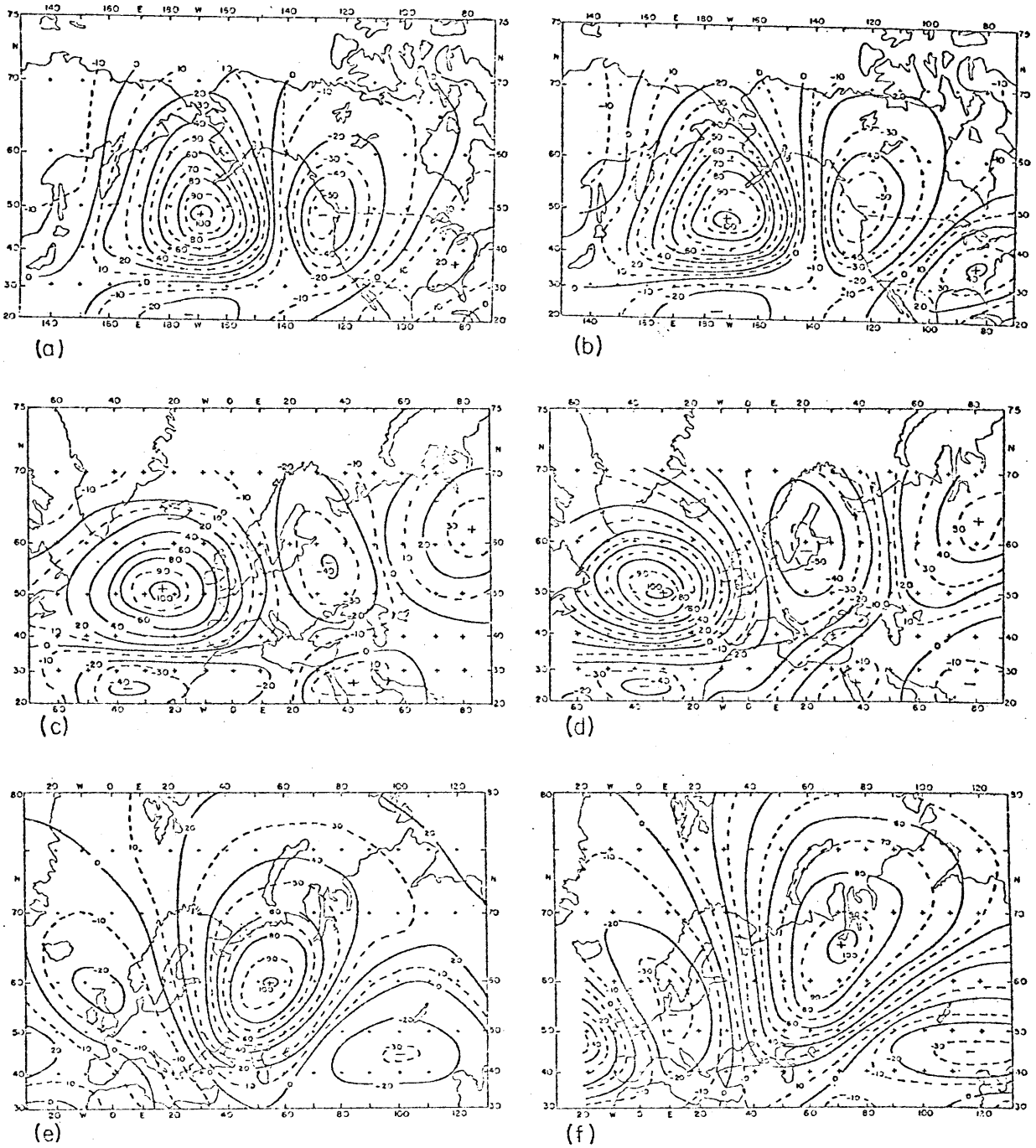


Fig. 4.4. (a) The first EOF of the PAC persistent anomaly cases; (b) the corresponding first EOF of the low-pass filtered anomaly data; (c) as in (a) for the ATL cases; (d) as in (b) for the ATL region; (e) as in (a) for the NSU cases; and (f) as in (b) for the NSU region.

Table 4.1
Explained Variance by
Case and Low-Pass EOF's
by Region

PAC

<u>EOF</u>	<u>CASE</u>		<u>LOW-PASS</u>	
	<u>EX VAR</u>	<u>CUM EX VAR</u>	<u>EX VAR</u>	<u>CUM EX VAR</u>
1	.54	.54	.21	.21
2	.14	.68	.15	.36
3	.07	.75	.12	.48
4	.06	.81	.09	.57
5	.04	.85	.07	.64
6	.03	.88	.06	.70
7	.02	.90	.05	.75
8	.01	.91	.04	.79
9	.01	.92	.03	.82
10	.01	.93	.02	.84

ATL

1	.48	.48	.19	.19
2	.16	.64	.15	.34
3	.11	.75	.13	.47
4	.06	.81	.11	.58
5	.04	.85	.07	.65
6	.04	.89	.05	.70
7	.03	.92	.04	.74
8	.02	.94	.04	.78
9	.02	.96	.03	.81
10	.01	.97	.03	.84

NSU

1	.44	.44	.20	.20
2	.22	.66	.13	.33
3	.10	.76	.12	.45
4	.07	.83	.09	.54
5	.05	.88	.07	.61
6	.04	.92	.07	.68
7	.03	.95	.05	.73
8	.02	.97	.04	.77
9	.01	.98	.03	.80
10	.01	.99	.03	.83

In evaluating predictability experiments, Hollingsworth et al., (1980) have determined that anomaly correlations of .60 or greater between observed and predicted fields correspond quite well with independent subjective evaluations of useful predictability. By analogy, we will call two patterns "useful analogues" if their spatial correlations are at or above .60. Table 4.2 presents the spatial correlations between each of the case means and the corresponding dominant case EOF. We see that over 75% of the spatial correlations have magnitudes greater than .60. These results clearly demonstrate that the dominant patterns are not simply manifestations of single, particularly intense events, but rather reflect the recurrence of certain preferred anomaly patterns in these regions.

An indication of the direction of meridional energy propagation can be obtained from the horizontal phase structures of the patterns. Dickinson (1980), among others, has noted that for Rossby waves, the phase shifts westward in the direction of energy propagation. In order to examine the phase structures in more detail, the 500 mb grand mean height anomaly fields were decomposed into zonal Fourier components. Expansions were performed over the zonal wavenumber band $k = 0 - 8$ between 20 N and the pole. The expansion for $z(\lambda, \theta)$ at longitude λ and latitude θ is expressed as

$$z(\lambda, \theta) = a_0 + \sum_{k=1}^m a_k \cos [k(\lambda - \Phi) - \phi_k] \quad (4.1)$$

where $a_k(\theta)$ is the amplitude and $\phi_k(\theta)$ the phase of the k^{th}

Table 4.2
Spatial Correlations Between
Case Mean Anomaly Patterns
and Case EOF 1 by Region

<u>Region</u>	<u>Case Number</u>	<u>Pos. Case Correlation</u>	<u>Neg. Case Correlation</u>
PAC	1	.85	-.76
	2	.93	-.57
	3	.71	-.48
	4	.71	-.75
	5	.61	-.88
	6	.63	-.64
	7	.78	-.82
ATL	1	.87	-.65
	2	.74	-.72
	3	.68	-.57
	4	.69	-.67
	5	.73	-.55
	6	.41	-.84
	7	.67	----
	8	.68	----
	9	.84	----
NSU	1	.72	-.78
	2	.85	-.57
	3	.81	-.64
	4	.64	-.53
	5	.77	-.73
	6	.58	-.47
	7	.54	----
	8	.29	----

Fourier component at latitude θ in a coordinate system having longitude ϕ as the origin. The reference longitude ϕ was chosen as the longitude of the key point used in selecting cases; e.g., 20 W for the ATL cases, 165 W for the PAC cases and 50 E for the NSU cases.

Fig. 4.5 presents vector plots of the amplitudes and phases of wavenumbers $k = 0 - 8$ of the anomaly fields and of the climatological-mean height field between 20 N and 80 N. Inspection of these figures reveals that, for each pattern, several Fourier harmonics are required to account for the composite structure. Also evident are near or complete phase reversals when comparing positive to negative anomaly patterns for each region. In addition, phase reversals generally occur between the latitudes of the anomaly maxima and latitudes about 20 to 30 degrees further south. We see that most of the major components have no, or small westward, phase changes between 60 N and 30 N, suggesting that the net meridional propagations at these latitudes are, if anything, predominantly southward. The phase relationships between the anomaly components and the corresponding climatological mean components for the PAC patterns are somewhat reminiscent of the responses seen in simple models when crossing through a resonance.

We can gain some insight into the temporal variability of the patterns by analyzing characteristics of the associated EOF time coefficients* generated for the 14 winter seasons of the (unfiltered)

* The spatial structure is defined by the dominant EOF for the cases. Similar analyses with the low-pass EOF patterns yielded highly similar results.

Fig. 4.5. Vector plots of the amplitudes and phases of zonal Fourier components $k=0 - 8$ of the grand-mean anomaly fields and of the climatological mean height field between latitudes 20°N and 80°N . Solid vectors are for the positive cases, dashed vectors are for the negative cases and dotted vectors are for the climatological mean field. The amplitude is proportional to the length of the vector, the phase is given by the angle measured in the clockwise direction between the positive vertical axis through the origin of the vector and the vector itself (positive angles eastward). The vertical component of a vector is proportional to the contribution by that wavenumber to the observed anomaly at the reference longitude. The scales are adjusted such that the distance between either vertical tick marks or wavenumber tick marks corresponds to 100m wave amplitude. (a) PAC cases; (b) ATL cases; and (c) NSU cases.

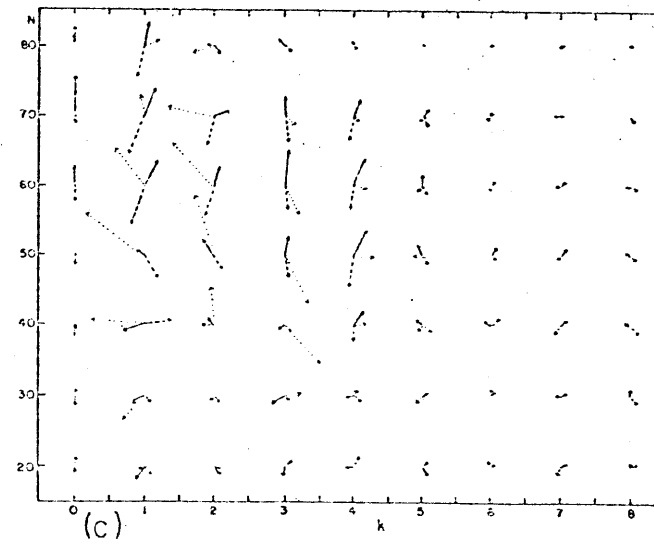
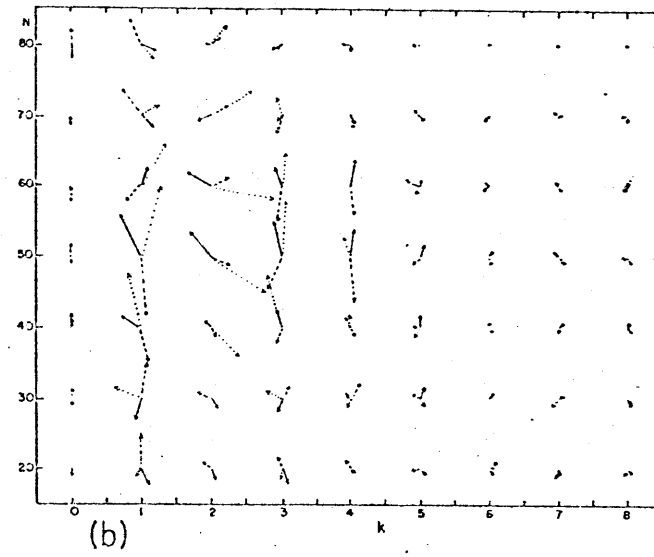
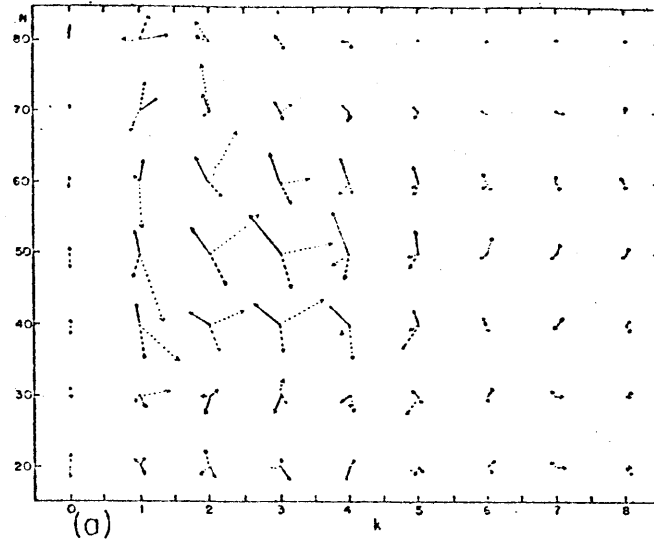


Fig. 4.5

twice-daily anomaly data. A first indication of the character of the fluctuations is provided by comparing the relative importance of the within-season to the between-season (e.g., interannual) variability. Fig. 4.6 displays for each of the three regions the seasonal means and standard deviations about the seasonal means of the dominant EOF time coefficients. We see that in most years the seasonal means are not far removed from the long-term mean. We can decompose the total variance of the EOF time series into a sum of the within-season variance and the between-season variance. The percentages of the total variance contributed by intra-seasonal fluctuations are 75% for PAC, 80% for ATL and 87% for NSU. Thus, for all three regions, most of the variance in the patterns is contributed by within-season, rather than between-season fluctuations.

Nevertheless, there are a few seasons where the mean value deviates substantially from zero. The most extreme example is the persistent negative PAC pattern occurring during the 1976-1977 winter, which was associated with record-breaking weather over almost all of North America (see e.g., Namias, 1978). Not only is the seasonal-mean anomaly during this winter the largest we observed, but the standard deviation about the seasonal mean is smaller than for any other season. Our analyses suggest that the abnormal circulation of the 1976-1977 winter can be interpreted as an unusually extreme and persistent realization of a frequently recurring persistent anomaly pattern.

So far, we have not explicitly considered the changes in storm paths associated with persistent anomalies. The variance in geo-

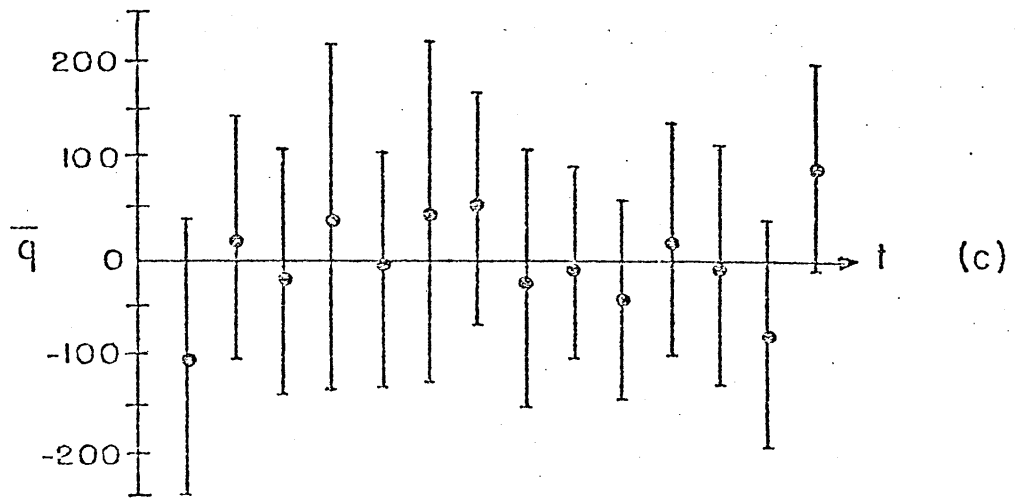
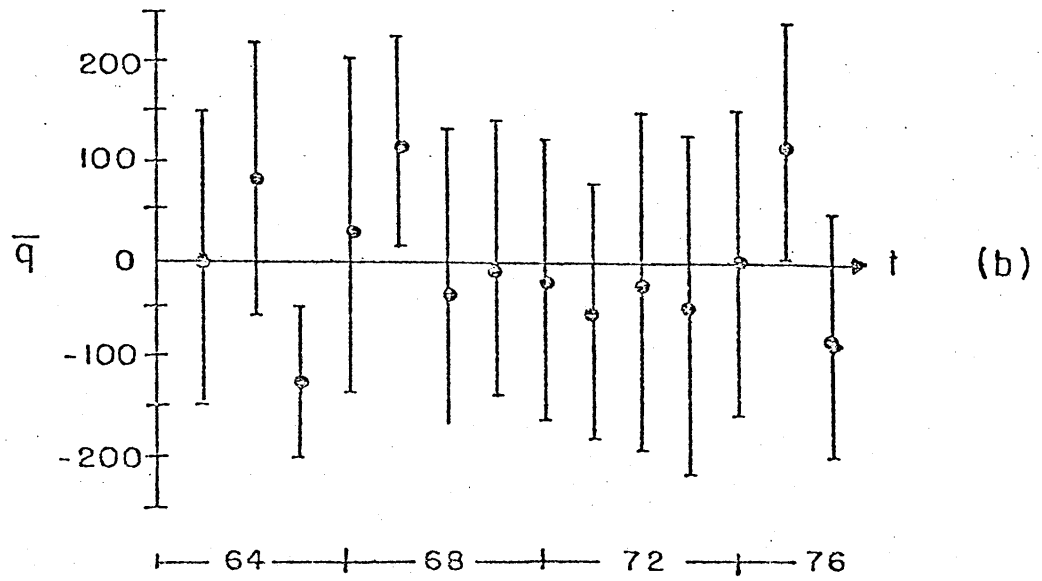
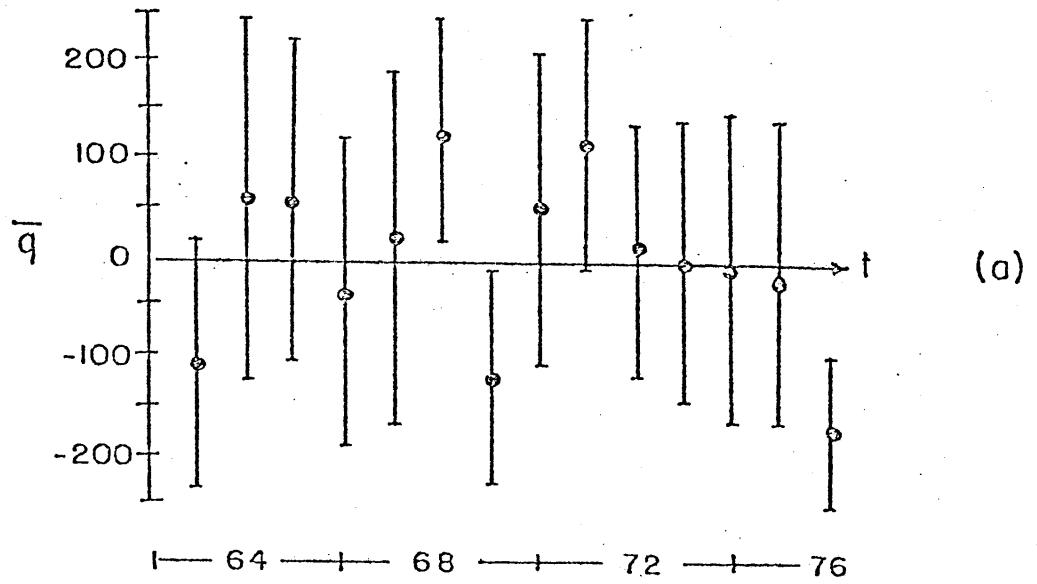


Fig. 4.6. The seasonal means \bar{q} and standard deviations about the seasonal means of the time coefficient of the first case EOF for each of the regions (units: arbitrary). The seasonal mean is give by the dot, the vertical bars denote ± 1 standard deviation and the dates refer to the start of the season (e.g., 76 refers to the 1976-77 winter season). (a) PAC ; (b) ATL and (c) NSU.

potential heights having periods of roughly 2.5 - 6 days* has recently been found to bear a close geographic relation to the major storm paths (e.g., Blackmon, 1976; Lau, 1978). This measure is reminiscent of indices provided in earlier observational research on mean storm paths (e.g., the local rate of alternation of cyclones and anticyclones presented by Pettersen, 1956). For convenience, we adopt the terminology of Blackmon (1976) and Lau (1978) and call regions of maximum band-pass height variance "storm paths."

Fig. 4.7 presents composite averages of the root-mean-square (rms) bandpass 500 mb heights** for positive and negative cases in each of the three regions. For the PAC positive cases (Fig. 4.7a), there appear to be two major Pacific storm paths: one starting over eastern Asia and curving abruptly northeastward toward the Bering Sea, and the other beginning over the northern Gulf of Alaska and dropping sharply southeastward toward the Pacific northwest. A local minimum in activity occurs near and immediately southeast of the key region. In contrast, the PAC negative cases (Fig. 4.7b) display a single, nearly zonally-oriented storm path across the Pacific at about 40 N, with maxima south and southeast of the key region. Note that differences between positive and negative cases appear small in the cyclogenetic region over eastern Asia.

*The periods retained by Blackmon band-pass filter.

**The band-pass heights are not normalized by sine as in the previous calculations.

Similar analyses for the ATL positive and negative cases, presented in Figs. 4.7c and 4.7d respectively, display differences reminiscent of their PAC counterparts. The positive cases' storm path turns sharply northeastward from eastern North America to over Iceland and thence southeastward to the Baltic Sea. The negative cases' path appears comparatively stronger over eastern North America and, in parallel to the PAC negative pattern, extends nearly zonally across the Atlantic near 40 N. The NSU positive cases (Fig. 4.7e) display little transient activity near the NSU blocking ridge, while the NSU negative cases (Fig. 4.7f) show a well-defined storm path forming near and downstream of the anomalous trough in the key region. Another major difference between NSU positive and negative cases is evident over the Pacific: the positive cases have the weakest, and the negative cases the strongest, activity of any of the patterns.

Thus, corresponding positive and negative cases display sharp variations in the locations of the storm paths. For the PAC and ATL regions, intensities of the positive and negative storm paths appear comparable; if, however, we had normalized the height fields by $\sin \theta$ as in the earlier calculations, the negative maxima would be larger, since the locations are much further south. The origins do not appear greatly different when comparing positive and negative cases for the PAC and ATL regions, but show substantial differences for the NSU cases. The differences for all three regions support the notion that blocking is associated with major deviations in the storm paths.

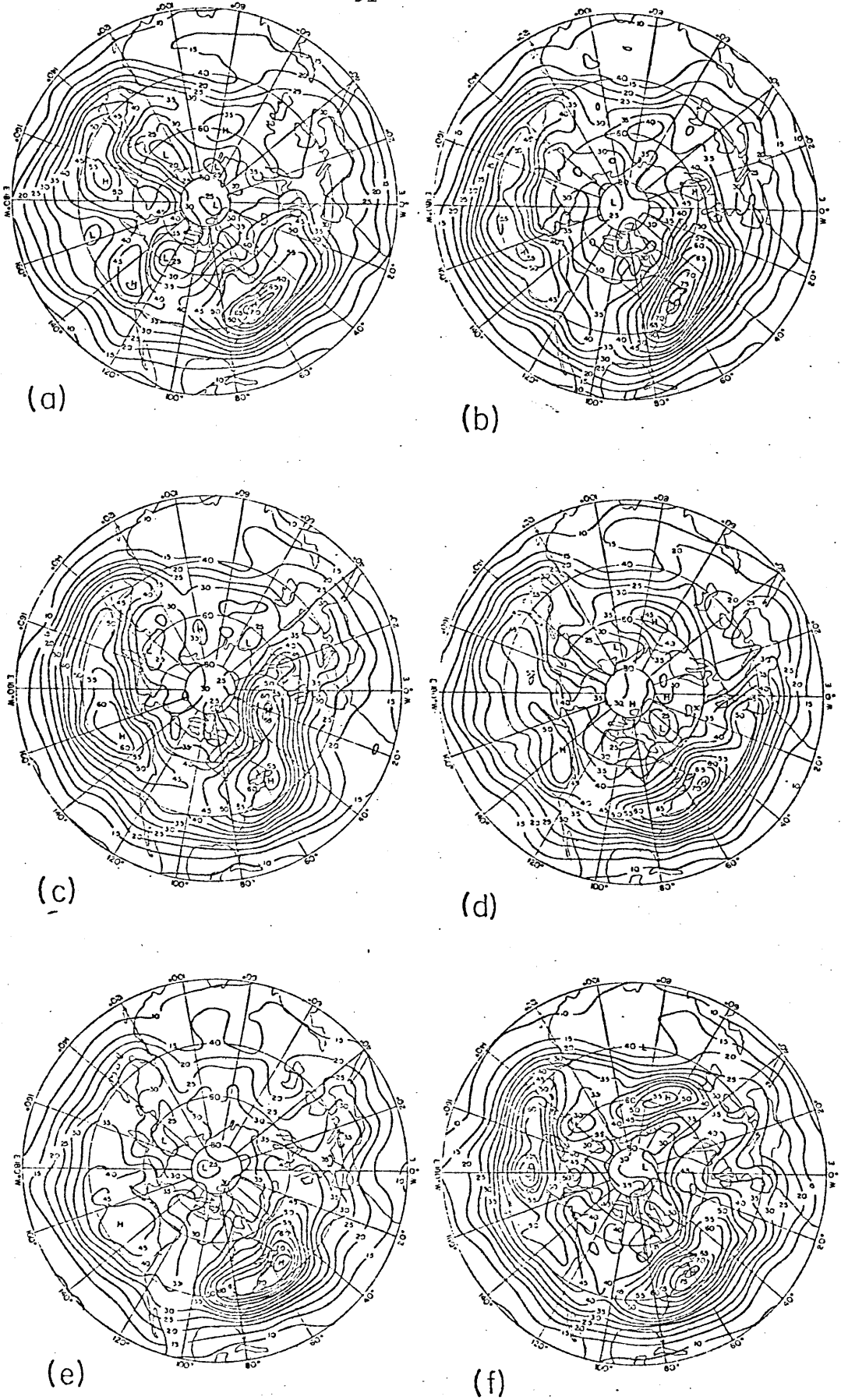


Fig. 4.7. Composite averages of the rms band-pass 500 mb heights (units:m) (a) PAC positive; (b) PAC negative; (c) ATL positive; (d) ATL negative; (e) NSU positive; and (f) NSU negative.

In addition to the 500 mb heights, the horizontal structures of the 1000 mb heights and of the 1000 mb - 300 mb layer mean temperatures have been analyzed for a set of cases studied extensively in the following chapters. The cases were extracted from the 10 winter seasons 1966-67 through 1975-76. Cases were selected by applying our usual procedure to low-pass filtered* 500 mb height anomaly data with selection criteria (+100m, 10 days) and (-100m,10 days). A list of the cases is provided in Appendix 2. The mean 500 mb height patterns for these cases (not shown) are generally highly similar to the patterns previously described.

*The low-pass filter ("Blackmon" low-pass filter) removes periods of under 10 days (Blackmon, 1976).

Fig. 4.8a and 4.8b display the composite 1000 mb height anomalies* for 14 PAC positive cases and 9 PAC negative cases, respectively. In contrast to the 500 mb patterns, the 1000 mb height anomalies are mainly confined to the key region, with only a weak suggestion of downstream wavetrains evident. Anomalies of opposite sign to the main center are located over the central North Atlantic, reflecting a tendency for the intensity of the Aleutian and Icelandic lows to vary inversely, as noted elsewhere (Kutzbach, 1970; Van Loon and Rogers, 1978). The variations in the 1000 mb height patterns are striking: in the positive cases (Fig. 4.8c) there is a weak ridge to the south of the Aleutians; the remnants of the Aleutian low appear as two centers, one located over the Kamchatka peninsula and the other over the southeastern Gulf of Alaska. The negative cases (Fig. 4.8d), in contrast, display a single intense low to the south of the Aleutians, considerably eastward of the long-term mean position. Differences between positive and negative means (Fig. 4.8e) exceed 250m to the south of the Aleutians and 100m over a small portion of the central North Atlantic. The t-test results for the significance of the difference between means (Fig. 4.8f) indicate that a huge area of the central North Pacific has differences exceeding the 99% confidence level. Additional areas exceeding the

* The height anomalies are determined from 11 winter means calculated by Lau (1979) and archived at NCAR; the anomalies are not normalized by sine (latitude) as in the earlier calculations.

99% level are located over a rather large area of southeastern Asia and the southwest North Pacific, and over smaller parts of the Pacific northwest and the central North Atlantic.

Fig. 4.9 displays the corresponding 1000 mb - 300 mb layer-mean temperature* analyses for the same PAC cases. There is a considerable positive correlation between the temperature anomalies and the 1000 mb height anomalies, indicating that the magnitudes of the height anomalies typically increase with height above 1000 mb with little, if any, westward tilt in the anomaly axes indicated through the troposphere. The major exception to this relationship is associated with the center over southeast Asia; the structure of this feature suggests that it may be a manifestation of a local response to thermal forcing, as discussed later.

Figs. 4.10 and 4.11 present similar analyses for the ATL 1000 mb heights and 1000 - 300 mb layer mean temperatures, respectively. Compared to the PAC height anomaly patterns, the ATL height anomaly patterns display more evidence of a wavetrain structure. The differences between the 1000 mb height patterns are, if anything, even more impressive than for the PAC cases. In the ATL positive cases, a surface blocking high is established in the eastern Atlantic; the Icelandic low has essentially vanished. The negative cases, in contrast, display an intense Icelandic low displaced somewhat south of its mean position. The patterns for the temperature anomalies

* Derived hydrostatically from the 1000 mb - 300 mb thickness.

Fig. 4.8. (a) Composite 1000 mb height anomalies for 14 PAC positive cases (units:m); (b) as in (a) for 9 PAC negative cases; (c) composite 1000 mb heights for the positive cases (units:m); (d) as in (c) for the negative cases; (e) (positive-negative) 1000 mb height differences (units:m); and (f) confidence levels for a two-sided t-test for the difference between means. Solid lines are positive differences as expressed in (e), dashed lines are where the differences are negative.

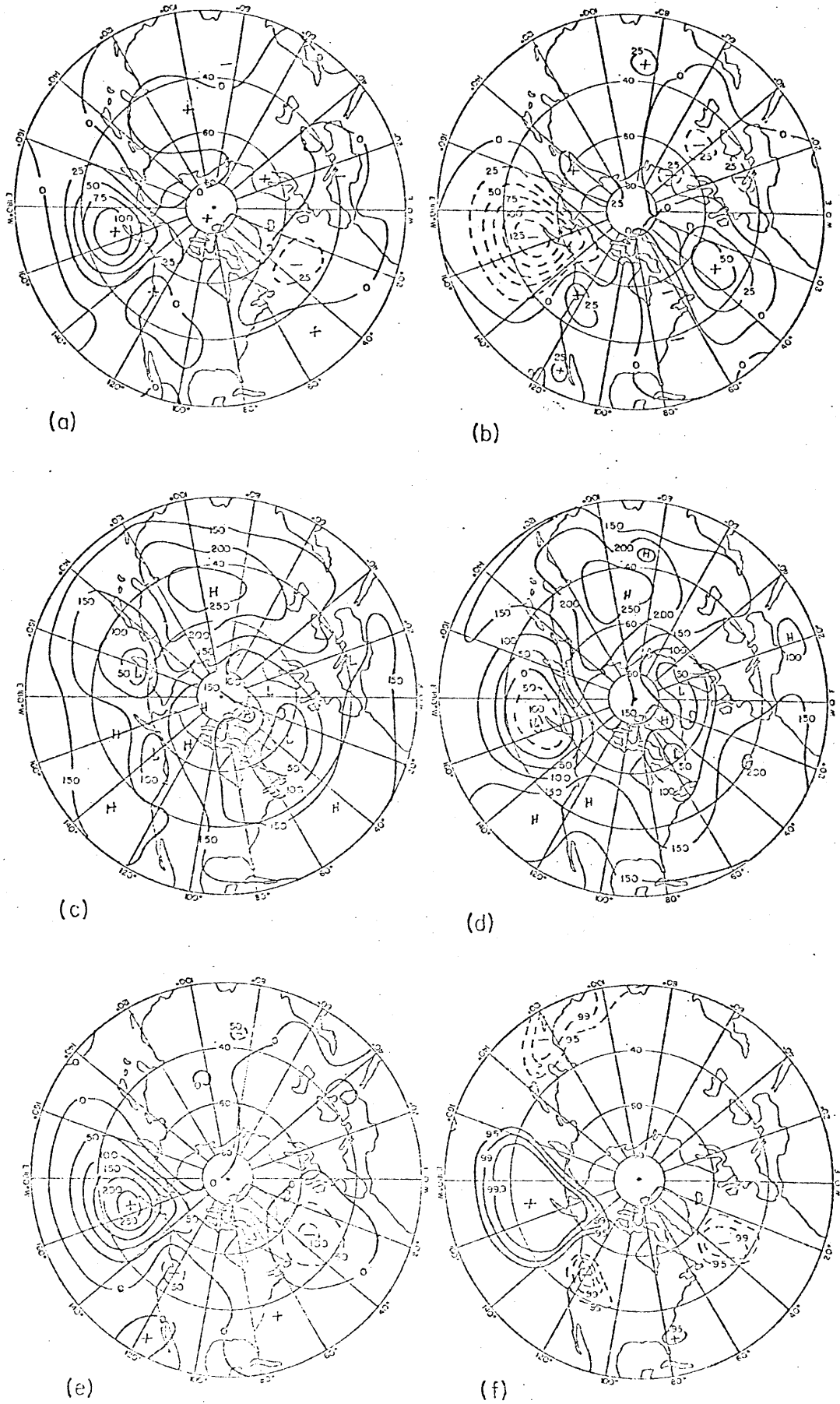


Fig. 4.8

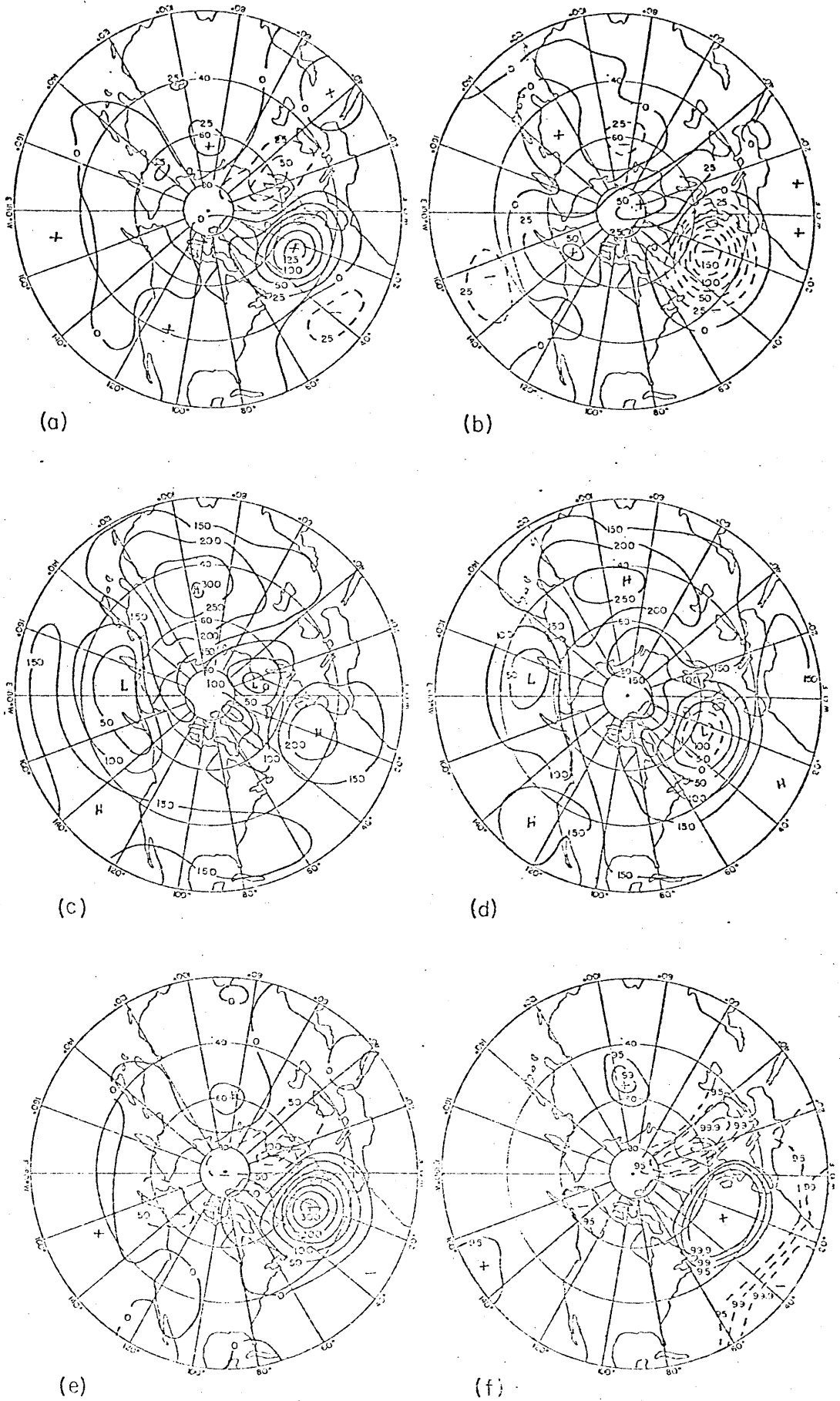


Fig. 4.10. As in Fig. 4.8 for the 1000 mb heights for 12 ATL positive cases and 12 ATL negative cases.

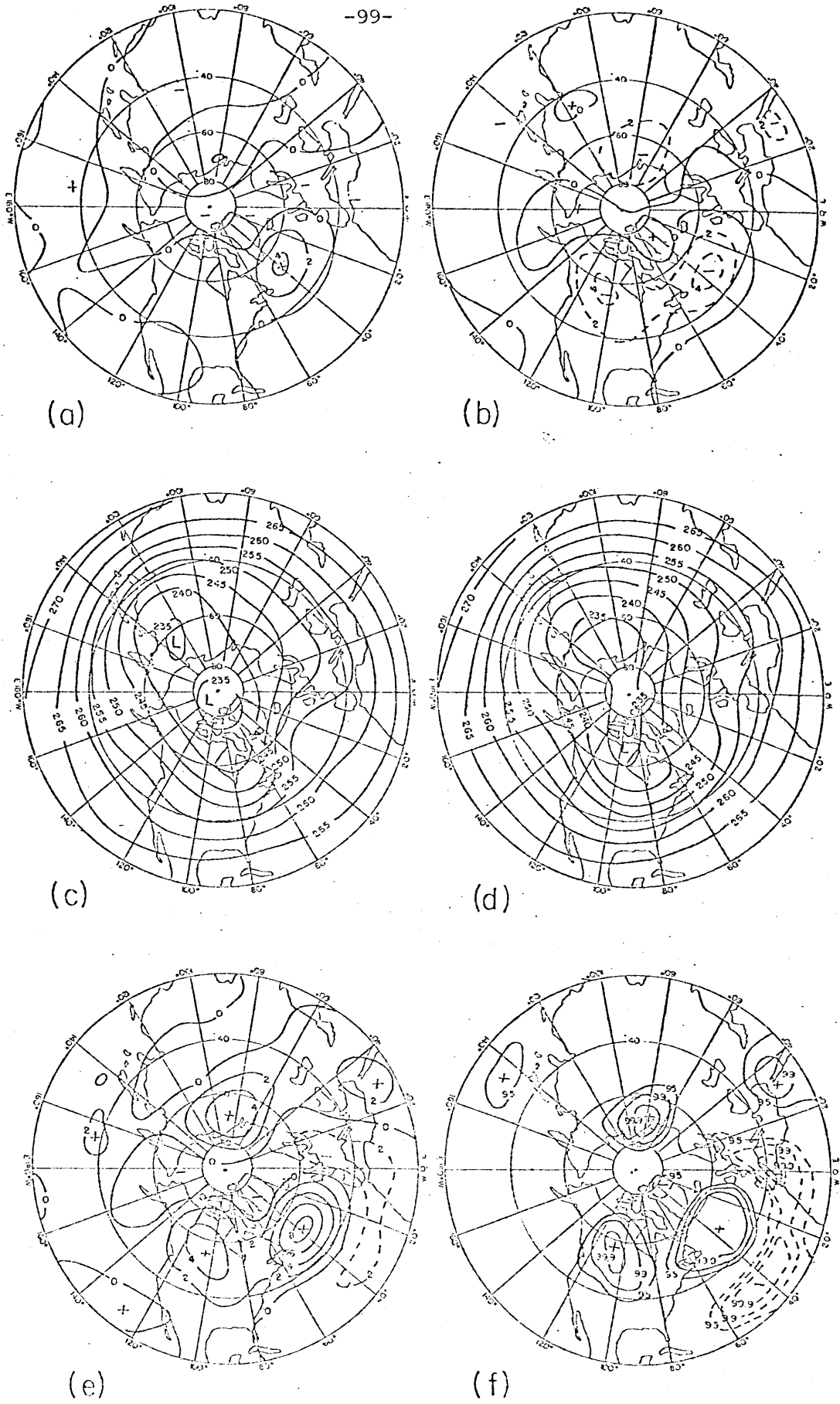


Fig. 4.11. As in Fig. 4.9 for the 1000 - 300 mb layer-mean temperatures for the ATL cases.

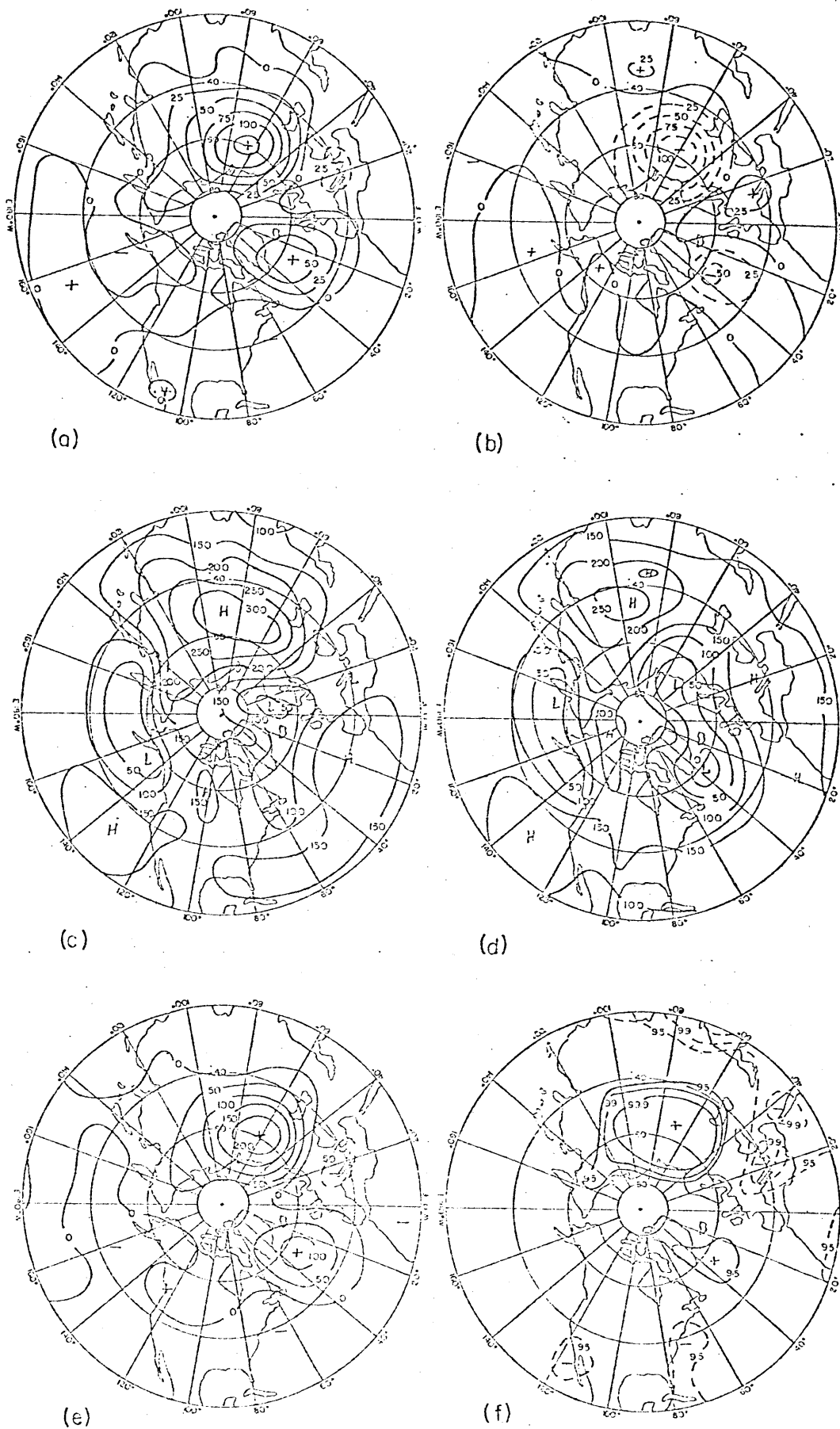


Fig. 4.12. As in Fig. 4.8 for the 1000 mb heights for 8 NSU positive cases and 9 NSU negative cases.

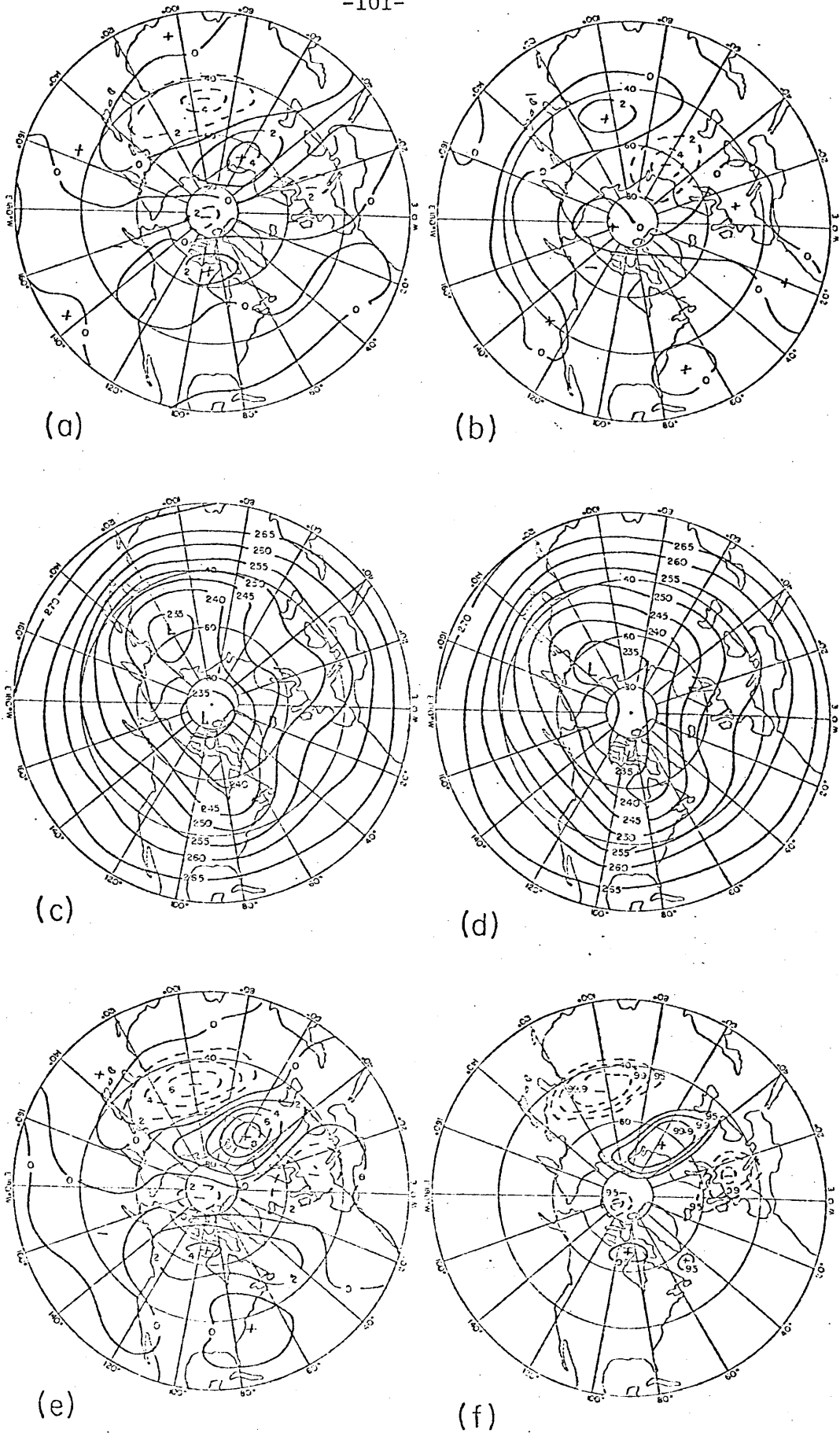


Fig. 4.13. As in Fig. 4.9 for the 1000 - 300 mb layer-mean temperatures for the NSU cases.

again primarily mirror the height anomalies, although the positions of the temperature anomaly centers associated with the main height centers appear shifted relatively further westward than for the corresponding PAC patterns. Also evident in the temperature analyses are significant centers over Northern Canada and near the Red Sea which have no clear counterparts in the 1000 mb height fields.

The NSU 1000 mb height anomalies (Fig. 4.12) appear to be primarily associated with variations in the location and strength of the Siberian High: the positive cases with a strengthening and westward movement, the negative cases with a weakening and eastward movement. Significant 1000 mb height anomalies having opposite sign to the main center are located mainly to the southwest and far to the south of the key region. The temperature anomaly patterns (Fig. 4.13) display a wavetrain structure similar to the 500 mb height anomaly patterns described earlier.

For all three regions, then, pronounced anomalies in the patterns of surface pressure and tropospheric mean temperatures accompany the persistent 500 mb height anomaly patterns.

C. Vertical Structure

The next stage in our analysis is the description of the vertical structure of persistent anomalies. Our data base consists of twice-daily N.M.C. analyses of the geopotential height, temperature and wind fields at 10 pressure levels (1000, 850, 700, 500, 400, 300, 250, 200, 150 and 100 mb) for the 11 winter seasons 1966-67 to 1976-77. Using the selection criteria (+100m, 10 days), 24 cases (15 positive, 9 negative) were chosen from this period for more detailed study.

The case locations, starting dates and durations are listed in Appendix 2. All of the cases are derived from the three key regions and are among the most persistent events which occurred during the 11 winter seasons. In addition to persistence, data availability was considered in selecting cases. All of the cases had at least 88 per cent of the observations available at all levels, and no more than 1 missing observation. Missing data were not interpolated, so that time-averages over the duration of a case are weighted by the number of available observations. All calculations were performed on a 2.5 degree latitude by 5.0 degree longitude grid. Data were spatially interpolated to the latitude-longitude grid as previously described. Anomalies are defined as departures from the 11 winter season means. The structures of the mean fields are described by Lau (1979).

Zonal cross-sections of height, temperature and vorticity anomalies were prepared at selected latitudes for each case. Examination of these cross-sections revealed certain typical features, which we will illustrate first by describing a single case and then by providing results of composite analyses.

Figure 4.14a presents a longitude-pressure cross-section at 50N of the time-average geopotential height anomalies for PAC positive case 2. This case is the most long-lived of those selected. It is also of interest as an example of concurrent persistent anomalies. In addition to the major positive anomaly near 160W, the strong negative anomalies centered near 120W, 20W and 70E all satisfied the selection criteria for at least part of the 27 day period. They

appear in this figure as a train of anomalies of alternating sign extending downstream from the center near 160W and having a wavelength of about 90 degrees longitude. These anomalies share similar vertical structure characteristics: they display little or no tilt with height, have maxima at about 300 mb (near the tropopause) and are relatively weak near the surface. The associated temperature anomalies (Fig. 4.14b) show a consistent thermal structure: through the troposphere, the positive height anomalies are warm-core and the negative anomalies cold-core, with a pronounced reversal of the sign of the anomaly and secondary maxima in the lower stratosphere. These features are particularly evident for the anomalies near 160W and 120W. Note that the latter center is in a region of dense data coverage over western North America. The accompanying vorticity anomalies (Fig. 4.14c) similarly display little vertical tilt, with maximum departures exceeding $6 \times 10^{-5} \text{ sec}^{-1}$ in the upper troposphere.

Estimates of typical anomaly vertical structures for cases of like sign and region were obtained as averages at each level of the positions and values of the corresponding maxima. Positions were defined for each case relative to the longitude of the largest height anomaly at 500 mb (positive displacements eastward). Fig. 4.15 presents the average vertical variations in height anomaly values for both positive and negative cases for all three regions. The gross features are highly similar, with anomalies increasing in magnitude from the surface upward to about 300 mb and decreasing above that level. Typical magnitudes for the 500 mb anomalies are about 250 m and thus are substantially larger than the maximum climatological

mean zonal departures (cf Fig.3.3b) The corresponding position analyses (Fig. 4.16) indicate that, with the exception of the NSU positive cases, the axes of the persistent anomalies typically slope slightly westward with height. Note, however, that none of the differences between the 1000 mb and 100 mb positions exceed 10 degrees longitude. These observations suggest that the anomalies are predominantly equivalent-barotropic in vertical structure.

The average vertical variations in temperature anomaly values are shown in Fig 4.17. The overall characteristics are consistent with hydrostatic considerations: the temperature anomalies are positively correlated with height anomalies in the troposphere and negatively correlated in the stratosphere. This thermal structure implies that, near the tropopause, positive anomalies are associated with anomalously low, and negative anomalies with anomalously high, static stabilities. A reversal in the static stability anomaly is evident above 200 mb for all but the ATL positive cases.

The corresponding vorticity anomaly values (Fig. 4.18) display peaks between 200 and 300 mb. The relation between vorticity and thermal anomaly structures has a further implication. Hartmann (1977) shows that for large scale, highly stratified flows ($Ro \ll 1$, $Ri \cdot Ro^2 \geq 1$), the potential vorticity may be approximated by $P = -(\zeta+f) \frac{\partial \theta}{\partial p}$, where the relative vorticity ζ is evaluated on a constant pressure surface. Near the tropopause (approximately 300 mb), positive (negative) anomalies are characterized by anomalously low (high) values of ζ and $-\frac{\partial \theta}{\partial p}$. This correlation suggests that

near the tropopause, positive (negative) anomalies will be associated with abnormally low (high) values of potential vorticity.

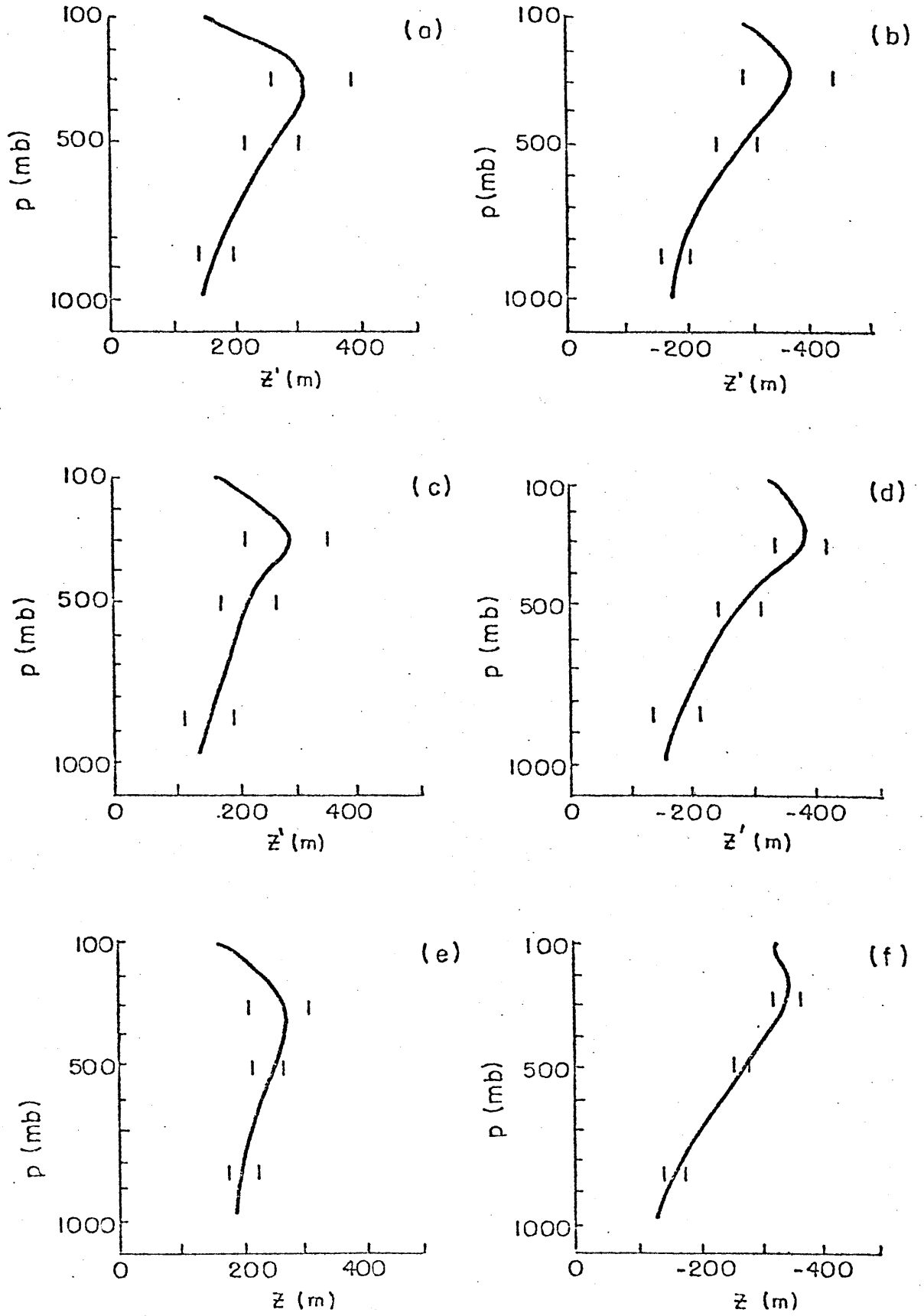


Fig. 4.15. Average vertical variations of anomaly maxima (units:m) for (a) PAC positive cases; (b) PAC negative cases; (c) ATL positive cases; (d) ATL negative cases; (e) NSU positive cases; (f) NSU negative cases. Vertical bars mark ± 1 standard deviation about the mean value at the corresponding level.

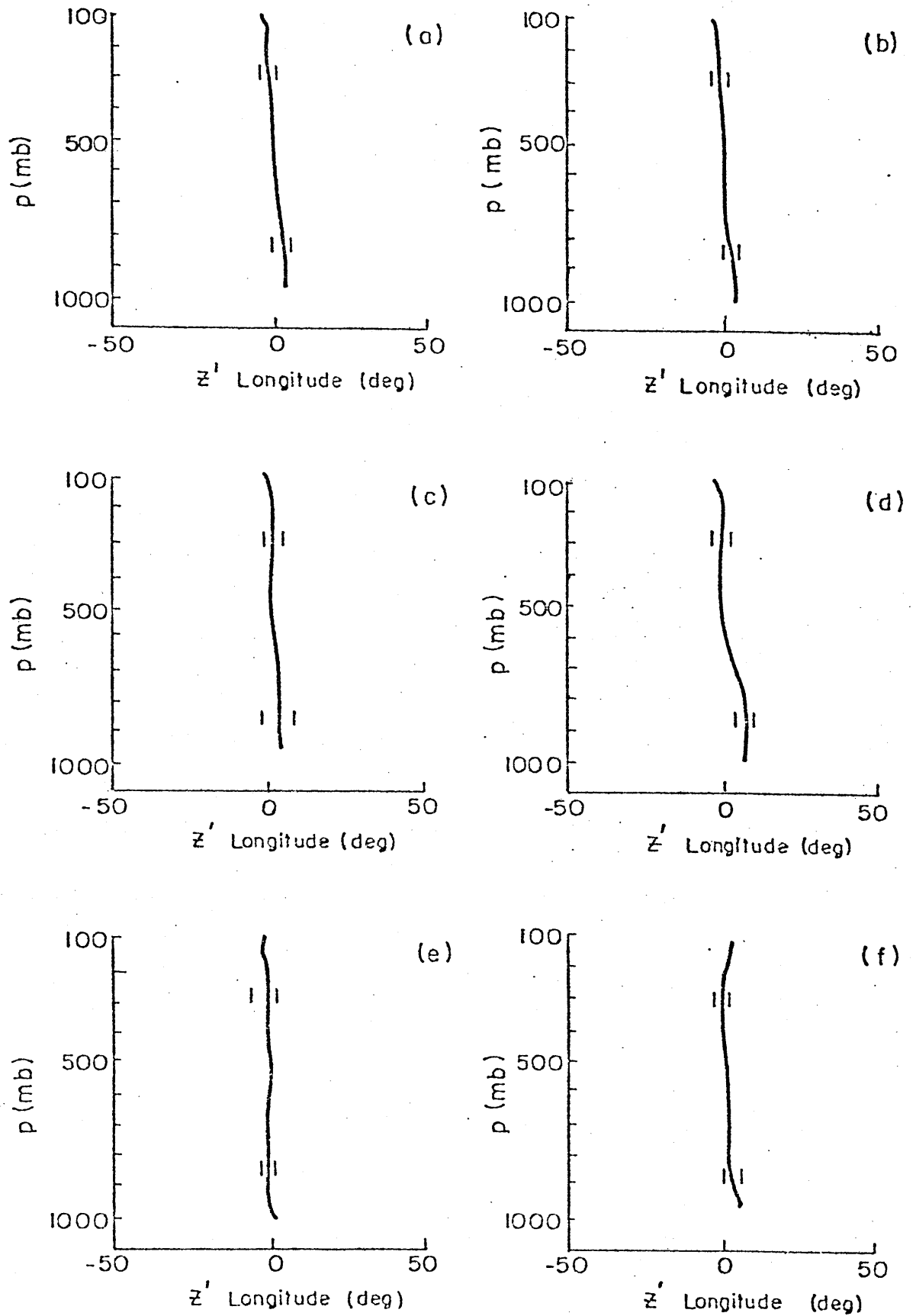


Fig. 4.16. Average zonal displacement ($^{\circ}$ longitude) of the height anomaly maxima relative to the 500 mb position (eastward displacements positive) (a) PAC positive cases; (b) PAC negative cases; (c) ATL positive cases; (d) ATL negative cases; (e)

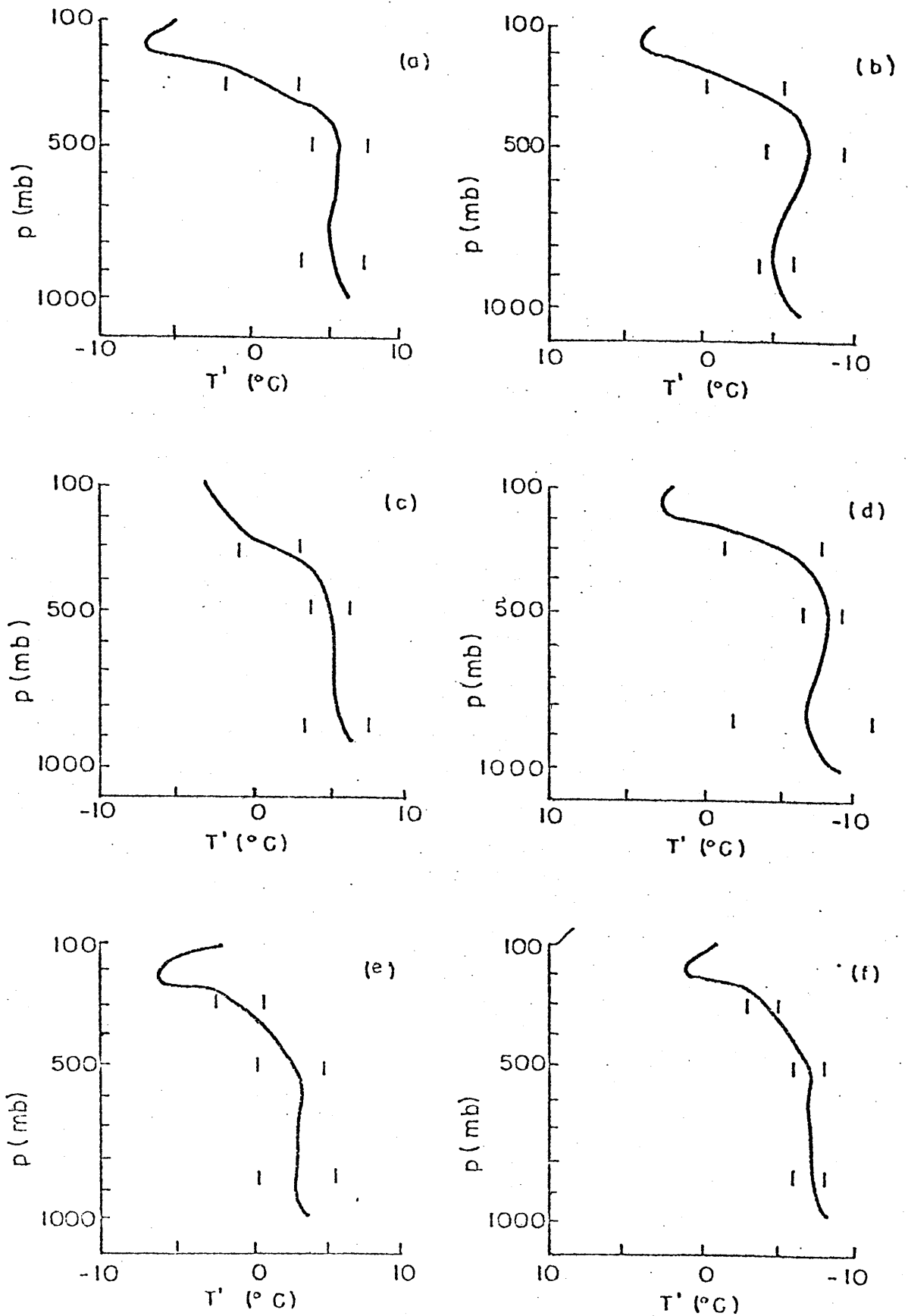


Fig. 4.17. As in Fig. 4.15 for the temperature anomalies (units: $^{\circ}\text{C}$).

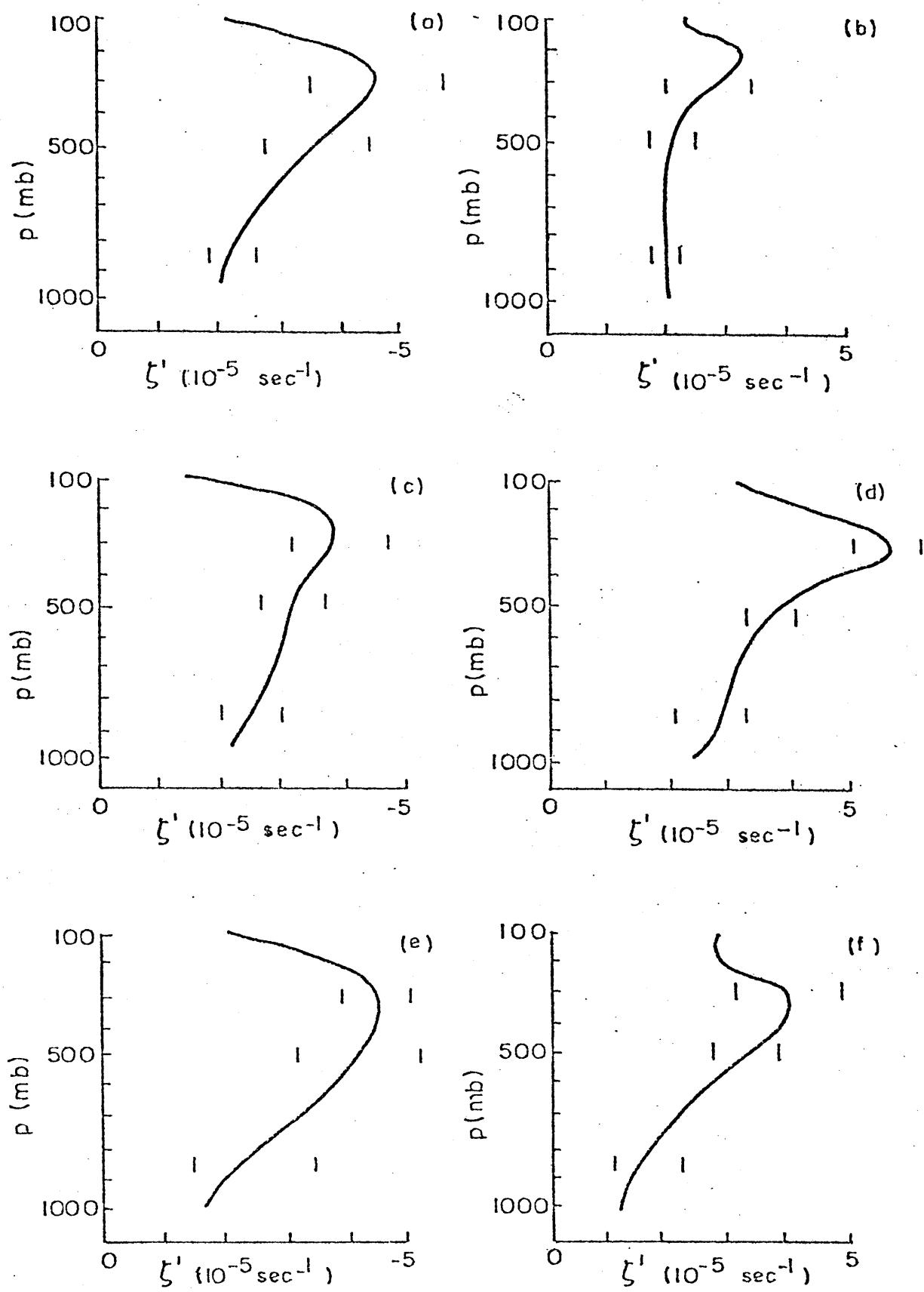


Fig. 4.18. As in Fig. 4.15 for the vorticity anomalies (units: 10^{-5} sec^{-1}).

D. Discussion

Before proceeding, we summarize the main aspects of the structure of persistent anomalies. From the horizontal structure analyses, we determined that:

1) there is strong evidence for the recurrence of certain preferred patterns for the persistent anomalies;

2) although apparently real asymmetries exist, to a first approximation persistent positive and negative anomaly patterns can often be described as opposite phases of the same basic pattern;

3) the positive phase of the pattern usually resembles blocking, the negative phase can often be associated with a regional "high-index" flow. Systematic changes in storm paths accompany the mean flow changes

4) the majority of the cases appear to be associated with unusually strong enhancements of the primary regional patterns of low-frequency variability. Most of the variance in these patterns is contributed by within-season, rather than between-season, fluctuations.

5) the persistent anomaly patterns are accompanied by pronounced changes in the location and intensity of the major centers of action (the Aleutian low in the PAC cases, the Icelandic low in the ATL cases and the Siberian high in the NSU cases). Concurrent with the height anomalies, there are large-scale tropospheric temperature anomalies having patterns mainly in-phase with the height anomalies.

The vertical structure analyses showed:

1) maximum height anomaly values near the tropopause;

2) nearly equivalent-barotropic anomaly structures;

- 3) typical temperature anomaly magnitudes of about 5°C in the troposphere (positive anomalies warm-core, negative anomalies cold-core) with low-level maxima;
- 4) abrupt sign reversals in the temperature anomalies above the tropopause;
- 5) vorticity peaks in the upper troposphere; and,
- 6) abnormally low values of potential vorticity for the positive cases and high values for the negative cases, with maxima near the tropopause.

It is interesting that some simple theoretical models do produce analogues to the persistent patterns we observe. Charney and DeVore (1979) find in a low-order barotropic channel model two stable equilibrium states, one characterized by an enhanced zonal flow and relatively weak wave perturbations and the other by a weak zonal flow and a highly amplified wave resembling blocking. The wave patterns between the two states are nearly anti-phase. The high- and low-index equilibria correspond, respectively, to zonal flows above and slightly below the values for linear resonance of the forced wave. Charney and Strauss (1980) obtain low- and high-index equilibria in a highly truncated, two-layer baroclinic model. Recent analyses of quasi-stationary waves in simple time dependent models (Reinhold, 1981; Kalnay-Rivas and Merkine, 1981) also disclose pairs of flow states.

A behavior suggestive of multiple equilibria would be the occurrence of multiple well-separated modes in suitably defined frequency distributions. If the features identified are manifestations of multiple equilibria, we might hope that a distribution representing their behavior would exhibit a multi-modal structure. To construct such a distribution, we have assumed that the first eigenvector of the low-pass EOF analyses adequately defines the spatial patterns of the hypothesized positive anomaly and negative anomaly quasi-equilibria and then have generated a corresponding time series from the daily low-pass filtered anomaly data. From these time series,

histograms were constructed of the values of the first EOF time coefficient (Fig. 4.19). Although each of the distributions are somewhat flatter than corresponding normal distributions, none shows a strongly bimodal character. Examination of similar distributions calculated for unfiltered data yields qualitatively similar behavior.*

These results suggest that, if these patterns are associated with two quasi-equilibrium states, then it is likely that either the means of the states are not well separated or that the time spent between the two quasi-equilibrium states is not small compared to the time spent within the states. Alternatively, the forcing may vary sufficiently between seasons (or perhaps within seasons) to alter the attractor set and thus preclude simple identification in long-term statistics.

The horizontal structures of the patterns bear some qualitative resemblance to solutions of the linearized barotropic vorticity equation obtained in studies of forced stationary waves on a sphere (Grose and Hoskins, 1979; Hoskins, 1978; Hoskins and Karoly, 1981). Hoskins (1978), following Bjerknes (1966), suggests that over tropical regions warm sea surface temperature anomalies may lead

* We have also constructed distributions of the local values of the geostrophic zonal wind speeds for the unfiltered data for points on a 5 degree latitude by 5 degree longitude grid (results not shown; results of similar calculations for the height data are displayed in Fig. 3.7). Consistent with the EOF 1 time coefficient distributions, we were unable to find evidence of bimodality.

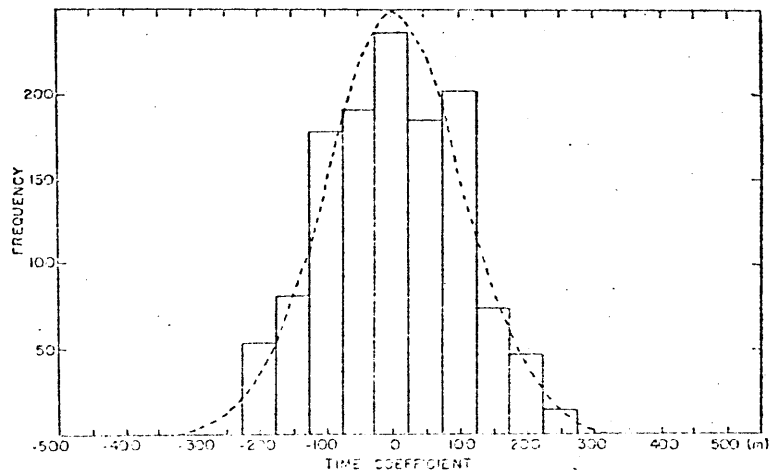
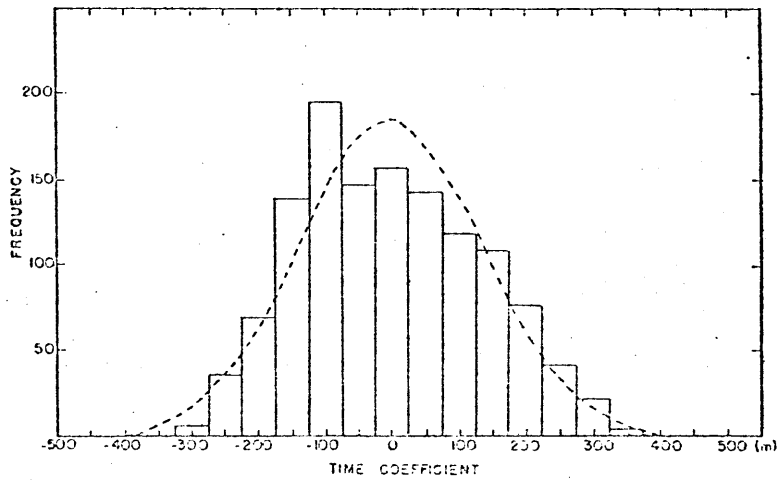
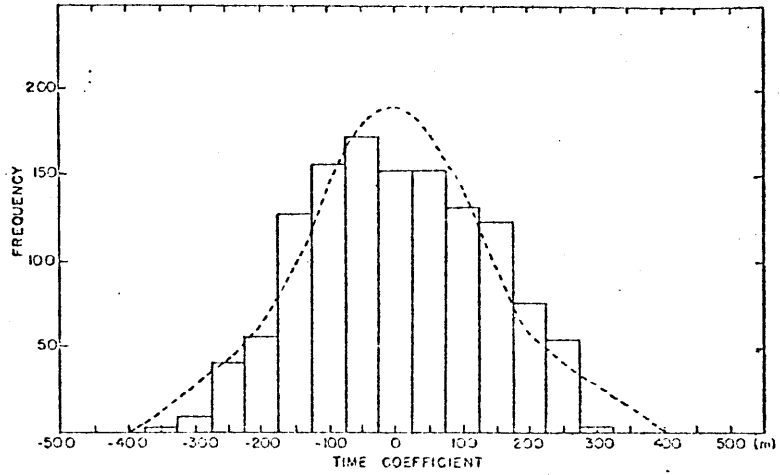


Fig. 4.19. Histograms of the values of the time coefficient of EOF 1 of the low-pass data: (a) PAC region; (b) ATL region; and (c) NSU region.

to enhanced convection. He proposes that increased convective heating will be balanced by adiabatic cooling through upward motions, so that upper-level divergence and therefore forcing of anticyclonic vorticity can be expected over the abnormally warm water. To simulate the effects of convective heating in the tropics on the large-scale flow, Hoskins forces the linearized barotropic vorticity equation with a prescribed divergence over a region 60° longitude by 30° latitude centered at 15°N. He uses for a basic state a "realistic" zonally-averaged 300mb zonal flow. Vorticity damping is included to suppress resonance and to remove extremely strong gradients occurring near critical lines.

Steady-state solutions to this problem give positive height anomalies centered near 55°N downstream from the forcing region. The ratio of the magnitude of the vorticity perturbation at 55°N (the "blocking" anticyclone) to that over the source is about 2/5. If we assume a similar ratio for the positive anomaly cases, then our data indicate the corresponding tropical vorticity perturbation is approximately $-1.3 \times 10^{-4} \text{ sec}^{-1} < -f_{60N}$, which would strongly suggest the possibility of inertial instability, even at mid-latitudes. The reduction in the magnitudes of the vorticity maxima away from the source region in Hoskins' experiment may in part be attributable to the strength of the dissipation, although this does not seem particularly excessive. In fact, Grose and Hoskins (1979) reported earlier that, in similar experiments with topographic forcing, the results were insensitive to a doubling of the drag

coefficient. Note, however, that even if we assume that the tropical and mid-latitude vorticity perturbations are comparable, the absolute vorticity would become negative at latitudes south of about 20 N. It appears that if the source for the positive anomalies that we observe is anomalous heating in the tropics, then the vorticity maxima near the source must be weaker than the vorticity maxima corresponding to the mid-latitude positive anomaly.

Although some theoretical work suggests that this may be possible (Karoly, 1978 ; Hoskins and Karoly, 1981), recent numerical results with a five-layer baroclinic model (Hoskins and Karoly, 1981) are consistent with the earlier barotropic calculations in showing the maximum vorticity perturbation near the tropical heat source. The vorticity response in this model appears to be mainly determined by three effects:

- 1) conservation of wave action implies that the streamfunction amplitude $A(k, \ell)$ for zonal wavenumber k and meridional wavenumber ℓ is proportional to $\ell^{-1/2}$. This suggests that the streamfunction maxima will occur near the turning point, which for low total wavenumbers typically occurs at mid to high-latitudes.

- 2) the vorticity response essentially increases as the square of the total wavenumber. For tropical forcing and a realistic zonally-averaged mean flow Hoskins and Karoly find that the higher wavenumbers are mainly trapped to the south of the jet maxima. This, in addition to the coherence of the high wavenumber response over the tropical source, favors a maximum vorticity response at low latitudes.

3) The dissipation on the wave depends on the time away from the source region. This effect tends to reduce the distant response mainly for low zonal wavenumbers since they have the smallest energy propagation speeds.

In the experimental results presented, effects 2) and 3) apparently dominate over 1), giving the largest vorticity response near the tropical source.

Whether the apparent discrepancies between our observations and the results presented by Hoskins and Karoly can be accounted for by changes in the structure of the basic state or the form or location of the forcing, or whether more sophisticated approaches are required, remains to be seen. Recent work in introducing zonal variations in the mean flow (Simmons, 1981; Branstator, personal communication) provides some encouraging preliminary results. We note, however, that any acceptable theory will still have to account for the strong geographical preferences for the anomaly centers, as well as the co-location of the positive and negative frequency maxima.

The vertical structures suggest clues to possible forcing mechanisms. Hoskins and Karoly (1981) and Held (1981) indicate that, away from source regions, the long-time scale response should have an equivalent-barotropic structure. Held argues that outside source regions, the only significant responses are from waves with turning points at or below the tropopause, and of these, destructive interference occurs for all except the external Rossby wave, which therefore dominates the distant response. The structure of this mode strongly resembles the vertical structures we find for the persistent anomalies. In addition to these forced responses, numerical studies (Simmons and Hoskins, 1978) suggest that finite amplitude waves arising from baroclinic instabilities may also attain vertical structures similar to those observed here.

The vertical structures of the patterns do not appear consistent with certain other forcing mechanisms. Gall, et al., (1979) propose that ultra-long waves in the atmosphere may be forced by nonlinear interactions with cyclone-scale waves. In their model, the maximum eddy forcing is near the surface. The resulting long wave structures are characterized by cold-core anticyclones and warm-core cyclones, in opposition to what we observe. Similarly, Hoskins and Karoly (1981) present simple arguments indicating that the local response to near surface heating at mid-latitudes should display strong westward tilts in the anomaly maxima with height, contrary to our observations. We also note that in the PAC and ATL positive cases, the subtropical negative anomaly centers are cold-core, with little or no evidence of tilts throughout the troposphere. This structure

does not resemble that found by Hoskins and Karoly for the local response to forcing by a deep heat source, suggesting that local* thermal forcing is probably not the proximate cause of its existence.

E. Conclusions

Our principal aims in this chapter were to identify and describe the structure of persistent anomalies. From the horizontal structure analyses we determined that, for each of the three regions, a certain pattern appeared to characterize the majority of both the positive and negative anomaly case mean patterns. This pattern was also identified as the dominant pattern of low-frequency variability for the region. These results indicate that, first, persistent anomalies have strongly preferred scales, which are nearly the same for positive and negative cases and, second, persistent anomalies have strongly preferred phases, with the most intense centers typically located near the previously identified key points.

The calculations provide a quantitative basis for describing the recurrence of certain preferred anomaly patterns. As such, they support earlier qualitative notions that at least some cases of blocking are associated with recurrent flow configurations. For each of the three regions, blocking patterns appeared in our analyses as the positive phase of the dominant anomaly pattern. For the ATL and PAC regions, the negative phase of this pattern was characterized by high-index zonal flows. Thus, for these regions both low- and high-index zonal flows appear as different manifestations of the

* The present structure may still be a manifestation of a forced response to tropical or subtropical heating, if the source of the forcing is sufficiently distant that the external Rossby wave response dominates.

same basic anomaly pattern.

Analyses of vertical structure also revealed a number of highly typical characteristics. We found that persistent anomalies have little vertical tilt, with maximum height anomalies in the upper troposphere. Associated with these departures were pronounced anomalies in the temperature, vorticity and potential vorticity fields. In later chapters, we exploit these distinct structural characteristics in analyzing the problem of the maintenance of persistent anomalies.

V. TIME EVOLUTION

A. Introduction

The previous chapters have established the geographical distribution and structural characteristics of persistent anomalies without regard to their specific temporal behaviors. We now consider the question of how persistent anomalies evolve in time, placing particular attention on identifying typical time scales and isolating systematic propagation characteristics. We first study the development of persistent anomaly patterns by constructing composites from 500 mb height data, and then briefly consider the vertical structures of the developing patterns. Following this, we examine composites of the breakdown of the persistent anomalies. We then compare our observations with the behaviors suggested by certain simple theories.

B. Data Set

The data base is that of the previous chapters. For this portion of the study the winter season is defined as the 120-day period beginning November 16; extending the data set in this manner allows us to examine more readily the evolution of events occurring near the beginning and end of the three month (Dec.-Feb.) period. Anomalies are obtained as departures from seasonal trend values and are normalized by sine (latitude) as previously described. Long term seasonal trends are calculated at each point by the procedure described in Chapter II. Cases are selected by applying our usual procedure to low-pass filtered 500 mb height anomaly data with selection criteria (+100m, 10 days) and (-100m, 10 days)*. A list of the cases is provided in Appendix 2.

*Data were filtered with the "Blackmon" low-pass filter (Blackmon, 1976).

The "key" points are identified by the "maximum number of cases" criterion described previously. The use of low-pass filtered, rather than unfiltered, data, as well as the increased length of the period considered, approximately doubles the number of available cases.

C. Development

We first study the "slow" time evolution of the 500 mb anomaly patterns by constructing composites from low-pass filtered data. This provides an overview of the development and allows us to identify certain subtle features that are partially obscured by high frequency transients. We then examine corresponding composites constructed from unfiltered data around certain key times when the patterns rapidly evolve. Following this, we present additional simple analyses to provide a more complete view of the developments.

Composites in this section are constructed relative to the time when the low-pass filtered anomaly first reaches the threshold value at the key point. This time is defined as day zero. Composite analyses cover the thirty day period from 10 days prior to onset (day -10) to 19 days after onset (day 19). In the following discussion, we will primarily focus on selected times around day 0.

Fig. 5.1 presents composite anomaly maps and associated confidence levels for 15 PAC positive anomaly cases at 2 day intervals from 4 days before onset (day -4) to 6 days after onset (day +6)*. There is little evidence in these analyses of a precursor until a few days prior to onset; indeed, at day -4, only a limited region of the northern Soviet Union to the northwest of the Tibetan Plateau has t-values

*The statistical significances of the composite anomalies are estimated by a two-sided t-test (null hypothesis of zero mean).

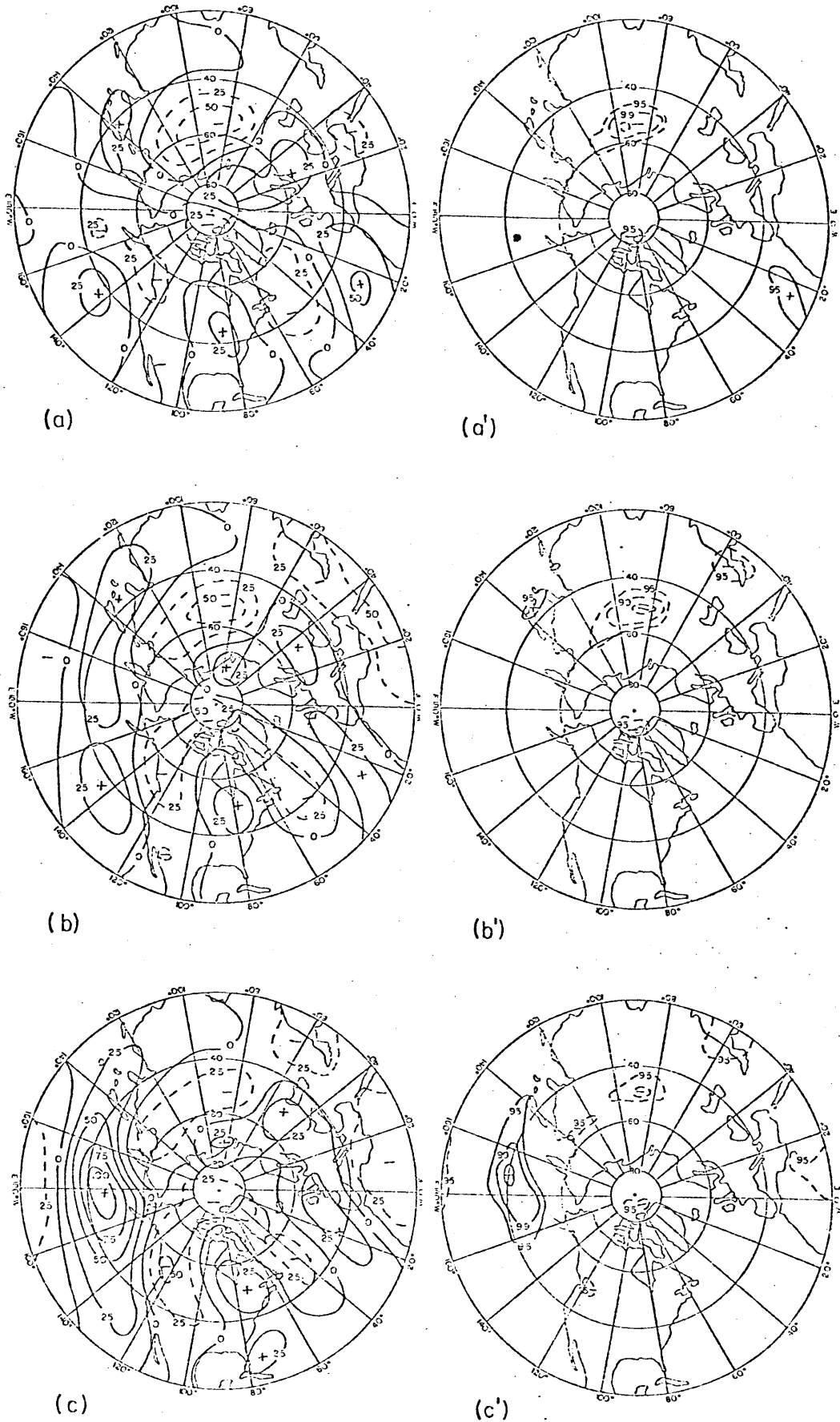
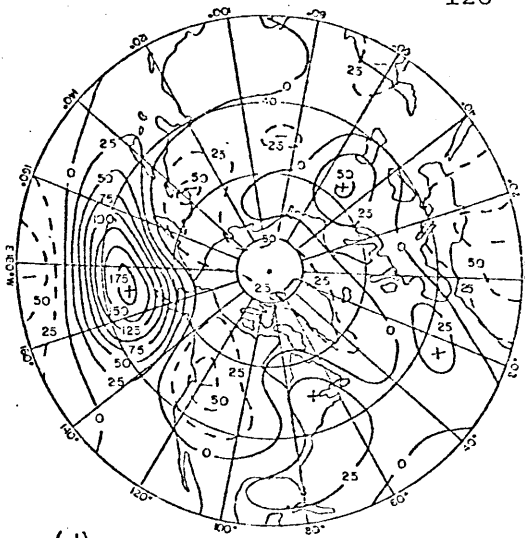
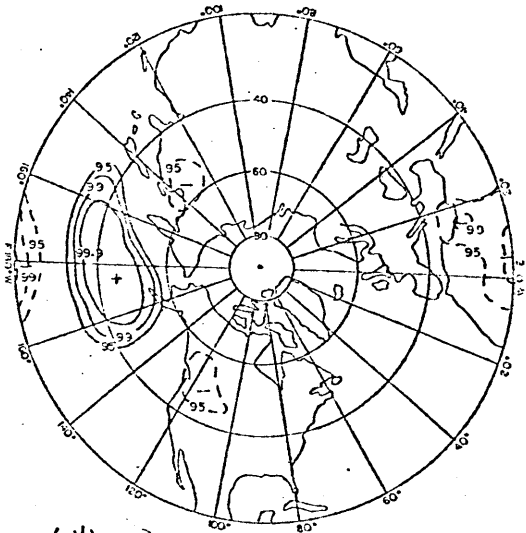


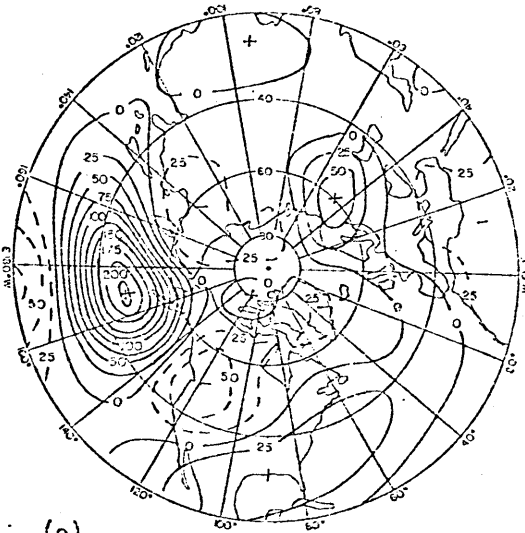
Fig. 5.1: Time composites of low-pass filtered anomalies (units:m) for 15 PAC positive cases at day (a) -4; (b) -2; (c) 0; (d) +2; (e) +4; and (f) +6. Corresponding confidence levels are displayed in (a') - (f'). Negative anomaly values are



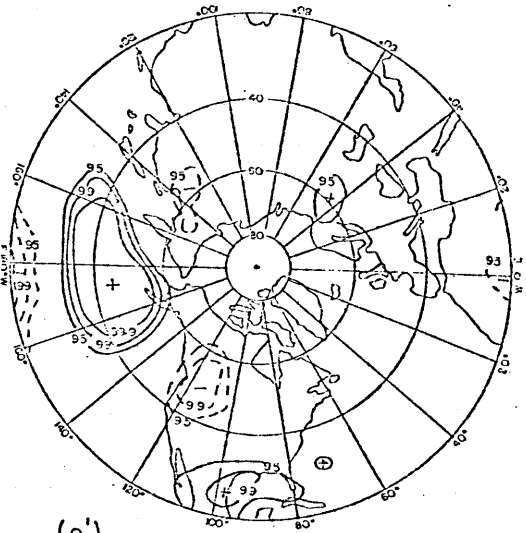
(d)



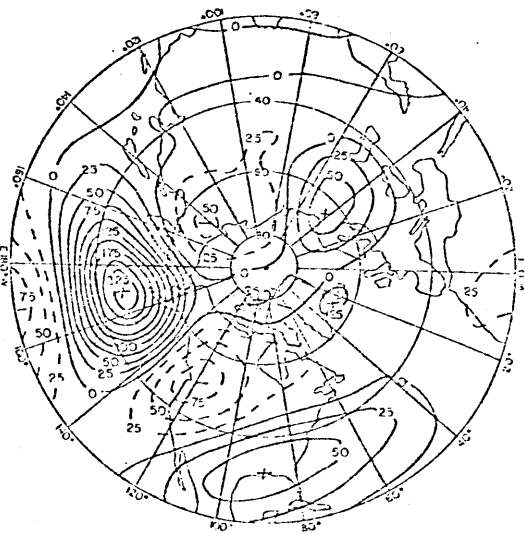
(d')



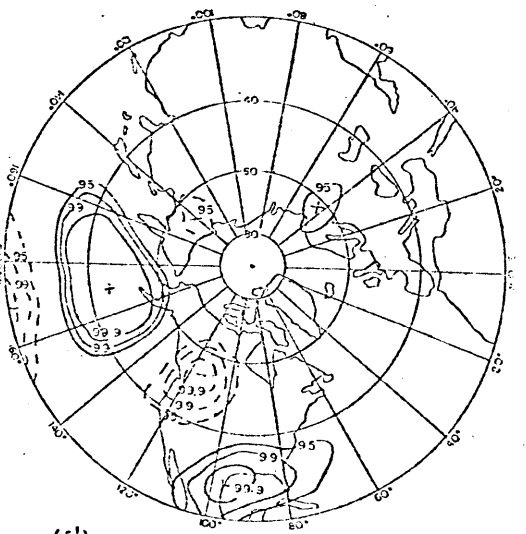
(e)



(e')



(f)



(f')

Fig. 5.1 (cont.)

exceeding the 99% confidence level. Note that, through day -2, the mean anomalies over the entire North Pacific north of 20N are not significantly different from zero. The structure of the anomaly patterns prior to (and to a lesser extent following) onset suggests that the associated wind anomalies are primarily in the zonal component.

A single major positive center becomes established over the key region at day 0. Subsequent to this time, anomaly centers form to the south of, and in sequence downstream from, the main center. Intensification of these centers occurs with little evidence of phase propagation. By day +4 the PAC positive pattern is established. The gross features of the development are strongly reminiscent of the behavior seen in simple models of energy dispersion on a sphere away from a localized, transient (e.g., switch-on) source of vorticity (Hoskins, et al., 1977; Hoskins, 1978). Over the Pacific, however, the near simultaneity of development, the almost north-south orientation of the centers and the absence of tilts in the anomaly axes make determination of the meridional component of energy propagation difficult; indeed, the pattern somewhat resembles a standing wave in the north-south direction.

Similar maps of the PAC negative anomaly composites and corresponding t-statistics are presented in Fig. 5.2. The pattern of evolution displays considerable similarity to the sequence seen previously for the positive cases. At day -4, the largest area of significant anomalies is again located upstream over the Asian continent, with t values exceeding the 99% level over a large region extending

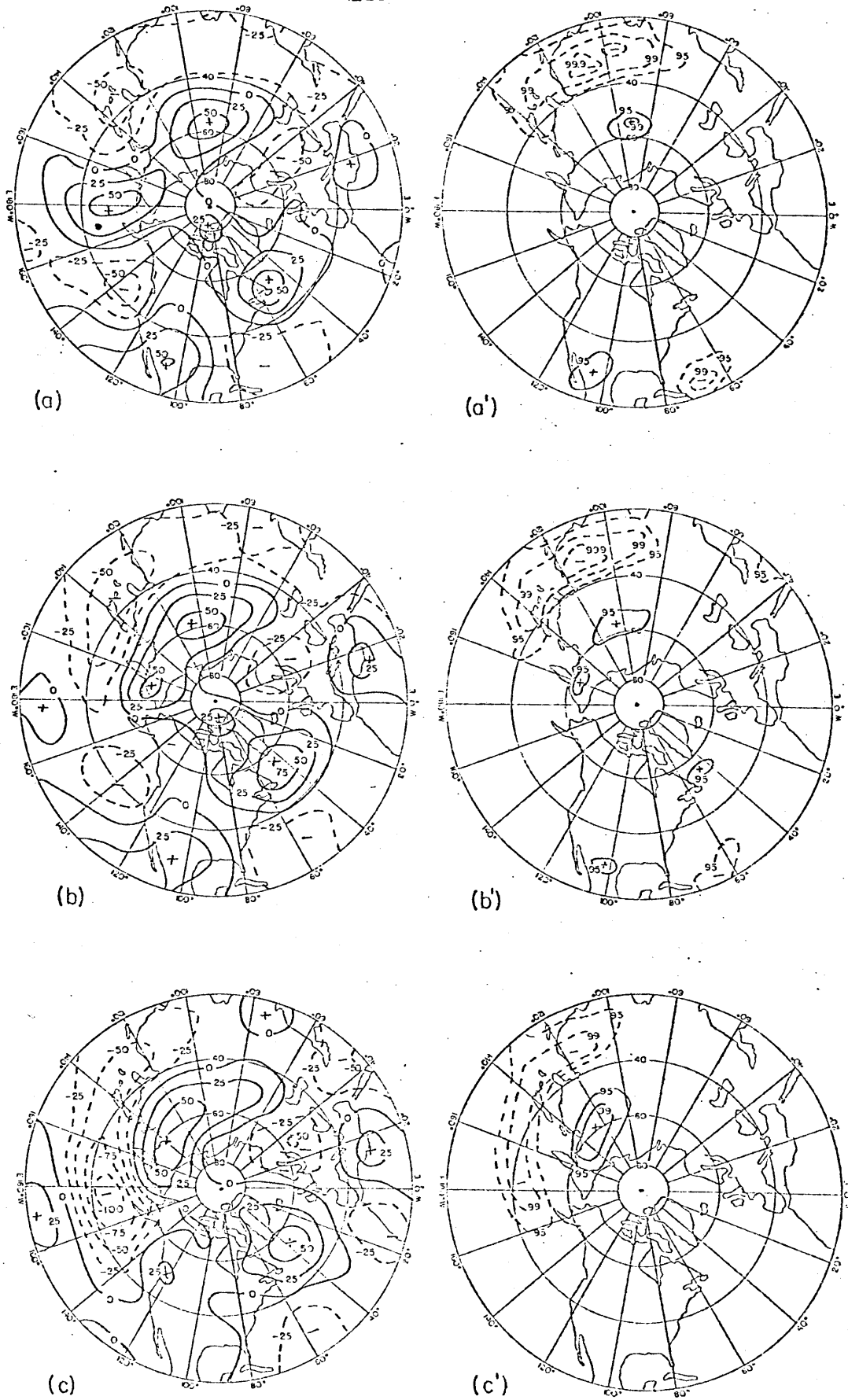


Fig. 5.2. As in Fig. 5.1 for 13 PAC negative cases.

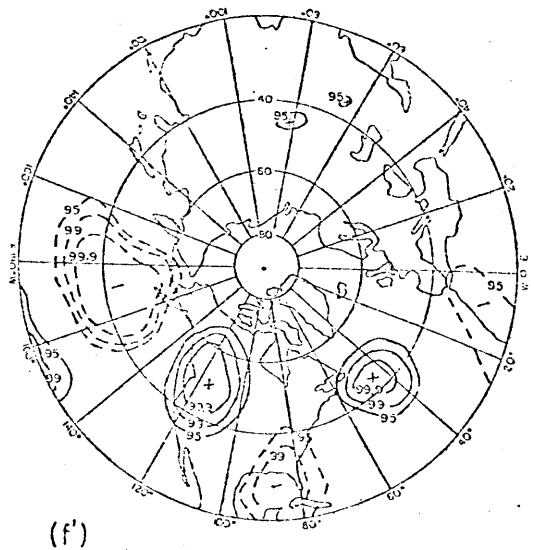
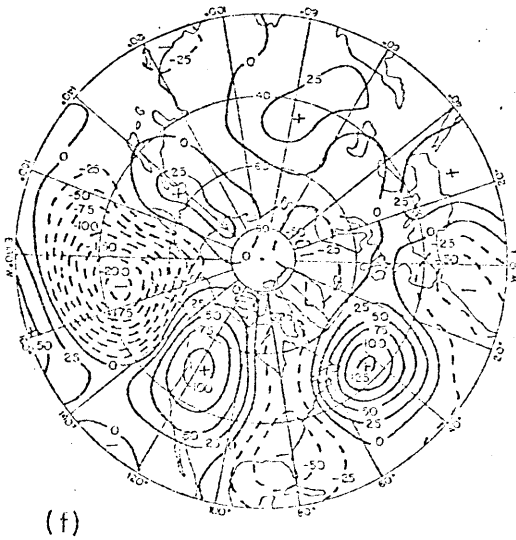
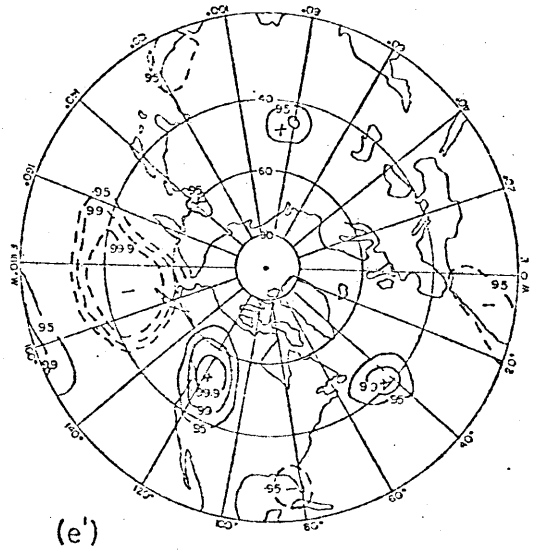
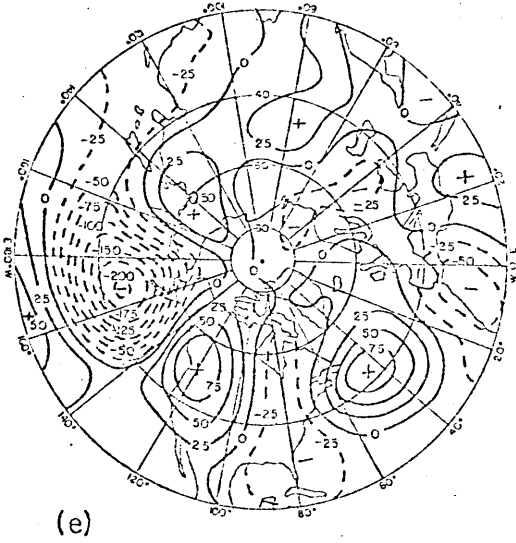
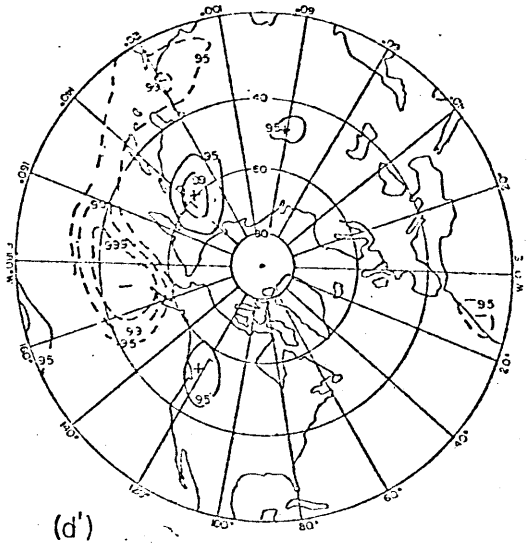
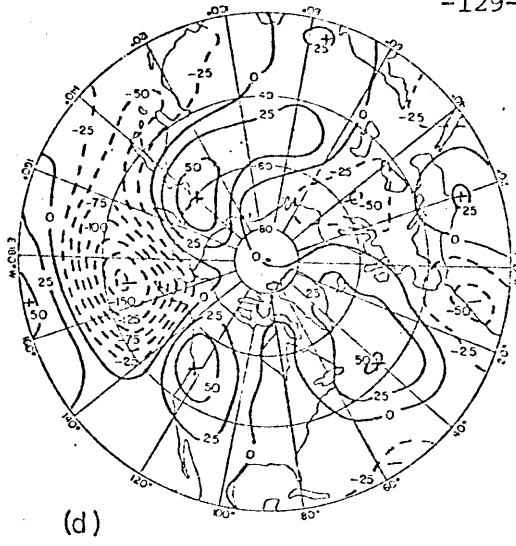


Fig. 5.2 (cont.)

from the Tibetan Plateau eastward to Japan. In contrast to the positive cases, however, the major area of significant anomalies is now located principally over and to the south of the Himalayas. Through day -2, the significant anomalies are mainly confined to this region; as for the positive cases, anomalies over the northern North Pacific are not significantly different from zero. A single major center becomes established over the key region at day 0 and, subsequently, centers deepen in sequence downstream. The largest discrepancies between the positive and negative patterns appear from day 4 onwards over the North Atlantic, where the intense positive anomaly center seen in the negative cases has no counterpart in the positive cases.

The symmetry in development (with sign reversal) can be evaluated more readily by constructing difference maps of the evolutions of the positive and negative cases. Fig. 5.3 displays the composite anomaly differences (positive-negative) at two day intervals from day -4 to day +6 and the associated confidence levels for the statistical significances of the differences between the means (null hypothesis of no difference between means). As suggested by the previous analyses, prior to the development of the main center, the principal differences between the positive and negative cases appear upstream, primarily over eastern Asia. At day -2 the southern portion of high differences extends eastward into the western North Pacific; note, however, that over the North Pacific north of 20N and east of 170E differences between the mean anomalies for the positive cases and negative cases are not statistically significant until day 0. These analyses suggest that, in 500 mb height data, the most prominent features preceding

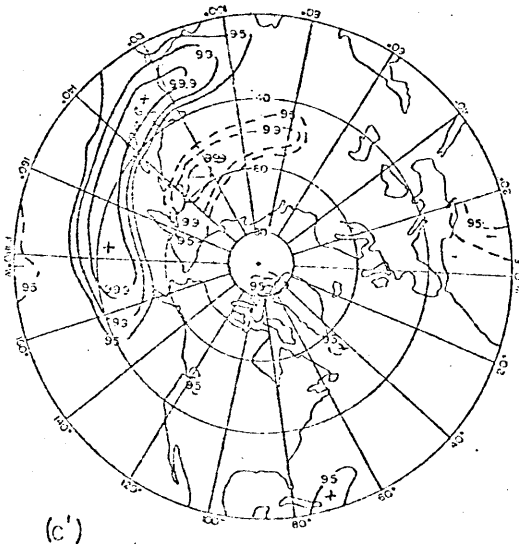
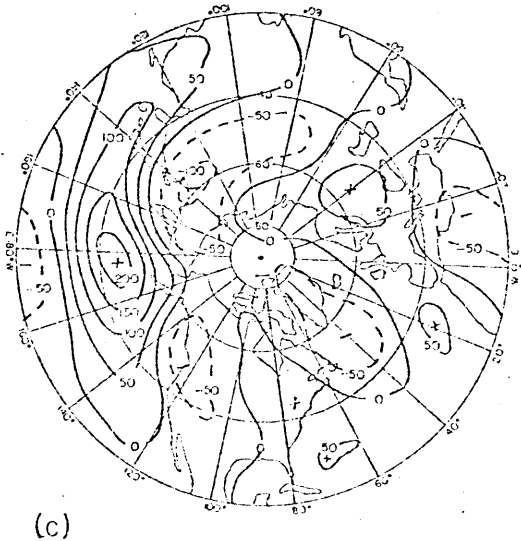
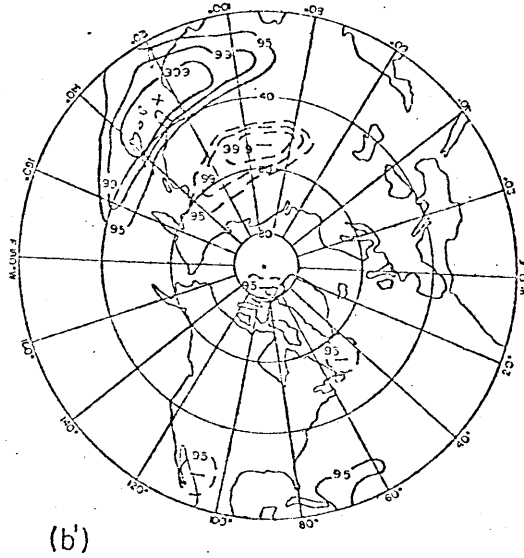
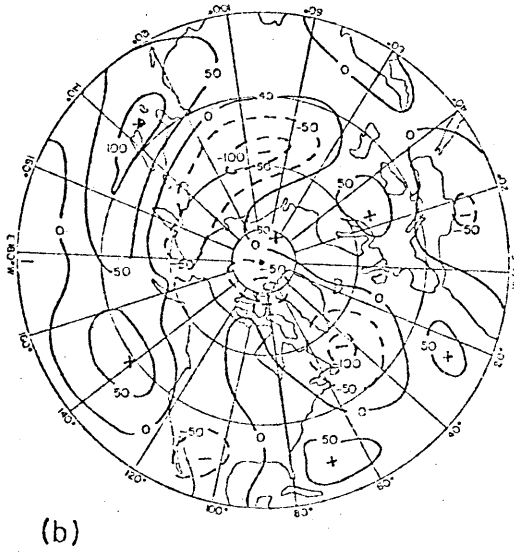
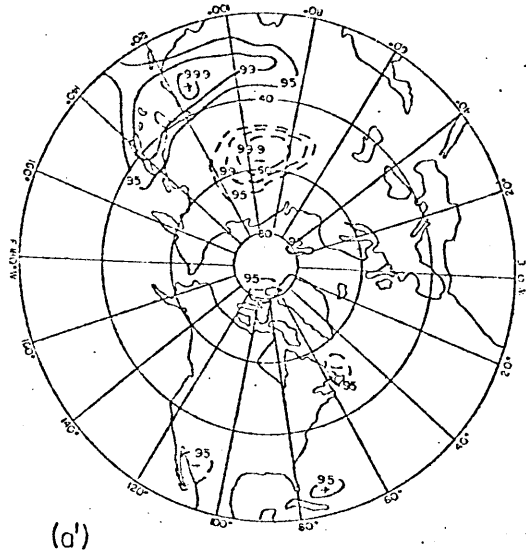
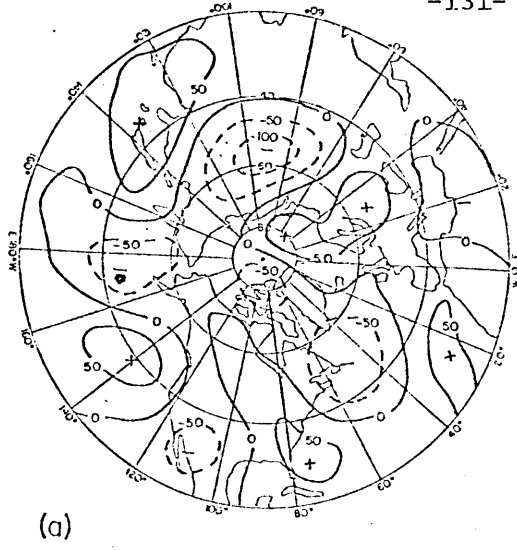


Fig. 5.3. As in Fig. 5.1 for differences (positive - negative).

the development of the North Pacific anomaly pattern are located upstream, and are primarily associated with the zonal flow over eastern Asia and the extreme western North Pacific (relatively stronger westerlies occur before onset of the positive cases). In contrast, knowledge of the sign of the anomalies over the central North Pacific immediately preceding development is likely to be of little value in distinguishing whether a positive case or negative case will subsequently occur.

Although data used in the above analyses were low-pass filtered, the main centers appeared to develop quite rapidly. We now examine similar analyses conducted on unfiltered data for further clues to the character of this rapid development. The starting dates are identical, so that the only difference from the previous analyses is the filtering process.

Fig. 5.4 displays the unfiltered composites for the positive cases at 1 day intervals from day -3 to day 0. The major differences in evolution are mainly associated with a positive anomaly center located to the east of Japan at day -3. This center propagates eastward and intensifies through the period, reaching the key region at day 0. In advance of this feature, a negative center moves southeastward to the subtropical central North Pacific by day 0. This sequence of development suggests that the initial rapid growth of the main center is primarily associated with the propagating, intensifying disturbance which originates in mid-latitudes near Japan. This disturbance slows up but continues to intensify as it approaches the key region. The main center over the subtropical North Pacific also apparently originates

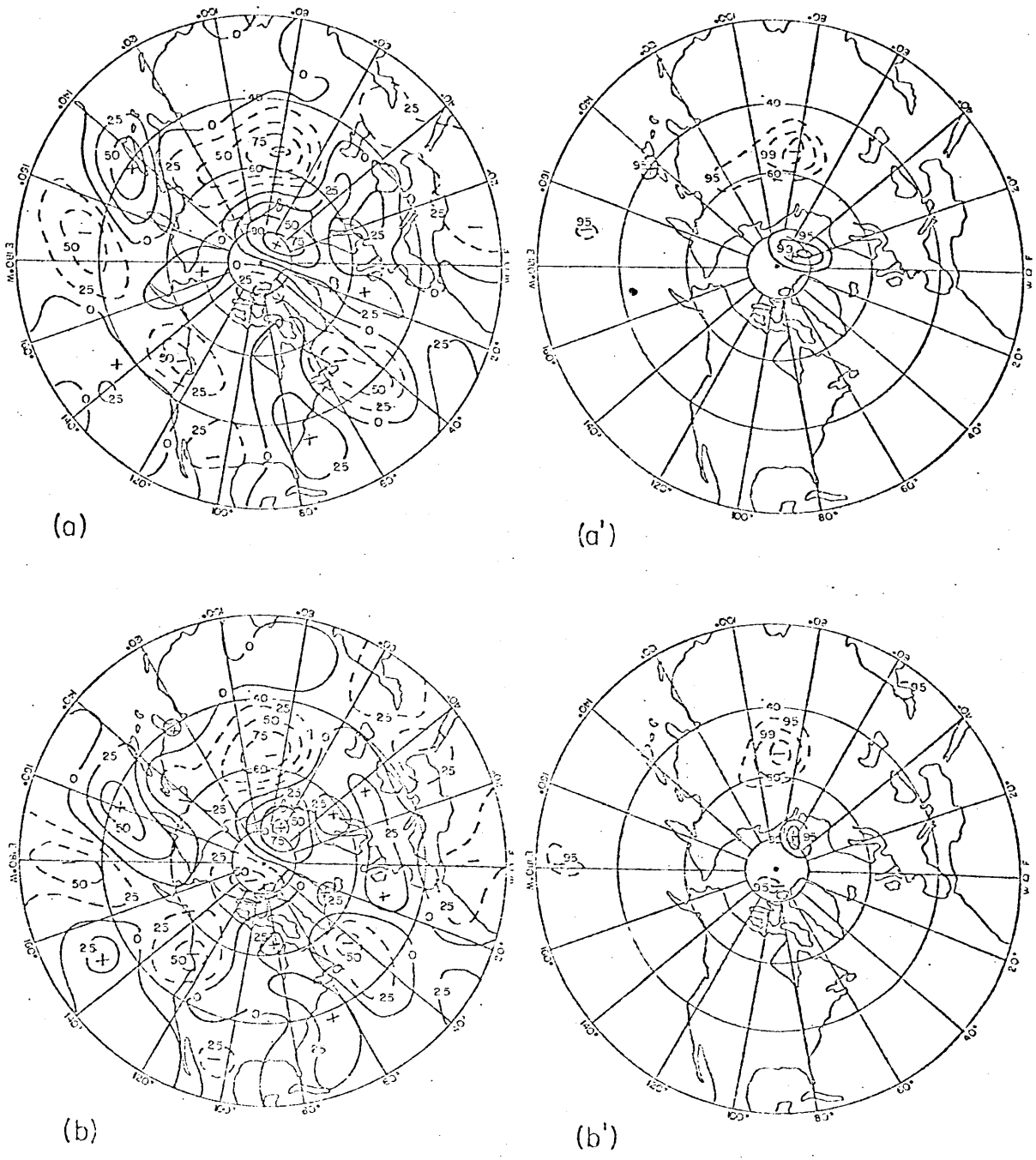
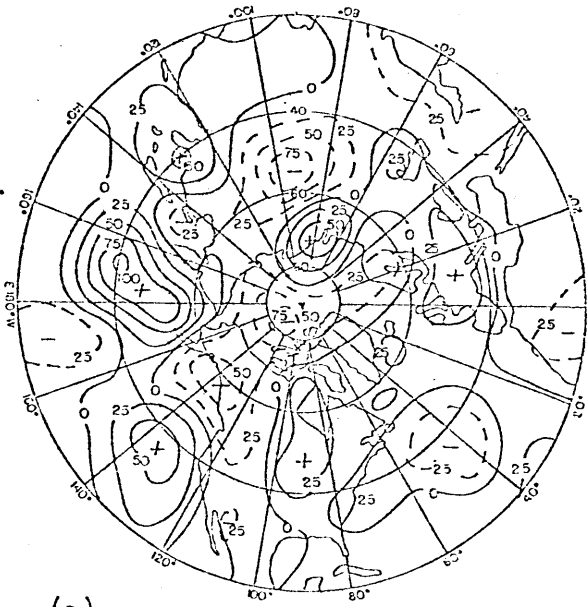
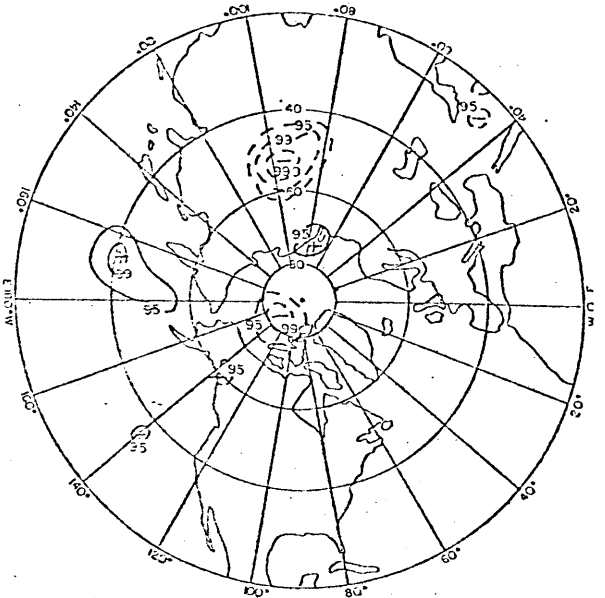


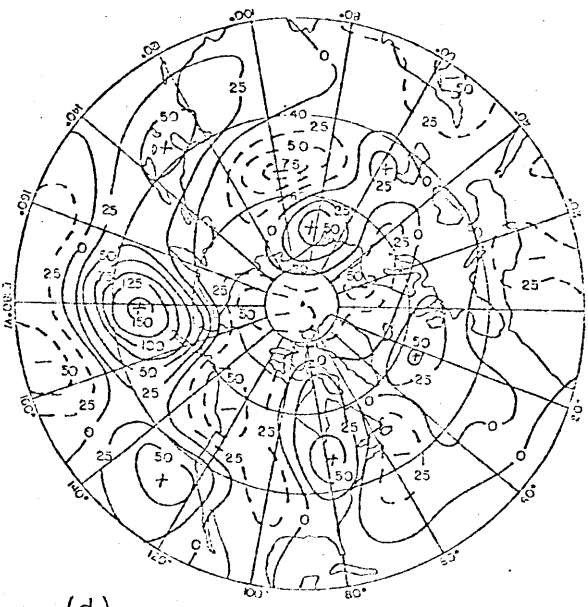
Fig. 5.4. Time composites of unfiltered anomalies for the same 15 PAC positive cases as in Fig. 5.1 at day (a) -3; (b) -2; (c) -1; and (d) 0. Corresponding confidence levels are displayed in (a') - (d').



(c)



(c')



(d)



(d')

Fig. 5.4 (cont.)

from a mid-latitude disturbance. Concurrent with these developments, a larger scale pattern of height rises over the mid-latitude North Pacific with falls to the south is again evident. Maps following day 0 (not shown) indicate that subsequent developments are qualitatively similar to those displayed in the low-pass analyses.

Like the filtered analyses, the unfiltered PAC negative evolution (Fig. 5.5) resembles the corresponding positive sequence. The negative center to the east of Japan on day -3 in the negative analyses, however, is considerably more intense than its positive counterpart. This negative center intensifies and moves eastward to the key region by day 0; the second negative anomaly center over the East China Sea on day -2 follows a similar course, eventually merging with the main center after day 0 (not shown). An interesting feature in the negative case composites is the strong positive anomaly center initially near the key region; the subsequent evolution of this center appears typical of the breakdown of the PAC positive cases (to be discussed later). The difference and corresponding t-test results (Fig. 5.6) confirm our expectations based on the separate positive and negative analyses: immediately in advance of development, the major differences between positive and negative cases are associated with the anomaly pattern over eastern Asia and with the propagating, intensifying mid-latitude disturbance initially near Japan.

Both the ATL and NSU cases, like the PAC cases, exhibit roughly parallel positive and negative evolutions. For brevity, then, only the (positive-negative) difference sequences are presented for these regions.

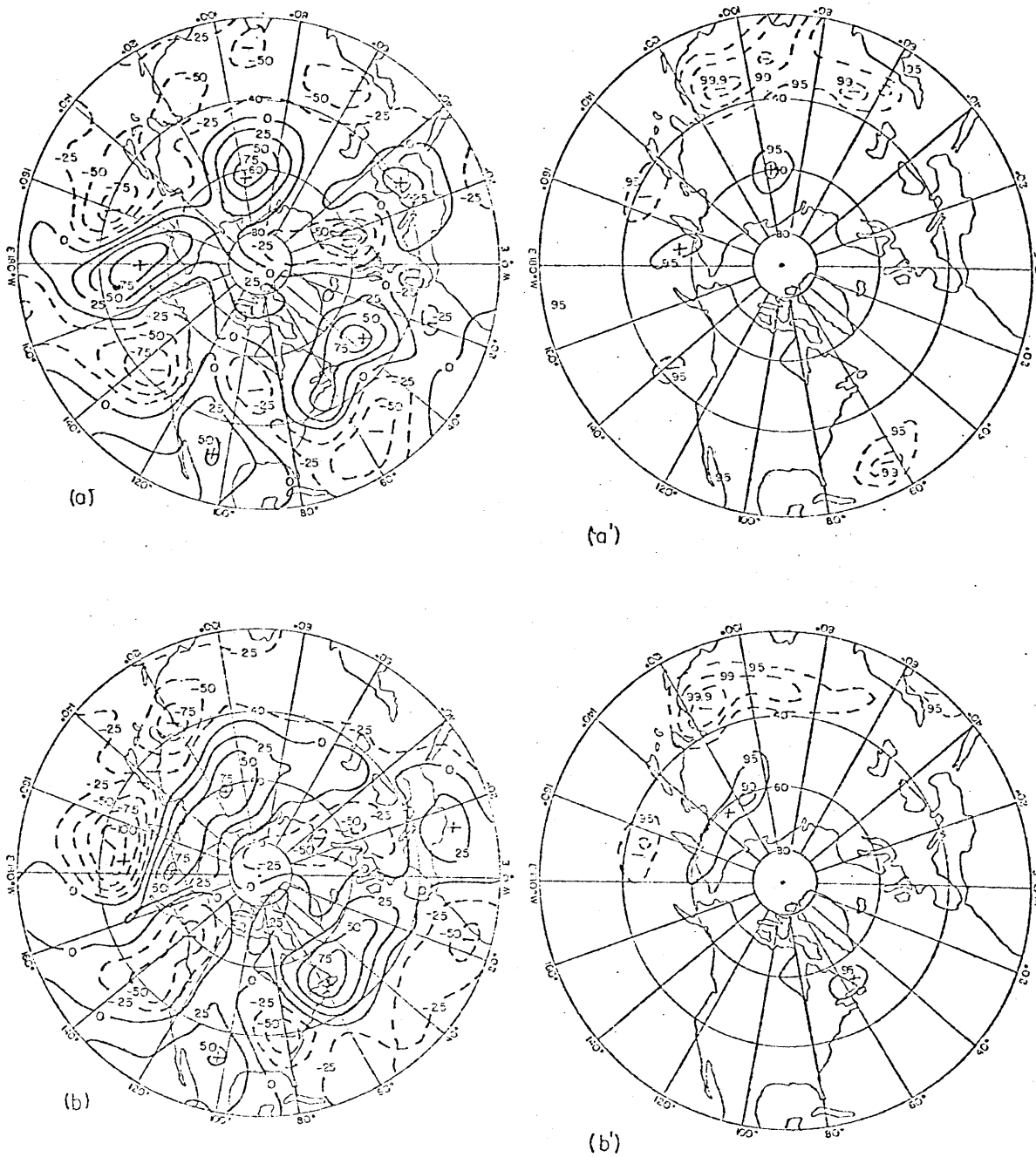


Fig. 5.5. As in Fig. 5.4 for 13 PAC negative cases.

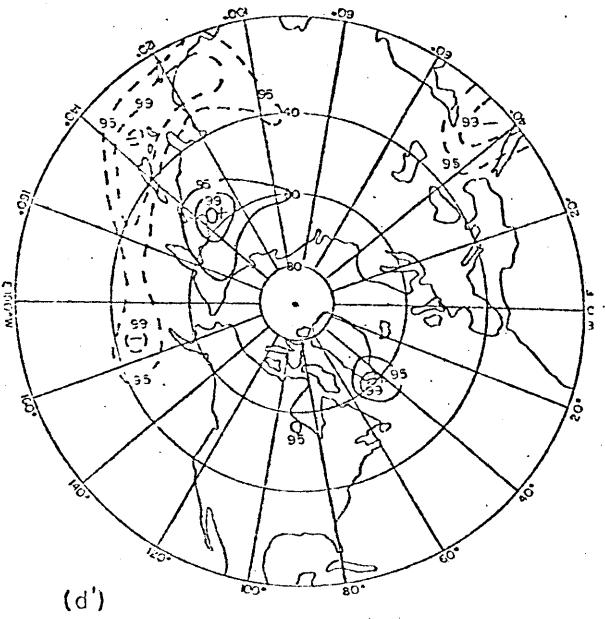
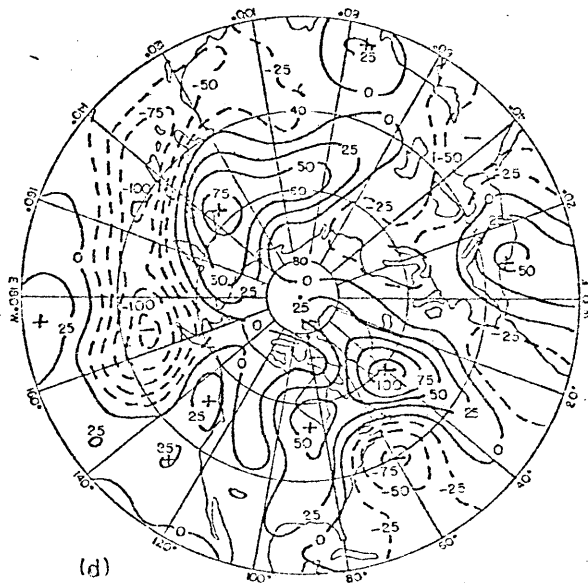
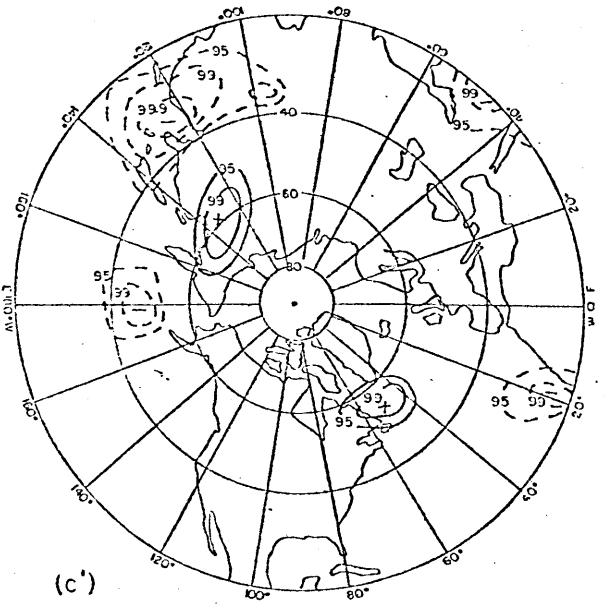
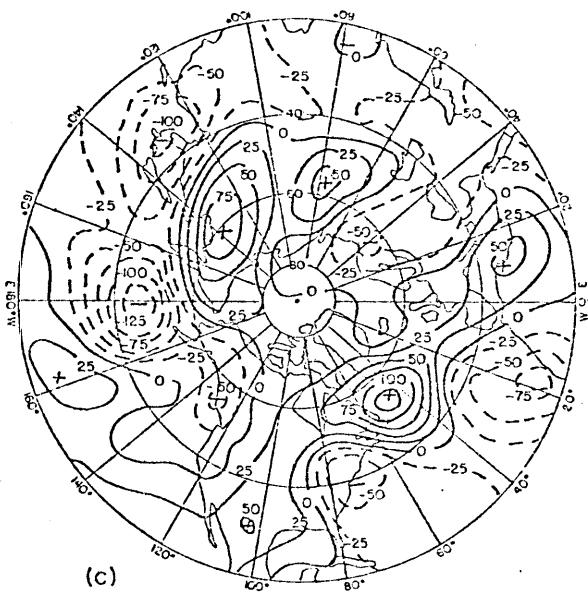


Fig. 5.5 (cont.)

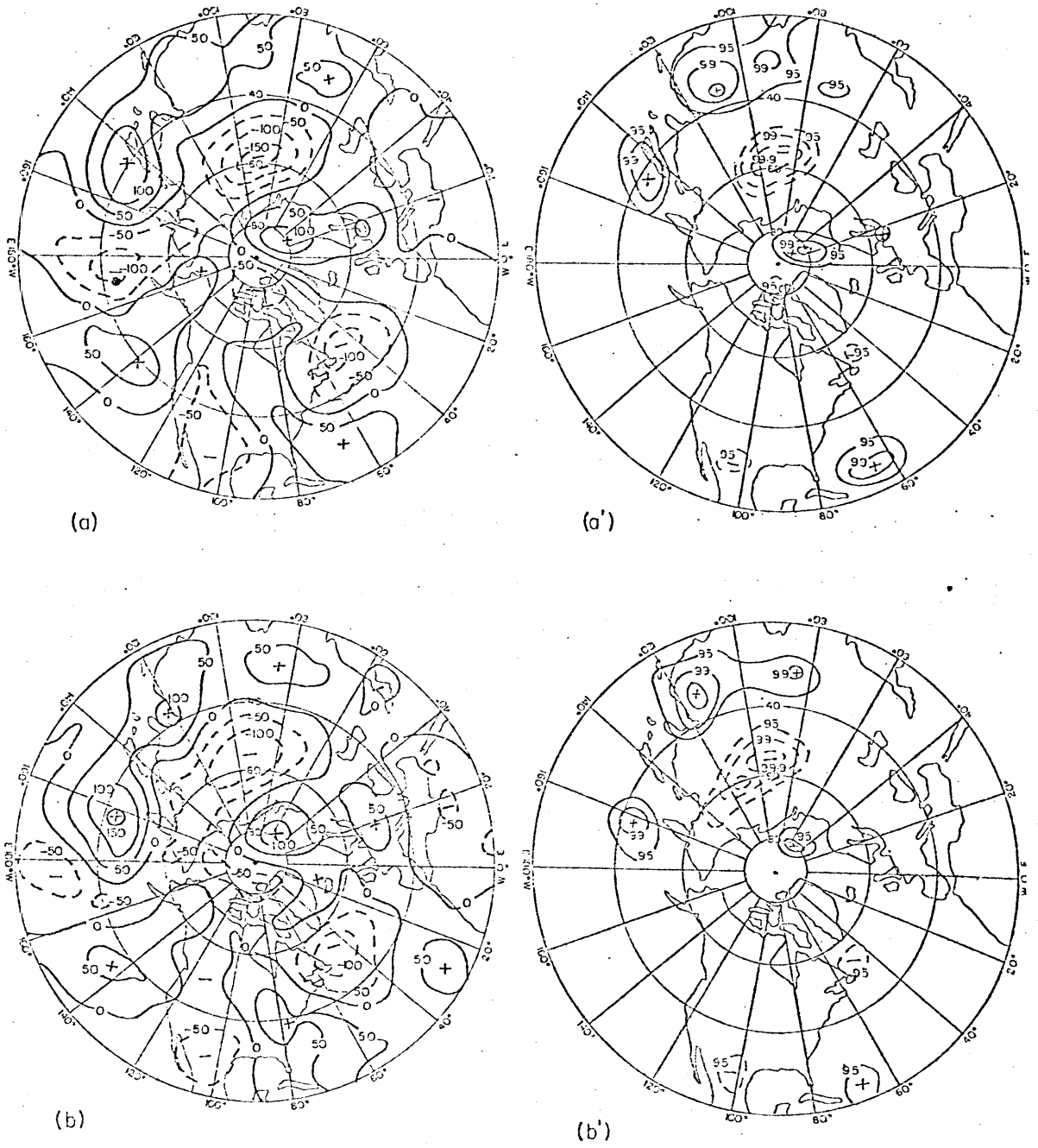


Fig. 5.6. As in Fig. 5.4 for anomaly differences (positive - negative).

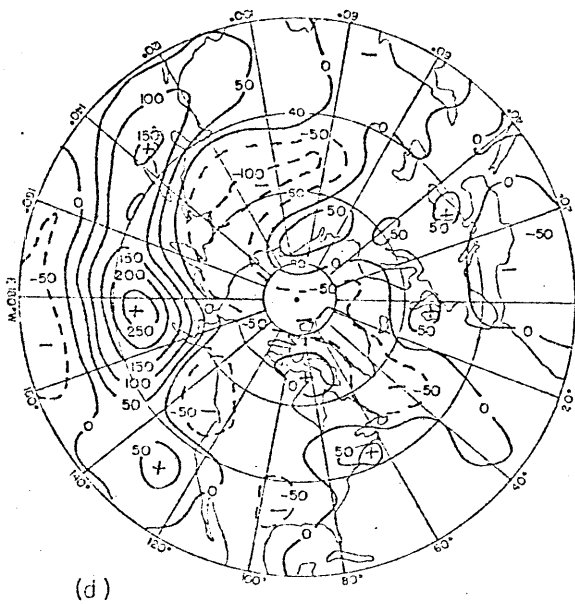
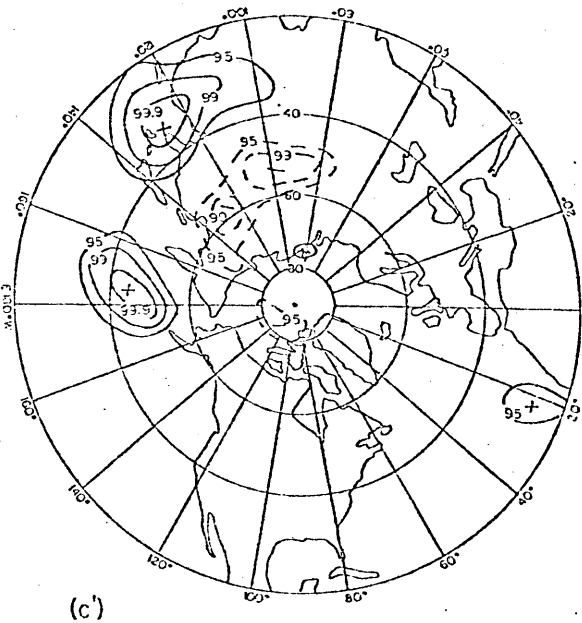


Fig. 5.6 (cont.)

Fig. 5.7 presents the ATL low-pass composite anomaly differences and associated confidence levels at two day intervals from day -4 to day +6; Fig. 5.8 shows similar sequences for the NSU cases. Comparing these evolutions with the corresponding PAC sequences, we see that, particularly preceding onset, the developing patterns for the three regions display several qualitative differences. Nevertheless, in several aspects these evolutions do resemble those just described for the PAC cases. First, the differences between positive and negative means over the key regions are not significant until just prior to onset. Second, both the ATL and NSU composites suggest that energy dispersion occurs downstream from the key region following the development of the main center. The sequence for the NSU cases also indicates that the development of the main center is preceded by a well-defined wavetrain upstream with centers initially over the Atlantic and Europe. The poleward increase in amplitude of the successive centers in this pattern qualitatively agrees with predictions of simple theories of Rossby wave propagation on a sphere (Hoskins and Karoly, 1981). For all three regions, then, downstream energy propagation appears to follow (and, at least for the NSU region, also precedes), the development of the main center, leading after a few days to the establishment of the persistent anomaly pattern.

Parallel unfiltered ATL composites (not shown) also suggest that, at least in the negative cases, an amplifying, eastward propagating, baroclinic disturbance is involved in the initial growth of the main center. The NSU unfiltered composites (not shown), in contrast, provide no significant indication of phase propagation immediately preceding development.

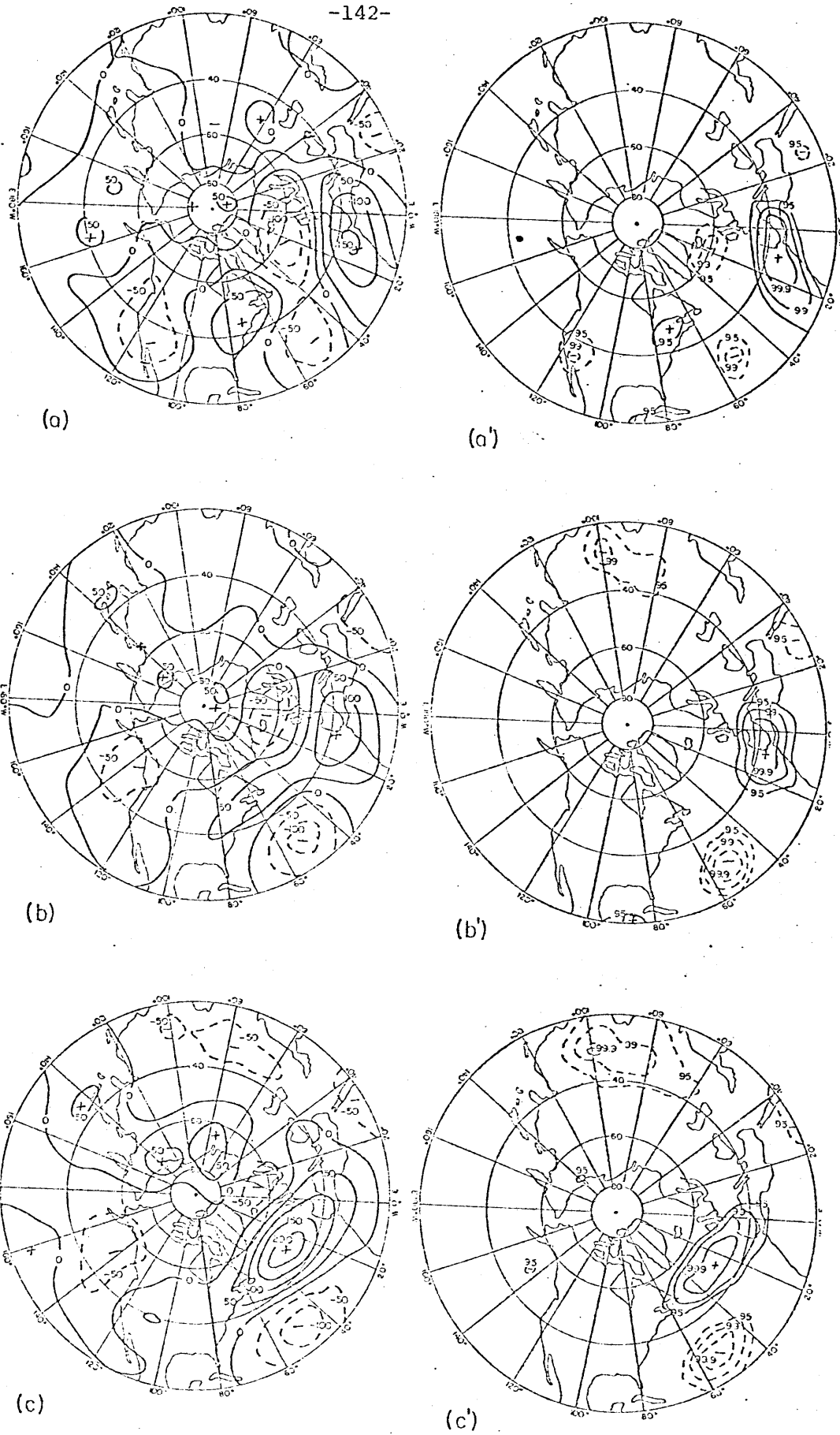
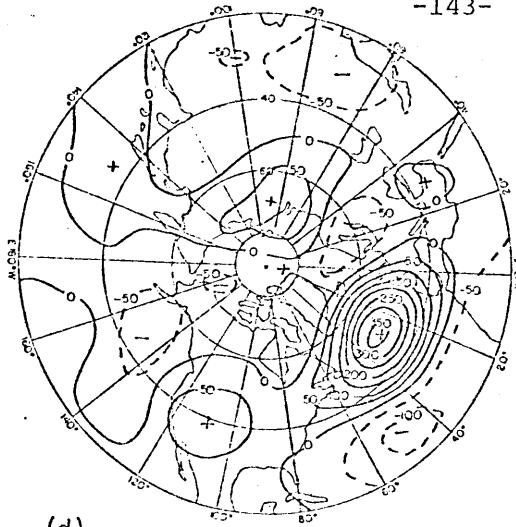
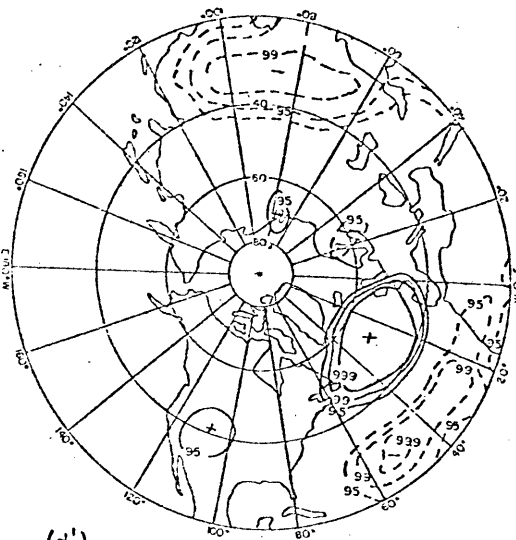


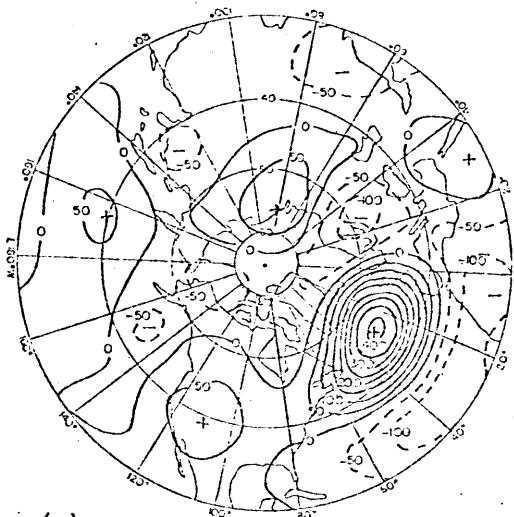
Fig. 5.7. As in Fig. 5.1 for ATL low-pass anomaly differences.



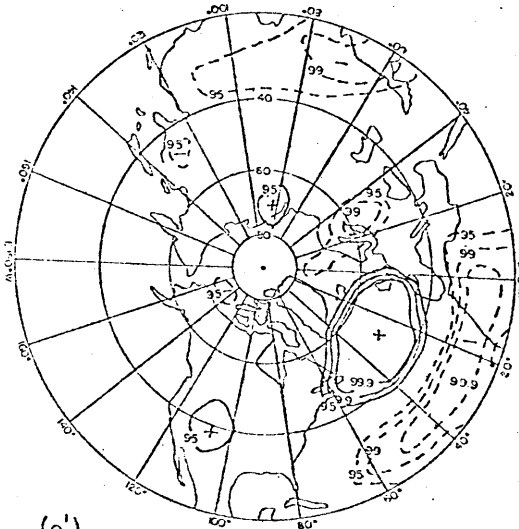
(d)



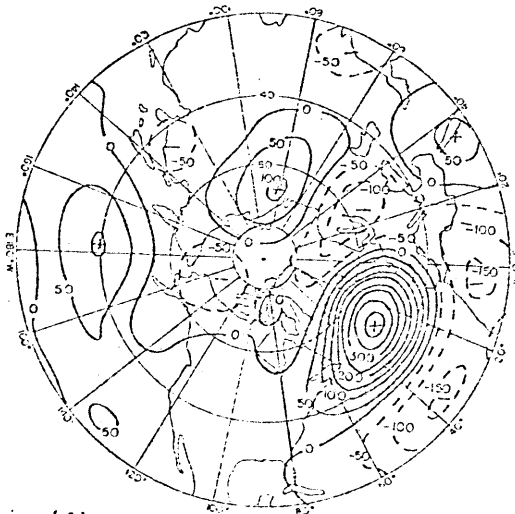
(d')



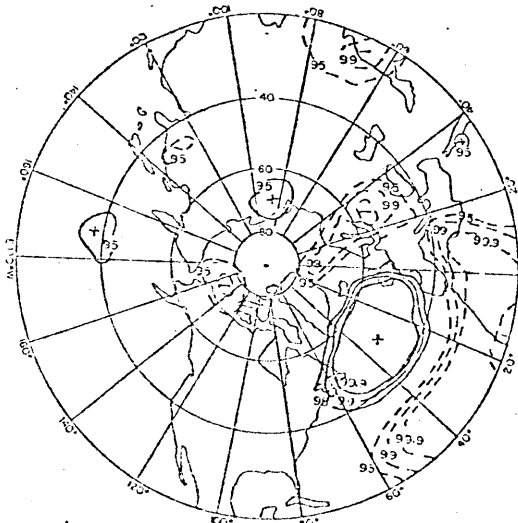
(e)



(e')



(f)



(f')

Fig. 5.7 (cont.)

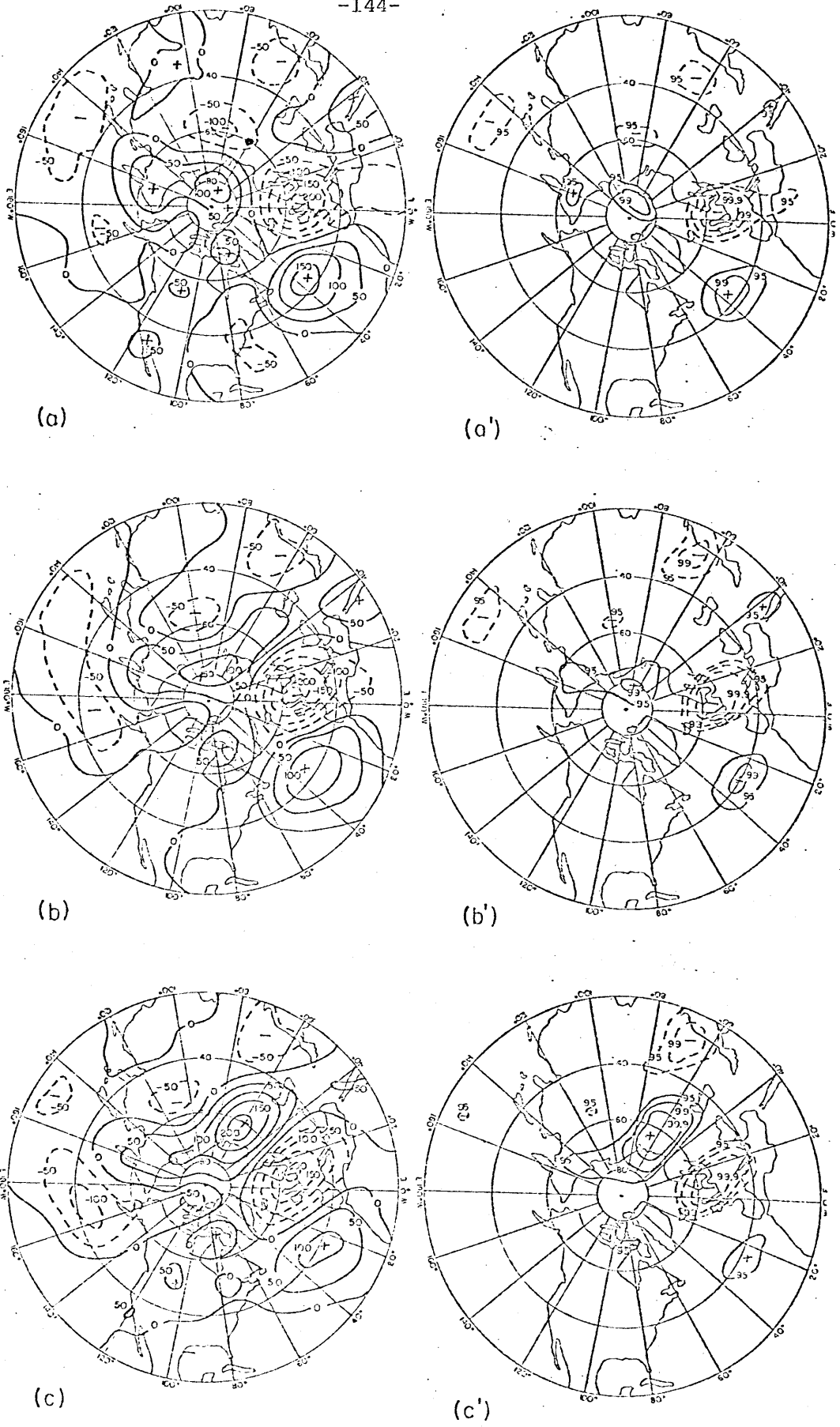


Fig. 5.8. As in Fig. 5.1 for NSU low-pass anomaly differences.

Investigators have suggested that blocking over the oceans is often characterized by the amplification of certain zonal wavenumbers of the 500 mb heights (Austin, 1980; Colucci, et al., 1981). We have examined this possibility for our cases by constructing composite vector time series of zonal Fourier components $k=0-6$ of the anomalies at the corresponding "key" latitudes (Fig. 5.9). Consistent with the time mean composites presented in the previous chapter, we see that important contributions to the observed anomalies at the key point are provided by a relatively broad band of components, primarily wavenumbers $k=0-4$. Thus, these analyses do not suggest a strong dominance by a particular wavenumber in the development of the patterns. Nor do they suggest a systematic precursor: prior to onset the amplitudes are small, typically under 10m, and the vectors tend to have a haphazard orientation with respect to the vertical axis, indicating a lack of wave coherence locally. Before the major amplification most components show some rotation, indicating propagation. During the period of maximum amplification, however, little propagation is evident for wavenumbers $k < 5$ consistent with an interpretation of the development in terms of stationary waves. Wavenumbers 6 and greater continue to propagate with little change through the event, indicating that they are not contributing significantly to the representation* of the stationary pattern.

Simple models of Rossby wave propagation away from a localized source (Hoskins and Karoly, 1981) suggest that, if the source of the forcing is in the tropics, shorter wavelengths (roughly, $k > 4-5$)

*This observation does not preclude the possibility that the propagating short waves may still be important to the underlying dynamics, as suggested by some recent theories (Green, 1977; Austin, 1980; Reinhold, 1981).

Fig. 5.9. Composite vector time series of zonal Fourier components $k = 0 - 6$ of the low-pass anomalies at the "key" latitude Θ . The amplitude is proportional to the length of the vector. The phase is given by the angle measured in the clockwise direction between the positive vertical axis through the origin of the vector and the vector itself (positive angles eastward); thus clockwise (counter-clockwise) rotation with increasing time indicates eastward (westward) propagation. The vertical component of a vector is proportional to the contribution by that wavenumber to the observed anomaly at longitude $\tilde{\lambda}$ (the reference longitude) on that day. (a) PAC positive cases; (b) PAC negative cases; (c) ATL positive cases; (d) ATL negative cases; (e) NSU positive cases; (f) NSU negative cases.

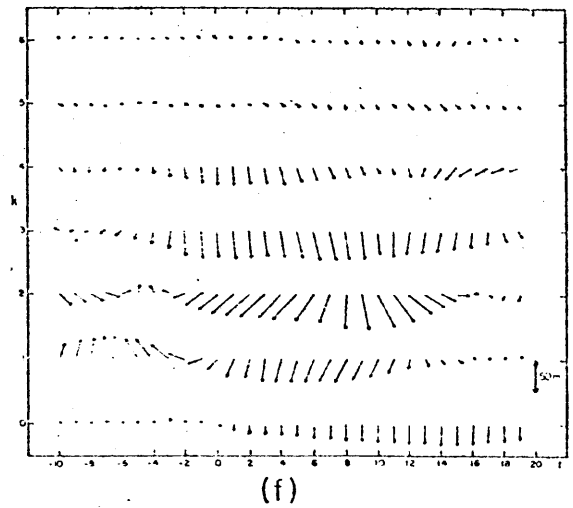
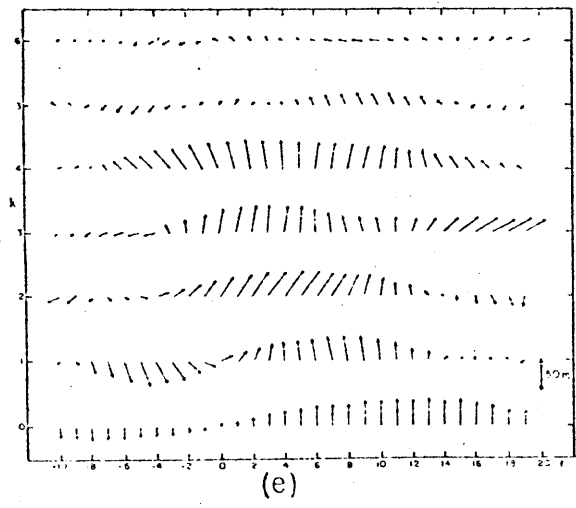
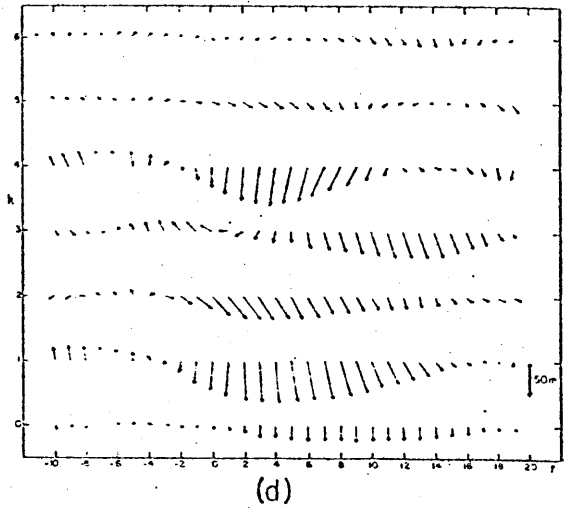
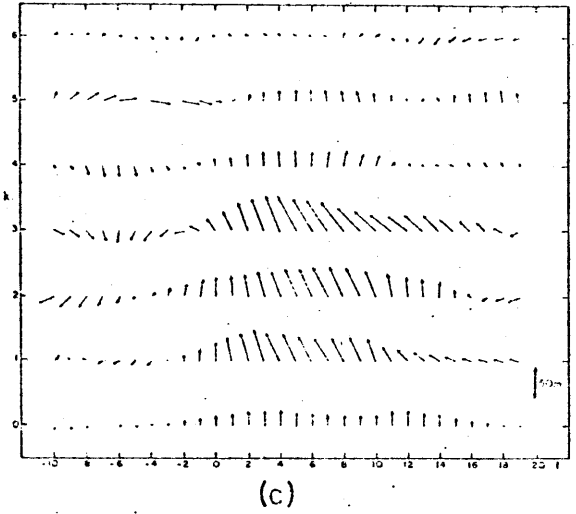
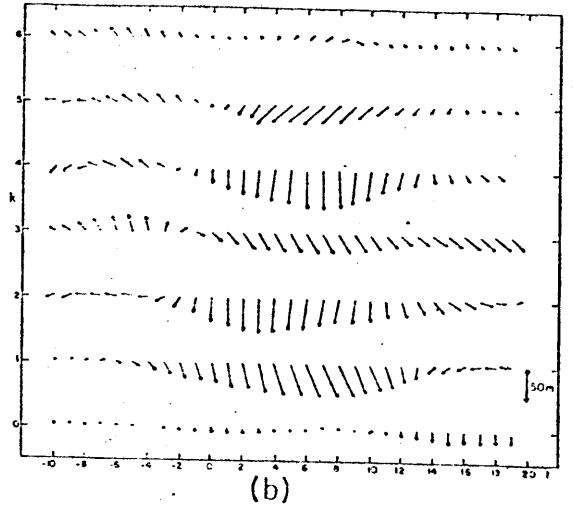
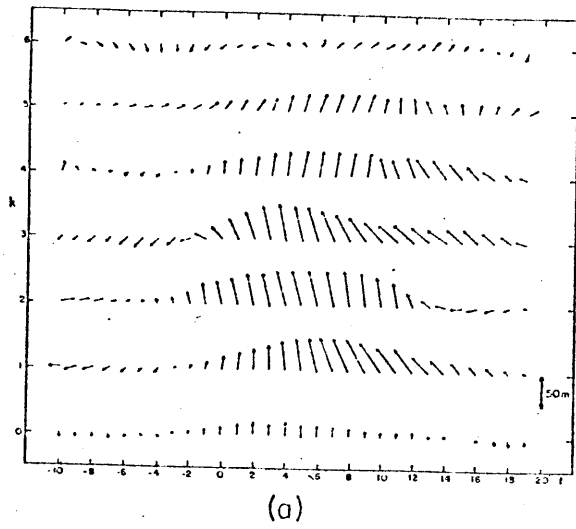


Fig. 5.9

will be trapped equatorward of the poleward side of the jet so that only the very long wavelengths will appear with significant amplitudes at high latitudes. The low wavenumber predominance of the observed patterns is consistent with a tropical source, although alternative mechanisms may also lead to this result. The composite development, however, is not consistent with certain other simple models of wave amplification, e.g., free barotropic resonant triad interactions, since all significant components appear to grow simultaneously.**

A further indication of the character of the developments is obtained by examining how the vertical structures evolve in time. For this purpose, parallel development composites for the 1000, 700, 500, 300 and 100 mb height anomalies were prepared from unfiltered data following the procedures described previously. Data at these levels were available for the 11 winters from 1965-1966 through 1975-1976, so that the composites were formed from the previously listed cases (Appendix 2) that fell within this period. For brevity, only the PAC evolutions are discussed in detail.

Fig. 5.10 presents longitude-pressure cross sections at 45N and 20N of the unfiltered PAC positive composite anomalies at one-day intervals from day -3 to day 0. We see that, consistent with the previous 500 mb analyses, the rapid development of the main center appears to be primarily associated with an amplifying, eastward propagating mid-latitude disturbance. This feature has pronounced westward tilts with height during this period, suggesting that a

**Resonant interactions may still be important in particular blocking cases (Colucci, et al., 1981).

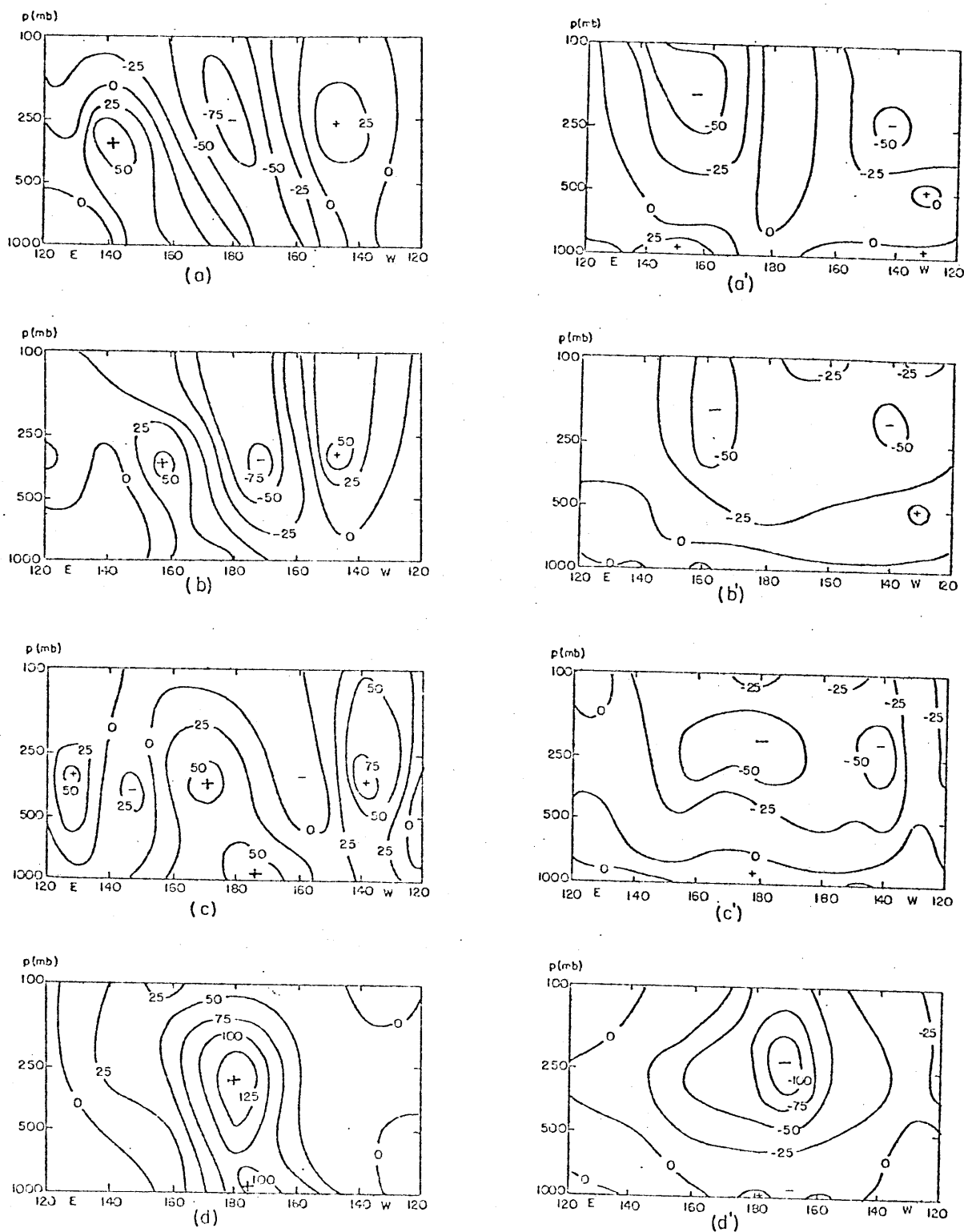


Fig. 5.10. Composite longitude-pressure cross-sections of unfiltered anomalies (units: m) for 15 PAC positive cases at 45 N on (a) day -3; (b) day -2; (c) day -1; (d) day 0. Parallel analyses at 20 N are presented in (a') - (d').

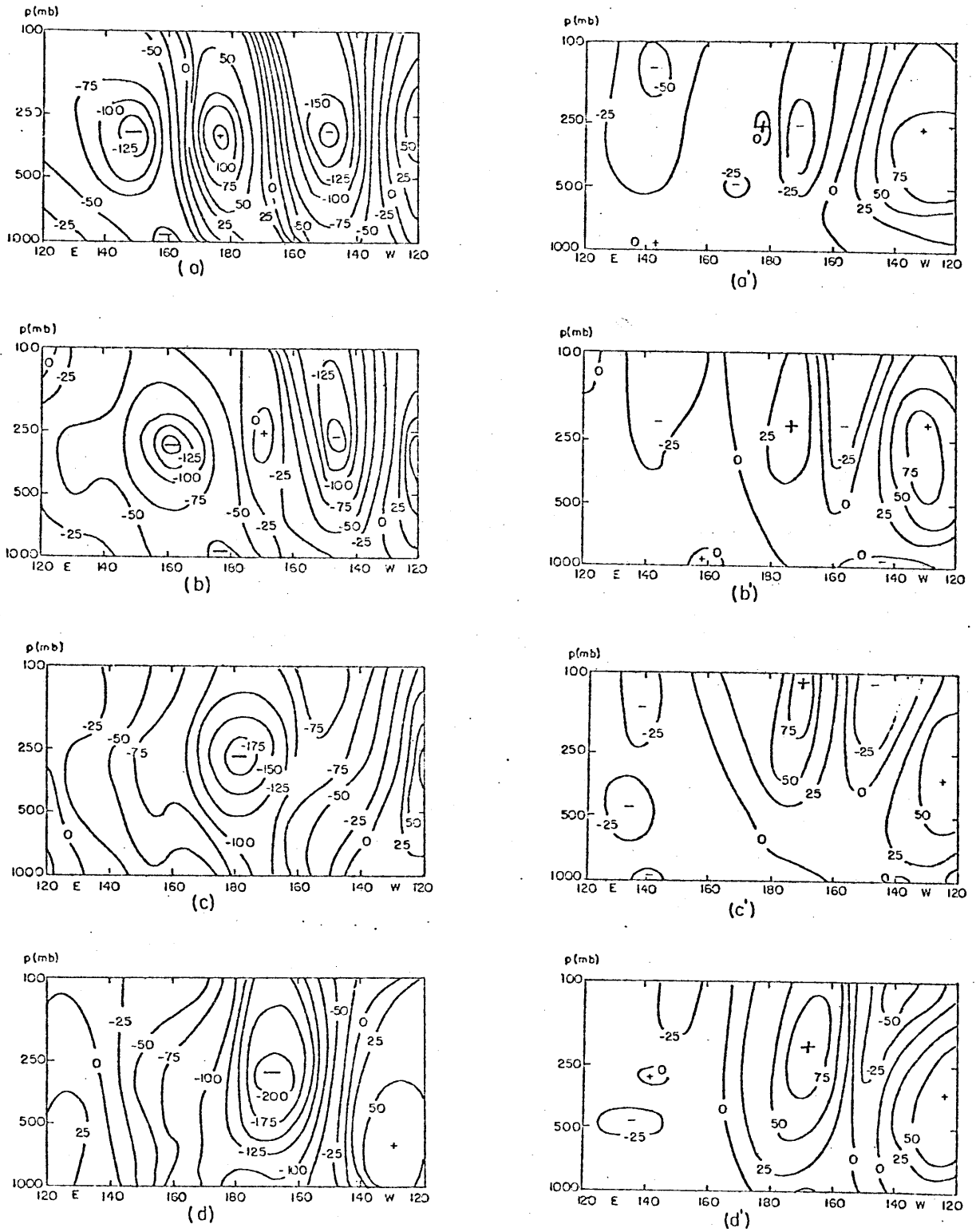


Fig. 5.11. As in Fig. 5.10 for 9 PAC negative cases.

substantial baroclinic contribution is involved in its amplification. There are two maxima in the vertical structure, with peaks at 1000 mb and near 300 mb. A similar structure is observed in numerical studies of nonlinear effects on growing baroclinic waves of long synoptic scales (Gall, 1976; Simmons and Hoskins, 1978). Such a structure, however, may also be partly an artifact of data coverage since, over this region, data are more plentiful at these levels. Nevertheless, comparison of the relative positions of the centers at the data-rich levels suggests that there are pronounced westward tilts with height throughout the troposphere, and that, at an early stage in the development, the maximum anomalies are realized in the upper troposphere.

The corresponding development at 20N indicates that, in parallel with its mid-latitude positive counterpart, the main negative center progresses eastward across the Pacific through day 0. Subtropical negative anomalies are initially confined primarily to the upper troposphere. Following day 0 (not shown), however, 1000 mb heights continue to fall over the central Pacific, leading to the establishment of a cold-core negative center with little or no evidence of tilts throughout the troposphere.

Fig. 5.11 shows similar analyses for the PAC negative cases. In many respects, the vertical evolution parallels that of the positive cases. The main center propagates eastward and intensifies through the period. The associated trough axis initially tilts strongly westward with height, but becomes nearly vertical by day 0. Double maxima are also evident in the vertical structure early in the evolution, giving way to a single major center in the upper troposphere.

by day 0. The subtropical patterns are initially rather ill-defined, but a positive center is evident over the subtropical mid-Pacific from day -2 onwards. By day 0 positive anomalies associated with this feature extend with little vertical tilt from the surface to above 100 mb.

Similar analyses for the ATL and NSU regions (not shown) also indicate that maximum amplitudes are reached in the upper troposphere at an early stage in the development, and suggest predominantly weak westward vertical tilts in the anomaly axes during amplification.

D. Breakdown

The previous analyses suggest that persistent anomaly patterns often develop rapidly, with corresponding positive and negative cases displaying several parallel features. We now briefly examine the subsequent breakdowns of the patterns for further evidence of systematic behaviors. Composites for this section are constructed relative to the time when the anomaly first falls below the threshold value at the key point. The unfiltered analyses provided no obvious indication that small-scale, mobile disturbances were systematically involved in the breakdowns; for this reason, only low-pass composites are presented.

Figs. 5.12 and 5.13 present, respectively, composite low-pass analyses for the PAC positive cases and negative cases at two-day intervals from 4 days prior to breakdown (day -4) to 6 days following breakdown (day +6). We see that during breakdown the evolutions also display a number of striking similarities. Up until day -2, the patterns strongly resemble the PAC composite patterns described previously. Breakdown then precedes rapidly. By day 0, the main

centers have moved northwestward to the Bering Sea and have weakened considerably. These features than remain nearly quasi-stationary and continue to decay. Anomalies over the key region are not significantly different from zero beyond day +2.

Differences between the composite maps immediately preceding breakdown and the corresponding maps following development may suggest clues to the cause of the breakdown. Comparison of the maps 2 days before breakdown with (for example) the maps 6 days after onset, however, reveals few striking changes. For the positive cases, the most noticeable difference is the intensification and displacement of the downstream center to just west of the Washington coastline. We suspect that this development, which is also reflected in an asymmetry between the positive and negative case mean composites discussed in the previous chapter, is at least partly the result of orographic effects: in particular, the anomalous northerly flow over the Alaska Range into the Gulf of Alaska in the positive cases is often followed by intense cyclogenesis off the northwest coast (see Winston, 1955). The negative cases, in contrast, show little change in the location or intensity of the downstream center.

Another difference evident in both the positive and negative cases when comparing post-development with pre-breakdown maps is the change in sign of the anomaly centers near Japan: whereas at and following development anomalies in this region have the same sign as in the key region, immediately preceding breakdown, anomalies in this area and in the key region are of opposite sign. This change may be related to variations in the zonal wind over the southwestern

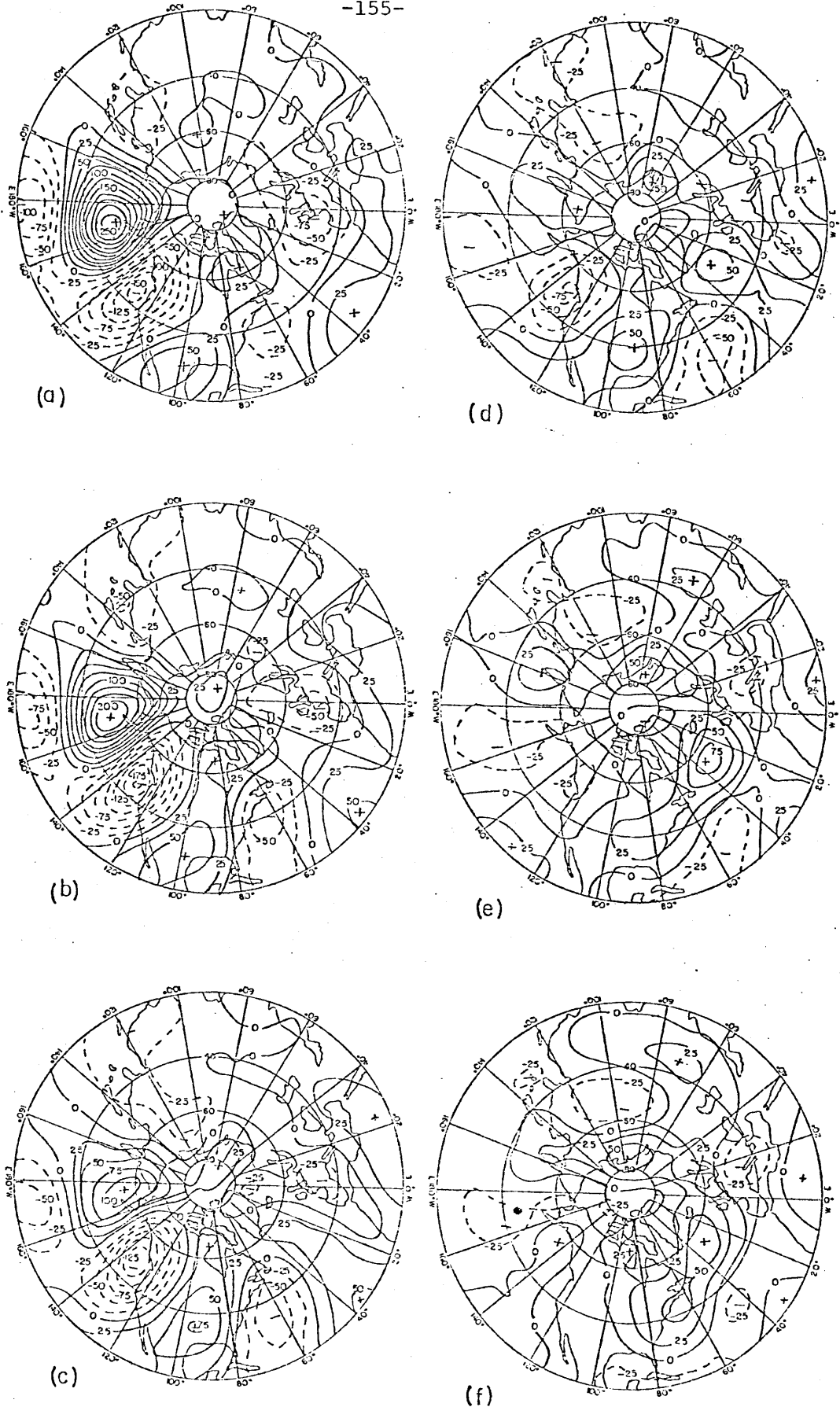


Fig. 5.12. Composites of the breakdown of the PAC positive cases, low-pass filtered anomalies (units:m) at (a) day -4; (b) day -2; (c) day 0; (d) day +2; (e) day +4; and (f) day +6.

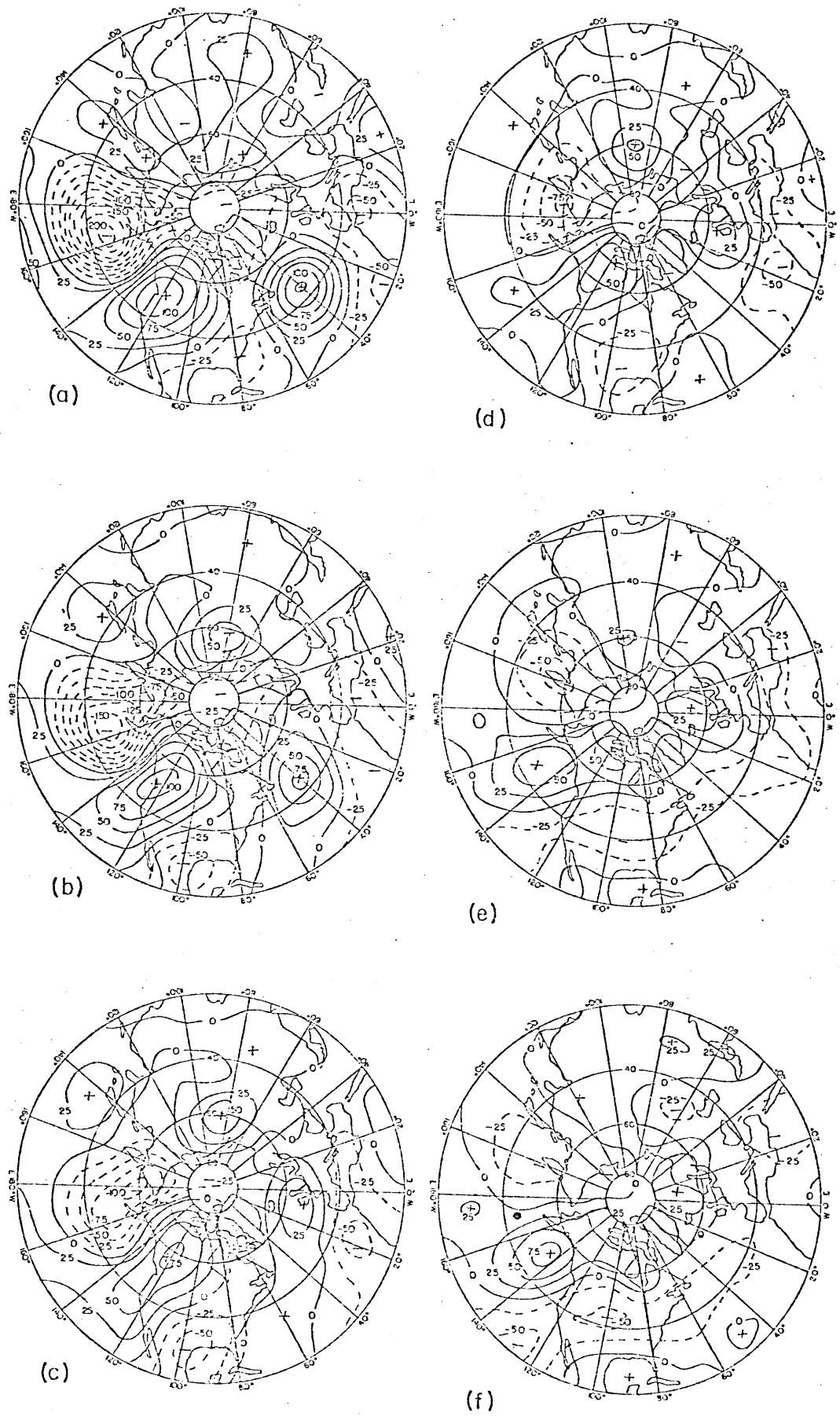


FIG. 5.13. As in Fig. 5.12 for PAC negative cases.

North Pacific; differences are so small, however, that we are presently disinclined to attribute much significance to this result.

Similar composite maps for the ATL cases are displayed in Figs. 5.14 and 5.15. Again, up until 2 days before breakdown the primary features of the ATL pattern are evident. The subsequent evolutions of the main centers bear some resemblance to the behavior seen for the PAC cases. Between day 0 and day 2 these centers have retrogressed and weakened. At day 4 these centers have drifted slightly northwest with little change in intensity. There is some indication in these analyses that, initially, the main center decays and retrogresses, and, subsequently, changes occur in the remainder of the pattern. As for the PAC cases, however, slight differences between corresponding post-development and pre-breakdown maps are evident, but are of dubious significance.

Similar sequences for the NSU cases are shown in Fig. 5.16 and 5.17. Comparing these maps to the earlier development composites, we see that the NSU patterns display somewhat greater differences than found for either the PAC or ATL patterns. The most striking change from the earlier maps is the absence of major anomaly centers upstream of the key region immediately prior to breakdown. The somewhat greater transience of the upstream and downstream NSU anomaly centers was reflected earlier in the case mean composites, where the NSU patterns had relatively weaker contemporaneous correlations and appeared to have a more regional character than their PAC and ATL counterparts. The subsequent downstream deepening (and also successive downstream weakening) of the centers in the NSU pattern thus provides

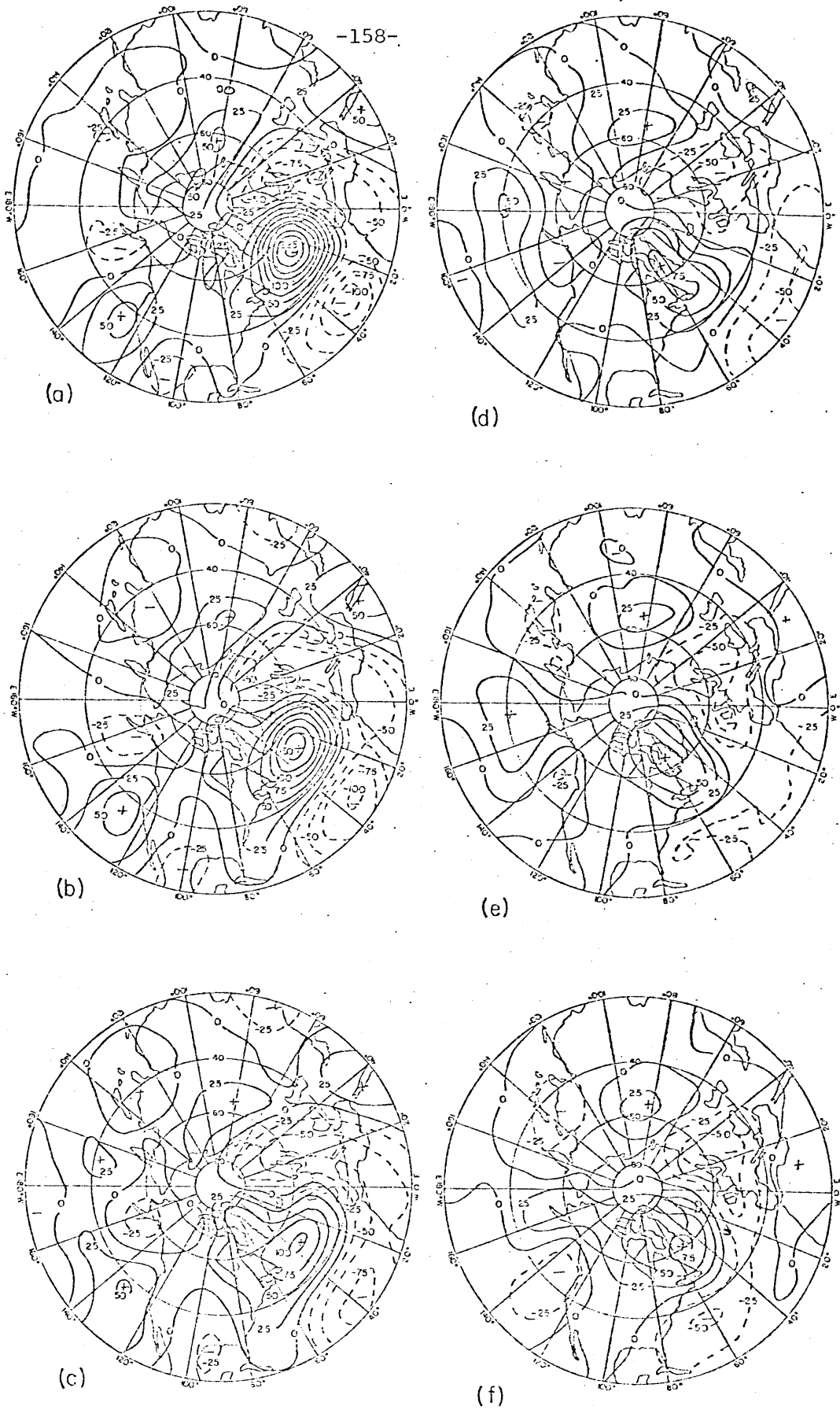


Fig. 5.14. As in Fig. 5.12 for ATL positive cases.

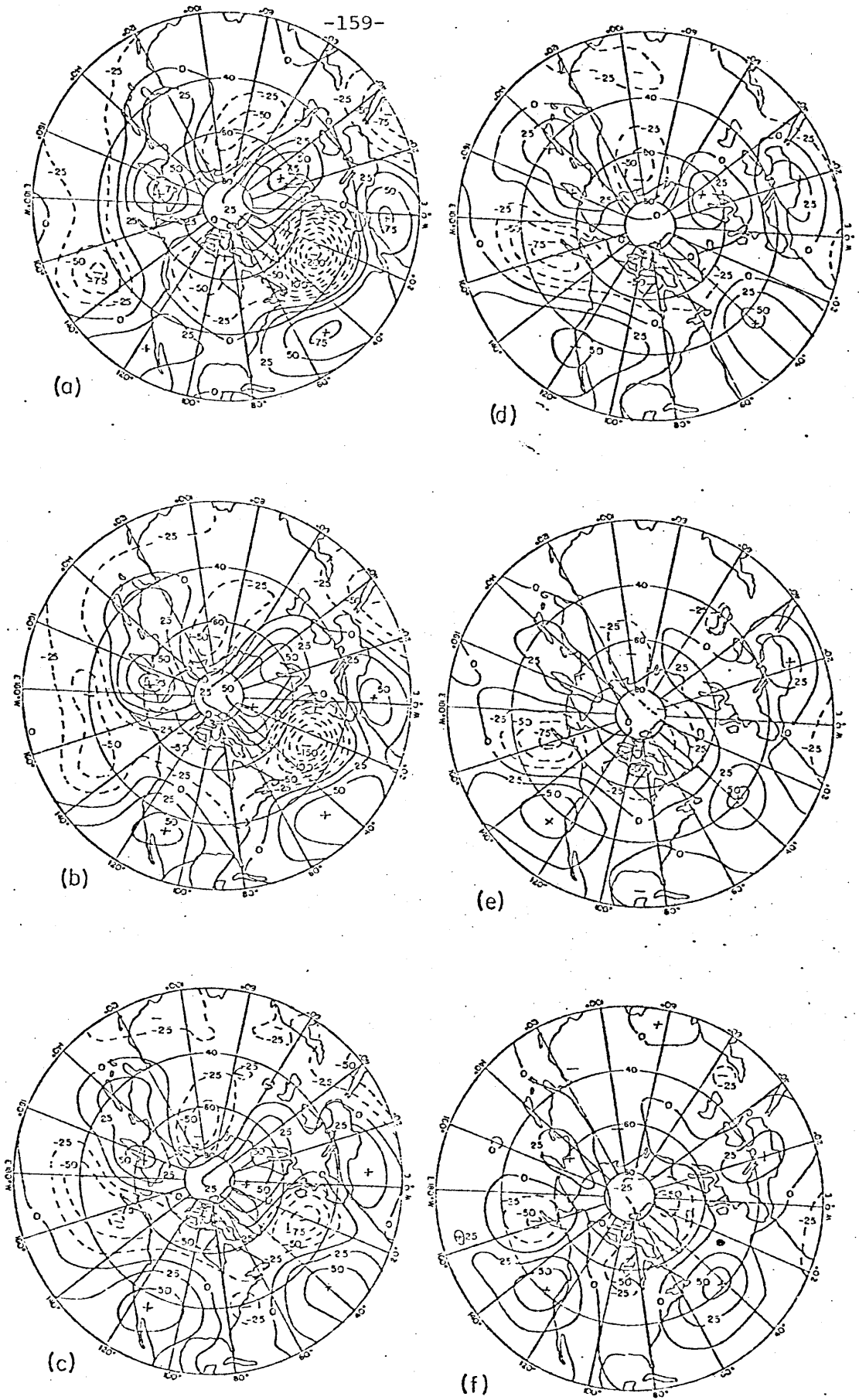


Fig. 5.15. As in Fig. 5.12 for ATL negative cases.

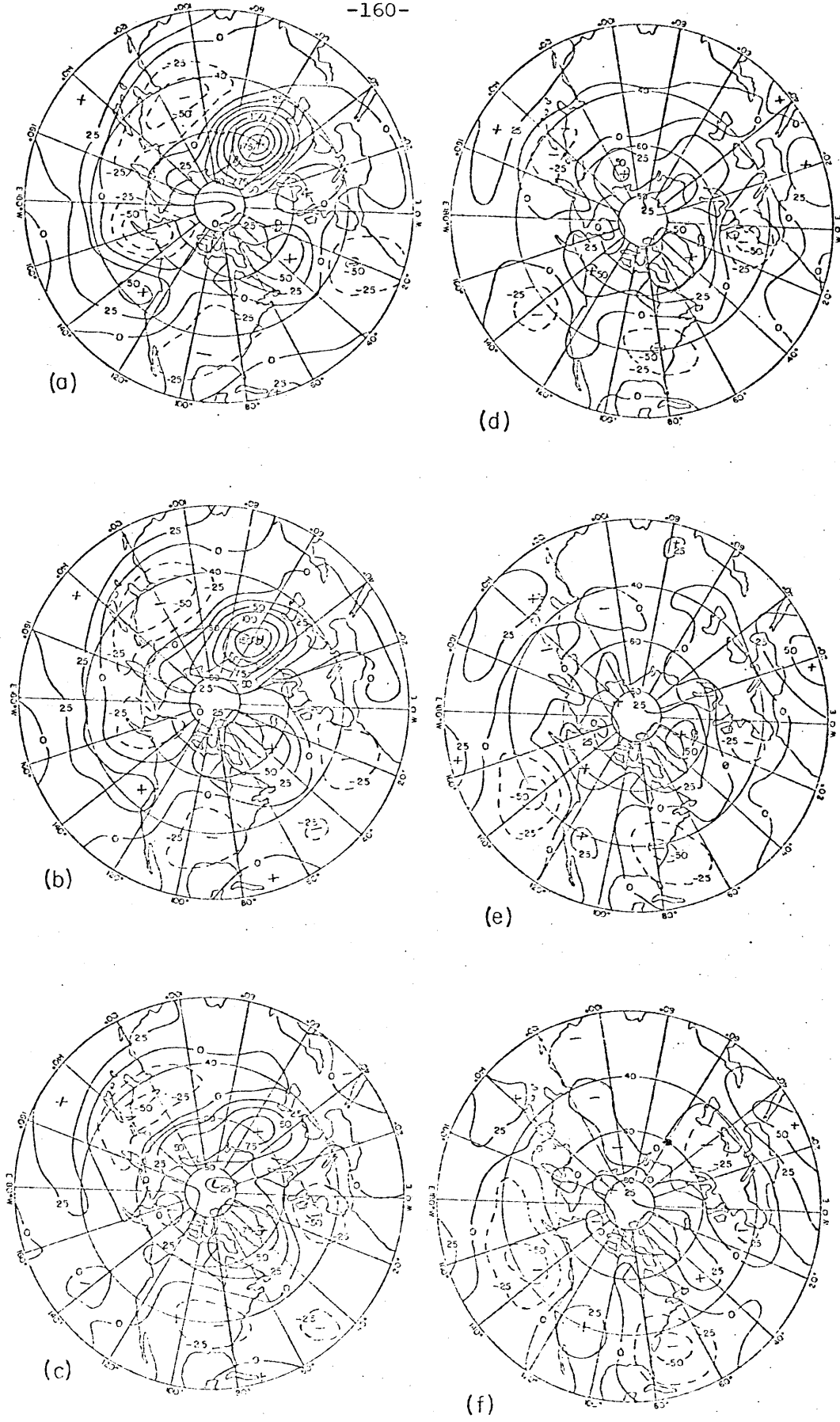


Fig. 5.16. As in Fig. 5.12 for NSU positive cases.

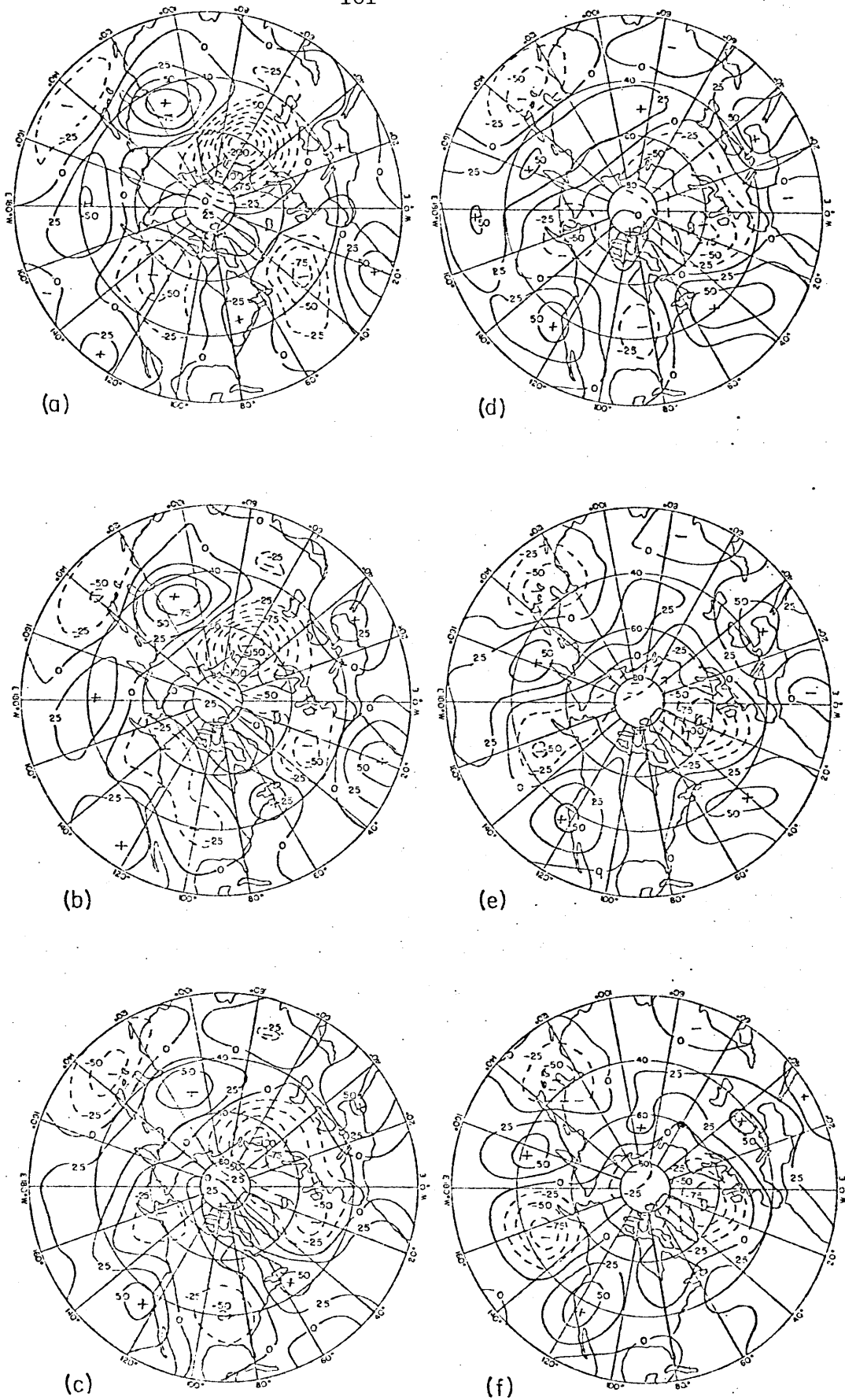


Fig. 5.17. As in Fig. 5.12 for NSU negative cases.

a preliminary basis for predicting the onset and also the decay of this pattern several days in advance.

E. Discussion

The results of the previous analyses suggest a number of typical characteristics in the evolution of persistent anomaly patterns:

1) Development rates are often rapid (full establishment in less than a week).

2) Over the key region, there is little evidence of an atmospheric precursor until just prior to onset.

3) Following onset, anomaly centers develop and intensify in sequence, forming a quasi-stationary wavetrain downstream from the main center. Intensification occurs with little indication of phase propagation. This leads to the establishment of the persistent anomaly pattern.

4) Breakdown rates are also often rapid. Until immediately prior to breakdown, the patterns closely resemble the corresponding patterns obtained following development.

5) From development through decay, corresponding positive and negative patterns display striking similarities in their evolutions.

The development of the wavetrains downstream from the main centers qualitatively agrees with simple time-dependent models of energy dispersion on a sphere away from a localized, transient source of vorticity (Hoskins, et al., 1977; Hoskins, 1978). The NSU cases are also typically preceded by a well-defined upstream wavetrain. The sequence of development for the PAC cases suggests that the initial rapid growth of the main center is primarily associated with

a propagating, intensifying disturbance which originates in mid-latitudes. The vertical structure of this disturbance somewhat resembles that found in numerical studies of nonlinear amplifying baroclinic waves of long synoptic scales (Gall, 1976; Simmons and Hoskins, 1978).

Horel and Wallace (1981) have recently presented convincing observational evidence indicating some relationship between tropical Pacific sea-surface temperature anomalies and the sign of the North Pacific anomaly pattern. Their work is supported by results obtained from general circulation studies on the atmosphere's response to changes in external forcing (particularly to tropical sea-surface temperature anomalies) (e.g., Rowntree, 1972, 1976; Opsteegh and Van Den Dool, 1980; Webster, 1981). The time scales for changes in such forcing, however, is presumably much longer than the time scales that we typically find for the development and decay of persistent anomalies. This suggests that these patterns often, and perhaps primarily, grow and decay while the external forcing remains nearly fixed. Further support for the view that the patterns evolve mainly by internal processes comes from recent modelling studies by Lau (1981) and Blackmon (personal communication), which demonstrate that anomalies in the external forcing are not required to produce patterns similar to those described here.

A possible interpretation for the correlation between tropical Pacific sea-surface temperatures and the PAC pattern is provided by Hoskins (1978). He suggests that enhanced convection may be expected over an anomalously warm tropical ocean, leading to increased upper

level divergence and therefore to enhanced forcing of anticyclonic vorticity. This may be expected to produce an anomalous wavetrain extending into the extratropics downstream from the forcing region.

Our results, however, suggest that the causal link between tropical sea-surface temperatures and the Pacific pattern may be more subtle than indicated by this picture. An intriguing clue is provided by the significant pattern located upstream over Asia and the extreme western Pacific preceding the development of the PAC cases. This pattern somewhat resembles that of composite pressure anomalies associated with the southern oscillation (see, e.g., Troup, 1965), a phenomenon clearly linked to tropical Pacific sea-surface temperatures (Horel and Wallace, 1981, and refs.). The structure of this pattern suggests that the associated wind anomalies are primarily in the zonal flow over both the Himalayas and the southwestern North Pacific. Whether such anomalies will give rise to significant anomalous wavetrains remains to be seen; recent theoretical work (Branstator, personal communication; Karoly, personal communication), tends to support the idea that relatively modest changes in the mean flow may give rise to significant anomalous wavetrains, even for fixed forcings. These mean flow changes may themselves reflect changes in tropical forcing, or alternatively, may bias the character of the disturbances forming in the major cyclogenetic region over eastern Asia and the western North Pacific. The resolution of these issues is beyond the scope of the present study.

The sequential character of the development of the anomaly centers favors the view that local or quasi-local sources are asso-

ciated with their origins. This does not, however, entirely rule out the possibility of quasi-resonant behaviors. Although the structures and evolutions of the patterns indicate that the waves are generally significantly refracted or attenuated before travelling far zonally, the PAC and ATL patterns, in particular, somewhat resemble standing meridional modes, suggesting that north-south reflections may occasionally be important in these regions.

Although our results suggest certain statistical approaches toward forecasting the evolution of the persistent patterns, we have not attempted to do that here. On the longer term, a better approach toward forecasting these features will likely come from a more thorough understanding of their sources and dynamics; in that respect, then, our results provide some potentially fruitful direction.

VI. INTERACTIONS WITH TRANSIENT EDDIES AND THE MAINTENANCE OF PERSISTENT ANOMALIES

A. Introduction

The relationship between stationary waves and transient eddies is of considerable theoretical as well as practical interest. Reinhold (1981) demonstrates that recurrent, persistent flow patterns in a low-order, time-dependent spectral model often bear little resemblance to the equilibrium solutions obtained by neglecting transient eddies. Recent simple theoretical studies (Frederiksen, 1979; Niehaus, 1980) suggest that the presence of a stationary wave can organize preferred regions for cyclogenesis. In contrast, Green (1977) and Austin (1980) propose that persistent large-scale features such as blocking can be dynamically maintained by forcings due to synoptic-scale eddies.

The analyses of Chapter 4 established that persistent height anomalies are associated with highly significant anomalies in the fields of vorticity, temperature and potential vorticity. In this chapter, we examine the contributions of transient eddies toward maintaining local balances in these fields in order to address the question of how changes in the transient eddies are related to changes in the mean flow. This question is intimately related to the basic concept of blocking; that is, that major deformations of the mean flow are accompanied by significant changes in storm activity.

Our approach is as follows: We first describe the procedure for analyzing the budgets. Following this, we review the differences in the mean flows and storm paths for positive and negative cases. We then compare contributions by selected terms to the local,

time mean balances of heat, vorticity and potential vorticity.

The data base for this portion of the study consists of twice-daily NMC final analyses of geopotential height and temperature at 8 levels (1000, 850, 700, 500, 300, 250, 200, 100 mb) for the 11 winter seasons 1965-66 to 1976-77. All calculations were performed on a 5° by 5° latitude-longitude grid. Data were spatially interpolated from the NMC grid to the latitude-longitude grid as described previously. Missing data were linearly interpolated in time. Winds are calculated geostrophically. Composites are constructed from the same cases as in the vertical evolution analyses; case dates are listed in Appendix 2.

B. Procedure

The procedure for comparing budget fields is straightforward. In brief: We first calculate the spatial distribution of any one of the fields, say f_j^+ , for each of the $j=1,2,\dots,M$ positive cases, and similarly determine the corresponding distributions f_k^- for the $k=1,2,\dots,N$ negative cases. We then define ensemble averages of f for the positive cases

$$\langle f^+ \rangle = \frac{1}{M} \sum_{j=1}^M w_j^+ f_j^+ \quad (6.1)$$

and for the negative cases

$$\langle f^- \rangle = \frac{1}{N} \sum_{k=1}^N w_k^- f_k^- \quad (6.2)$$

where the weighting factors are proportional to the duration of the particular case.

Following this, we construct the spatial distribution of the t-statistic for the difference between means (null hypothesis of no difference between means), identifying those regions where the differences exceed certain significance levels. For the selected fields we present maps of $\langle f \rangle$, $\langle f \rangle$, the difference ($\langle f \rangle - \langle f \rangle$) and the results of the t-test.

We will sometimes present the linear spatial correlation coefficient between two fields. Since our primary interest is in comparing eddy structures, the mean values of the fields at each latitude (the zonal averages) are first removed before calculating correlations. The area-normalized correlation of two fields and between latitudes 30 N and 80 N is then defined by

$$r(f, g) = \frac{\int_{30^\circ}^{80^\circ} a(\theta) [f^* g^*] d\theta}{([f^{*2}] [g^{*2}])^{1/2}} \quad (6.3)$$

where the square brackets denote zonal averages, the asterisks departures from zonal averages, and $a(\theta)$ is the normalization factor at latitude θ .

C. Differences in mean flows and storm paths

The structural characteristics of persistent anomalies have been analyzed in detail in Chapter 4; our objective here is to briefly review those features particularly salient to the budget discussion. We will subsequently focus mainly on the ATL cases. Our rationale is that:

1) there is a better balance between the numbers of positive (12) and negative (12) cases, as well as a larger total number of cases than for the other regions;

2) there are significant and well-defined differences in storm tracks associated with the positive and negative cases; and

3) the data coverage over the North Atlantic is superior to that over the North Pacific.

The latter issue is more crucial here than in our earlier calculations, since we anticipate that the covariances (and their derivatives) required in the budget calculations will be more sensitive to data deficiencies than the mean fields studied earlier. We will, however, also present summaries of results for the other two regions.

Analyses of the 500 mb heights for the ATL cases are presented in Fig. 6.1. Figs. 6.1a and 6.1b show composite 500 mb height anomaly maps for the 12 positive and the 12 negative anomaly cases, respectively. As we found earlier in a smaller set of ATL cases (cf. Fig. 4.2), the corresponding positive and negative anomaly patterns are highly similar, with a major center near the key point, anomalies of opposite sign over the subtropics to the south of the center, and a train of anomalies at mid- and high-latitudes extending mainly downstream from the dominant center. The composite 500 mb heights for the positive cases (Fig. 6.1c) strongly resemble typical Atlantic blocking patterns; in contrast, the 500 mb heights for the negative cases (Fig. 6.1d) are characterized by a regional high index flow. Anomaly differences (Fig. 6.1e) between the positive and the negative cases are in excess of 400 m over the North Atlantic; elsewhere, peak anomaly differences

are around 100 m. The t-test results (Fig. 6.1f) indicate that differences between means are highly significant over a vast portion of the North Atlantic; a train of centers of high significance is also located downstream from the key region. Additional centers exceeding the 99% confidence level are located upstream over north-central Canada and over a small region near the Red Sea.

Fig. 6.2a displays the root-mean-square (rms) 500 mb* geopotential heights in the 2.5-6 day range** for the positive cases. We see that a broad region of high variability extends northeastward from the eastern United States to Scandinavia, with maxima over Nova Scotia and to the southeast of Iceland. The negative cases (Fig. 6.2b), in contrast, display high variability in a zonally-oriented band extending across the central North Atlantic, with a single, relatively intense maximum located to the east of Newfoundland. The differences between means (Fig. 6.2c) and associated t-test results (Fig. 6.2d) suggest that the significant changes are primarily associated with the relatively more northward displacement of the storm paths in the positive cases.

* Parallel distributions (not shown) calculated for levels near the surface (1000 mb) and tropopause (300 mb) show qualitatively similar characteristics.

** The periods retained with the Blackmon band-pass filter.

Fig. 6.1. (a) Composite 500 mb height anomalies for 12 ATL positive cases (units:m); (b) as in (a) for 12 ATL negative cases; (c) composite 500 mb heights for the positive cases (units:m); (d) as in (c) for the negative cases; (e) (positive-negative) 500 mb height differences (units:m); and (f) confidence levels for a two-sided t-test for the difference between means. Negative values are dashed.

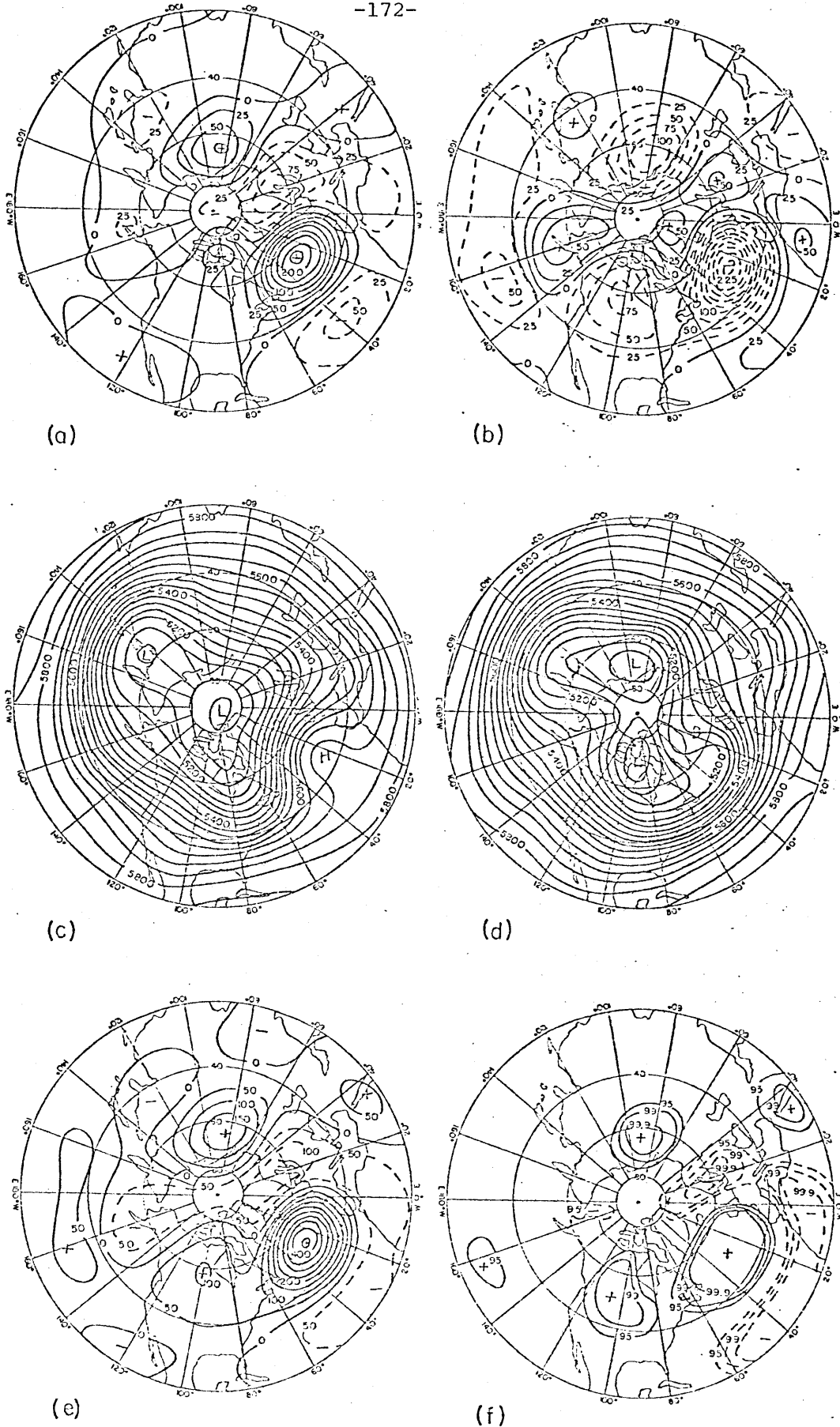


Fig. 6.1

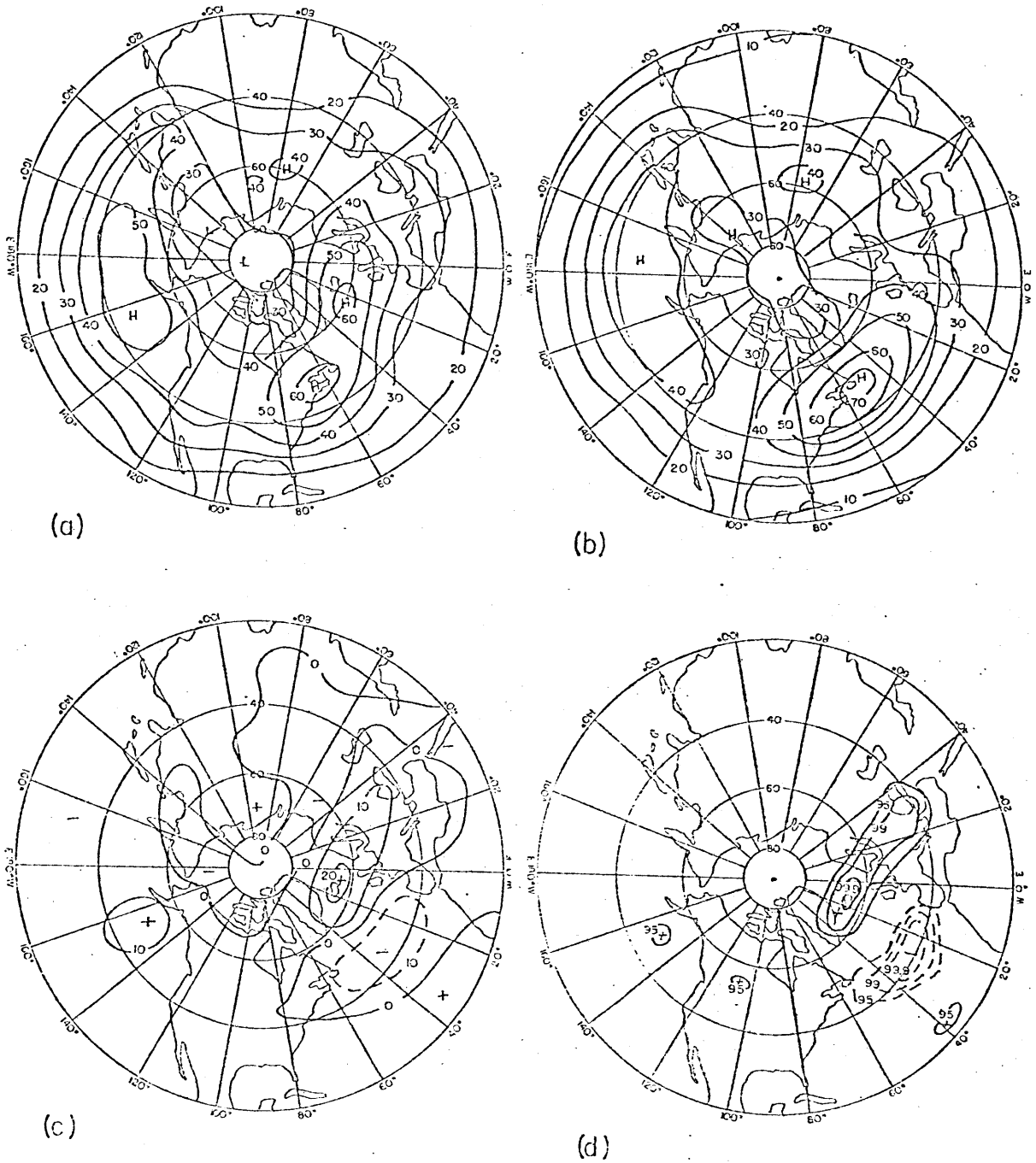


Fig. 6.2. (a) Composite band-pass 500 mb heights for the positive cases (units:m); (b) as in (a) for the negative cases; (c) (positive-negative) differences rms heights (units:m); (d) confidence levels for a two-sided t-test for the difference between means. Negative values are dashed.

D. Budgets

In the following discussions, we will first discuss the character of the mean fields and then present selected terms from the ATL budget calculations. At the end of each subsection, we present brief summaries of the results for all three regions.

1. Heat budgets

Fig. 6.3 displays composite analyses of time-mean temperature fields at 700 mb, representative of temperature patterns throughout most of the troposphere (cf. Fig. 4.11). Comparing these analyses with the corresponding 500 mb height analyses described earlier, we see that the positive height anomalies are predominantly warm-core and the negative anomalies cold-core, with the ATL thermal anomaly centers displaced slightly westward of the corresponding 500 mb height maxima. The strongest temperature gradients associated with the positive cases extend in a band from near Nova Scotia northeastward to Iceland. In contrast, the strongest gradients in the negative cases occur from eastern North America eastward across the Atlantic near 40 N. Mean temperature differences between the positive and negative cases exceed 8°C over the northern North Atlantic and are above 5°C in several other regions. Mean temperatures in the positive cases are greater (less) than those in the negative cases over virtually the entire North Atlantic north (south) of about 35 N. The t-test results strongly resemble those obtained earlier for the 500 mb height analyses, consistent with the earlier observation that the tropospheric height and temperature anomaly patterns are highly positively correlated.

The time-average thermodynamic equation may be written as

$$\begin{aligned}
 \frac{\overline{\partial T}}{\partial t} &= - \overline{\underline{V} \cdot \nabla T} - \nabla \cdot \overline{\underline{V}' T'} - \overline{\omega \left(\frac{\partial T}{\partial p} - \frac{R T}{p c_p} \right)} \\
 \text{(HT)} & \quad \text{(HA)} \quad \text{(HB)} \quad \text{(HC)} \\
 & - \left(\frac{\partial}{\partial p} \overline{\omega' T'} - \frac{R}{p c_p} \overline{\omega' T'} \right) + \overline{Q} \\
 & \quad \text{(HD)} \quad \text{(HE)}
 \end{aligned} \tag{6.4}$$

where the overbar represents a time-average over the duration of a case and a prime indicates a deviation from that average. All other symbols have their conventional meanings. Term HT is a heat storage* term. Term HA represents the advection of time-mean temperature by the horizontal component of the time-mean flow. Term HB is the eddy heat flux convergence. Term HC represents adiabatic temperature changes associated with time-mean vertical motions; term HD, the effects of the vertical eddy transports of heat; and term HE, the time-mean diabatic heating. In practice, HT, HA, HB, and HC are calculated from the data, so that the residual, HD + HE, represents a "virtual" time-mean heating. Lau (1978) suggests that for climatological-mean data, the ratio HE/HD is typically >2 over the storm track regions. For brevity we subsequently refer to the residual as the mean diabatic heating.

The composite 700 mb distribution of term HA, the horizontal advection of time-mean temperature by the time-mean flow, is presented in Fig. 6.4a for the positive cases and in Fig. 6.4b for the negative cases. The positive cases are characterized by weak warm advection to the west of the key region, with slight cold-advection to the east;

*For all of the budgets, the composite storage terms provide negligible contributions and so will not be discussed.

the negative cases, in contrast, display strong cold advection to the west of the key region, with largest values extending from eastern North America to the central North Atlantic. Differences between means (Fig. 6.4c) are strongest over the northwest North Atlantic, locally exceeding over $5^{\circ}\text{C}/\text{day}$. The difference pattern rather closely resembles the corresponding difference pattern for 700 mb temperatures described previously (spatial correlation .67); the t-test analysis for term HA (Fig. 6.4d) indicates that the major regions of significant differences are centered over the North Atlantic and western Europe.

Similar maps for term HB, the 700 mb eddy heat flux convergence, are presented in Fig. 6.5. In contrast to the term HA, the eddy flux convergence patterns are negatively correlated with the temperature patterns (correlation between difference fields = $-.61$); thus, the direct effect of this eddy term mainly weakens the mean temperature anomalies by transporting heat down the local temperature gradient. Hololpainen (1970) and Lau (1979) report a similar relationship for transient eddies and climatological mean flows. The adiabatic heating and cooling associated with time-mean circulations induced by the transient disturbances may, however, partially oppose the direct effect of the eddy heat flux convergences. We discuss this issue and the problem of interpreting these and subsequent relations in terms of energetics in the following section.

Distributions of the time-mean adiabatic term HC (not shown) have patterns nearly identical to the corresponding mean vertical motion

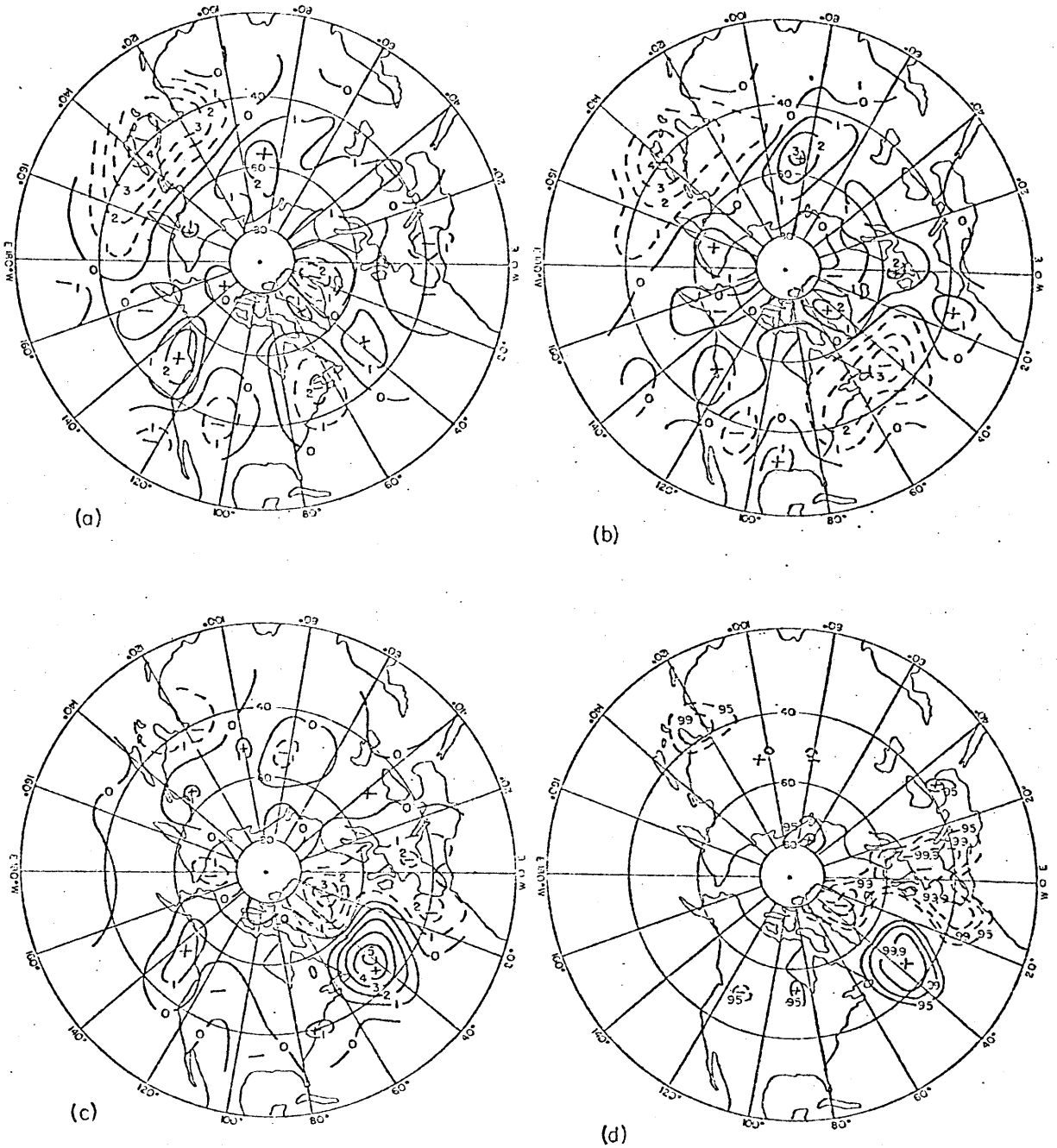


Fig. 6.4. As in Fig. 6.2 for 700 mb analysis of term HA, the advection of time-mean temperature by the time-mean flow (units: °C/day).

patterns ($\bar{\omega}$) at 500 mb (Fig. 6.6), which display significantly greater ascent upstream and descent downstream in the positive cases.* In brief, the correlation between HC and T difference fields is slightly negative (-.06), suggesting that the anomalous time mean vertical motions have, if anything, a weak tendency to reduce the temperature anomaly locally. Similar correlations between HC and T but calculated instead for the positive cases fields together and for the negative cases fields together are, respectively, -.35 and -.37, suggesting this effect acts more directly in the long-term mean fields than in the anomaly fields.

Fig. 6.7 displays the distributions for the time mean diabatic heating term. The principal areas of heating appear to be connected with the oceanic storm paths. In the positive cases, weak cooling occurs near and just to east of the key region, likely mainly due to radiative cooling. In contrast, in the negative cases relatively stronger warming occurs over and to the south-west of the key region, apparently associated with increased sensible heat transfers and with enhanced precipitation accompanying more vigorous storm activity in that area. This suggests that some asymmetries between positive and negative cases may be introduced by the dominance of different physical processes in the two regimes. The correlation between differences in temperature and differences in diabatic heating is -.23, suggesting that this term also acts mainly to damp the mean temperature anomalies.

* The vertical motions are obtained by a vorticity method as described in Appendix 4.

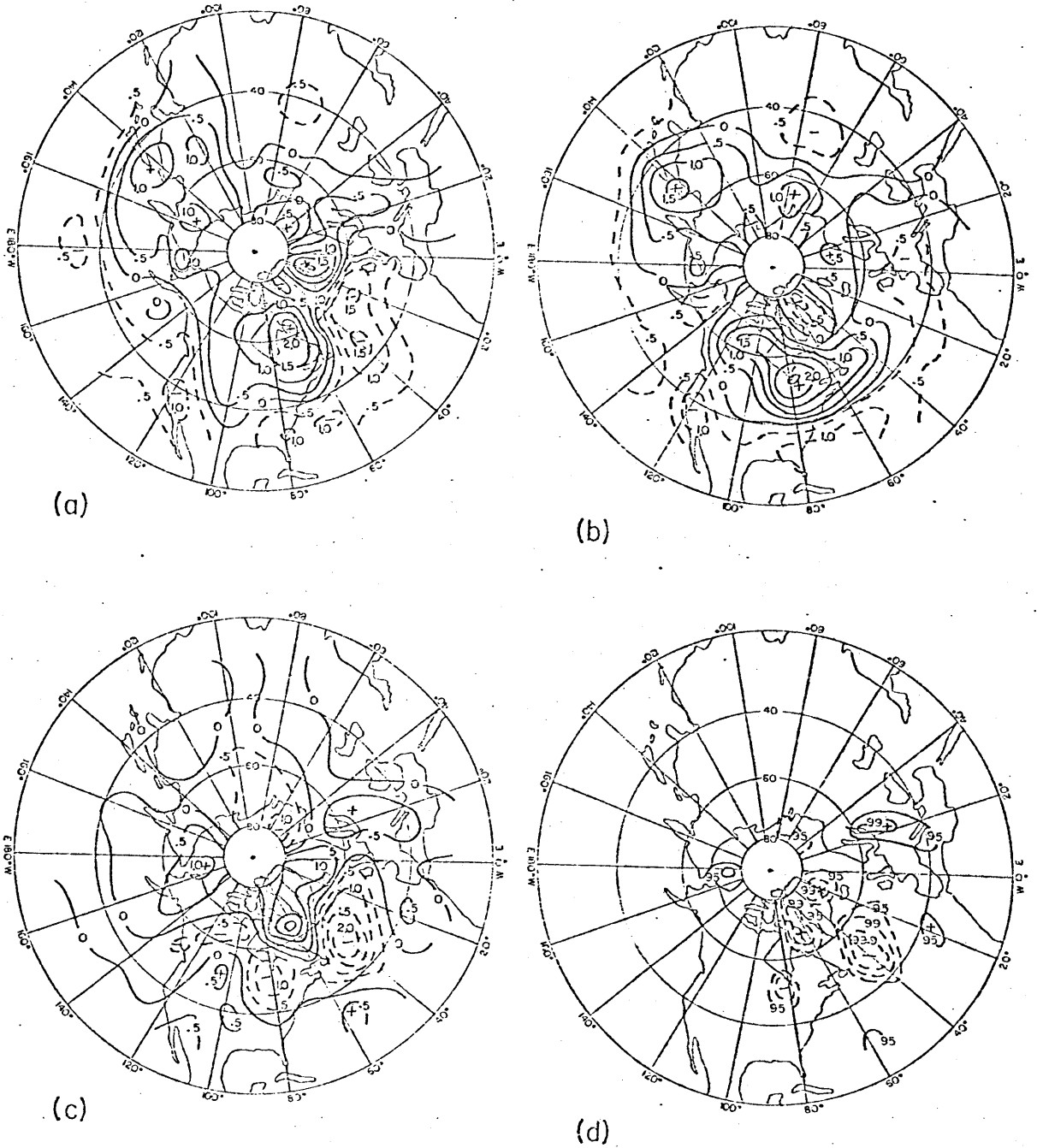


Fig. 6.5. As in Fig. 6.2 for 700 mb analyses of term HB, the horizontal eddy heat flux convergence (units: °C/day).

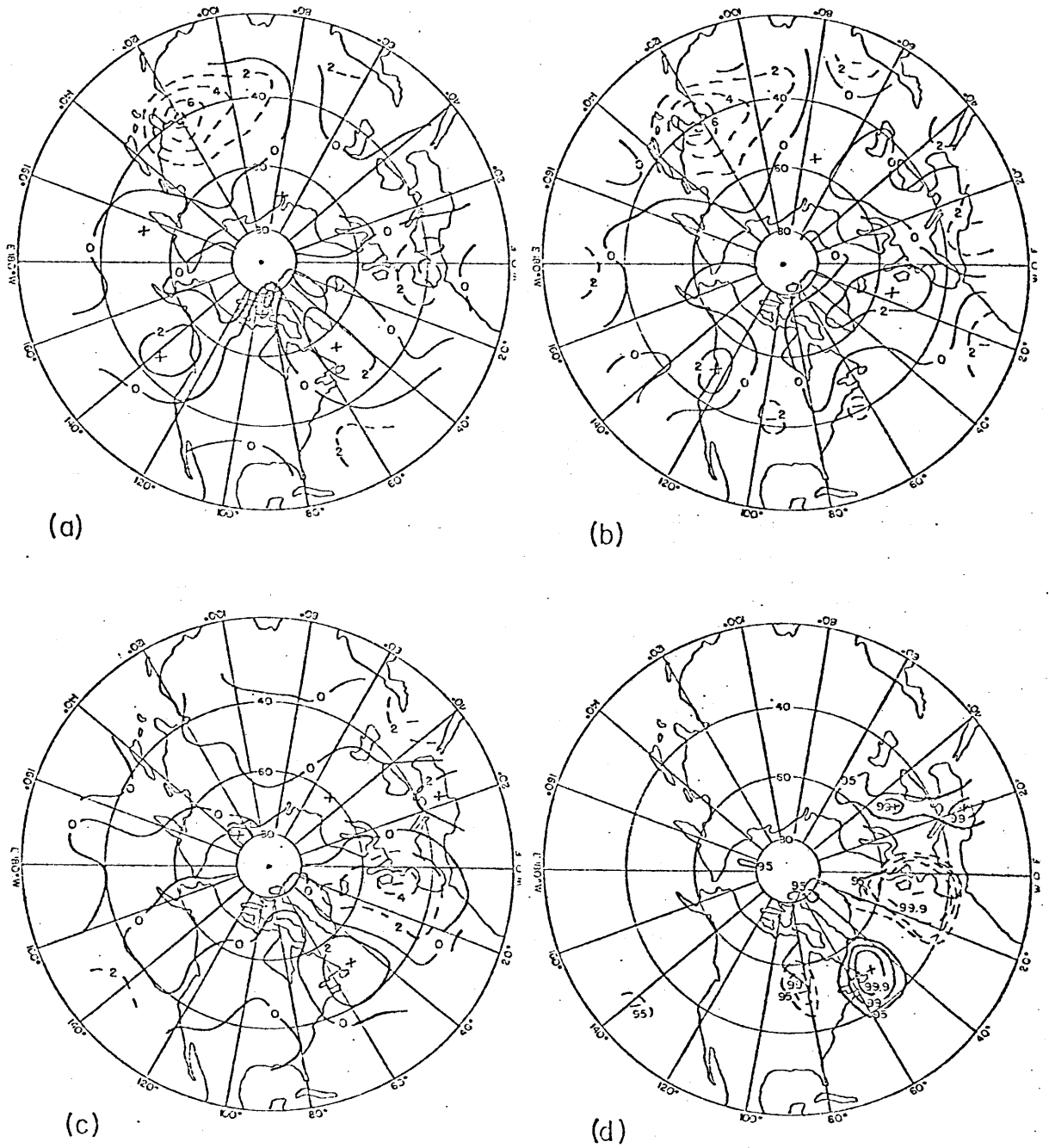


Fig. 6.6. As in Fig. 6.2 for 500 mb analyses of $\bar{\omega}$ (units: 10^{-4} mb/sec $^{-1}$). The values have been multiplied by -1 so that positive values correspond with rising motion.

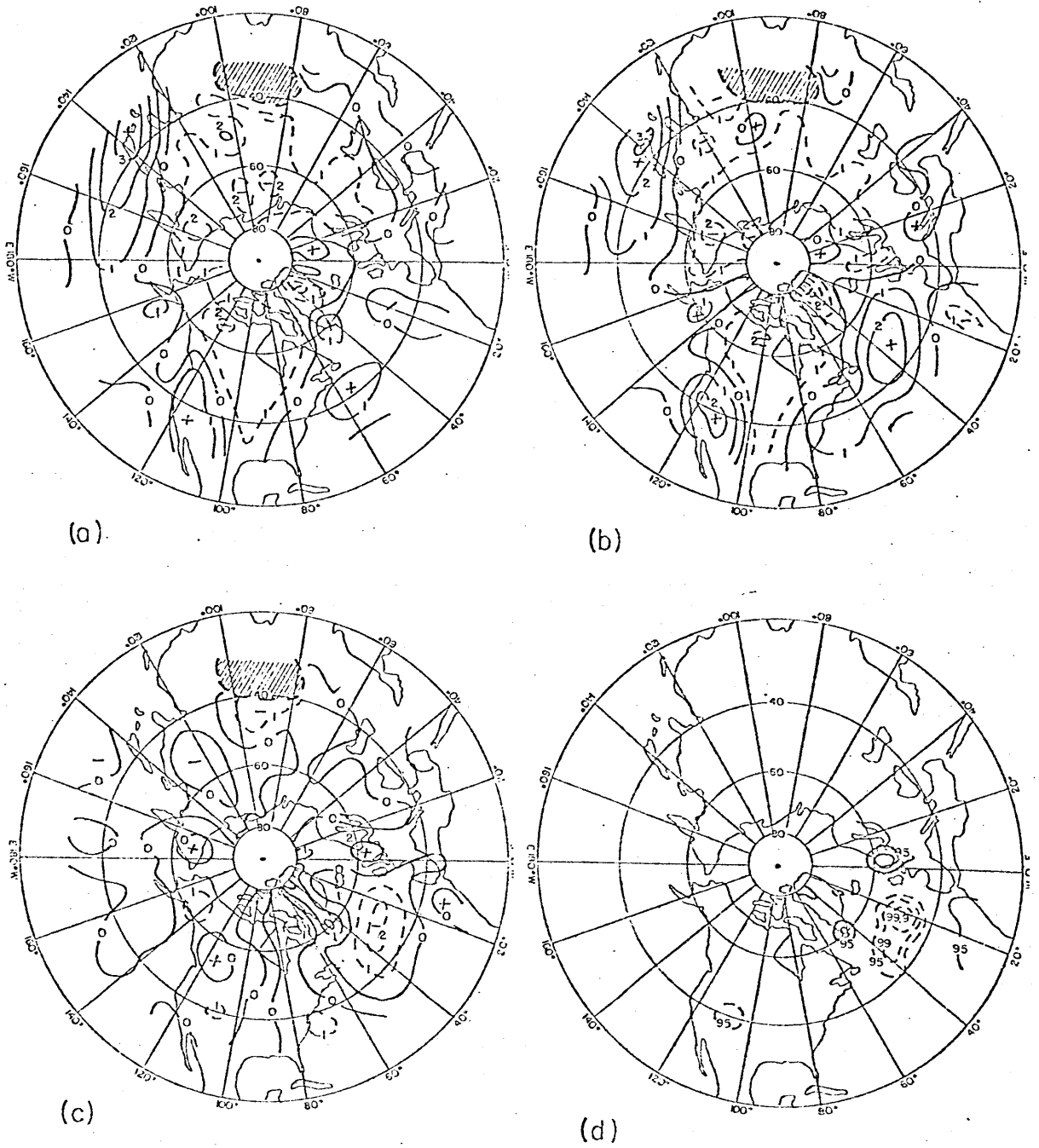


Fig. 6.7. As in Fig. 6.2 for term HE, the time-mean diabatic heating (units: °C/day).

Heat budget calculations for all three regions display qualitatively similar results: through the lower and mid-troposphere, differences in temperatures between positive and negative cases are positively correlated with differences in the time mean advection (typical correlations are 0.60 to 0.70) and are negatively correlated with differences in the eddy heat flux convergence (typical values of -.60 to -.70). Differences in the adiabatic cooling and heating terms show no or only slightly negative correlations with the temperature differences (.00 to -.20). Differences in the diabatic heating appear mainly related to changes in the storm paths. In the PAC cases (not shown), this tendency appears to be enhanced by orographic effects in the Far West (positive cases have greater precipitation). Corresponding differences for the eddy terms and the diabatic heating terms have comparable magnitudes.

2. Vorticity Budgets

Fig. 6.8 displays analyses of the vorticity fields at 300 mb, near the level of maximum vorticity anomalies (cf. Fig. 4.17). The overall patterns closely resemble the structures seen in the height fields. Peak magnitudes of the vorticity anomalies are about $3 - 4 \times 10^{-5} \text{ sec}^{-1}$. Vorticities associated with the positive center (Fig. 6.8a) are characteristic of values at latitudes about 20° further south. The vorticity pattern associated with the negative center (fig. 6.8b) indicates that a band of high vorticity extends eastward from a region of typically high values over northeastern Canada across the northern North Atlantic to the key region. The major regions of significant differences are associated with the vorticity pattern over

the North Atlantic.

The time-mean vorticity equation can be written as

$$\begin{aligned}
 \frac{\partial \bar{\zeta}}{\partial t} &= - \bar{\mathbf{v}} \cdot \nabla (\bar{\zeta} + f) - \nabla \cdot \bar{\mathbf{v}}' \zeta' + (\bar{\zeta} + f) \frac{\partial \bar{\omega}}{\partial p} + \\
 \text{(VT)} & \qquad \qquad \text{(VA)} & \qquad \qquad \text{(VB)} & \qquad \qquad \text{(VC)} & \qquad \qquad + \\
 & \left(- \bar{\omega} \frac{\partial \bar{\zeta}}{\partial p} - \frac{\partial}{\partial p} \overline{\omega' \zeta'} + \bar{R} \cdot \nabla \times \bar{\mathbf{F}} + \bar{R} \cdot \left(\frac{\partial \bar{\mathbf{v}}}{\partial p} \times \nabla \bar{\omega} \right) \right) \text{(6.5)} \\
 & \text{(VD)} & \qquad \qquad \text{(VE)} & \qquad \qquad \text{(VF)} & \qquad \qquad \text{(VG)}
 \end{aligned}$$

$\bar{\mathbf{F}}$ represents the frictional force; all other symbols have their conventional meanings. Terms VT, VA and VB have analogous interpretations to the corresponding terms in the time-average thermodynamic equation. Term VC represents the effect of time-mean divergence on altering the time-mean vorticity. Term VD is the vertical advection of time-mean vorticity by the time-mean vertical motion; VE is the vertical eddy vorticity flux convergence; VF is the time-average frictional force; and VG is the time-average twisting term. Terms VT, VA and VB can be calculated directly from the data. Terms VT, VA, VB and VC contain all the terms of the time-average quasi-geostrophic vorticity equation, in addition to certain smaller terms that are readily calculable from the observations. Scale analysis and observational data suggest that, at least in the free atmosphere at middle and high latitudes, the terms in parentheses are relatively small. Thus, to a first approximation, we may determine VC as a residual of the other three principal terms.

Distributions of term VA (not shown) strongly resemble the patterns of term VD displayed later (correlations about $-.90$). In brief, at 300 mb, the advection of relative vorticity ($-\bar{v} \cdot \nabla \bar{\zeta}$) generally opposes and exceeds the advection of planetary vorticity ($\frac{\bar{v}df}{dy}$). Typically then, positive (negative) vorticity advection occurs downstream from the major troughs (ridges) at upper levels. This balance is consistent with long wave rather than ultra-long wave scales (Burger, 1958). At lower levels (below 500 mb) the advection of planetary vorticity dominates. This structure appears consistent with trapping of the waves near the tropopause, as discussed earlier.

Fig. 6.9 presents distributions of VB, the eddy vorticity flux convergence. Although the patterns are noisy with much small-scale variability evident, comparison of the corresponding maps in Figs. 6.9 and 6.2 suggests predominantly positive vorticity flux convergence to the north of the storm paths with negative vorticity flux convergence to the south. This structure is consistent with a maximum of eddy momentum flux convergence into storm paths, as observed in climatological studies (e.g., Blackmon, et al., 1977), numerical studies of baroclinic instability (Simmons and Hoskins, 1976; 1977; 1978) and as predicted by recent theories (Held, 1975). The difference map (Fig. 6.9c) and associated t-test (Fig. 6.9d) indicate that only a small area upstream of the key region has differences exceeding the 99% confidence level.

Although we are presently disinclined to attach much significance to this feature, this pattern is somewhat intermediate between relations suggested by Green (1977) and Austin (1980) in simple theories of the forcing of mean flows by transient eddies. Austin suggests

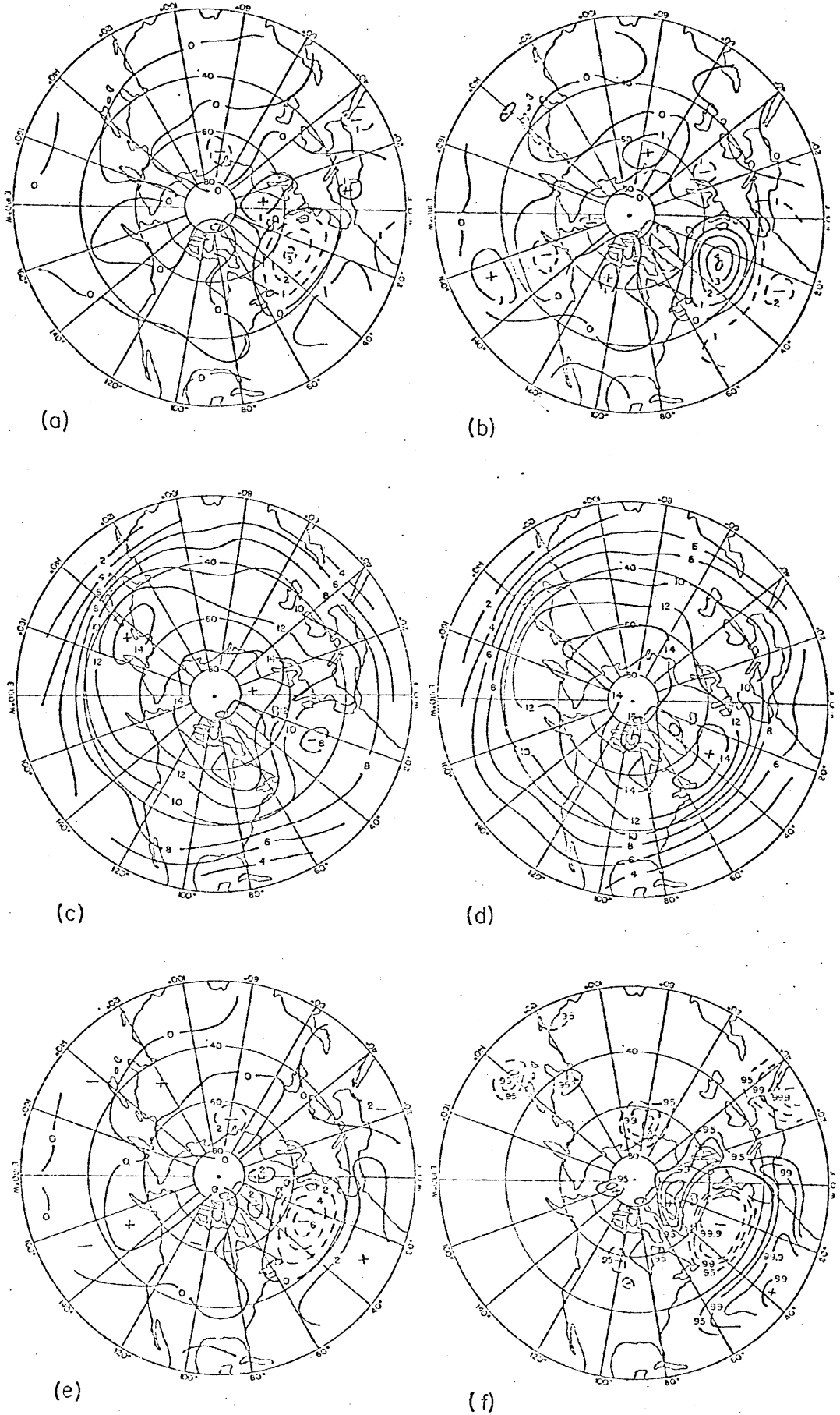


Fig. 6.8. As in Fig. 6.1 for 300 mb vorticities (units: 10^{-5}sec^{-1}).

that for long waves, a forcing of anticyclonic vorticity concentrated at upper levels will tend to produce a warm-core anticyclone with a maxima one quarter-wavelength downstream from the forcing maxima. The location of the maximum anticyclonic forcing we observe, however, appears more nearly in phase with the maximum anticyclonic vorticity, consistent with the relationship suggested by Green (1977). Austin's theory predicts the maxima in the vertical structure of the vorticity response will occur near the level of largest forcing; above that level, the anticyclone decays with height. We have noted before, however, that other mechanisms may also produce a similar vertical structure. The magnitudes of the eddy vorticity forcing we observe are roughly consistent with the magnitudes that Austin's model requires to produce steady-state vorticity anomalies of the right magnitudes.

Fig. 6.10 presents distributions for the divergence forcing term VC. We see that the VC and VB terms have magnitudes of similar order, although VC is typically larger (rms values about 50-90% higher). The difference maps indicate that at upper levels, the positive cases have relatively greater upstream divergence and downstream convergence, consistent with the greater upstream ascent and downstream descent seen in the vertical motion patterns. Only very small areas, primarily over the eastern Atlantic, have differences exceeding the 95% confidence level.

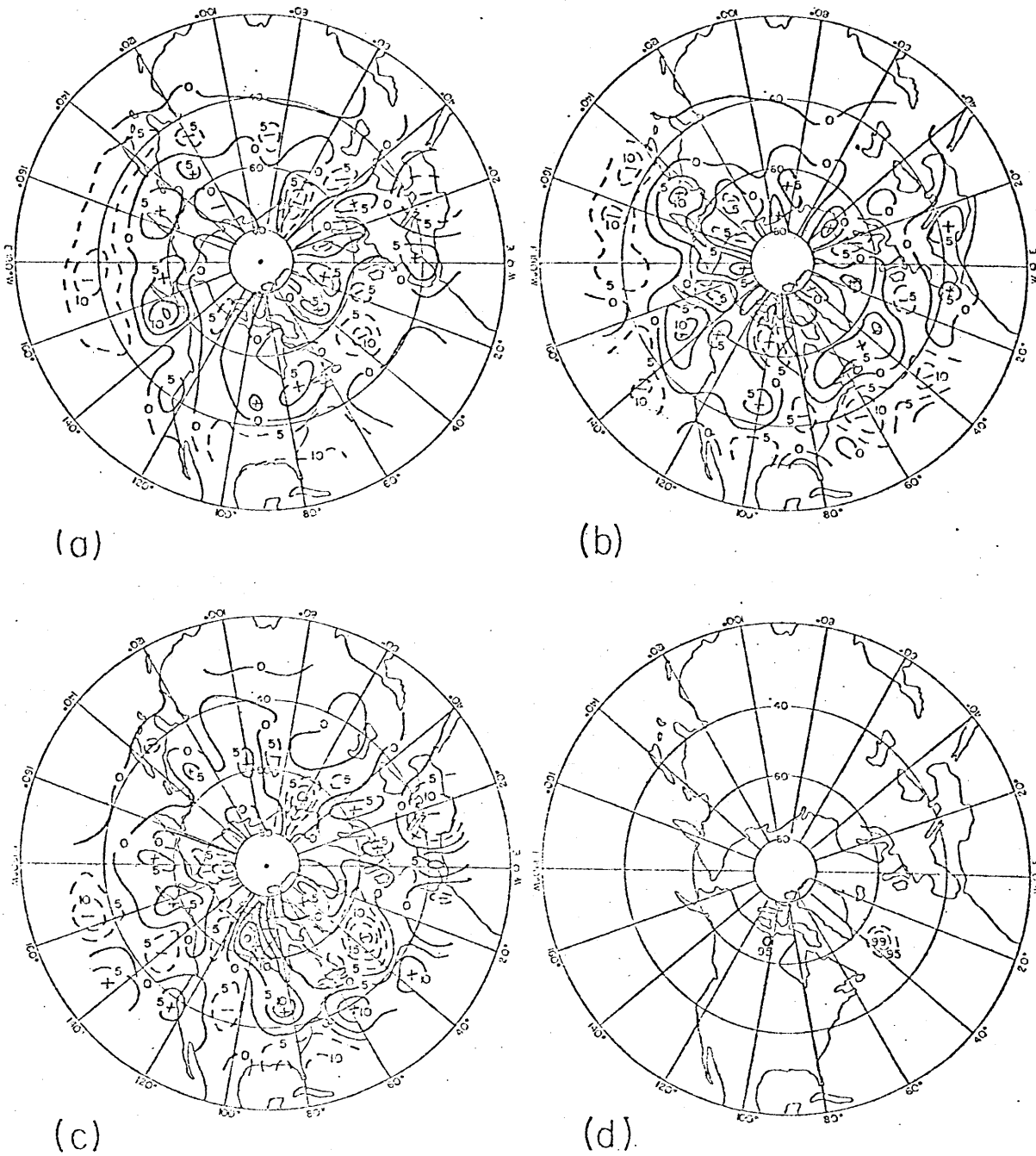


Fig. 6.9. As in Fig. 6.2 for term VB, the horizontal eddy vorticity flux convergence (units: 10^{-12}sec^{-2}).

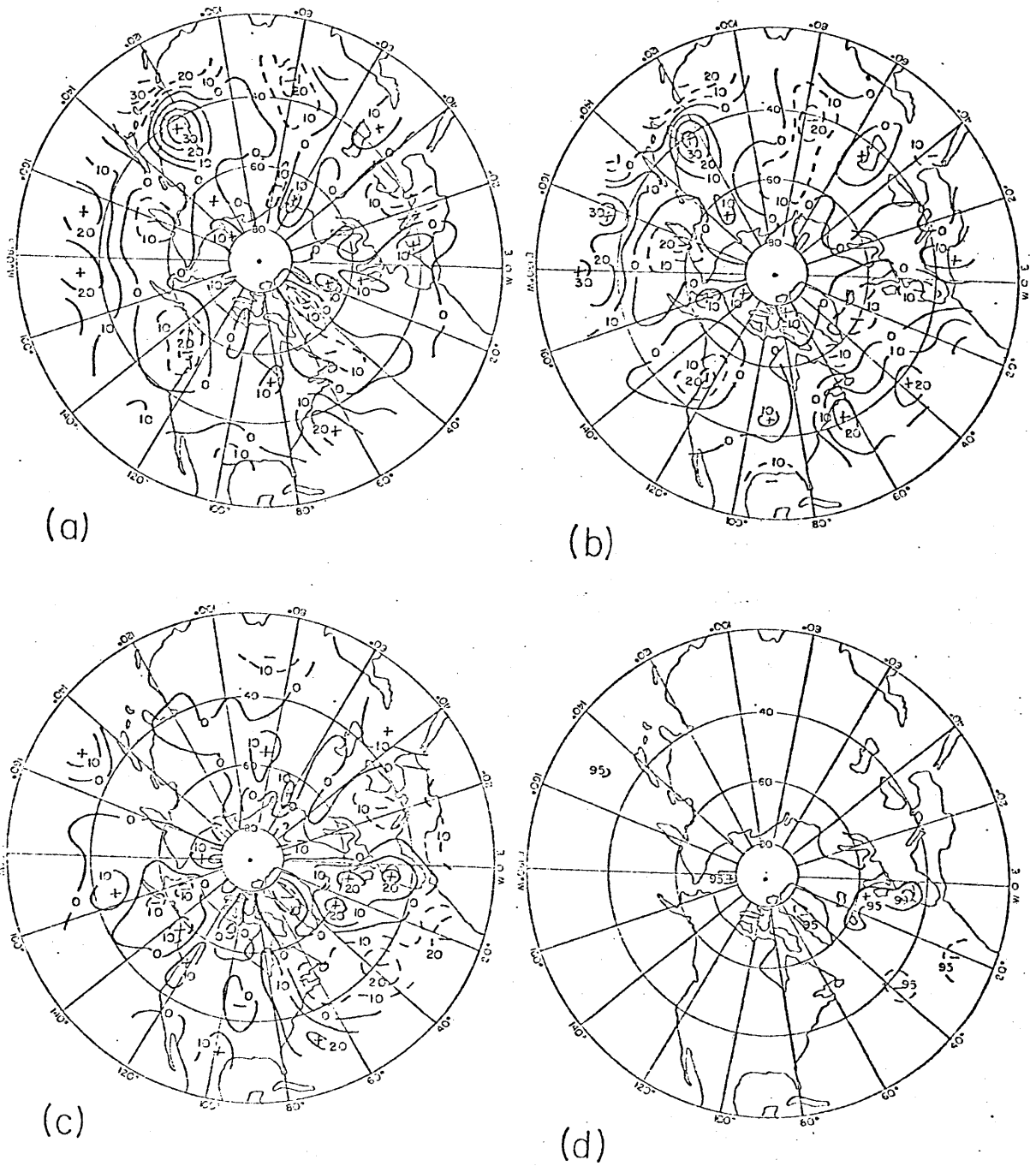


Fig. 6.10. As in Fig. 6.2 for term VC, the vorticity forcing by time-mean divergence.

Figs. 6.11a, 6.11b, and 6.11c display, respectively, for levels from 1000 mb to 100 mb the correlations between vorticity difference fields and corresponding differences in terms VA, VB, and VC. We see that correlations are weak for all terms at all levels. Correlations for most terms reverse sign between the lower and upper troposphere, with strongest correlations near the tropopause. At upper levels, correlations are positive between vorticity and eddy differences and negative between vorticity and convergence differences.

Values for the rms differences in terms VA, VB and VC are presented in Figs. 6.11d, 6.11e and 6.11f, respectively. All terms display pronounced peaks near the tropopause. The 1000-100 mb vertical averages (not shown) typically resemble the patterns at these levels. The rms values for VA and VC differences are comparable and generally exceed VB by about 50-200%. Near the surface, VC exceeds VA, reflecting weak positive correlations between VA and VB; at upper levels, VC is usually slightly smaller than VA, reflecting weak negative correlations between VA and VB (typically about $-.3$). These relations appear qualitatively consistent with expectations from quasi-geostrophic theory (e.g., Holton, 1972): that is, cyclogenesis (as suggested by the eddy vorticity flux divergence) tends to occur in regions of mean low-level convergence and upper-level divergence (upper-level positive vorticity advection) downstream from the major long wave troughs.

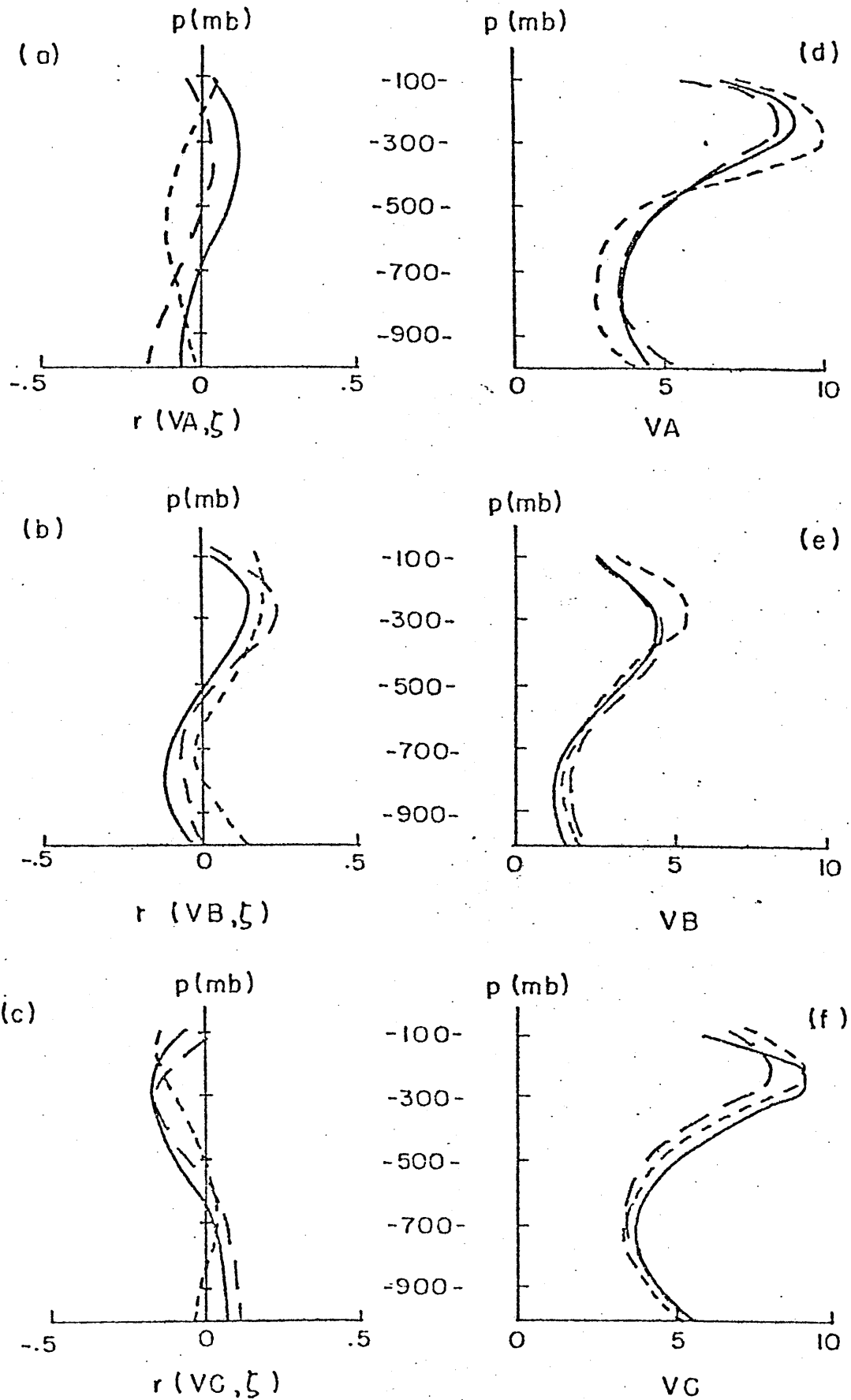


Fig. 6.11. Vertical distributions of the spatial correlations between vorticity differences fields and differences in term (a) VA; (b) VB; and (c) VC. Vertical distribution of the rms values (units: 10^{-12}sec^{-2}) of term (d) VA; (e) VB; and (f)

We have additionally calculated 250 mb distributions of the eddy flux convergence for an approximate* form of the potential vorticity

$$p = (\beta + f) \frac{\partial \phi}{\partial p} \tag{6.6}$$

and for the quasi-geostrophic pseudo-potential vorticity (Charney, 1973)

$$q = \frac{g}{f} \nabla^2 z + f + \frac{g}{\beta} \frac{\partial}{\partial p} \left(\frac{T}{\frac{\partial T}{\partial p} - \frac{RT}{pC_p}} \right) \tag{6.7}$$

The patterns (not shown) are highly similar to the patterns of the eddy vorticity flux convergences, with maximum positive (negative) potential vorticity flux convergences near and slightly upstream of the potential vorticity maxima (minima).

* Hartmann (1977) shows that evaluation of the relative vorticity on an isobaric rather than an isentropic surface is a valid approximation for large-scale, highly stratified flows.

E. Discussion

The main relations to emerge from the budget analyses are,

For the heat budgets:

1) Through most of the troposphere, differences in temperature between positive and negative cases are positively correlated with differences in the time-mean advection, negatively correlated with differences in the eddy heat flux convergence and mean diabatic heating and almost uncorrelated with the diabatic warming accompanying time-mean vertical motions.

2) Differences in the diabatic heating appear mainly related to changes in the storm paths. In the positive cases weak cooling occurs near and just to the east of the key region, likely mainly due to radiative cooling. In the negative cases relatively stronger warming occurs over and to the southwest of the key region, apparently associated with enhanced sensible and latent heating.

3) Corresponding rms values for the differences in eddy terms and diabatic heating terms have comparable magnitudes.

For the vorticity budgets:

1) Correlations between vorticity differences and corresponding differences in budget terms are small for all terms at all levels. Correlations for most terms reverse sign between the lower and upper troposphere. At upper levels, correlations are positive between vorticity and eddy term differences (the eddies tend to increase the vorticity anomalies locally) and negative between vorticity and mean convergence differences (the mean convergence tends to reduce the vorticity anomalies locally).

2) Values for the rms differences in all terms display pronounced peaks near the tropopause; vertical average patterns typically resemble patterns at these levels. The rms values for mean advection and mean convergence differences generally exceed eddy differences by about 50 - 200%.

3) Patterns of eddy flux convergences of potential vorticity and pseudo-potential vorticity at 250 mb are highly similar to the patterns of the eddy vorticity flux convergences, with maximum positive (negative) potential vorticity flux convergences near and slightly upstream of the potential vorticity maxima (minima).

Our results are generally consistent with similar calculations for climatological mean flows (Lau, 1979; Blackmon, et al., 1978; Holopainen, 1978) and seasonal-mean flows (Edmon, 1980), suggesting that the relations between mean flows and storm paths are also established for persistent anomalous flows having durations that are short compared with a season (on the order of a few weeks or less). We are able to identify well-defined differences between positive and negative cases in most of the heat budget terms, but find few significant differences in the vorticity budget terms. This is undoubtedly partly due to the greater sensitivity of the vorticity calculations to analysis errors, but may also reflect the less systematic character of the momentum transports compared with the heat transports in baroclinic waves as discussed, for example, by Hoskins (1978). In many respects, those systematic changes we have identified appear qualitatively consistent with changes expected for growing baroclinic waves on a locally varying mean flow.

There are severe difficulties in determining the importance of the eddies in maintaining persistent anomalies. The results clearly point to ambiguities in distinguishing eddy from time-mean effects: we noted, for example, that differences in the time-mean diabatic heating appear closely related to differences in the storm paths, primarily through changes in latent, but also through changes in sensible, heating patterns. The relations between latent and sensible heating patterns and storm paths are poorly understood, but are certainly at least partly geographically dependent.

Another ambiguity arises from the tendency for the eddies to drive mean secondary circulations, so that, for example, the eddy heat flux divergence may indirectly contribute significantly to the vorticity balance through the time-mean divergence term. Comparisons of typical values suggest that the magnitudes of these indirect eddy contributions are of the same order as, although generally smaller than, the other terms.

We note, however, that even if the eddy terms were much smaller than the mean terms, the importance of the eddies could not be ruled out: conceivably, eddy-mean flow interactions might occur until the flow approaches a "quasi-equilibrium" where the interactions appear small. The quasi-equilibria need bear no obvious relation to equilibria calculated by neglecting transient eddies. Reinhold (1981) finds such a behavior in a low-order spectral model. Even the sign of the eddy forcing may not indicate the role of the eddies: although observational studies of the zonal-average circulation (e.g., Starr, et al., 1970) often suggest that eddies provide positive contributions

toward maintaining the jet stream, some theoretical studies of symmetric circulations (Schneider, 1977; Schneider and Lindzen, 1977) obtain stronger jets by neglecting eddies, suggesting the effect of the eddies may be inhibitive. Our diagnostic calculations are not intended to address these problems, nor questions of cause and effect. Rather, they attempt to ascertain what systematic eddy changes are observed between widely varying mean states.

Our analyses suggest potential difficulties in attempting to determine the energetics of persistent anomalies by standard methods (e.g., Holopainen, 1970). We noted, for example, that correlations between temperature and vertical motion anomaly fields appear to be negligibly correlated, although correlations between temperature fields and vertical motion fields during anomalous periods appear to have modest correlations. The correlations, apparently due to the long-term mean circulation, are of the proper sign to suggest a conversion from standing eddy available potential energy to standing eddy kinetic energy. Nevertheless, we cannot conclude that the persistent anomalies are maintained by baroclinic processes; our opinion is that there may be slight positive conversions, but that once developed the persistent anomalies are likely to be substantially less baroclinic than the long-term mean perturbations. Alternative approaches, perhaps involving a different reference state, may be required to adequately define the energetics of persistent anomalies.

F. Conclusions

Comparisons of local contributions by selected terms to the time-mean balances of heat, vorticity and potential vorticity show

well-defined differences between corresponding positive and negative cases in most of the heat budget terms, but few statistically-significant differences in most vorticity and potential vorticity terms. Many of the systematic differences in the eddy terms appear qualitatively consistent with changes expected for developing baroclinic waves on a spatially varying mean flow. Differences in the time-mean diabatic heating appear mainly related to changes in the storm paths. The results are generally consistent with similar calculations for climatological-mean flows. Thus, the relations already established between long-term mean flows and storm paths also appear in anomalous flows with durations of a few weeks.

VII. CONCLUSION

We have studied the geographical, structural and temporal characteristics of anomalies that have persisted beyond the periods associated with synoptic-scale variability and have examined the relationship of these persistent anomalies to changes in storm activity. Our analyses revealed a number of highly systematic features.

The geographical distribution calculations indicate that there are preferred regions for the occurrence of persistent anomalies, with three favored regions for persistence: the north-central North Pacific (PAC), the eastern North Atlantic (ATL) and the northern Soviet Union (NSU). For each region, the maximum in the frequency of occurrence of positive anomalies is approximately co-located with, and has comparable values to, the corresponding maxima of negative anomalies. For durations beyond about a week, there are slightly more positive than negative anomaly cases.

Our results do not suggest a preferred duration for persistent anomalies, nor indicate any strong periodicities. Rather, for sufficiently long durations, the number of events decays nearly exponentially with increasing durations, resembling the distributions obtained from a first-order autoregressive process. Nevertheless, the features in the PAC, ATL and NSU regions appear to decay somewhat more slowly than in other regions. Our results suggest that in the three persistent anomaly regions anomalies persisting beyond about 5 days are almost entirely associated with this slow decay process.

The results of the geographic distribution calculations focused our attention on three key regions. We then examined the structures of persistent anomalies occurring in these regions in order to determine whether persistent anomalies are associated with recurrent flow patterns. Our results provide evidence for the recurrence of certain preferred persistent anomaly patterns. To a first approximation, the persistent positive and negative anomaly patterns in a region can be described as opposite phases of the same basic pattern. The positive phase of the pattern usually resembles blocking; the negative phase can often be associated with a regional "high-index" flow. Systematic changes in the storm paths accompany the mean flow changes.

The majority of the cases appear to be associated with unusually strong enhancements of the primary regional patterns of low-frequency variability. Most of the variance in these patterns is contributed by within-season, rather than between-season (e.g., interannual), variability. The persistent mid-tropospheric anomalies are accompanied by pronounced changes in the location and intensity of the major surface centers of action (the Aleutian low in the PAC cases, the Icelandic low in the ATL cases and the Siberian high in the NSU cases). Concurrent with the height anomalies, there are large-scale tropospheric temperature anomalies having patterns mainly in-phase with the height anomalies.

Analyses of the vertical structure also reveal a number of highly typical characteristics. The anomalies display little vertical tilts, with maximum height anomalies in the upper troposphere.

Associated with these departures are pronounced anomalies in the temperature, vorticity and potential vorticity fields.

Our next goal was to ascertain typical life cycles of persistent anomalies. From growth to decay, the time evolutions of corresponding positive and negative cases display a number of striking similarities. Development rates are often rapid; there is little evidence of an atmospheric precursor until just prior to onset. Following onset, anomaly centers develop and intensify downstream from the main center, leading to the establishment of the persistent anomaly pattern. Intensification occurs with little evidence of phase propagation. There is some indication that the anomalies display greater westward vertical tilts during than following development. Breakdowns occur rapidly. Until immediately prior to breakdown, the patterns closely resemble the patterns following development.

We then examined the contributions of transient eddies toward maintaining local, time-mean balances of heat, vorticity and potential vorticity in order to study how changes in storm activity are related to changes in the mean flow. Comparisons between positive and negative cases show well-defined differences in most of the heat budget terms, but few statistically-significant differences in most vorticity and potential vorticity terms. Many of the systematic differences in the eddy terms appear qualitatively consistent with changes expected for developing baroclinic waves on a spatially varying mean flow. Differences in the time-mean diabatic heating appear mainly related to changes in the storm paths. The results are

generally consistent with similar calculations for climatological-mean flows; thus, the relations already established between long-term mean flows and storm paths also appear in anomalous flows having durations of a few weeks.

Our analyses provide a basis for addressing the theoretical issues raised in the review (chapter II). The observations that persistent anomalies occur mainly in specific geographic regions, that the spatial scales are large and that much of the development takes place while the patterns are nearly stationary all favor the importance of geographically-fixed forcings. Nevertheless, in the PAC evolutions the rapid development of the main center appears to be associated with an eastward propagating, mid-latitude disturbance. In some respects, then, the relative roles of free and forced motions cannot be considered as completely resolved.

The time scales for changes in external forcing are presumably much longer than the time scales that we typically find for the growth and decay of persistent anomalies. This suggests that these patterns often, and perhaps primarily, grow and decay while the external forcing remains nearly fixed. Further support for the view that the patterns evolve mainly by internal processes comes from recent modelling studies by Lau (1981) and Blackmon (personal communication), which demonstrate that anomalies in the external forcing are not required to produce patterns similar to those described here. Nevertheless, there is convincing observational evidence (Horel and Wallace, 1981) indicating some relationship between tropical Pacific sea surface temperature anomalies and the sign of the North Pacific anomaly pattern. The explanation for this relationship

remains an important unsolved problem.

The sequential character of the development of the anomaly centers favors the view that local or quasi-local sources are associated with their origins. This does not, however, entirely rule out the possibility of quasi-resonant behaviors. Although the structures and evolutions of the patterns indicate that the waves are generally significantly refracted or attenuated before travelling far zonally, the PAC and ATL patterns, in particular, somewhat resemble standing meridional modes, suggesting that north-south reflections may occasionally be important in these regions.

Our observations provide a basis for more detailed comparisons with theoretical and numerical modelling results, although we will not attempt to do that here. Among the fundamental results we consider as currently unexplained, however, are the geographic distributions and the nearly constant decay rates for the numbers of persistent events. Comparison of the values for the decay rates with time scales for other atmospheric processes suggests possible clues: the values appear comparable with estimates of time scales (Stefanick, 1981) for fluctuations in the tropical atmosphere, and also for variations in the zonal flow.

The development of wavetrains downstream from the main centers following onset qualitatively agrees with simple time-dependent models of energy dispersion on a sphere away from a localized, transient source of vorticity (Hoskins, et al., 1977; Hoskins, 1978). The gross horizontal and vertical structures of the patterns resemble external Rossby wavetrains (Held, 1981), although we have not attempted

a detailed comparison with theory. The evolution analyses suggest, however, that the explanation for the initial developments may be rather subtle. In the PAC cases, an intriguing clue is provided by the significant pattern located upstream over Asia and the extreme western Pacific preceding the development. The structure of this pattern suggests that the associated wind anomalies are primarily in the zonal flow over both the Himalayas and the southwestern North Pacific. Whether such anomalies will give rise to significant wavetrains remains to be seen.

Our results provide no convincing evidence for the occurrence of multiple quasi-equilibria; neither do they rule out the possibility. Distributions of several atmospheric parameters hint at, but do not clearly show, multi-modality. The internal mechanisms for variability suggested by multiple equilibria theory appear broadly consonant with observations, as do the nearly symmetric pairs of patterns usually predicted, although the latter may be generated for spurious reasons (e.g., resonances in the model that may not have counterparts in the atmosphere). It is probably fair to say that such models are presently too crude to provide detailed explanations of atmospheric behavior, but serve valuable heuristic purposes.

Throughout this thesis we have emphasized symmetries between positive and negative patterns. This is partly related to what we regard as a striking result: that by compositing cases with respect to the sign of the anomaly at a single point, and then comparing the result to a similar composite for anomalies of opposite sign, we are able to recover similar significant patterns over a large portion

of the hemisphere. Nevertheless, asymmetries between patterns are evident in all the analyses and also require explanation. We have suggested that some asymmetries may be related to orographic influences and others to the dominance of different physical processes in the corresponding positive and negative cases. Perhaps slight differences in the mean flow structure also substantially affect the character of the patterns. Both observational and theoretical approaches may prove useful in ascertaining the causes of significant asymmetries.

Finally, we note that the relatively small shift in time scales between persistent and non-persistent anomalies appears somewhat discouraging from the point of view of long range forecasting. Nevertheless, we find some encouragement in the ability of recent theoretical models to qualitatively replicate important aspects of structure and development. We are also heartened that the observed features of persistent anomalies are often rather simple; indeed, in many respects far simpler than we might have originally anticipated.

Appendix 1. NMC data set.

The data base for the present study consists of twice-daily National Meteorological Center (NMC) analyses of geopotential height, temperature and wind fields for the Northern Hemisphere at 10 pressure levels (1000, 850, 700, 500, 400, 300, 250, 200, 150 and 100 mb). The analyses are products of the forecast-analysis cycle at NMC. The "first guess" for the analyses is the previous (12 hour) model forecast. This first guess is then updated by observations obtained from the surface and radiosonde observational networks, aircraft reports, winds inferred from satellite imagery, etc. The transient data sources often compose a significant fraction of the total number of reports: Jenne (1975) presents a typical time in July 1968 in which 48% of the upper-air reports were from conventional sources (RAOB and RAWIN reports) and 52% were from other sources (primarily aircraft winds and winds inferred from satellite data). The latter sources are probably most valuable in filling gaps over otherwise data-sparse regions such as the North Atlantic and North Pacific oceans. Over these regions, the NMC analyses should have an advantage over other analysis schemes that incorporate only fixed base data.

Up through 1965, the first guesses for both the 0000Z and 1200Z analyses were based on a 3-level baroclinic model.

From 1966 through 1972, this model was usually operational at 1200Z; a 6-layer primitive equation model (Shuman and Hovermale, 1968) was operational at 0000Z. Between 1972 and September 1974 the 6-layer model was used for both analyses. Through the period, numerous lesser changes in models and procedures also occurred, some of the most important of which are discussed by McDonnell (1974). Although these changes undoubtedly introduce changes in the first-guess fields and hence in the analysis fields over data sparse regions, results obtained by Lau (1978) and ourselves suggest that systematic changes during this time are generally small. Throughout this period, the observed data were incorporated into the analysis through a successive correction scheme similar to that described by Cressman (1959).

In September 1974, NMC introduced a global spectral forecast model together with a Hough function analysis scheme (Flattery, 1971). As noted by Rosen and Salstein (1980), the Hough scheme places a strong constraint on the analyzed winds such that they are essentially non-divergent. This eliminates features such as the mean meridional cells. Rosen and Salstein indicate, however, that for analyses of mid-latitude waves and transports the Hough analyses appear quite acceptable.

Comparison of the NMC schemes with schemes using only fixed station data (Lau and Oort, 1981) suggests that over data-rich regions the analyses are highly similar, whereas in

data-sparse regions the NMC analyses show a more detailed structure. For our purposes, the incorporation of the additional data sources in the NMC analyses offsets the possible disadvantages of the loss of "observational purity" resulting from the combining of model forecast and observational data.

Appendix 2. Case dates.

Selection criteria were (100m, 10 days) and (-100m, 10 days) for all positive cases and negative cases, respectively.

The following cases were used in the horizontal structure and case EOF analyses. Cases were selected from unfiltered data for the 14 winter seasons from 1963-64 to 1976-77. The winter was defined as the 90-day period from 1 December through 28 February.

<u>No.</u>	<u>Reg.</u>	<u>Loc.</u>	<u>Type</u>	<u>Yr.</u>	<u>Mo.</u>	<u>Day</u>	<u>Hr.</u>	<u>Dur.</u>
1	PAC	50N 165W	POS	64	12	16	00	23.0
2				65	12	23	00	11.0
3				68	1	3	00	15.0
4				69	1	5	00	10.5
5				69	1	21	00	12.0
6				72	2	17	12	11.5
7				75	1	25	00	19.5
1			NEG	63	12	18	00	16.0
2				70	12	12	00	11.0
3				72	12	16	00	10.5
4				73	12	15	12	14.0
5				75	12	15	12	13.0
6				77	1	9	12	13.0
7				77	2	7	12	15.0
1	ATL	50N 20W	POS	64	1	20	12	22.0
2				65	2	1	12	19.5
3				67	1	5	00	10.5
4				67	1	31	00	10.5
5				68	1	17	12	13.5
6				69	2	2	12	10.5
7				73	2	17	12	11.5
8				74	12	29	12	10.5
9				76	1	9	12	17.5
1			NEG	66	2	7	12	20.5
2				68	12	12	12	10.5
3				69	1	6	12	13.0
4				71	1	16	00	11.5
5				72	1	7	12	10.0
6				74	1	2	00	12.0

<u>No.</u>	<u>Reg.</u>	<u>Loc.</u>	<u>Type</u>	<u>Yr.</u>	<u>Mo.</u>	<u>Day</u>	<u>Hr.</u>	<u>Dur.</u>
1	NSU	60N 60E	POS	66	12	17	00	21.0
2		60N 50E		68	12	22	12	17.0
3		65N 55E		69	2	8	12	15.0
4		65N 40E		72	1	14	00	20.5
1		60N 65E	NEG	71	12	26	00	15.5
2		60N 45E		75	2	7	00	13.5
3		60N 45E		75	12	31	12	19.5

The following cases were used in the 1000 mb height and 1000-300 mb layer mean temperature, time evolution and budget analyses. For the 500 mb time evolutions, cases were selected from low-pass filtered data for the 14 winter seasons from 1963-64 through 1976-77. For all other analyses, cases were obtained from the 11 winters 1965-66 through 1975-76. In these analyses, the winter season is defined as the 120-day period beginning 15 November.

<u>No.</u>	<u>Reg.</u>	<u>Loc.</u>	<u>Type</u>	<u>Yr.</u>	<u>Mo.</u>	<u>Day</u>	<u>Hr.</u>	<u>Dur.</u>
1	PAC	45N 170W	POS	64	12	10	00	10.0
2				64	12	23	12	14.0
3				65	12	21	00	13.0
4				66	2	10	00	25.0
5				67	12	29	12	20.5
6				68	12	9	12	11.5
7				68	12	31	00	15.0
8				69	1	23	00	16.5
9				70	12	16	00	13.5
10				71	1	17	12	10.0
11				71	2	24	1	10.5
12				71	12	8	12	17.0
13				72	2	16	12	11.5
14				74	2	22	12	12.5
15				75	1	25	00	20.0
1			NEG	63	12	16	00	17.0
2				64	1	24	00	12.5
3				65	1	9	00	12.0
4				67	1	30	00	12.0
5				68	2	5	00	30.0
6				69	12	16	12	17.5
7				70	1	28	12	25.5
8				71	2	4	12	15.5
9				73	12	17	00	11.0
10				75	12	16	12	12.0
11				76	1	24	00	10.5
12				76	12	10	00	15.0
13				77	1	1	00	52.5

<u>No.</u>	<u>Reg.</u>	<u>Loc.</u>	<u>Type</u>	<u>Yr.</u>	<u>Mo.</u>	<u>Day</u>	<u>Hr.</u>	<u>Dur.</u>
1	ATL	50N 25W	POS	64	1	21	12	20.0
2				64	12	17	00	10.0
3				65	2	1	00	21.0
4				67	1	2	12	12.5
5				67	12	24	12	11.5
6				68	1	20	00	15.5
7				68	12	25	00	10.5
8				69	1	30	12	16.5
9				70	2	24	12	10.5
10				73	1	23	12	36.0
11				74	12	29	12	10.0
12				75	12	3	00	26.5
13				76	1	8	00	18.5
1			NEG	63	12	9	12	12.0
2				64	2	13	12	17.5
3				65	12	31	12	11.5
4				66	1	17	00	42.5
5				67	1	18	00	11.5
6				67	2	12	12	13.5
7				69	1	8	00	18.5
8				70	1	8	00	20.5
9				71	1	4	00	23.5
10				72	1	5	12	12.0
11				72	1	30	12	13.0
12				74	1	1	00	14.0
13				74	1	24	00	10.0
1	NSU	60N 60E	POS	64	2	3	12	17.0
2				64	12	4	00	12.0
3				65	12	13	12	10.5
4				66	12	17	00	20.0
5				68	12	22	00	16.0
6				69	2	11	12	11.5
7				70	2	17	12	17.5
8				71	1	23	00	13.0
9				74	2	20	12	14.5
10				76	12	3	12	12.0
1			NEG	63	12	6	12	14.0
2				64	1	4	12	21.5
3				66	1	29	00	15.5
4				70	1	24	12	10.0
5				71	1	5	12	13.0
6				71	12	21	00	23.5
7				75	1	3	12	10.0
8				75	2	6	00	10.0
9				75	12	16	12	19.5

<u>No.</u>	<u>Reg.</u>	<u>Loc.</u>	<u>Type</u>	<u>Yr.</u>	<u>Mo.</u>	<u>Day</u>	<u>Hr.</u>	<u>Dur.</u>
1	NSU	60N 50E	POS	64	12	5	12	10.0
2				66	12	24	00	13.0
3				68	12	22	12	17.0
4				69	2	9	12	15.0
5				70	2	18	12	12.5
6				71	1	23	12	12.5
7				74	1	9	00	10.0
8				76	12	12	00	10.0
1			NEG	63	12	8	00	12.5
2				66	1	29	12	14.0
3				68	12	1	00	13.5
4				73	12	1	00	10.5
5				75	2	5	00	11.0
6				76	1	1	00	12.0

The following cases were used in the vertical structure analyses. Cases were selected from unfiltered data for the 11 winter seasons 1966-67 through 1976-77.

<u>No.</u>	<u>Reg.</u>	<u>Loc.</u>	<u>Type</u>	<u>Yr.</u>	<u>Mo.</u>	<u>Day</u>	<u>Hr.</u>	<u>Dur.</u>
1	PAC	50N 150W	POS	67	12	24	12	17.0
2		50N 160W		69	1	6	00	27.0
3		50N 160W		72	11	30	00	15.0
4		55N 165W		73	12	30	12	16.5
5		50N 160W		75	1	25	00	19.5
1		50N 165W	NEG	73	12	15	12	14.0
2		45N 160W		77	1	4	00	22.0
3		50N 165W		77	2	7	12	15.0
1	ATL	45N 25W	POS	67	12	24	12	19.0
2		55N 30W		68	12	24	12	14.0
3		50N 30W		69	1	28	00	20.5
4		50N 5W		71	12	4	00	14.0
5		45N 30W		73	2	9	00	18.5
6		45N 15W		76	1	1	00	24.0
1		50N 20W	NEG	69	1	6	00	13.0
2		50N 10W		69	2	12	12	13.0
3		55N 40W		74	1	3	00	17.5

Appendix 3. Empirical Orthogonal Function Analysis.

The theories and methods of empirical orthogonal function (EOF) analysis are discussed in detail elsewhere (Lorenz, 1956; Davis, 1976) and so will only briefly be outlined here. The general problem is to approximate a function of space and time $h(x,y,t)$ for which data values at M spatial grid points are known over N consecutive observations by the series \hat{h} :

$$h(x_j, y_j, t_i) \equiv h_{ij} \\ \hat{h}_{ij} = \sum_{k=1}^m g_{ik} f_{kj} \quad (A.1)$$

Choosing the functions of grid position f_{kj} as the dominant m empirical orthogonal functions yields the smallest sample mean square error

$$E(m) = (NM)^{-1} \sum_{i=1}^N \sum_{j=1}^M (h_{ij} - \hat{h}_{ij}(m))^2 \quad (A.2)$$

which can be obtained from any choice of m functions (Lorenz, 1956).

Additional properties are that the functions are orthonormal

$$\sum_{j=1}^M f_{rj} f_{sj} = \delta_{rs} \quad r, s = 1, 2, \dots, m \quad (A.3)$$

while the time coefficients are uncorrelated at zero lag:

$$\sum_{i=1}^N g_{ik} g_{il} = d_k \delta_{kl} \quad (\text{A.4})$$

The empirical orthogonal functions are obtained as eigenvectors of the matrix

$$\tilde{A} = \sum_{i=1}^N h_{ij} h_{ik}, \quad j, k = 1, 2, \dots, M \quad (\text{A.5})$$

When the elements h_{ij} are anomaly values, $N^{-1}A$ is a covariance matrix; if the h_{ij} are further normalized by their standard deviations, then $N^{-1}A$ is a correlation matrix. The time coefficients q_{ik} , which play a role analogous to the coefficients of the sine and cosine functions in the Fourier harmonic analysis previously discussed, are obtained by solving

$$g_{ik} = \sum_{j=1}^M h_{ij} f_{kj} \quad (\text{A.6})$$

A basic hypothesis of this analysis is that the appropriate error measure is the sum of squares over all grid points, from which the criterion (eq. A.2) follows. The choice of equal weighting of the square error from each grid point can be replaced by other weightings, such as a weighting proportional to the 5° by 5° tessera corresponding to the grid point. Calculations have also been performed using this weighting, with only minor differences in the results.

EOF 's were determined for each region over M grid points and N cases: for ATL, $N = 15$, for PAC, $N = 14$ and for NSU, $N = 14$. The number of grid points, M , is limited by practical considerations; hence, the analyses were performed over limited regions (50° latitude by 160° longitude, $M = 363$) for which the previous analyses provided the strongest indication of pattern recurrences. The spatial structure of the first EOF was found to be insensitive to changes in the location of the boundaries.

Appendix 4. Vertical motion calculations.

The time-mean motions $\bar{\omega}$ are obtained by integrating the time-mean divergence with respect to pressure

$$\bar{\omega}(p) = \bar{\omega}(p_0) + \int_{p_0}^p \frac{\partial \bar{\omega}}{\partial p} dp \quad (\text{A.1})$$

where $\bar{\omega}(p)$ denotes the time-average vertical velocity at pressure level p and $\bar{\omega}(p_0)$ represents the corresponding quantity (assumed known) at level p_0 . The mean divergences are determined as residuals from the vorticity balance (eq. 6.5). Following O'Brien (1970), the divergence in (A.1) is adjusted so that boundary conditions at lower and upper levels are simultaneously satisfied. The divergence adjustment is independent of pressure (e.g., the systematic part of the divergence error is assumed to be uniformly distributed throughout the column). The adjusted vertical motions are given by

$$\bar{\omega}''(p) = \bar{\omega}(p) - \frac{(p_B - p)(\bar{\omega}(p_T) - \bar{\omega}_T)}{(p_B - p_T)} \quad (\text{A.2})$$

where $\bar{\omega}''(p)$ is the adjusted vertical motion at level p , $\bar{\omega}(p)$ the usual estimate obtained from eq. A.1, p_B and p_T the pressures at lower and upper boundaries, respectively, and $\bar{\omega}_T$ the independently calculated value of $\bar{\omega}_T$ at level p_T .

The vertical motion at the lower boundary (850 mb) is assumed to be composed of three terms:

$$\bar{\omega}(850) = \bar{\omega}_M + \bar{\omega}_F + \bar{\omega}_D \quad (\text{A.3})$$

where the first term on the right hand side of (A.3) is due to the topography, the second due to friction and the third to quasi-geostrophic divergence in the surface to 850 mb layer. The topographic vertical motion is approximated by

$$\bar{\omega}_m = - \frac{gRT}{P} \bar{\nabla} \cdot \nabla h \quad (\text{A.4})$$

where h is the height of the local terrain obtained from NCAR (Jenne, personal communication) on a 2.5 grid. All other symbols have their conventional meanings.

The frictional term is obtained as

$$\bar{\omega}_F = \frac{g}{f} \left[\frac{\partial}{\partial y} \bar{p} C_D \bar{\pi} |\bar{\nabla}| - \frac{\partial}{\partial x} \bar{p} C_D \bar{v} |\bar{\nabla}| \right] \quad (\text{A.5})$$

The drag coefficient C_D is assumed to be a linear function of the terrain height

$$C_D = 1.0 \times 10^{-3} + 8.0 \times 10^{-3} \frac{h}{h_{\max}} \quad (\text{A.6})$$

where h_{\max} is the maximum terrain height. The values for the drag coefficient correspond approximately with the values in Cressman (1960).

The quasi-geostrophic divergence term is determined by

$$\bar{\omega}_D = \delta \int_{1000}^{950} \left(\frac{\partial \omega}{\partial p} \right) dp \quad (\text{A.7})$$

where the divergence is obtained as a residual from the vorticity balance as described earlier. The weight factor δ depends on the fraction of the layer above the surface

$$\delta = \begin{cases} 0 & \bar{p}_{sfz} < 850 \text{ mb} \\ 1 - \frac{(1000 - \bar{p}_{sfz})}{(1000 - 850)} & 1000 \text{ mb} \leq \bar{p}_{sfz} \leq 850 \text{ mb} \\ 1 & \bar{p}_{sfz} > 1000 \text{ mb} \end{cases} \quad (\text{A.8})$$

The upper boundary condition is determined by assuming that the virtual heating vanishes at 200 mb

$$\bar{\omega}_+ \Big|_{200} = - \left(\frac{\partial \bar{T}}{\partial p} - \frac{R \bar{T}}{p C_p} \right)^{-1} \left(\bar{\mathbf{v}} \cdot \nabla \bar{T} + \nabla \cdot \bar{\mathbf{v}}' T' \right) \quad (\text{A.9})$$

This term is generally small except in the descent to the region east of the Himalayas where its neglect would imply unreasonably strong 200 mb heating rates.

Recent calculations by White (1981) indicate that large-scale climatological-mean vertical motions obtained by the vorticity balance method and by the quasi-geostrophic omega equation (Holton, 1972) are very similar. The patterns obtained by these methods largely agree with the vertical velocity patterns implied by cloudiness and precipitation.

The mean vertical motions obtained above have also been used to perform an a posteriori check on the adequacy of neglecting terms involving the time-mean vertical motions. The neglected terms appear at least an order of magnitude smaller than the retained terms, suggesting the consistency of our approximations.

REFERENCES

- Austin, J.F., 1980: The blocking of middle latitude westerly winds by planetary waves. Quart. J. R. Met. Soc., 106, 327-350.
- Bjerknes, R., B. Bolin and C.G. Rossby, 1949: An aerological study of zonal motion, its perturbation and breakdown. Tellus, 1, 14-37.
- Bjerknes, J., 1966: Atmospheric teleconnections from the equatorial Pacific. Mon. Wea. Rev., 97, 163-172.
- Blackmon, M.L., 1976: A climatological spectral study of the 500 mb geopotential height of the Northern Hemisphere. J. Atmos. Sci., 33, 1607-1623.
- _____, J.M. Wallace, N.C. Lau, and S.L. Mullen, 1977: An observational study of the Northern Hemisphere wintertime circulation. J. Atmos. Sci., 34, 1040-1053.
- Brezowsky, H., H. Flohn and P. Hess, 1951: Some remarks on the climatology of blocking action. Tellus, 3, 191-194.
- Brooks, C.E.P., and N. Carruthers, 1953: Handbook of Statistical Methods in Meteorology. Her Majesty's Stationary Office.
- Burger, A.P., 1958: Scale consideration of planetary motions of the atmosphere. Tellus, 10, 195-205.
- Charney, J.G., 1947: The dynamics of long waves in a baroclinic westerly current. J. Meteor., 4, 135-163.
- Charney, J.G., 1973: Planetary fluid dynamics, in Dynamic Meteorology, ed. by P. Morel, p. 97, D. Reidel Publishing, 1973.
- _____, and A. Eliassen, 1949: A numerical method for predicting the perturbations of the middle latitude westerlies. Tellus, 1, 38-54.
- _____, and J.G. DeVore, 1979: Multiple flow equilibria in the atmosphere and blocking. J. Atmos. Sci., 36, 1205-1216.
- _____, and D.M. Strauss, 1980: Form-drag instability, multiple equilibria and propagating planetary waves in the baroclinic, orographically forced, planetary wave systems. J. Atmos. Sci., 37, 1157-1176.
- Colucci, S.J., and A.Z. Loesch, L.F. Bosart, 1981: Spectral evolution of a blocking episode and comparison with wave interaction theory. J. Atmos. Sci., 38, 2092-2111.

- Cressman, G.P., 1959: An operational objective analysis system. Mon. Wea. Rev., 87, 367-374.
- _____, 1960: Improved terrain effects in barotropic forecasts. Mon. Wea. Rev., 88, 327-342.
- Davis, R.E., 1976: Predictability of sea surface temperature and sea level pressure anomalies over the North Pacific Ocean. J. Phys. Oceanogr., 6, 249-266.
- Dickson, R.R. and J. Namias, 1976: North American influences on the circulation and climate of the North Atlantic sector. Mon. Wea. Rev., 104, 1255-1265.
- Dickinson, R.E., 1978: On Planetary Waves. The General Circulation Theory, Modelling and Observations. NCAR Summer 1978 Colloquium, NCAR/CQ-6+ 1978-ASD, 59-82.
- Eady, E.T., 1949: Long waves and cyclone waves. Tellus, 1, 33-52.
- Edmon, H.J., Jr., 1980: A study of the general circulation over the Northern Hemisphere during the winters of 1976-77 and 1977-78. Mon. Wea. Rev., 108, 1538-1553.
- Egger, J., 1978: Dynamics of blocking highs. J. Atmos. Sci., 35, 1788-1801.
- _____, 1979: Stability of blocking in barotropic channel flow. Atmos. Phy. 52, 27-43.
- Elliott, R.D. and T.B. Smith, 1949: A study of the effects of large blocking highs on the general circulation of the Northern Hemisphere westerlies. J. Meteor., 6, 67-85.
- Flattery, T.W., 1971: Spectral models for global analysis and forecasting. Proc. Sixth AWS Tech. Exchange Conf., Air Weather Service Tech. Rep. 242, 42-54.
- Fredericksen, J.S., 1979: The effects of long planetary waves on the regions of cyclogenesis: linear theory. J. Atmos. Sci., 37, 195-204.
- Gall, R., 1976: Structural changes in growing baroclinic waves. J. Atmos. Sci., 33, 374-390.
- Geisler, J.E., 1977: On the application of baroclinic instability and sensible heat exchange to explain blocking ridge development. J. Atmos. Sci., 34, 216-218.
- _____, and R.P. Garcia, 1977: Baroclinic instability at long wavelengths on a β plane. J. Atmos. Sci., 34, 311-321.
- Green, J.S.A., 1977: The weather during July 1976: some dynamical considerations of the drought. Weather, 32, 120-128.

- Grose, W.L., and B.J. Hoskins, 1979: On the influence of orography on large-scale atmospheric flow. J. Atmos. Sci., 36, 223-234.
- Haltiner, G.J., 1967: The effects of sensible heat exchange on the dynamics of baroclinic waves. Tellus, 19, 183-198.
- Hartmann, D.L., 1977: On potential vorticity and transport in the stratosphere. J. Atmos. Sci., 34, 968-977.
- _____, and S.J. Ghan, 1980: A statistical study of the dynamics of blocking. Mon. Wea. Rev., 108, 1144-1159.
- Held, I.M., 1975: Momentum transport by quasi-geostrophic eddies. J. Atmos. Sci., 32, 1494-1497.
- _____, 1981: Stationary and quasi-stationary eddies in the extra-tropical troposphere: theory, to be in The Dynamics of the Extratropical Troposphere, ed. by B. Hoskins, Academic Press.
- Hollingsworth, A., K. Arpe, M. Tiedtke, M. Capaldo and H. Savijarvi, 1980: The performance of a medium range forecast model in winter - impact of physical parameterizations. Mon. Wea. Rev., 108, 1736-1773.
- Holopainen, E.O., 1970: An observational study of the energy balance of the stationary disturbances in the atmosphere. Quart. J. Roy. Met. Soc., 96, 626-644.
- Horel, J.D., and J.M. Wallace, 1981: Planetary-scale atmospheric phenomena associated with the Southern Oscillation. Mon. Wea. Rev., 109, 813-829.
- Hoskins, B.J., 1978: Horizontal wave propagation on a sphere. The General Circulation: Theory, modeling and observations. N.C.A.R. Summer Colloquium, 1978. Boulder, Colorado.
- _____, A.J. Simmons and D.G. Andrews, 1977: Energy dispersion in a barotropic atmosphere. Quart. J. Roy. Meteor. Soc., 103, 553-567.
- _____, and D. Karoly, 1981: The steady linear response of a spherical atmosphere to thermal and orographic forcing. J. Atmos. Sci., 38, 1179-1196.
- Holton, J.R., 1972: An Introduction to Dynamic Meteorology. Academic Press, pp. 391.
- Jenne, R.L., 1970: The NMC octogonal grid. NCAR, Boulder, CO, 14 p.

- Kalnay-Rivas, E., and L. Merkin, 1981: A simple mechanism for blocking. J. Atmos. Sci., 38, 2077-2091.
- Karoly, D.J., 1978: Rossby wave ray paths and horizontal wave propagation. The General Circulation: Theory, Modeling and Observations. N.C.A.R. Summer 1978 Colloquium, NCAR/CQ-6+ 1978 ASP, 478-484.
- Kutzbach, J.E., 1970: Large-scale features of monthly mean Northern Hemisphere anomaly maps of sea-level pressure. Mon. Wea. Rev., 98, 708-716.
- Lau, N.C., 1978: On the three-dimensional structure of the observed transient eddy statistics of the Northern Hemisphere wintertime circulation. J. Atmos. Sci., 35, 1900-1923.
- _____, 1979: The observed structure of tropospheric stationary waves and the local balance of vorticity and heat. J. Atmos. Sci., 36, 996-1016.
- _____, 1981: A diagnostic study of recurrent meteorological anomalies appearing in a 15-year simulation with a GFDL general circulation model, to be in The Dynamics of the Extratropical Troposphere, ed. B. Hoskin
- Lau, N.C. and A.H. Oort, 1981: A comparative study of observed Northern Hemisphere circulation statistics based on GFDL and NMC analyses. Part I: The time-mean fields. Mon. Wea. Rev., 109, 1380-1403.
- Leith, C.E., 1973: The standard error of time-average estimates of climatic means. J. Appl. Meteor., 12, 1066-1069.
- Leith, C.E., 1978: Objective methods for weather prediction. Ann. Rev. Fluid Mech., 10, 107-128.
- Lin, C.A., 1980: Heat transport by stationary and transient waves. M.I.T. Dept. of Meteorology, Ph.D. Thesis.
- Lorenz, E.A., 1956: Empirical orthogonal functions and statistical weather prediction. Sci. Rep. No. 1, M.I.T. Statistical Forecasting Project, Contract no. AF19 (604), 49 pp.
- Madden, R.A., 1976: Estimates of the naturally occurring variability of time-averaged sea-surface pressure. Mon. Wea. Rev., 104, 942-952.
- Martin, D.E., 1953: Anomalies in the Northern Hemisphere 5-day mean circulation patterns. Air Weather Service Rep. No. 105-100, 39 pp.
- McDonnell, J.E., 1974: Notes on operational objective analysis procedures, unpublished manuscript prepared for "advanced prediction techniques course", NWS, Washington, DC, 50 p.
- McWilliams, J.C., 1980: An application of equivalent modons to atmospheric blocking. Dyn. of Atm. and Oceans, 5, 43-66.

- Namias, J., 1947: Extended range forecasting by mean circulation methods. Washington, D.C., U.S. Weather Bureau, 55 pp.
- _____, 1950: The index cycle and its role in the general circulation. J. Meteor., 7, 130-139.
- _____, 1964: Seasonal persistence and recurrence of European blocking during 1958-1960. Tellus, 13, 394-407.
- _____, 1972: Large-scale and long-term fluctuations in some atmospheric and oceanic variables. Nobel Symp., 20, 27-48.
- Namias, J., 1978: Multiple causes of the North American abnormal winter 1976-1977. Mon. Wea. Rev., 106, 279-295.
- Niehaus, M.C.W., 1980: Instability of non-zonal baroclinic flows. J. Atmos. Sci., 37, 1447-1463.
- O'Brien, J.J., 1970: Alternative solutions to the classical vertical velocity problem. J. Appl. Meteor., 9, 197-203.
- O'Conner, J.T., 1969: Hemispheric teleconnections of mean circulation anomalies at 700 mb. ESSA Tech. Rep. WB-10, 103 pp.
- Opsteegh, J.D., and H.M. Van Den Dool, 1980: Seasonal differences in the stationary response of a linearized primitive equation model: Prospects for long-range forecasting. J. Atmos. Sci., 37, 2169-2185.
- Palman, E., and C.W. Newton, 1969: Atmospheric Circulation Systems. Academic Press, 603 pp.
- Parzen, E., 1962: Stochastic Processes. San Francisco. Holden-Day.
- Petterssen, S., 1956: Weather Analysis and Forecasting, Vol. 1, McGraw-Hill, 267-276.
- Reinhold, B., 1981: Dynamics of weather regimes: quasi-stationary waves and blocking. M.I.T. Dept. of Meteorology and Physical Oceanography, Ph.D. Thesis.
- Rex, D.D., 1950a: Blocking action in the middle troposphere and its effects on regional climate. I. An aerological study of blocking. Tellus, 2, 196-211.
- _____, 1950b: Blocking action in the middle troposphere and its effect on regional climate. II. The climatology of blocking action. Tellus, 2, 275-301.

- Rex, D.D., 1951: The effect of Atlantic blocking action upon European climate. Tellus, 3, 1-16.
- Rosen, R.D., and D.A. Salstein, 1980: A comparison between circulation statistics computed from conventional data and NMC Hough analyses. Mon. Wea. Rev., 108, 1226-1247.
- Rosby, C.G., 1950: On the dynamics of certain types of blocking waves. J. Chinese Geophys. Soc., 2, 1-13.
- Rowntree, P.R., 1972: The influence of tropical east Pacific Ocean temperature on the atmosphere. Quart. J. R. Meteor. Soc., 98, 290-321.
- _____, 1976: Tropical forcing of atmospheric motions in a numerical model. Quart. J. R. Meteor., 102, 583-605.
- Sanders, R.A., 1953: Blocking highs over the eastern North Atlantic ocean and western Europe. Mon. Wea. Rev., 81, 67-73.
- Sanders, F. and J.R. Gyakum, 1980: Synoptic-dynamic climatology of the "bomb". Mon. Wea. Rev., 108, 1589-1606.
- Savijarvi, H.I., 1977: The interaction of the monthly mean flow and large-scale transient eddies in two different circulation types. Part II. Vorticity and temperature balance. Geophysica, 14, 207-229.
- Sawyer, J.S., 1970: Observational characteristics of atmospheric fluctuations with a time scale of a month. Quart. J. R. Met. Soc., 96, 610-625.
- Schneider, E.K., 1977: Axially symmetric steady-state models of the basic state for instability and climate studies. II. Nonlinear calculations. J. Atmos. Sci., 34, 280-296.
- _____, and R.S. Lindzen, 1977: Axially symmetric steady-state models of the basic state for instability and climate studies. I. Linear calculations. J. Atmos. Sci., 34, 263-279.
- Shapiro, R., 1970: Smoothing, filtering, and boundary effects. Rev. Geophys. and Space Phys., 8, 359-387.
- Shuman, F.G., and J.B. Hovermale, 1968: An operational six-layer primitive equation model. J. Appl. Meteor., 108, 1226-1247.
- Simmons, A.J., 1981: The forcing of stationary wave motion by tropical diabatic heating. Unpublished manuscript.
- _____, and B.J. Hoskins, 1976: Baroclinic instability on a sphere: Normal modes of the primitive and quasi-geostrophic equations. J. Atmos. Sci., 33, 1454-1477.

- Simmons, and B.J. Hoskins, 1977: Baroclinic instability on the sphere: solutions with a more realistic troposphere. J. Atmos. Sci., 34, 581-588.
- _____, and _____, 1978: The life-cycles of some nonlinear baroclinic waves. J. Atmos. Sci., 35, 414-432.
- Smagorinsky, J., 1953: The dynamical influence of large-scale heat sources and sinks on the quasi-stationary mean motions in the atmosphere. Quart. J. Roy. Meteor. Soc., 79, 342-366.
- Starr, V.P., J.P. Peixoto and N.E. Gaut, 1970: Momentum and zonal kinetic energy balance of the atmosphere from five years of hemispheric data. Tellus, 22, 251-274.
- Stefanick, M., 1981: Space and time scales of atmospheric variability. J. Atmos. Sci., 38, 988-1002.
- Sumner, E.J., 1954: A study of blocking in the Atlantic-European sector of the Northern Hemisphere. Quart. J. R. Meteor. Soc., 80, 402-416.
- _____, 1959: Blocking anticyclones in the Atlantic-European sector of the Northern Hemisphere. Meteor. Mag., 88, 300-311.
- Thompson, P.D., 1957: A heuristic theory of large-scale turbulence and long-period velocity variations in baroclinic flow. Tellus, 9, 69-91.
- Troup, A.J., 1965: The Southern Oscillation. Quart. J. R. Met. Soc., 91, 490-506.
- Tung, K.K., and R.S. Lindzen, 1979a: A theory of stationary long waves. Part I. A simple theory of blocking. Mon. Wea. Rev., 107, 714-734.
- _____, and _____, 1979b: A theory of stationary long waves. Part II. Resonant Rossby waves on the presence of realistic vertical shears. Mon. Wea. Rev., 107, 735-750.
- van Loon, H., and J.C. Rogers, 1978: The see-saw in winter temperature between Greenland and northern Europe. Part I. General description. Mon. Wea. Rev., 106, 296-310.
- von Neumann, J., 1960: Some remarks on the problem of forecasting climatic fluctuations, in Dynamics of Climate, ed. by R.L. Pfeffer, Pg. 9, Pergamon Press.
- Wallace, J.M., and D.S. Gutzler, 1981: Teleconnections in the geopotential height field during the Northern Hemisphere winter. Mon. Wea. Rev., 109, 784-912.

- Webster, P.J., 1981: Mechanisms determining the atmospheric response to sea surface temperature anomalies. J. Atmos. Sci., 38, 554-571.
- White, G.H., 1980: Skewness, kurtosis and extreme values of Northern Hemisphere geopotential heights. Mon. Wea. Rev., 108, 1446-1455.
- White, W.B., and N.E. Clark, 1975: On the development of blocking ridge activity over the central North Pacific. J. Atmos. Sci., 32, 489-502.
- White, G.H., 1981: Estimates of the seasonal mean vertical velocity fields of the extratropical northern hemisphere. Submitted to Mon. Wea. Rev.
- Winston, J.S., 1955: Physical aspects of rapid cyclogenesis in the Gulf of Alaska. Tellus, 7, 481-566.
- Yeh, T.C., 1949: On energy dispersion in the atmosphere. J. Met., 6, 1-16.

BIOGRAPHICAL NOTE

The author was born Sept. 29, 1951 in Sacramento, California. Family and old friends recall that he displayed an intense interest in natural, particularly weather, phenomena from an early age. While at Gunn high school in Palo Alto, California, he was a research observer at the National Center for Earthquake Research and at Pacific Weather Analysis Corporation (now Oceanroutes, Inc.). Both positions presented fascinating and challenging problems in predicting natural events. During this time, he also studied pattern recognition techniques under the tutelage of scientists at the Stanford Artificial Intelligence Project.

The author attended Cornell University in Ithaca, New York from 1971-1975. During his junior and senior years, he was a teaching assistant in synoptic meteorology, helping to organize and write notes for, in addition to teach, an undergraduate synoptic lab course. He was also a resident advisor in an undergraduate dormitory, where he was fortunate to meet another resident advisor, Ellen Perry, who became his wife in June, 1980. The author graduated with a B. S. degree in 1975 with honors and distinction; he also received an A. A. degree with highest honors in Aeronautical Science from Foothill College in Los Altos Hills, California for work done prior to, and concurrent with, his studies at Cornell.

The author entered the graduate program at MIT in September, 1975. For the first two years, he was a teaching assistant in synoptic meteorology under Prof. Sanders; subsequently, he has been a research assistant. He has published one paper: "The Objective Representation of Blocking Patterns" in The General Circulation: theory, modelling and observations (NCAR Summer 1978 colloquium). A second paper, "Persistent anomalies of the extratropical Northern Hemisphere wintertime circulation", will appear later this year in Dynamics of the Extratropical Atmosphere, Brian Hoskins, ed., published by Academic Press.

The author has accepted a postdoctoral research fellowship at the Center for Earth and Planetary Physics at Harvard University.